A study on Optical Labelling Techniques for All-Optical Networks

Holm-Nielsen, Pablo Villanueva

Publication date:
2005

Document Version
Publisher's PDF, also known as Version of record

Pablo V. Holm-Nielsen

A STUDY ON OPTICAL LABELLING TECHNIQUES FOR ALL-OPTICAL NETWORKS

20th of April, 2005

Research Center COM
Technical University of Denmark

Contents

Abstract

Optical switching has been proposed as an effective solution to overcoming the potential electronic bottleneck in all-optical network nodes carrying IP over WDM. The solution builds on the use of optical labelling as a mean to route packets or bursts of packets through the network. In addition to the selected wavelength, a short label of fixed length can be added to the information flow in order to be processed in intermediate nodes.

The main advantage of this approach is the ability to route packets or bursts independently of bit-rate, packet format and packet length, increasing network flexibility and granularity. In this thesis the systems aspects of optical labelling will be investigated for several labelling techniques, in order to identify the strengths and drawbacks of each one with respect to system performance.

Orthogonal labelling has been proposed as one of the potential labelling techniques. It is based on the transmission of two types of modulation on the same optical carrier. The orthogonal nature of the signal ensures that the label and the payload would be able to be detected independently of each other.

In order to asses the limits and possibilities of such schemes, several orthogonal labelling schemes will be investigated with regard to generation, transmission, wavelength conversion and label swapping. The resulting subsystems are then combined in order to emulate the functionalities of a network node within a transmission system.

The two main addressed labelling schemes are the IM/DPSK and the IM/FSK schemes. In IM/DPSK the payload is modulated in the intensity of the carrier, while the label is differentially encoded on its phase. The IM/FSK labelling scheme, on the other hand, modulates the payload on the intensity, while the label is modulated on the frequency of the signal. Other labelling techniques are also presented and analyzed, including carrier-suppressed sideband labelling and the DPSK/IM scheme that interchanges the roles of the modulation formats from the IM/DPSK scheme. A mention on time-serial labelling is done with regard to wavelength conversion and an experimental assessment of a packet switching node.

Several methods for generating the labelled signals are studied. For the FSK transmitter, a novel method is presented, which is based on direct modulation of a DFB laser, accompanied by an intensity stabilization using the

conjugated data on a EAM. The receiver performance is also analyzed with respect to several filtering schemes.

A major performance limitation of orthogonal labelling comes from the crosstalk between the two modulation formats induced by the simultaneous amplitude and phase/frequency modulation on the same optical carrier. The receiver sensitivity of the IM signal improves as the IM extinction ratio is increased, while the sensitivity of the DPSK or FSK label deteriorates. Thus, the IM extinction ratio has to be optimized in order to correctly detect the information in the phase or frequency modulation. This requirement on the IM extinction ratio limits the network scalability and the system transparency to signal format. However, the need to use a poor extinction ratio can be completely eliminated by utilizing special line coding on the IM signal, such as Manchester coding or 8B/10B coding.

The degradation of the orthogonal modulation formats, due to transmission over fiber spans, is compensated in single channel and WDM systems. Several compensation schemes are compared and limits to channel spacing and receiver performance are identified. The stabilization of filtering process throughout the systems are shown to be of importance.

Wavelength conversion of orthogonally labelled signals is performed on passive and active devices. In HNLF both the FWM and XPM effects are exploited in order to achieve wavelength conversion of 40 Gb/s signals. Active devices as SOA, EAM and SOA-MZI are also investigated for wavelength conversion of labelled signals. Most of the employed wavelength conversion processes are only sensitive to the amplitude of the incoming signal, and can therefore effectively be used for label erasure. Label insertion can in some cases also be done in the same device, thus performing label swapping and wavelength conversion in a single device. However, this method is unable to re-use the same wavelength for the output signal, and requires a fast tunable filtering scheme at the network node. These limitations are overcome by performing wavelength conversion and label swapping in a double stage system, that makes use of an intermediate wavelength between label erasure and label insertion.

The above mentioned functionalities are assembled in whole network systems experiments that validates the different labelling schemes with respect to transmission, wavelength conversion, label swapping and re-transmission. Optical labelling and specially the orthogonal schemes for optical labelling, are thus shown to be an effective solution to all-optical networks.

Resumé

Optisk *switching* er blevet foreslået som en effektiv løsning til den mulige elektroniske flaskehals i alt-optiske netværks knudepunkter, som behandler IP over WDM. Løsningen bygger på brugen af optiske mærker til at dirigere pakker eller *bursts* af pakker gennem netværket. Udover den valgte bølgelængde kan et kort mærke af fast længde blive lagt til informationsstrømmen, så den kan blive processeret i de mellemliggende knudepunkter. Den største fordel ved denne løsning er muligheden for at dirigere pakker eller *bursts* af pakker uafhængig af bit-hastighed, pakke-format eller pakke-længde. Derved forøges netværkets fleksibilitet og granularitet. Denne ph.d. afhandling omhandler systemaspekterne ved optisk mærkning. Flere optiske mærkningsmetoder er blevet undersøgt, med henblik på at finde fordele og ulemper med hensyn til deres system præstationsevne.

Ortogonal mærkning er blevet foreslået som en af de lovende mærkningsteknikker. Den er baseret på transmissionen af to typer af modulationer på samme optiske bærebølge. Signalets ortogonale natur garanterer at mærke og nyttelast vil kunne modtages uafhængigt af hinanden.

For at kunne måle begrænsningerne og mulighederne for disse metoder er flere sådanne ortogonale markeringsmetoder blevet undersøgt med hensyn til frembringelse, transmission, bølgelængdekonvertering og mærkeombytning. Derefter, bliver de resulterende under-systemer samlet med henblik på at efterligne funktionaliteterne, som et netværksknudepunkt ville have i et transmissionssystem.

De to mærkningsmetoder, som får den største opmærksomhed, er IM/DPSK og IM/FSK metoderne. I IM/DPSK er nyttelast moduleret på signalets intensitet, medens mærket er differential-kodet på fasen af den optiske bærebølge. I modsætning hertil, består IM/FSK metoden af en nyttelast som også er intensitetsmoduleret, medens mærket denne gang er moduleret på signalets optiske frekvens. Andre mærkningsmetoder er imidlertid også præsenteret og analyseret. Blandt andet *carrier-suppressed sideband* mærkning og DPSK/IM metoden, som ombytter modulationsformaterne mellem mærke og nyttelast, i forhold til IM/DPSK metoden. *Time-serial* metoden til mærkning bliver også nævnt hvad angår bølgelængdekonvertering og målinger på et eksperiment omkring et pakke-*switching* knudepunkt.

Flere metoder til frembringelse af mærkede signaler bliver studeret. En ny metode for FSK senderne præsenteres, som er baseret på direkte modulation

af en DFB laser sammen med undertrykkelse af intensitetsvariationer ved hjælp af en EAM. Modtagerens præstationsevne bliver også studeret med hensyn til flere filtreringsmetoder.

En af de største begrænsninger ved ortogonal mærkning er krydstale mellem de to modulationsformater. Intensitetsmodulationens modtagerfølsomhed bliver forøget, når dennes udslukningsforhold forbedres, medens følsomheden for DPSK eller FSK mærket forværres. Derfor er det vigtigt at optimere intensitetsmodulationens udslukningsforhold for at modtage mærkets information. Denne begrænsning på intensitetsmodulationens udslukningsforhold betyder, at netværkets skalerbarhed og systemets uafhængighed med hensyn til signal format bliver reduceret. På den anden side kan man undgå dette ellers nødvendige begrænsede udslukningsforhold ved at benytte specielle kodningsmetoder for intensitetsmodulationen, som for eksempel Manchester kodning eller 8B/10B kodning.

Påvirkningen af transmission på de ortogonalt modulationerne signaler bliver målt i enkelt kanal og WDM systemer. Flere kompensations metoder er sammenlignet, og begrænsninger i kanalafstand samt modtagerpræstationsevne bliver målt. De optiske filtres stabilitet og indflydelse under filtreringsprocessen gennem hele systemet viser sig at have stor betydning.

Bølgelængdekonvertering af ortogonalt mærkede signaler er blevet udført på passive samt aktive komponenter. I HNLF bliver både FWM og XPM brugt til bølgelængdekonvertering af 40 Gb/s signaler. Aktive komponenter som SOA, EAM og SOA-MZI er også undersøgt til bølgelængdekonvertering af ortogonalt mærkede signaler. De fleste af de benyttede bølgelængdekonverteringsmetoder reagerer kun på intensiteten af det indkommende signal, og kan derfor effektivt benyttes som mærkeudviskning. Mærkeindsætning kan nogle gange også foretages i den samme komponent, og på den måde kan man opnå mærkeombytning og bølgelængdekonvertering i en og samme komponent. Dette fører imidlertid til, at man ikke kan benytte den samme bølgelængde for outputsignalet, og desuden kræves en hurtig tunbar filtermetode i netværksknudepunkterne. Disse begrænsninger kan overvindes ved at anvende bølgelængdekonvertering og mærkeombytning i et to-trins system, som benytter en mellemliggende bølgelængde mellem udviskning og indsætning.

Alle disse funktionaliteter bliver så sat sammen i et helt netværkssystemeksperiment, som demonstrerer de forskellige metoder til transmission, bølgelængdekonvertering, mærkeudskiftning og gen-transmission som et samlet hele. Optisk mærkning og specielt de ortogonale metoder for optisk mærkning er derved vist at være en effektiv løsning til alt-optiske netværk.

Acknowledgements

I would like to thank my supervisors Palle Jeppesen and Christophe Peucheret, for kind guidance and an exceptionally achieved balance between professional effectiveness and a friendly treatment.

Most of the lab work throughout the thesis was done in cooperation with Jianfeng Zhang and Nan Chi, that also were very helpful with any research matter that might come up along the way. The whole of the systems group have contributed to the notorious good atmosphere and high level of performed research, which is also distinctive of the whole of Research Center COM. I am very grateful to Christophe, Torger, Alvaro, Leif, Anders and Michael for reading the thesis and coming with valuable comments. To my office mates Peter and Andrea for keeping it lively. And also thanks to Jorge, Beata, Emir, Darko, Yan, Zhenbo, Brian, Jose and Heidi. Contributions of the other STOLAS and LASAGNE partners (IMEC, Lucent, UC Dublin, Hymite, NKT Integration, Telenor, UPVL, NTUA, TU/e, TI-Labs, Fibernet, Intune Technologies) are also gratefully acknowledged.

On the personal level, there are lots of people whom I would like to thank for accompanying me during the last years and specially these last months. Juan-Pedro, Naja and the girls for IT assistance and quality moments. My parents for multiple forms of support. My extended Danish family for being a constant reference. Toni and Helena for sweets and music. Maria, Emma, Mile and Mia for good times. Peter, Dan, Torger, Mogens, and Troels for constantly helping me being on the move. The FOM Commission for keeping us on our toes. David for problem solving at my most busy time. SOL for constant comfort and an escape from the ordinary. Anna, Dani, Mireia, the Wolves family and the many friends from Barcelona for numerous uplifting mails and encouragement. Roel, Martine, Luciana and other friends out in the world for making me feel welcome in this vast planet. And friends that were there for me even when I didn't have the time to correspond Maj, Eva, Trine, Stine, Charlotte, Thomas, Marlene, Gitte, and Lise.

Other people, that I might have forgotten, are acknowledged for not being cross about it.

This thesis is dedicated to the memory of my grandparents.

Ph.D. publication list

[1] N. Chi, B. Carlsson, J. Zhang, P. V. Holm-Nielsen, C. Peucheret and P. Jeppesen, "Transmission performance of all-optically labelled packets using ASK/DPSK orthogonal modulation", in Tech. Dig. IEEE Laser and Electro-Optics Society Annual Meeting, LEOS'2002, paper MF3, vol. 1, pp. 51-52, Glasgow, U.K., November 2002.

[2] Nan Chi, Birger Carlsson, Pablo V. Holm-Nielsen, Christophe Peucheret, Palle Jeppesen, "Dispersion management for two-level optically labeled signals in IP-over-WDM networks", in Proc. European Conference on Optical Communication, ECOC'2002, paper 5.5.1, vol. 2, Copenhagen, Denmark, September 2002.

[3] J. Zhang, N. Chi, P. V. Holm-Nielsen, C. Peucheret and P. Jeppesen, "10 Gbit/s Manchester encoded FSK-labelled optical signal transmission link", Electronics Letters, vol. 39, no. 16, pp. 1193-1194, 2003.

[4] J. Zhang, N. Chi, P. V. Holm-Nielsen, C. Peucheret and P. Jeppesen, "An optical FSK transmitter based on an integrated DFB laser-EA modulator and its application in optical labeling", IEEE Photonics Technology Letters, vol. 15, no. 7, pp. 984-986, 2003.

[5] J. Zhang, N. Chi, P. V. Holm-Nielsen, C. Peucheret and P. Jeppesen, "Method for optical subcarrier label generation using carrier suppression technique", Electronics Letters, vol. 39, no. 4, pp. 388-389, 2003.

[6] J. Zhang, N. Chi, P. V. Holm-Nielsen, C. Peucheret and P. Jeppesen, "Performance of Manchester-coded payload in an optical FSK labeling scheme", IEEE Photonics Technology Letters, vol. 15, no. 8, pp. 1174-1176, 2003.

[7] Tafur Monroy, A. M. J. Koonen, J. Zhang, N. Chi, P. V. Holm-Nielsen, C. Peucheret, J. J. Vegas Olmos and G.-D. Khoe, "Techniques for labeling of optical signals in burst switched networks", First International Workshop on Optical Burst Switching (WOBS), Dallas, Texas, 2003.

[8] N. Chi, C. Mikkelsen, L. Xu, J. Zhang, P. V. Holm-Nielsen, H. Ou, J. Seoane, C. Peucheret and P. Jeppesen, "Transmission and label

encoding/erasure of orthogonally labelled signal using 40 Gbit/s RZ-DPSK payload and 2.5 Gbit/s IM label", Electronics Letters, vol. 39, no. 18, pp. 1335-1337, 2003.

[9] Nan Chi, Birger Carlsson, Jianfeng Zhang, Pablo V. Holm-Nielsen, Christophe Peucheret, Palle Jeppesen, "Transmission properties for two-level optically labeled signals using ASK/DPSK orthogonal modulation in IP-over-WDM networks", Journal of Optical Networking, vol. 2, no. 2, pp. 46-54, 2003.

[10] J. Zhang, N. Chi, P. V. Holm-Nielsen, C. Peucheret and P. Jeppesen, "A novel method for optical subcarrier label generation", in Technical Digest Optical Fiber Communication Conference, OFC'03, Atlanta, Georgia, U.S.A., paper FD5, vol. 2, pp. 653-654, 2003.

[11] J. Zhang, N. Chi, P. V. Holm-Nielsen, C. Peucheret and P. Jeppesen, "A novel optical labeling scheme using a FSK modulated DFB laser integrated with an EA modulator", in Technical Digest Optical Fiber Communication Conference, OFC'03, Atlanta, Georgia, U.S.A., paper TuQ5, vol. 1, pp. 279-280, 2003.

[12] N. Chi, L. Xu, L. J. Christiansen, K. Yvind, J. Zhang, P. V. Holm-Nielsen, C. Peucheret, C. Zhang and P. Jeppesen, "Optical label swapping and packet transmission based on ASK/DPSK orthogonal modulation format in IP-over-WDM networks", in Technical Digest Optical Fiber Communication Conference, OFC'03, Atlanta, Georgia, U.S.A., paper FS2, vol. 2, pp. 792-794, 2003.

[13] N. Chi, J. Zhang, P. V. Holm-Nielsen, C. Peucheret and P. Jeppesen, "Transmission and transparent wavelength conversion of an optically labeled signal using ASK/DPSK orthogonal modulation", IEEE Photonics Technology Letters, vol. 15, no. 5, pp. 760-762, 2003.

[14] N. Chi, J. Zhang, P. V. Holm-Nielsen, L. Xu, I. T. Monroy, C. Peucheret, K. Yvind, L. J. Christiansen and P. Jeppesen, "Experimental demonstration of cascaded transmission and all-optical label swapping of orthogonal IM/FSK labelled signal", Electronics Letters, vol. 39, no. 8, pp. 676-678, 2003.

[15] N. Chi, L. J. Christiansen, P. Jeppesen, I. T. Monroy, P. V. Holm-Nielsen, C. Peucheret, K. Yvind, L. Xu, J. Zhang, "Optical label switching in telecommunication using semiconductor lasers, amplifiers and electro-absorption modulators", in Laser Optics'2003, paper WeR3-05, St.Petersburg, Russia, 2003.

[16] Pablo V. Holm-Nielsen, N. Chi, J. Zhang, C. Peucheret, I. T. Monroy and P. Jeppesen, "Experimental investigation of transmission

properties of all-optical label swapping of orthogonal IM/FSK labeled signals", in Proceedings Optoelectronics and Communications Conference, OECC'03, Shanghai, China, pp 679-680, 2003.

[17] N. Chi, J. Zhang, P. V. Holm-Nielsen, B. Kozicki, C. Peucheret and P. Jeppesen, "Transmission properties of an all-optical labelled signal using orthogonal IM/FSK modulation format", in Proceedings European Conference on Optical Communication, ECOC'03, Rimini, Italy, paper Tu4.4.1 (invited), vol. 2, pp. 300-303, 2003.

[18] K. Vlachos, J. Zhang, J. Cheyns, Sulur, N. Chi, E. van Breusegem, I. Tafur Monroy, J. G. L. Jennen, P. V. Holm-Nielsen, C. Peucheret, R. O'Dowd , P. Demeester and A. M. J. Koonen, "An optical IM/FSK coding technique for the implementation of a label-controlled, arrayed waveguide packet router", Journal of Lightwave Technology, vol. 21, no. 11, pp. 2617-2628, Nov. 2003.

[19] N. Chi, P. V. Holm-Nielsen, L. Xu, J. Zhang, T. Tokle and P. Jeppesen, "Cascaded transmission, packet switching and all-optical wavelength conversion for 40 Gbit/s RZ payload with 10 Gbit/s serial-bit label", Electronics Letters, vol. 40, no. 21, pp. 1366-1367, 2004.

[20] Tafur Monroy, E. J. M. Verdurmen, S. Sulur, A. M. J. Koonen, H. de Waardt, G. D. Khoe, N. Chi, P. V. Holm-Nielsen, J. Zhang and C. Peucheret, "Performance of a SOA-MZI wavelength converter for label swapping using combined FSK/IM modulation format", Optical Fiber Technology, vol. 10, no. 1, pp. 31-49 (invited paper), 2004.

[21] P. V. Holm-Nielsen, J. Zhang, J.J. Vegas Olmos, I. Tafur Monroy, C. Peucheret, V. Polo, P. Jeppesen, A.M.J. Koonen and J. Prat, "Experimental investigation of WDM transmission properties of optical labeled signals using orthogonal IM/FSK modulation format", in Proceedings International Conference on Telecommunications, ICT'04, Fortaleza, Brazil, pp753-759, August 2004.

[22] J. J. Vegas Olmos, J. Zhang, P. V. Holm-Nielsen, I. Tafur Monroy, V. Polo, A. M. J. Koonen, C. Peucheret, and J. Prat, "Simultaneous optical label erasure and insertion in a single wavelength conversion stage of combined FSK/IM modulated signals", IEEE Photonics Technology Letters, vol. 16, no. 9, pp. 2144-2146, Sept. 2004.

[23] J. Zhang, P. V. Holm-Nielsen, N. Chi, C. Peucheret and P. Jeppesen, "DC-balanced line encoding for optical labeling scheme using orthogonal modulation", in Technical Digest Optical Fiber Communication Conference, OFC'04, Los Angeles, California, U.S.A., paper WF2, 2004.

[24] J. Zhang, N. Chi, P. V. Holm-Nielsen, C. Peucheret and P. Jeppesen, "Method for high-speed Manchester encoded optical signal generation", in Technical Digest Optical Fiber Communication Conference, OFC'04, Los Angeles, California, U.S.A., paper MF76, 2004.

[25] N. Chi, L. Xu, J. Zhang, P. V. Holm-Nielsen, C. Peucheret, C. Mikkelsen, H. Ou, J. Seoane and P. Jeppesen, "Orthogonal optical labeling based on a 40 Gbit/s DPSK payload and a 2.5 Gbit/s IM label", in Technical Digest Optical Fiber Communication Conference, OFC'04, Los Angeles, California, U.S.A., paper FO6, 2004.

[26] N. Chi, P. V. Holm-Nielsen, P. Jeppesen, C. Peucheret, J. Zhang, J. J. Vegas Olmos and I. Tafur Monroy, "Optical label swapping of payloads up to 40 Gb/s using an orthogonally modulated label", IEEE Lasers and Electro-Optics Society Annual Meeting, LEOS'04 (invited), Puerto-Rico, 2004.

[27] F. Ramos, E. Kehayas, J. M. Martinez, R. Clavero, J. Marti, L. Stampoulidis, D. Tsiokos,H. Avramopoulos, J. Zhang, P. V. Holm-Nielsen, N. Chi, P. Jeppesen, N. Yan, I. Tafur Monroy, A. M. J. Koonen, M. T. Hill, Y. Liu, H. J. S. Dorren, R. Van Caenegem, D. Colle, M. Pickavet, and B. Riposati, "IST-LASAGNE: Towards All-Optical Label Swapping Employing Optical Logic Gates and Optical Flip-flops", to be published in Journal of Lightwave Technology, 2005.

[28] N. Chi, L. Xu, J. F. Zhang, P. V. Holm-Nielsen, C. Peucheret and P. Jeppesen, "Optical Label Switching of 40 Gb/s Payloads Using Orthogonal ASK/DPSK Modulation Format", submitted to Journal of Lightwave Technology, 2005.

[29] N. Chi, L. Xu, J. Zhang, P. V. Holm-Nielsen, C. Peucheret, Y. Geng and P. Jeppesen, "Transmission and Optical Label Swapping for 4x40 Gb/s WDM signals deploying orthogonal ASK/DPSK labeling", IEEE Photonics Technology Letters, vol 17, no. 6, pp 1325-1327, 2005.

[30] P. V. Holm-Nielsen, J. Zhang, N. Chi and P. Jeppesen, "Combined Label Swapping and Wavelength Conversion in All-Optical Processing Nodes for 40 Gb/S Labelled Signals", International Conference on Telecommunications (ICT05), 2005.

[31] J.J. Vegas Olmos, I. Tafur Monroy, A. M. J. Koonen, C. Bock, V. Polo, J. Prat and P. V. Holm-Nielsen, "Unified optical access and metro network architecture based on agile tunable light sources and a combined FSK/IM modulation scheme", submitted to Journal of Optical Networking (JON), 2005.

List of acronyms

AOLS	All-Optical Label Swapping
AOWC	All-Optical Wavelength Converter
ASE	Amplified Spontaneous Emission
ASK	Amplitude Shift Keying
ATM	Asynchronous Transfer Mode
AWG	Arrayed Waveguide Grating
SDH	Synchronous Digital Hierarchy
B2B	Back-to-Back
BER	Bit-Error Rate
CSS	Carrier-Suppressed Side-Band
CW	Continuous Wave
DC	Direct Current
DCF	Dispersion Compensating Fiber
DFB	Distributed Feedback (laser)
DPSK	Differential Phase Shift Keying
EAM	Electro-Absorption Modulator
ECL	External-Cavity Laser
EDFA	Erbium Doped Fiber Amplifier
EOP	Eye-Opening Penalty
ER	Extinction Ratio
FBG	Fiber Bragg-Grating
FPF	Fabry-Perot Filter
FSK	Frequency Shift Keying
FWM	Four-Wave Mixing
GCSR	Grating Assisted Coupler Sampled Reflector (laser)
HNLF	Highly Nonlinear Fiber
IM	Intensity Modulation / Intensity Modulated
IP	Internet Protocol
ISI	Inter-Symbolic Interference
ITU	International Telecommunications Union
LASAGNE	All-Optical Label Swapping Employing Optical Logic Gates in Network Nodes
MC	Manchester Coding / Manchester Coded
MPLS	Multi-Protocol Label Switching.
MPλS	Multi-Protocol Lambda Switching
MZDI	Mach-Zehnder Delay Interferometer

MZI	Mach-Zehnder Interferometer
MZM	Mach-Zehnder Modulator
NRZ	Non-Return to Zero
NZDSF	Non-Zero Dispersion Shifted Fiber
OADM	Optical Add-Drop Multiplexer
OBPF	Optical Band-Pass Filter
OBS	Optical Burst Switching
OCDM	Optical Code Division Multiplexing
OEO	Opto-Electro-Optic (conversion)
OSNR	Optical Signal-to-Noise Ratio
OTDM	Optical Time-Division Multiplexing
PBS	Polarization Beam Splitter
PM	Phase Modulation
PRBS	Pseudo Random Bit Sequence
PSK	Phase Shift Keying
RF	Radio-Frequency
RZ	Return to Zero
SCM	Sub-Carrier Multiplexing
SMF	Single Mode Fiber
SNR	Signal-To-Noise Ratio
SOA	Semiconductor Optical Amplifier
SOA-MZI	SOA-Based Mach-Zehnder Interferometer
SPM	Self Phase Modulation.
STOLAS	Switching Technologies for Optically Labelled Signals
TL	Tunable Laser
TLLM	Transmission Line Laser Model
TWC	Tuneable Wavelength Converter
VPI	Virtual Photonics Incorporated
WC	Wavelength Conversion / Wavelength Converter
WDM	Wavelength Division Multiplexing
XAM	Cross-Absorption Modulation
XGM	Cross-Gain Modulation
XOR	Exclusive-OR
XPM	Cross-Phase Modulation

Chapter 1

Introduction

Despite the recent slowdown in the telecommunications industry, the amount of packet-based data traffic in today's telecommunication networks is still increasing steeply [1], [2]. The continuing growth of the Internet and the introduction of high-bit rate wavelength division multiplexing (WDM) connections in metro and backbone networks, is increasing the amount of data that has to be handled by Internet protocol (IP) routers [3]. Current electronic packet switches can handle high bit-rates, and their development is still increasing their capacity [4]. However, the demand and availability of bandwidth is raising at a much faster rate [5]. The need for effective and flexible switching solutions will therefore become more evident, in the sense that these increasing transmission rates will eventually create a bottleneck at the switching nodes [6], [7].

IP packet-based data traffic is currently carried over WDM, with SDH and/or ATM as the intermediate layers, while avoiding these intermediate layers by carrying IP directly over WDM would yields more efficient networks [8]. A novel approach termed lambda labelling or multi-protocol lambda switching (MPλS) has been presented for direct IP-over-WDM transport [9]. The scheme has been derived from the multi-protocol label switching (MPLS) protocols [10] and the label-switching concept to provision wavelength-switched channels. This technique uses the transmitted wavelength as a source of information about the packet. Optical packets are switched to other wavelengths at the network nodes and wavelength routers in the core nodes guide the packets along the appropriate network paths, while the label swapping can be done by wavelength converters [8].

However, in addition to the optical wavelength that can serve as an optical label in MPλS schemes, a second level of optical label is still necessary for provisioning, maintaining, and restoring switched light-paths [5].

Label switching would enable the implementation of packet routing and forwarding functions in IP-over-WDM [9]. At the same time it would

support high bit-rates for payload data transmission, while employing low speed electronics in the core nodes for label processing. Labels would be received and swapped at every node, while the payload information would be transparently forwarded with possible wavelength conversion [12].

Therefore, recent proposals [13], [14], [15] suggest to have two optical levels of packet labels. One level would be the wavelength to be assigned to the data stream. The second one would be an information label added along with the payload data using a particular modulation scheme different from the one used by the payload. In the edge nodes, both the wavelength and the label would be set and assigned to packets (or bursts of packets) according to their destination and/or class of service. In the network's core nodes, the wavelength and/or the label would be used for routing the packets, and would be able to be swapped [16], [17], [18].

All-optical packet switching using an optical label is being regarded as having a great potential in future IP-over-WDM networks in order to remove the bottleneck of IP packet routing [19], [20], [21]. By this method, individual packets could be switched through an optical network element without being converted from optical to electronic format [8]. An important characteristic and challenge of such an approach would be to enable transmitting payload information at high bit rates, while at the same time allowing label information to be easily extracted from the bit stream. The optical label format should be carefully chosen to satisfy such requirements [12].

1.1 Optical labelling methods

Several techniques have been proposed for labelling optical packets or burst of packets, amongst them time-serial labelling, [23], optical code division multiplexing (OCDM) labelling [24] and WDM labelling [7]. In the first two methods, the label is attached to the payload at the same wavelength channel as the one carrying these payload data, whereas in the third method, a separate wavelength channel is used to carry the labels.

The optical label can also be realized by a parallel modulation technique, meaning that the label would have a different modulation format than the payload, while being transmitted at the same carrier. The main advantages of the parallel techniques rely on the fact that the label data can be modulated at a significantly lower rate and separated from the payload by the type of modulation. Generally, the parallel modulation techniques for the label can be performed by subcarrier multiplexing [15], [25] or by an angle modulation that is orthogonal to the intensity modulated (IM) payload [16], [26], [27]. In

this context, orthogonal implies that the label and the payload can be detected independently of each other.

Time-serial labelling

In time-serial labelling (also called bit-serial labelling) the label information is attached in the time domain, by inserting it in front of the payload, separated by some guard time [28]. The payload and the attached label are encoded on the same wavelength carrier, as shown in fig. 1.1.

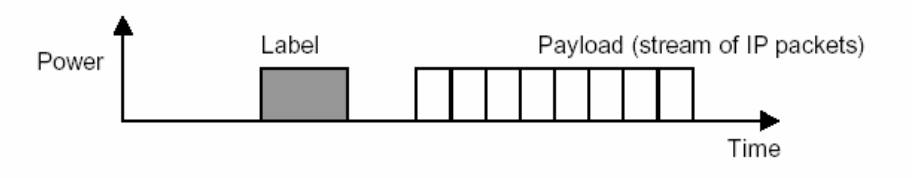

Fig. 1.1. *Serial transmission of label and payload on a single wavelength.*

The label information can be read and reinserted by O/E/O conversion, which would require reasonably fast 2×2 optical switches. The time-serial labels can also be swapped by optical means. Two techniques have been reported: wavelength conversion in a fiber loop mirror structure [29], or by optical XOR operations in an SOA-MZI wavelength converter [30].

However, a very careful synchronization for label and payload is required for label extraction and reinsertion of a new label, as well as for contention resolution purposes. This can be complex to achieve for optical channels arriving to a packet switching node from different origins.

Furthermore, bit serial multiplexing, imposes stringent processing requirements in the nodes, especially when the label rate is a high-speed signal, but on the other hand it is bandwidth wasting when label rate is a low rate signal [31], [32], [34].

WDM labelling

Another possibility is to aggregate all the label information for several WDM data channels on a single separate wavelength [35], [36], [37], as shown in fig. 1.2. This method was already adopted in [7].

Its advantage is the capability to separate the switching from the control plane, allowing easy label data extraction, detection and processing. As only the common label-wavelength channel needs to be inspected for label

processing and routing, the method would benefit from a quick and efficient single forwarding algorithm. In addition, a serious amount of high-speed O/E/O converters are avoided, as the payload data channels are delayed until the end of the electronic processing.

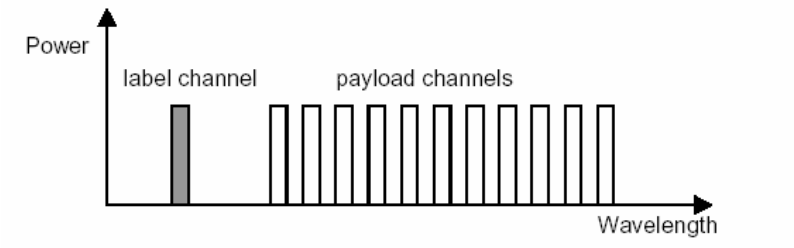

Fig. 1.2. *Single WDM channel carrying all the labels for all the bursts.*

However, the main disadvantage of this technique lays in the strict synchronisation of the individual label signals with the respective payload channels that needs to be maintained. It should also be ensured that the label reaches the nodes sufficiently earlier than the corresponding data packets in order to set the switches to the required state and to prepare the transmission of new packets on the idle wavelengths. Chromatic dispersion in the fibre links may affect this strict synchronisation by introducing group velocity differences between the label-channel and the various payload channels.

OCDM labelling

Optical code division multiplexing (OCDM) has been proposed for labelling in optical networks [24], [38]. In this method, the label information is attached by scrambling the payload with a specific code carrying the label information. Its implementation is quite complex. If a wavelength supports N OCDM codes, a bank of N optical auto-correlators per wavelength is needed for every channel in order to decode each possible label. This implies that a replica of the data of every channel should be provided to every auto-correlator of the bank. The number of network nodes is furthermore upper bounded by the nature of the code [39].

However, OCDM labelling offers possibilities to be combined with WDM (WDM sub-bands) and OTDM transmission techniques. An experiment of WDM-to-OTDM and back of 4×10 Gb/s OCDM coded channels was published in [38].

SCM labelling

Sub-carrier multiplexing (SCM) has been investigated as a possible implementation option of parallel payload-label multiplexing [40], [41], [42], where labelling information is carried on subcarrier frequency along with the payload data [15]. By intensity-modulating the subcarrier label on the optical carrier, two subcarrier sidebands next to the base-band will appear centered around the optical carrier, as shown in fig. 1.3. The wavelength channels need to be spaced at least by twice the subcarrier frequency.

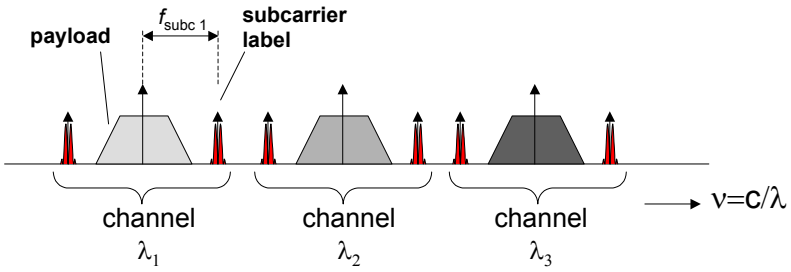

Fig. 1.3. *Subcarrier labelling in a multi-wavelength channel system.*

Reading the SCM label can be done in two ways: optical direct detection of a whole demultiplexed channel and converting the signal to base-band in the electrical domain; or alternatively, a narrow optical band-pass filter may be centred at the spectral location of a specific subcarrier band, thus detecting only the desired subcarrier information [25], [43]. Swapping of a subcarrier label is done in two steps: firstly erasure of the old label, and subsequently insertion of the new label. The sub-carrier can be suppressed by using a notch filter while the payload is left intact [25], [12].

Advantages of SCM labelling include that the label and payload are coupled in the same wavelength channel, easing the bookkeeping in the routing node. Moreover, the label data can be completely asynchronous to the payload data, avoiding strict synchronisation issues.

Some disadvantages are related to the fading of the subcarrier that may occur due to fibre dispersion [45], although, more complicated optical single-sideband modulation techniques have been explored to avoid the fading problem [46]. Furthermore, for high payload data rates, the subcarrier needs to be positioned at a very high frequency, which requires complicated electronics, and which enlarges the minimum allowed wavelength channel spacing.

Orthogonal labelling

In order to ease the above-mentioned drawbacks, the orthogonal modulation scheme has been proposed to all-optical labelling [16], [47]. Optical labelling can be achieved by a modulation which is orthogonal to the intensity modulated payload [48]. Therefore, if the wavelength is also kept as a label [8], a two-level optically labelled packet will be generated.

The intensity and angle (phase or frequency) of optical wave can be visualized as defining a two-dimensional space. When the payload is carried by intensity variations, one may code the label in the orthogonal direction in this space, using frequency shift keying (FSK) or phase shift keying (PSK), as shown schematically in fig. 1.4. In principle, this method permits label coding without a significant increase the optical bandwidth of the signal.

This labelling scheme relies on well known transmitters and receivers. Label erasure is accomplished by using a wavelength converter based on active devices, where only the IM payload information is transposed to a new wavelength channel, not the label information. Label rewriting in the FSK format can be done by FSK modulation of the tunable laser used as the wavelength converter input, while in DPSK format it would be achieved by means of a phase modulator following the wavelength converter.

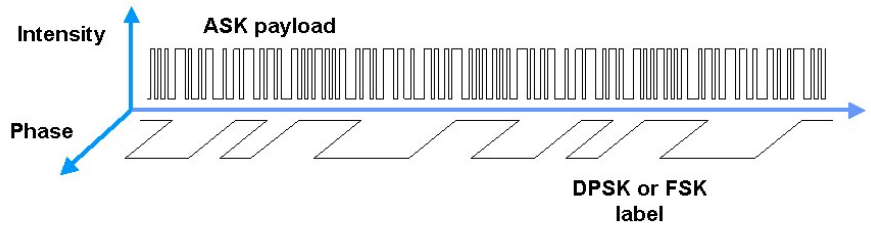

Fig. 1.4 . *Schematic description of orthogonal modulation.*

This technique has a compact spectrum and is scalable to high bit-rates, as well as permitting an upgrade in the payload bit-rate without severe changes in the labelling part of the system [49]. It enables transmitting payload information at high bit rates, while allowing label information to be easily extracted at a lower bit-rate, allowing for low-cost electronics in the network nodes [50]. The feasibility of combined intensity modulation and angle modulation has been shown in an experimental WDM network employing a coherent detection scheme [26].

Given that the data payload is coupled to the label in the same wavelength channel, the bookkeeping in the routing nodes is easily done

Table 1.1. *Comparison of labelling methods for multi-wavelength packet networks*

	Orthogonal labelling	**SCM labelling**	**TDM labelling**	**OCDM labelling**	**WDM labelling**
Synch. of payload and label	Not strict, at packet level	Not strict, at packet level	Moderate, at label level	Very strict, at payload bit level	Strict, at label bit level
Bandwidth penalty	Small increase in optical bandwidth	Increase in optical bandwidth	Increase in channel bit rate and optical bandwidth	Very large: Multiple of payload rate	Needs one additional WDM channel
Label reading	Demux of all λ-channels	OE label detection for all λ-channels	Demux of all λ-channels	Demux of all λ-channels	Demux of labels in common λ-channel
Label erasing	λ-demux + WC (XGM or XPM)	λ-demux + XGM WC, or optical notch filter	λ-demux + OE conv. of label required	λ-demux + OE conv. of payload + label + decoding	OE conv. + time demux of labels in common λ-channel
Label rewriting	By FSK mod. of tunable laser in WC, or DPSK external mod. after WC	By dual-drive external modulator, or driving SOA in SOA-MZI	EO conv. of label required, + time mux of new label with payload	EO conv. and decode of payload + label required, + encoding with new label code	OE conv. + time mux of new labels on common λ-channel
Trans-mission issues	Crosstalk between payload and label	Fading of subcarriers	Line rate somewhat higher than payload bit rate, tight synch.	High line rate	Multi-channel delineation of payload, chromatic dispersion

Moreover, the label and data payload are decoupled regarding timing, and thus only synchronisation at packet level is needed, not at bit level.

The disadvantages of orthogonal modulation scheme are mainly related to crosstalk. A limited extinction ratio on the payload is needed in order to minimize cross-talk between payload and label [51]. Besides, some payload to label crosstalk by chirp during generation and wavelength conversion could be expected; as well as a certain amount of crosstalk of label to payload by phase (or frequency) to intensity conversion, due to dispersion and interferometric effects in the fiber links during propagation [68].

Two schemes will be considered for orthogonal modulation. In the IM/DPSK scheme, the payload is intensity modulated, while the label is phase modulated employing differential phase shift keying (DPSK). It presents a compact spectrum, although at low label bit-rates the scheme imposes stringent requirements on the laser linewidth. Therefore, the scheme of combined intensity modulation with frequency shift keying (IM/FSK) has also been considered [52], [47], [53].

In the IM/FSK labelling scheme an optical FSK transmitter would impress the label information upon the optical carrier's frequency through FSK modulation without affecting its intensity. Then the optically labelled packet can be formed when the payload information is modulated on the carrier's intensity [54]. IM/FSK optical labelling offers a larger tolerance to the laser linewidth, which makes it easier to implement [16]. However, it requires careful fiber dispersion compensation due to its relatively larger optical spectrum, specially when large deviation FSK is employed [68].

The orthogonal angle/intensity modulation labelling method is extensively being studied in the framework of the IST–STOLAS (*Switching Technologies for Optical Labelled Signals*) research project.

The presented labelling methods are summarized in Table 1.1.

1.2 Optical networks

As observed earlier, all-optical packet switching is an important technique for future high-speed networks where the photonic routers can dynamically setup optical wavelength paths directly between edge nodes without electronic path termination at intermediate nodes [56].

An example of an all-optical label swapping network is shown in fig. 1.5. Bursts of data are composed by assembling several IP packets in the ingress nodes according to their destination or class of service. To each burst a label of a short fixed length is assigned and used by the core nodes to forward the packet through the network [9]. Labels are received and swapped at every node in a core network, while the payload information is transparently forwarded with possible wavelength conversion [12]. In this way packet forwarding decisions are taken by examining only short optical labels, supported by MPLS, yielding a low latency, low overhead routing technique that simplifies packet forwarding and enables scaling to very high bit rates [16].

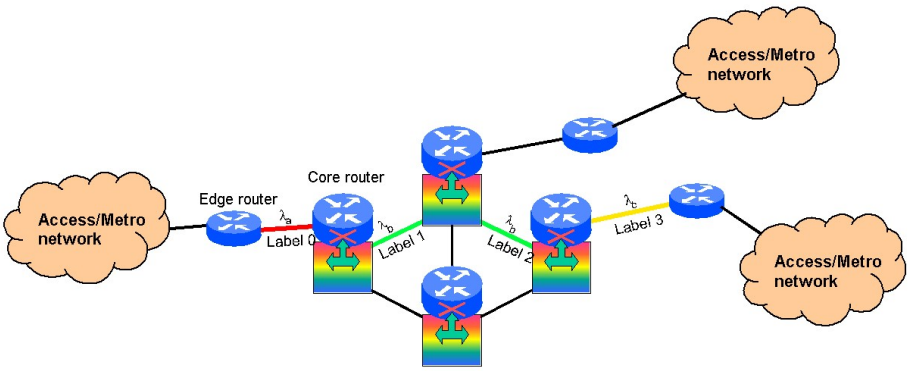

Fig. 1.5. *Network architecture of an optical labelled burst switched network. (Figure from [57]).*

The labelling process for the proposed angle modulation is illustrated in fig. 1.6. The high-speed payload data is transmitted using intensity modulation, while moderate-speed label data is transmitted on the same optical carrier by angle modulation. Once again, it is observed that the labels bit-rate can be different (much lower) than that of the payload. Then the payload information and label information can be detected using known demodulation techniques at the receiver.

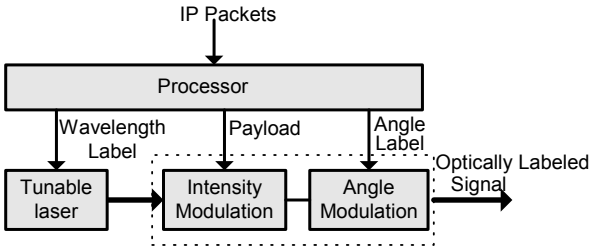

Fig. 1.6. *Optically labelled signal generation.*

At the node level, the core functionality of an optical packet switch would be to selectively transmit packets from a particular input port to a particular output port. Here a "port" implies a certain wavelength in a certain fibre. The structure of the optical label switching system for the labelled packets is illustrated in fig. 1.7 for the IM/DPSK labelling scheme. The payload, which does not need processing, can be kept in the optical domain and thus be transparently transported from inputs to outputs.

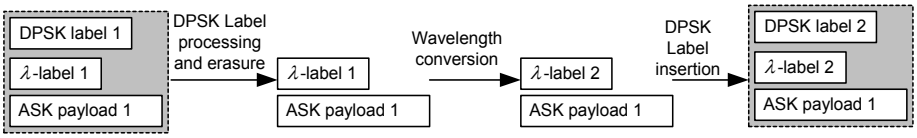

Fig. 1.7. *Schematics of two-level label swapping in an intermediate router for optical packet switching based on orthogonal modulation formats.*

The set-up of the label-controlled packet router is shown in fig. 1.8. Both the wavelength and the orthogonal (DPSK or FSK) label of each incoming packet burst are examined. After their inspection, the appropriate optical path is set through which the packet payload data are forwarded transparently. A delay line is used to buffer the incoming burst of data while the label is read, processed and the laser is tuned to the new wavelength. New labels are re-inserted for each burst, using a two-level integrated optical swapper [12],[16]. Subsequently, depending on the converted wavelength, each packet is directed to the appropriate output via an arrayed waveguide grating (AWG) [58],[59].

In order to avoid contention, packets can be buffered in variable switched-delay lines based on fibre loops and integrated optical 2×2 switches. By appropriately setting the wavelength label, packets can also be directed into feedback fibre loops for buffering or for multicasting. Similarly local dropping or adding of packets can be achieved [60], [61].

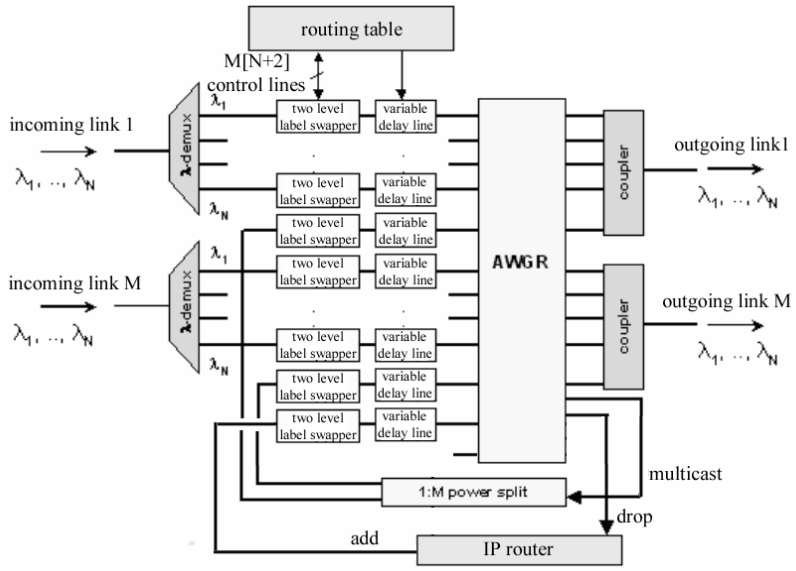

Fig. 1.8. *The label-controlled optical packet router set-up (Figure from [62]).*

At the label-swapping unit, both the label and the wavelength will be set according to the requirements of the routing process in the network. A label swapping unit is exemplified in fig. 1.9 for the IM/FSK labelling scheme. To perform label swapping a fraction of the incoming signal is tapped for opto-electronic label processing. The remaining part of the signal is input to a label eraser and 2R regenerator. Replacing the label can in many cases be achieved during wavelength conversion. After setting the new wavelength of the tunable laser and inserting the new label, the orthogonally modulated packet is ready for transmission over the next hop in the network.

Many open issues need to be determined when building such a network. Within the node the delay will depend on the label bit-rate and the electric processing time. This delay, plus the network functionality of contention resolution might call for the need of optical buffering. Also synchronization issues would demand an effective clock recovery circuit within the node. These are interesting topics of research, which are seeing advances in the research community [63], [64], [65], [67], but which fall outside the scope of this thesis.

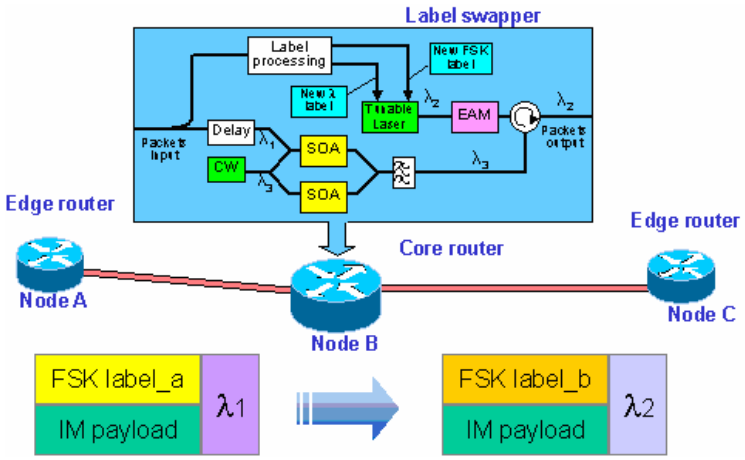

Fig. 1.9. *System architecture for orthogonal IM/FSK labelling.*

With regard to all-optical processing of the labels, the IST-LASAGNE (All-optical label swapping employing optical logic gates in network nodes) research project, aims at designing and implementing a truly all-optical photonic router capable of operating at 40 Gb/s. The employed optical logic gates are all implemented using commercially available SOA-based Mach-Zehnder interferometer (SOA-MZI) as fundamental building blocks [134].

1.3 Thesis structure

The goal for this thesis is to study orthogonal labelling techniques for future IP-over-WDM networks from a systems point of view. Within the project, different types of optical labelling will be compared systematically, in order to identify the strengths and drawbacks of each one, keeping the main focus on orthogonal labelling.

The components included in the experiments are treated in a broad perspective as integrating blocks in a system, leaving room for further optimization of the performance of a particular component. In this way, a proof of concept will be presented for each labelling technique with regard to the different system functionalities. The data that will be analyzed will in most cases be pseudo-random bit sequences (PRBS), while the specific content of the labels and their significance to protocols would be left for upper layers in the telecommunications hierarchy.

Throughout the thesis, the schemes will be mentioned in short by naming the modulation method for the payload first and then the modulation of the label. For example, IM/DPSK would be a scheme in which the payload is intensity modulated (IM) while for the label differential phase shift keying (DPSK) is used. On the other hand, DPSK/IM would be a scheme where the payload information is modulated on the phase of the carrier, while the label would be intensity modulated.

The analysis of the results will in most cases be done through the assessment of bit-error rate (BER) curves. The sensitivity of the system will always be measured for a BER of 1×10^{-9} (occasionally referred to as *error-free* performance) and the power penalty evaluated for the performance at this same BER. For the graphs in which the BER for a specific system is shown as a function of received power, the results are approximated by a linear fit for visualization purposes. The work was be carried out mainly in laboratory experiments, although some results based on numerical simulations (performed on VPI Transmission Maker) will support the analysis.

In chapter two, the generation of orthogonally labelled signals will be presented. Several transmitters and receiver models will be assessed at various bit-rates. Limits to each scheme will be identified, specially concerning the requirements on the sources and the extinction ratio (ER) of the intensity modulated part of the signal. An effective way to overcoming ER limitations for the orthogonally labelled signals through coding techniques, will be proposed and validated. The back-to-back performance of each labelling method will be measured in order to validate the realized transmitter and receiver as well as for comparing the results to later experiments.

The third chapter will investigate the transmission properties of orthogonally labelled signals. Some level of crosstalk between the label and the payload is expected when the orthogonally modulated signal propagates in optical fibres. For instance, phase to intensity modulation conversion induced by chromatic dispersion would result in degradation of the payload data by the label. On the other hand, non-linear effects such as self-phase modulation (SPM) would deteriorate the label data. Although extensively studied for standard ASK systems [55], [66], [101], the effects of these transmission degradations were not known for the orthogonal modulation schemes.

In a WDM context, additional non-linear effects as well as cross-talk should be considered, the impact of which would be related to channel spacing. While the multiplexing and demultiplexing operations, either at the transmitter/receiver or in network elements such as optical cross-connects, would introduce new signal degradation induced by imperfect filtering. This is studied in simulations and experiments in chapter four.

The next two chapters are devoted to the investigation of the most important functionalities in an all-optical network node from a systems point of view, which are wavelength conversion (WC) and label swapping. As will become clear from the discussion, these two subsystems are closely related. Wavelength conversion will be realized in passive and active components. The employed devices will include highly non-linear fibers (HNLF), semiconductor optical amplifiers (SOA) and SOA-MZI wavelength converters. The later will be theoretically investigated with respect to various configuration schemes for 40 Gb/s signals.

During the label erasing and insertion processes, the properties of the labelled signal might be affected. The sixth chapter will present experimental results on label swapping for orthogonal labelling, carrier-suppressed sideband (CSS) labelling and time-serial labelling, identifying in each case the requirements for this functionality. Most of the label-swapping techniques make use of some sort of wavelength conversion, which in many cases establish a limit on the possible output wavelengths to be used. Solutions to this problem are presented while performing label swapping.

The seventh chapter, will collect the knowledge gained throughout the thesis, in order to set-up laboratory prototypes for all-optical labelling systems. Several optical channels will be generated and transmitted, after which a selected channel will be wavelength converted and have its labels swapped, before being re-inserted as a WDM channel for re-transmission. Optical packets will be constructed for a time-serial labelling system. The results will validate the investigated labelling schemes for all-optical networks.

Finally, the thesis will be summarized and conclusions presented.

In the whole of the thesis, most of the lab work was realized in cooperation with Jianfeng Zhang and Nan Chi from Research Center COM, who also collaborated in the numerical investigation of the SOA-MZI wavelength converters.

In the second chapter, the development of the FSK source based on a distributed feed-back (DFB) laser followed by an integrated electro-absorption modulator (EAM) was due to a suggestion by Jianfeng Zhang, who also devised the proposed optical generation of the Manchester codification. The method for generating CSS labelling scheme was developed by Jianfeng Zhang and Nan Chi.

The simulations for the transmission of IM/DPSK labelled signals were performed with the assistance of Birger Carlsson, while the numerical results of transmission, filtering and WDM simulations for IM/FSK signals were obtained in cooperation with Bartłomiej Kozicki. Simulation of wavelength conversion in HNLF were carried out in collaboration with Michael Frosz, all at Research Center COM.

The single SOA used for wavelength conversion was optimized by Lotte Jin Christiansen and Kresten Yvind, while the EAM employed for label swapping was optimized by Lin Xu, all of them from Research Center COM. Both devices were kindly supplied by GIGA-Intel, while the HNLF was made available by Stig Knudsen from OFS Denmark.

The SOA-MZI used in experiments, was kindly borrowed from the COBRA Research Institute, part of the Eindhoven University of Technology (The Netherlands). The experiments related to label swapping of IM/FSK signals were performed in cooperation with Juan-José Vegas Olmos and Idelfonso Tafur Monroy form the COBRA Research Institute.

The GCSR-DBR laser modules used in the WDM transmission experiments, were kindly made available by the Optical Communications Group at the Universitat Politècnica de Catalunya (UPC), in Barcelona (Spain). Victor Polo from UPC assisted in the network experiments related to the IM/FSK labelled signals.

DPSK/IM experiments were carried out in cooperation with Lin Xu, Christophe Peucheret, Christian Mikkelsen, Haiyan Ou and Jorge Seoane, while the method for BER measurement for the packet transmission of IM time-serial labelled signals was suggested by Torger Tokle all of them from Research Center COM.

The performed work was supported by the 5th framework IST-project STOLAS (Switching Technologies for Optically Labelled Signals) and the 6th framework IST-project LASAGNE (All-optical Label Swapping Employing Optical Gates in Network Nodes) which were funded by the European Commission.

Chapter 2

Generation of orthogonally labelled signals

This chapter presents the all-optical orthogonally labelled schemes to be studied in the rest of the thesis. A detailed analysis of the transmitter and receiver needed in each case will be accompanied by considerations on the benefits and drawbacks of each scheme. Back-to-back measurements on the performance of these transmitters and receivers will be presented in each case. The performance will be based on the bit-error rate (BER) values as a function of the incoming power level into the receiver, as well as the sensitivity measured in dBm, for a BER of 10^{-9}.

The first section will investigate the orthogonally combined intensity and phase modulations (IM/DPSK) labelling scheme and introduce an alternative scheme where the modulation of payload and label are interchanged. After that, the IM/FSK scheme will be analyzed and a novel FSK source presented. The third section will examine the carrier-suppressed sideband (CSS) labelling scheme at different bit-rates. Finally, various encoding methods will be studied in order to minimize the limitation on the extinction ratio (ER) of the intensity modulated payload that is shown to limit several of the orthogonal labelling methods.

2.1 IM/DPSK signal generation and detection

This section will describe the theoretical and experimental results concerning IM/DPSK labelling. The principle of the generation of such signals is addressed in the first subsection. First the IM/DPSK scheme will be presented, where the payload is intensity modulated (IM) at 10 Gb/s and the label is differential phase shift keyed (DPSK) at 2.5 Gb/s. The issues on

detection, transmitter optimization and general requirements will be addressed. The theoretical maximum value of the ER of the IM payload will be calculated and requirements to the laser linewidth will be presented. Next, a DPSK/IM scheme is described, based on a 40 Gb/s DPSK payload and a 2.5 Gb/s IM label. In the second section, experimental results on the back-to-back performance of these labelling schemes will be presented.

2.1.1 The IM/DPSK scheme

The IM/DPSK labelling scheme consists of an intensity modulated payload accompanied by a DPSK modulated label on the same carrier and at a lower bit-rate. The two information streams are able to be detected separately, hence becoming an all-optical orthogonally modulated signal. Due to the cross-talk introduced between these two orthogonal channels during transmission and reception, the scheme has some limitations that will be addressed numerically in this subsection.

DPSK generation and detection

The numerical analysis on the IM/DPSK format presented in this subsection is based on an intensity modulated payload at 10 Gb/s accompanied by a DPSK modulated label at 2.5 Gb/s. The IM would be realized in an intensity modulator, such as a Mach-Zehnder modulator (MZM) and be detected directly by a photodiode [68]. The DPSK transmitter and receiver are shown in fig. 2.1. A laser output continuous wave (CW) is modulated by a phase modulator, which is driven by differential encoded electrical data. This differential encoding is necessary in order to generate the DPSK signal. The benefits of this differential encoded signal is mainly that the local oscillator, that a coherent light system would require, is avoided and the optical carrier only needs to be stable with regard to phase during the duration of 2 bits [69].

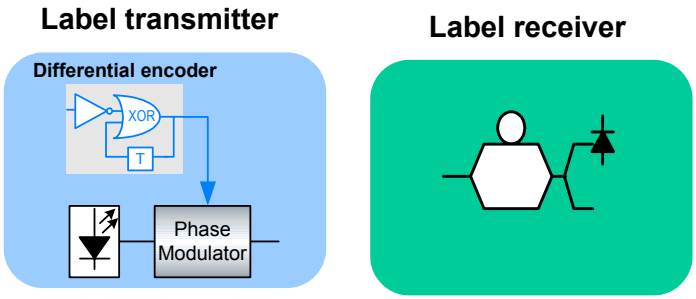

Fig. 2.1. *DPSK label (a) transmitter and (b) receiver.*

The differential encoding of the data stream is achieved by performing an XOR operation between the incoming bit and the previous bit of the encoded signal [70]. Fig. 2.2 (a) shows the truth table of the XOR operation. The phase modulator will then shift the phase of the carrier by π every time an encoded mark bit has to be transmitted. Fig. 2.2 (b) presents an example of this type of encoding. The upper row shows an example of a data stream, while the middle row shows the result of the XOR operation between a given bit and the previous one. This differential XOR operation is then translated into a π phase shift in the carrier whenever the differential XOR operation results in a '1', while leaving the phase untouched when the differential XOR operation results in a '0', thus producing the DPSK modulation.

d1	d2	XOR
0	0	0
0	1	1
1	0	1
1	1	0

(a)

data	1	1	0	1	0	0	1	0
differential	1	0	0	1	1	1	0	0
DPSK	π	0	0	π	π	π	0	0

(b)

Fig. 2.2. *(a) XOR truth table and (b) example of differential encoding for DPSK signals.*

In fact, when using pseudo-random bit sequences (PRBS) as the transmitted signal the first stage for the differential encoding can be avoided. A proof thereof is presented in Appendix A, where it is shown that the XOR operation with a one-bit delay of a PRBS signal gives as a result the same PRBS signal with a certain delay. For this reason the XOR operation will be avoided in all the experimental set-ups presented throughout this thesis.

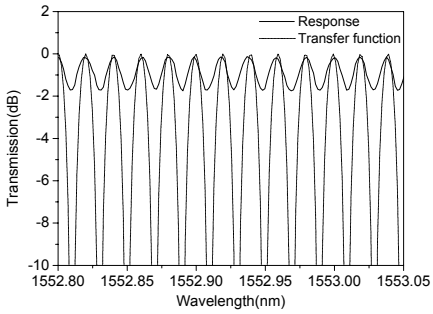

Fig. 2.3 *Measured transfer function of the 1-bit Mach-Zehnder interferometer.*

At the receiver side, a Mach-Zehnder interferometer (MZI) with a delay in one arm corresponding to the duration of one bit, can be used for the DPSK demodulation [60]. Obviously, the length of the delay has to match the data

speed of the signal. For example, for a 2.5 Gb/s DPSK signal the interferometer needs to have a difference in arm-lengths of 8 cm. In fig. 2.1 (b), such a one-bit delay MZI is used as a single arm receiver. A dual arm receiver can also be implemented if needed for enhancing the receiver sensitivity. Fig. 2.3 shows the measured transfer function of the one-bit delay MZI used in experiments as demodulator. When the signal crosses the interferometer, one arm delays the signal one bit relative to the other arm. When the signal is recombined at the output, a π difference in phase makes the signals interfere destructively and no signal is present at the output. If there is no phase difference between the two adjacent bits, the signals interfere constructively and a 1 would be present at the output. In this way, the DPSK signal has been converted into an intensity modulated signal and the differential codification has been removed. This signal can then be detected by a photodetector with the appropriate bandwidth.

Limitation on the payload extinction ratio

As mentioned earlier, in order to detect the label, a limited extinction ratio of the payload is required. An IM/DPSK modulated signal with a finite extinction ratio can be expressed in equation (1.1) [49],

$$S(t)=\sum_{n=-\infty}^{\infty}\left\{\sum_{m=1}^{4}\left[\varepsilon+(1-\varepsilon)q_{p,4n+m}g_p\left(t-(4n+m)T_p\right)\right]^{\frac{1}{2}}\cdot\exp\left[i\cdot\pi\cdot(1-q_{l,n})g_l(t-nT_l)\right]\right\} \tag{1.1}$$

where *p, l* and *q* stand for the payload, the label and the data sequence, respectively, *T* is the bit period and *g* the pulse shape. The extinction ratio of the payload expressed in dB is given by -10 log(ε). The output power of the one-bit delay demodulator can be expressed as,

$$P_{out,n}=\frac{P_n}{4}+\frac{P_{n-1}}{4}-\frac{1}{2}\sqrt{P_nP_{n-1}}\cos(\phi_n-\phi_{n-1}) \tag{1.2}$$

where *P* is the optical power, ϕ is the phase of the input field and the mark *n* denotes the *n*th label bit. Assuming the pulse shape of the label to be square, and a label bit rate of 2.5 Gb/s, five distinct power levels can be obtained at the output of the label demodulator. These power levels depend on the different possibilities for the payload data and label data, as shown in fig. 2.4. The corresponding values of these five levels are given in Table 2.1.

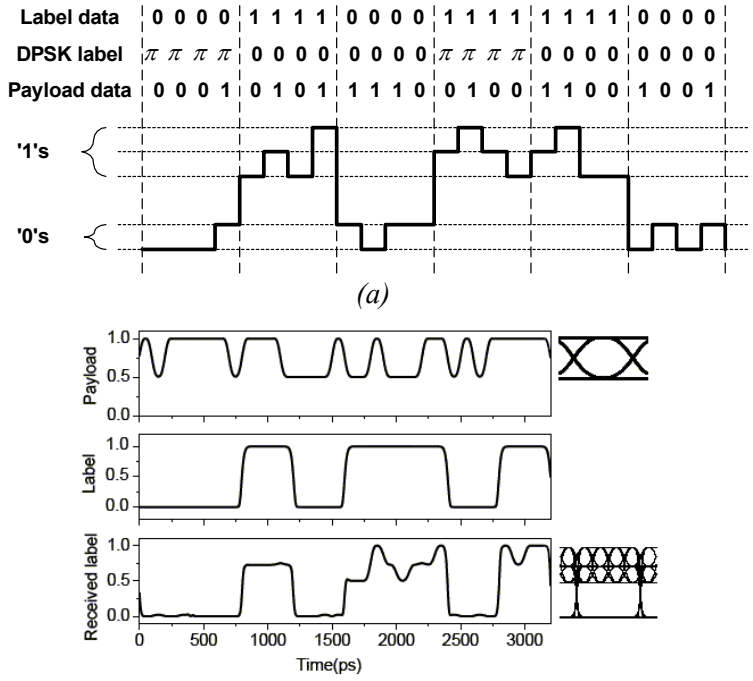

Fig. 2.4. *Multi-level structure of the demodulated DPSK labelled signal. (a) Theoretical analysis, (b) simulation results.*

From Table 2.1, the minimum eye opening of this multi-level label eye diagram can be derived. This minimum eye opening has the form (5ε-1)/4. Fig. 2.5 shows the received label eye opening as a function of the payload extinction ratio assuming ideally square pulses and in the absence of filtering, with the multilevel eye diagram as an inset. From this figure, it can be observed that, in order to obtain an open label eye, the extinction ratio of the payload must be no larger than 9.5 dB, thus setting a clear limit to the characteristics of the generated signal.

Table 2.1. *Power of the label after DPSK demodulation for different combinations of the payload data and label data.*

Label $q_{l,n}$	Payload $q_{p,4n}$, $q_{p,4(n+1)}$	Peak output power of label	Output power of label
1	1, 1	1	$g_p(t)$
	1, 0 and 0, 1	$\frac{1+3\varepsilon}{4}$	$\frac{g_p(t)}{4}+\frac{\varepsilon}{4}+\frac{\varepsilon\sqrt{g_p(t)}}{2}$
	0, 0	ε	ε
0	0, 1 and 1, 0	$\frac{1-\varepsilon}{4}$	$\frac{g_p(t)}{4}+\frac{\varepsilon}{4}-\frac{\varepsilon\sqrt{g_p(t)}}{2}$
	1, 1 and 0, 0	0	0

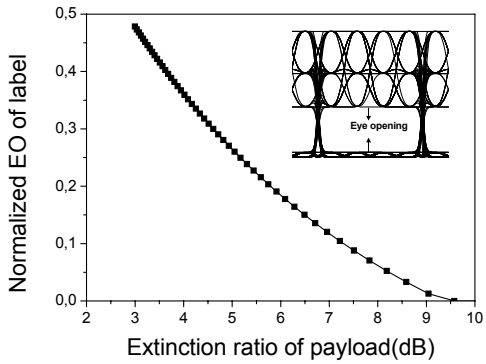

Fig. 2.5. *Received label eye opening normalized by the peak power of the demodulated label versus payload ER. The inset shows the multi-level eye diagram of the detected label.*

This analytical and numerical result was later observed in experiments. Fig. 2.6 shows an example of this multilevel effect at the receiver after a transmission over 50 km of single mode fiber (SMF), for a 10 Gb/s IM payload and a 2.5 Gb/s modulated label. The multilevel nature of the signal and interference of several payload bits for each label bit are clearly observable.

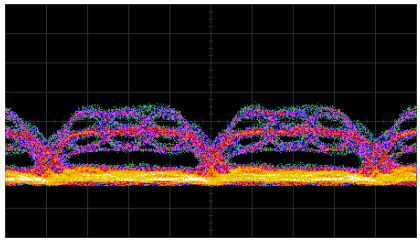

Fig. 2.6. *Example of the experimental validation of the multilevel signal received after transmitting a IM/DPSK modulated signal.*

This trade off between the ER of the payload and label is also clearly observed in fig. 2.7, that shows the simulation results of the receiver sensitivity defined for a BER of 10^{-9} vs. the extinction ratio of the payload for a label receiver respectively. The performance of the label would be enhanced by about 3 dB if a balanced receiver was to be used instead of a simple one [68], so a higher ER would be tolerable.

The choice of the optimum point of operation with regard to the IM payload ER, should take into account that an error in a label bit could lead to the whole packet being sent to a wrong address. The label performance is

therefore more critical than the performance of the payload. In that sense, the trade-off could be set to favour the label receiver to reduce this risk. An ER of the payload of less than 3 dB would then be preferred in order to enhance the receiver sensitivity of the label with regard to that of the payload.

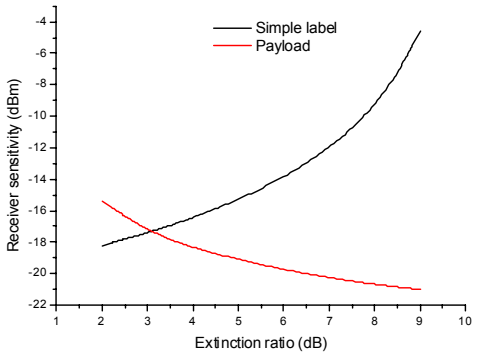

Fig. 2.7. *Receiver sensitivity vs. extinction ratio of the payload.*

Requirements to the laser linewidth

For a DPSK modulated label, the laser phase noise can have a important impact on performance [71], [69]. Fig. 2.8 shows simulation results on the influence of the laser linewidth at different label bit rates for a 10 Gb/s IM payload with an extinction ratio of 3 dB after transmission over 50 km of compensated SMF. The laser model contained a Gaussian white noise source with a variance of $2\pi\Delta f$ corresponding to the optical laser linewidth Δf. When the laser linewidth was increased from 0 to 4% of the label bit rate, the label receiver penalty at first showed a linear increase from 0 dB to 3 dB. If the laser linewidth was further increased, detection of the label became impractical.

The penalty shows a linear behaviour up to a laser linewidth of about 6.25 MHz for a 156.25 Mb/s label, and of about 100 MHz for a 2.5 Gb/s label. Defining the acceptable receiver power penalty of the label to be within 1 dB, then a linewidth requirement of less than 1.5% of the label bit rate should be applied. Considering a label-bit rate at 2.5 Gb/s, a laser with linewidth of less than 37.5 MHz would then be necessary, while a label bit-rate of 156 Mb/s would require a linewidth of 2.34 MHz, which, although achievable, would be a demanding feature for commercially available laser sources [72].

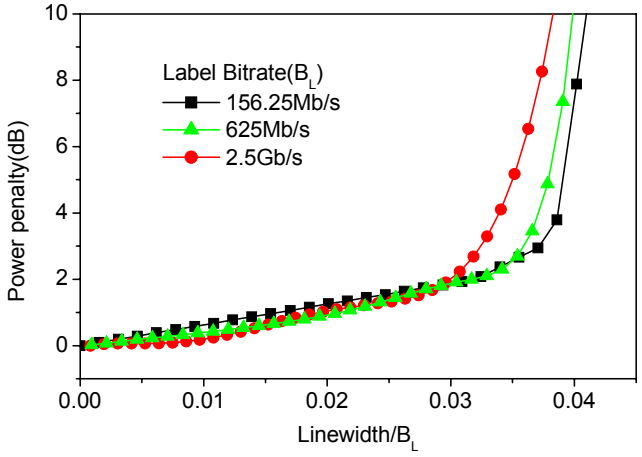

Fig. 2.8. *Simulated results of power penalty versus laser linewidth normalized to the label bit-rate for a 3 dB payload ER at different label bit rates.*

2.1.2 Back-to-back performance

The foregoing analysis on the IM/DPSK format was validated experimentally by measuring the back-to-back performance of transmitter and receiver. As explained in the introduction, one of the advantages of the orthogonal labelling scheme is that the bit-rate of the payload can be upgraded without having to change the label detection at each node. The performance will therefore be compared for payloads at 10 Gb/s and 40 Gb/s, while keeping the label bit-rate fixed at 2.5 Gb/s. After that, an alternative labelling scheme making use of the DPSK modulation will be introduced.

IM/DPSK signals at 10 / 2.5 Gb/s

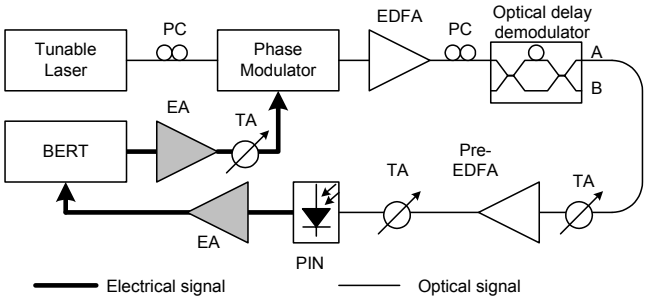

Fig. 2.9. *DPSK back-to-back experimental setup.*

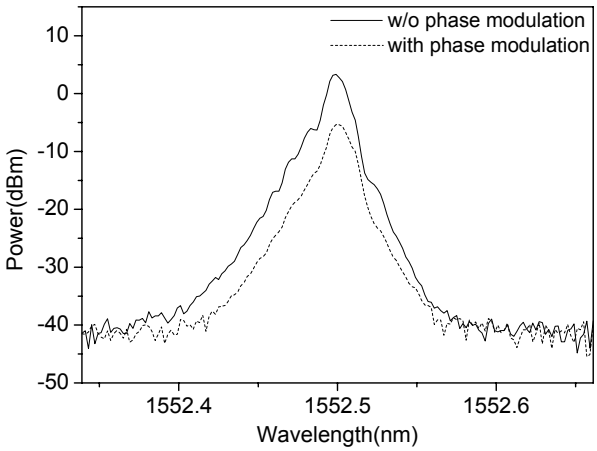

Fig. 2.10. *Measured optical spectra for the laser output with and without DPSK modulation.*

To begin with, the performance of the DPSK transmitter used in further experiments was assessed through the setup shown in fig. 2.9. The DPSK signal was generated by modulating a CW source through a phase modulator. The output power of the laser was set to 4 dBm. The electrical 2.5 Gb/s data was a PRBS of 2^9-1 length, which allowed for omitting the XOR differential encoding at the transmitter, as explained in Appendix A. Fig. 2.10 shows the measured optical spectra of the CW light compared to that of the DPSK

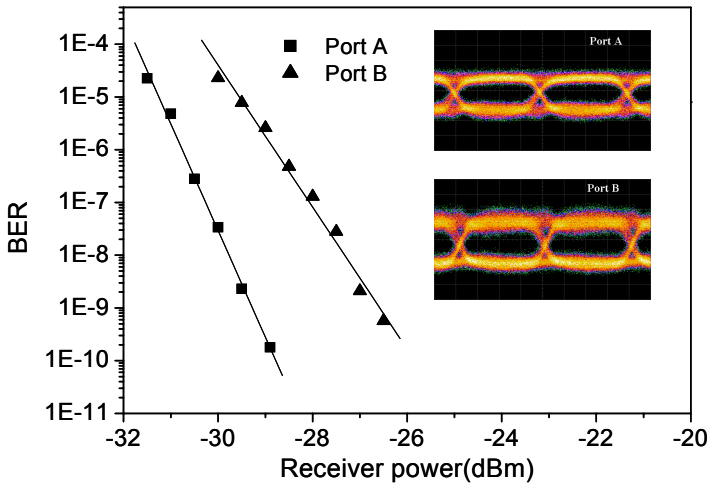

Fig. 2.11. *Measured BER curves and eye diagrams of the DPSK signal.*

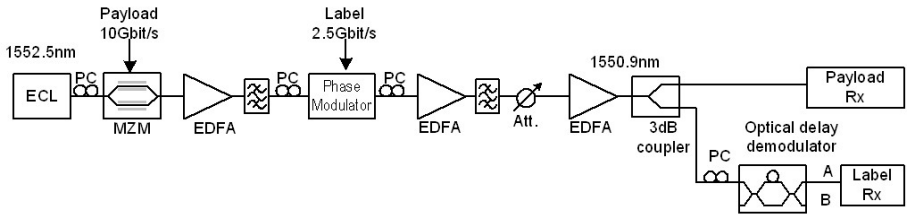

Fig. 2.12 *Experimental setup for the back-to-back performance of a IM/DPSK modulated signal.*

signal. The demodulated eye diagrams at each output port of the MZI, and the BER performance are shown in fig. 2.11. Both outputs of the delay interferometer receiver could be detected with a BER of less than 10^{-9}, although the constructive output of the interferometer showed a sensitivity that was about 2 dB better than the destructive output. The reason for this is believed to be the imperfections in the coupling ratio of the couplers involved in the interferometer. The sensitivity of the constructive output was found to be -29.5 dBm.

The next step was to add a 10 Gb/s IM payload to this 2.5 Gb/s DPSK label. The experimental setup for measuring this back-to-back performance is shown in fig. 2.12. The signal source was a wavelength tunable external cavity laser (ECL) working at 1552.5 nm. The signal was first intensity modulated at 10 Gb/s with a PRBS (2^7-1), by a Mach-Zehnder modulator. The DPSK label at 2.5 Gb/s was then impressed by the phase modulator. At the receiver, the signal was split equally in order to detect the payload and label separately.

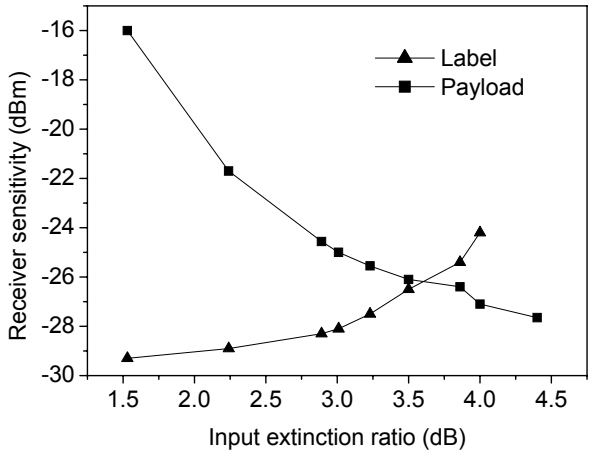

Fig. 2.13 *Measured back-to-back receiver sensitivity vs. payload extinction ratio for the label and the payload.*

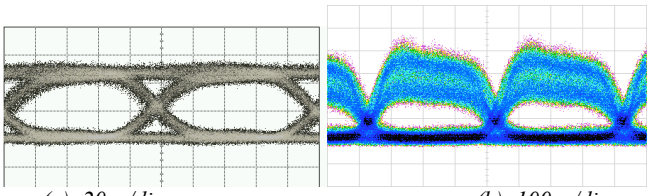

(a) 20ps/div *(b) 100ps/div*

Fig. 2.14. *Eye diagrams for (a) back-to-back payload at 10 Gb/s, (b) back-to-back label at 2.5 Gb/s.*

In order to find the optimum extinction ratio of the IM payload, this parameter was varied while keeping the rest of the system untouched. The measured receiver sensitivities for a BER of 10^{-9} for the payload and the label as a function of the extinction ratio are shown in fig. 2.13. As expected, a trade off between the intensity extinction ratio requirements for the payload and the label was observed. A degraded IM extinction ratio would result in penalty for the payload, whereas the extinction ratio should not be too large in order to recover the phase modulated label. In the experimental setup, the ER of the payload should be around 3.5 dB, in order to detect the payload and label with similar sensitivities. Because of the greater importance of the label information, it could also be chosen to enhance the performance of the label by reducing the payload extinction ratio further.

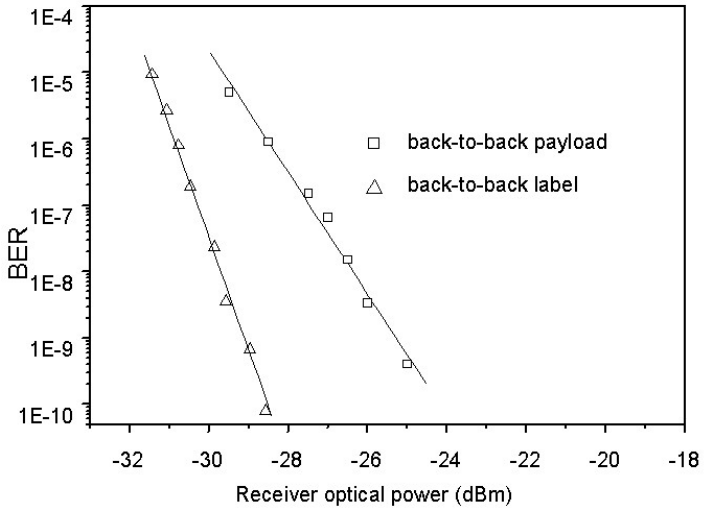

Fig. 2.15. *Measured BER performance for the back-to-back case of a IM/DPSK signal with a payload ER of 3 dB.*

The eye diagrams for the received back-to-back signals are shown in fig. 2.14, where the received label multi-level structure is observable. Fig. 2.15 shows the BER curves for the payload and label in the back-to-back

case with a payload ER of 3 dB. Both curves could be chosen to be shifted in opposite directions by changing the ER of the IM payload. For the chosen ER, the sensitivity of the payload and label was found to be -25 and -29 dBm respectively, which is in concordance with the results shown in fig. 2.13.

IM/DPSK signals at 40 / 2.5 Gb/s

As mentioned earlier, one of the advantages of orthogonal labelling is the possibility of changing the bit-rate of the payload independently of the one of the label. In order to confirm this, a back-to-back experiment was setup where the IM payload was modulated at 40 Gb/s while the DPSK label was kept at 2.5 Gb/s.

As shown in [73], the system performance shows an improvement with increasing values of the ratio between the payload and label bit rate, which means that if the label bit rate is fixed, increasing the payload bit rate will improve the DPSK detection. Hence, upgrading the payload capacity will improve the label performance. Alternatively, if the payload bit rate is fixed, a lower speed DPSK label would show a better performance, although the requirements on the laser linewidth would be more stringent.

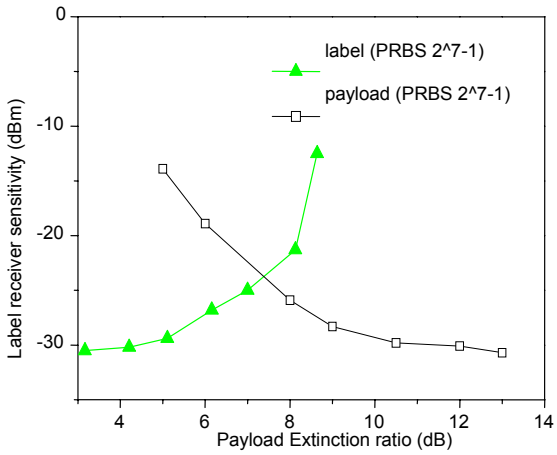

Fig. 2.16. *Measured receiver sensitivity for the payload and label vs. input extinction ratio of the payload for a payload bit-rate of 40 Gb/s and a label bit-rate of 2.5Gb/s.*

The measured receiver sensitivities of the payload and the label as a function of the extinction ratio (ER) are shown in fig. 2.16. As expected, a trade off between the ER requirements for the payload and label is observed. For a payload coded with a 2^7-1 PRBS sequence, an optimum value of 7 dB ER is now obtained where the payload and label have the same sensitivity. This

increase of the optimum value of the ER of the IM payload is due to the difference in bit-rate compared to the previous results. Furthermore, it was observed that this optimum value could be decreased when a longer PRBS sequence were used for the payload due to the increased length of the continuous 'mark's and 'space's. It was also found that the DPSK receiver sensitivity would be greatly enhanced at lower label rates. This conclusion is consistent with the theoretical results given in [74].

DPSK/IM scheme at 40 / 2.5 Gb/s

Alternatively to the IM/DPSK labelling method discussed so far, the modulation format of payload and label could be interchanged. In this sub-section the back-to-back performances of a 40 Gb/s DPSK payload and a 2.5 Gb/s IM label are presented. The benefits of this modulation scheme are that the DPSK modulation at high speed shows good transmission properties, the delay interferometer will be more stable as its difference in arms will be smaller, and that a balanced detection would improve the performance even under IM power fluctuations [75], [76]. On the other hand, the detection of the DPSK payload needs at all times the erasure of the IM label, which can only be done by detecting the label data stream first – as shall be described in Section 6.1.5 – which will bring synchronization issues to the receiver.

The experimental setup is shown in fig. 2.17. The RZ-DPSK generator consisted of an external-cavity laser at operating at 1550 nm, an external dual-drive Mach-Zehnder modulator and a phase modulator. The first modulator generated a 40 GHz RZ pulse by being biased at the peak of its transmission curve and differentially driven at twice the switching voltage with an ac-coupled half-bit-rate (20 GHz) sine wave. The phase modulator was driven by a 40 Gb/s (PRBS 2^{23}-1) NRZ data stream. A tunable optical delay line was inserted in between the two modulators to synchronize the pulse train and the 40 Gb/s data source. The IM label information at 2.5 Gb/s (PRBS 2^{7}-1) was added by a following EAM, thus producing an optically RZ-DPSK/IM labelled signal. An advantage of using the EAM for label insertion was found to be its negligible frequency chirp [78].

Similar to the IM/DPSK modulation, the receiver sensitivity of the IM label was found to improve as the IM extinction ratio was increased, while the sensitivity of the RZ-DPSK payload deteriorated due to the reduced signal power during a '0' IM transmission, which closes the demodulated DPSK eye-diagram. In this experiment an ER of 3 dB was selected for the extinction ratio of the IM label.

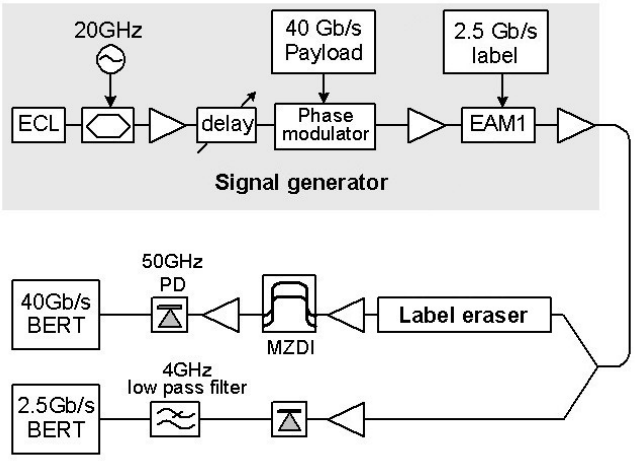

Fig. 2.17. *Experimental setup for a 40 Gb/s RZ-DPSK payload and a 2.5 Gb/s IM label.*

At the receiver, the labelled signal was divided using a 3 dB optical splitter. The output of one arm was directly detected by a photodiode and thus the optical label was converted into the electrical domain. The other arm underwent an optional label erasure process that will be discussed in Section 6.1.5 in order to optimize the payload receiver. The payload was then input to an integrated Mach-Zehnder delay interferometer (MZDI) – which was a prototype produced by C. Mikkelsen and H. Ou at Research Center COM – used to demodulate the RZ-DPSK signal. The length difference between the two arms of the MZDI was 5.049 mm, corresponding to a 25 ps delay. The signal at the output of the MZDI was detected by a 50 GHz photodiode and input into a 40 Gb/s BER test set.

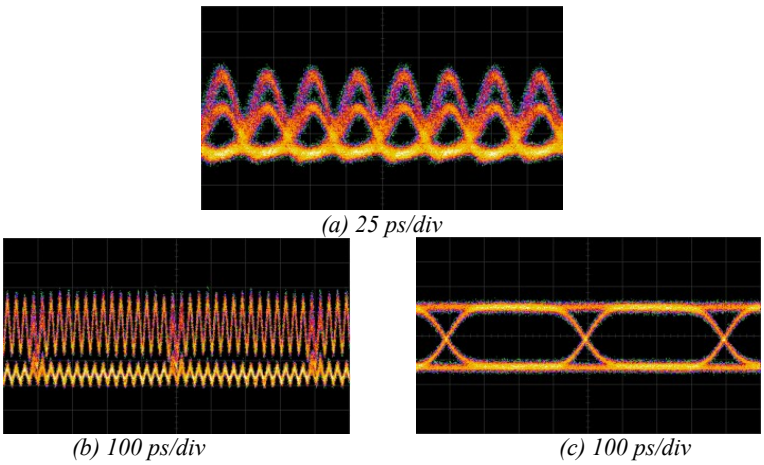

(a) 25 ps/div

(b) 100 ps/div *(c) 100 ps/div*

Fig. 2.18. *Eye diagrams for (a) payload without label erasure, (b) label before the low-pass filter, (c) label after the low-pass filter.*

The detected RZ-DPSK eye-diagram without label erasure is shown in fig. 2.18 (a). Obviously, due to the intensity crosstalk from the IM label, the demodulated RZ-DPSK payload eye-diagram presented a multi-level structure, which is why the label erasure process benefits the payload detection. The detected IM label eye diagrams are shown in figs. 2.18 (b) and (c). It is worth noting in fig. 2.18 (b), that the residual payload intensity was superimposed onto the label. Therefore a 4 GHz low-pass electrical filter was applied after the photodiode in order to remove the 20 GHz RZ pulses. In this way, a very clear and open 2.5 Gb/s label eye-diagram could be obtained, as shown in fig. 2.18 (c).

Fig. 2.19 shows the BER curves in the back-to-back case. The DPSK payload showed a sensitivity of -25 dBm, while the IM label had a B2B sensitivity of -32 dBm, which again could be modified by changing the ER of the IM.

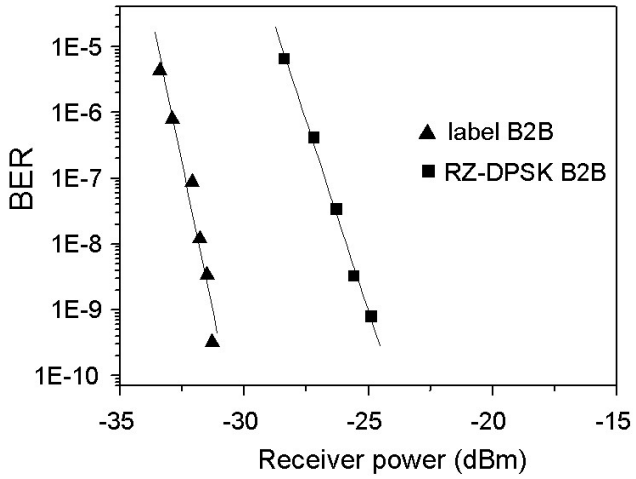

Fig. 2.19. *Measured BER results for the payload and label in the DPSK/IM labelling scheme.*

2.2 IM/FSK signal generation and detection

The IM/FSK scheme for orthogonal optical labelling, is based on an intensity modulated (IM) payload and a frequency shift keyed (FSK) label. The frequency modulation would assign a different frequency to the ‘mark’ and ‘space’ bits of the label pattern. For the scheme to work effectively, the FSK source should present a stable output with regard to intensity and the IM modulation should introduce no frequency chirp. These issues, along with possible solutions, will be investigated in the present sub-section.

2.2.1 FSK generation

In an IM/FSK label switched network, an optical FSK transmitter is necessary in both edge nodes and core nodes [16], [47]. As will be shown, the optical FSK transmitter plays an essential role in the performance of optical IM/FSK labelling. Ideally, the label information should be impressed upon the optical carrier's frequency through FSK modulation, while keeping its amplitude unaffected. On a second stage in the transmitter, the payload information would then be modulated on the carrier's amplitude. The experiments described in this section are mainly based on the definition of packets for the STOLAS concept [48], where the optical labelled signal would consist of an intensity modulated (IM) payload at 10 Gb/s and a frequency modulated (FSK) label at 312 Mb/s, with a tone-spacing of 20 GHz.

Three methods for FSK generation will be described: a scheme using two external-cavity lasers (ECL), a novel scheme using a directly modulated distributed feedback (DFB) laser and an electro absorption modulator (EAM), and finally a scheme using a grating assisted coupler sampled reflector (GCSR) laser source.

Using two tunable ECLs

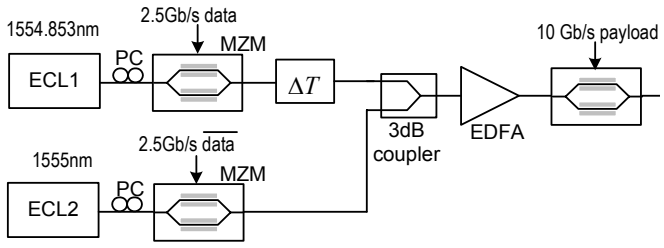

Fig. 2.20. *FSK generation based on two ECLs.*

Two lasers with different optical frequencies can be used to perform the FSK modulation. In this scheme, the two lasers' frequencies act as the FSK tones, while being intensity modulated by the conjugate data sources before being coupled together to form one FSK source. In this way, the label information can be impressed upon the frequency of the coupled light, while careful matching of the sources would keep the optical intensity constant, thus achieving FSK modulation.

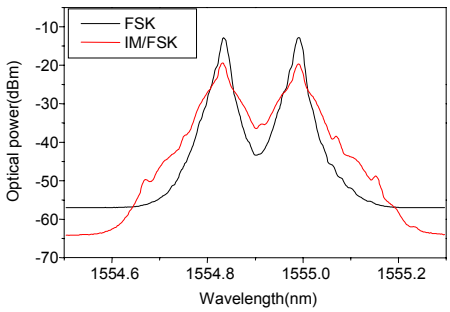

Fig. 2.21. *Optical spectra of the pure FSK signal and combined IM/FSK signal.*

In the setup shown in fig. 2.20, two tunable external-cavity-lasers (ECL), the frequencies of which were detuned by 20 GHz, were used to perform the FSK modulation. Before being coupled into one fiber, the two light beams were modulated by conjugate data at 2.5 Gb/s. The coupled light was then modulated by an intensity modulator operating at 10 Gb/s. Fig. 2.21 shows the optical spectra of the lightwave after FSK modulation and IM/FSK modulation respectively. Fig. 2.22 (a) shows the intensity waveform of the two sources before coupling. It is noticeable that the imperfect waveform match produces intensity ripples in the coupled light, which can be observed in fig. 2.22 (b).

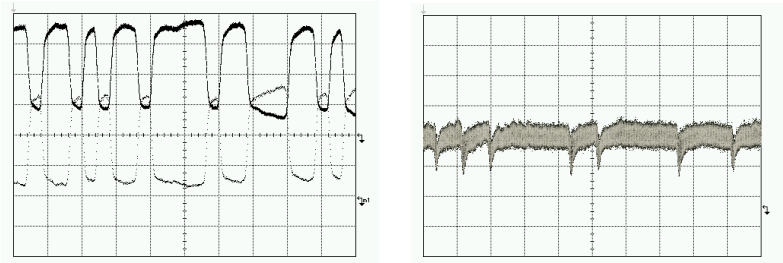

(a) *(b)*

Fig. 2.22. *(a) Wave pattern of the two ECL sources, and (b) coupled FSK intensity waveform.*

When no IM payload was added on the FSK modulation, the label could be detected satisfactorily. Fig. 2.23 shows the optical spectra of the generated FSK signal, the fiber Bragg grating used to filter out one of the FSK tones and the filtered signal suitable for direct detection. Fig. 2.24 shows the BER performance obtained through this method and an eye-diagram of the demodulated signal. The measured receiver sensitivity at a BER of 10^{-9} was -34.9 dBm.

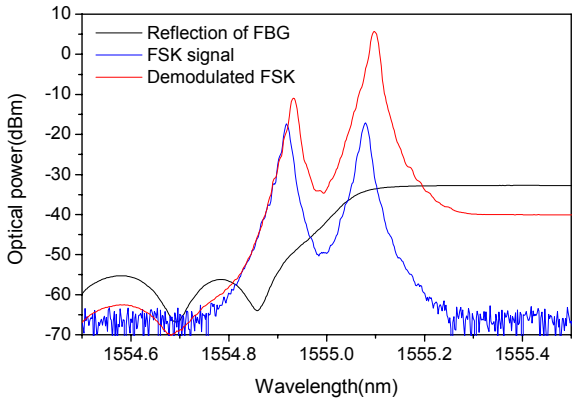

Fig.2.23. *Optical spectra of the reflection of the fiber Bragg grating, FSK signal and the demodulated FSK signal.*

However, when the IM modulation was added, the 10 Gb/s IM payload and 2.5 Gb/s FSK label could not be detected error-free simultaneously due to the intensity ripples observed in fig. 2.22 (b). In the experiment, the modulator impressing the payload information was polarization sensitive, which further aggravated the intensity ripples of the coupled light. It is expected that a tighter polarization control of the two sources before the coupler would improve the modulation performance.

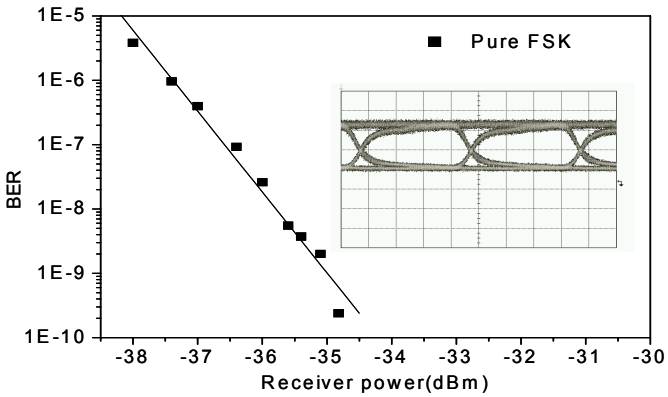

Fig. 2.24. *Measured BER curve and the eye diagram of the pure FSK signal.*

As shown in fig. 2.25 (b), an IM payload with a sufficiently high extinction ratio showed an acceptable tolerance to the intensity ripple to be detected. However, in this case, the FSK label had a much degraded receiver performance. When the IM payload was operated at 2.5 Gb/s, both the IM payload and FSK label could be detected with a BER of less than 10^{-9}, due to

a less demanding requirement on the matching of the ripple, as shown in fig. 2.25 (a).

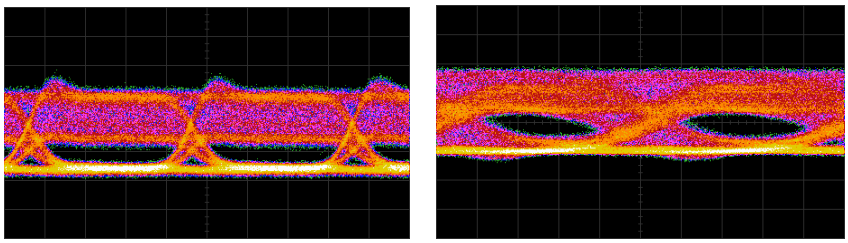

(a) *(b)*

Fig. 2.25. *(a) Payload at 2.5 Gb/s, simultaneously error-free detection of both payload and label (b) Payload at 10 Gb/s, no simultaneously error-free detection.*

Using DFB/EAM modules

In order to reduce the intensity ripples encountered in the last section, a new FSK source was designed and presented in [79]. The method is based on the fact that an optical FSK signal can be generated simply by directly modulating the electrical current of a DFB or DBR laser diode [80]. However, the drive current variation also results in a simultaneous intensity modulation of the emitted light [53]. Such residual intensity modulation has a detrimental effect on the optical signal when the IM payload information is added. To overcome this problem, a novel optical FSK label generation scheme is proposed, based on a commercially available integrated DFB laser/electroabsorption modulator (EAM).

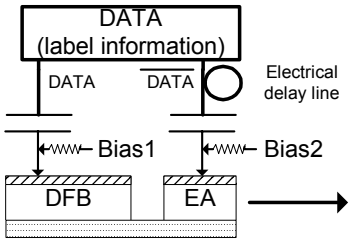

Fig. 2.26. *Configuration of the optical FSK transmitter.*

The configuration of the proposed optical FSK transmitter is shown in fig. 2.26. The DFB laser was driven with a bias current above threshold and a relatively small modulation current. The current modulation resulted in both intensity and frequency modulation of the output light. To remove the intensity variation of the laser's output, the inverse electrical data was injected into the integrated EAM with an appropriate time delay and modulation voltage. In this way, a constant amplitude optical FSK signal was generated. In reported experiments [26], the input current had to be kept at a

small value to minimize the residual IM, which also resulted in a small FSK tone spacing, thus a coherent detection scheme had to be employed.

The measured optical characteristics of the DFB laser and EAM are shown in fig. 2.27. The variation of injection current changed both output power and wavelength, as indicated in fig. 2.27 (a). In the high bias current regime, a modulation current of nearly 30 mA was needed to achieve a 20 GHz (~0.16 nm) frequency deviation, which was accompanied by a 3 dB intensity variation. The integrated EAM showed a modulation efficiency of nearly 5 dB/V, as shown in fig. 2.27 (b).

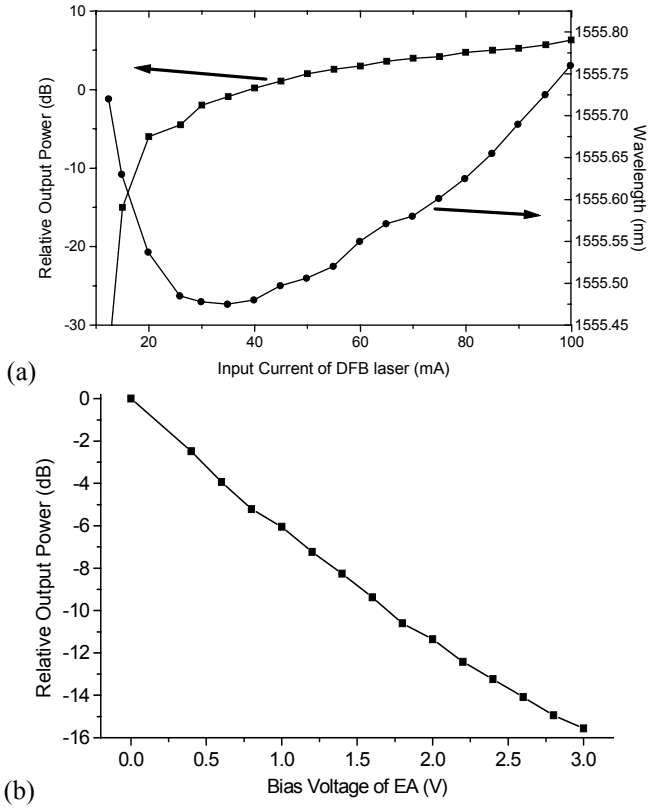

Fig. 2.27. *Optical characteristics of (a) DFB laser and (b) EAM.*

Both the measured DFB laser and the EAM had a 3 dB modulation bandwidth of 2.5 GHz. Figs. 2.28 and 2.29 show respectively the measured eye-diagrams and optical spectrum of the FSK modulated signal when the DFB laser was driven with a 90 mA bias current and a 30 mA modulation current at 1 Gb/s. Without intensity compensation, nearly 3 dB of intensity fluctuation was observed, as shown in fig. 2.28 (a). After optimizing the bias and modulation voltage of the EAM, the final output light had almost constant amplitude, as shown in fig. 2.28 (b). Thus, an FSK signal with a

peak-to-peak frequency deviation of 20 GHz was finally generated, as indicated by the spectrum of fig. 2.29. It can also be noted from this spectrum, that the direct modulation generated two asymmetric optical tones, indicating that the generated FSK signal was accompanied by a residual intensity modulation. After compensating for the residual intensity fluctuation, a symmetrical FSK spectrum around 1555 nm could be obtained.

The payload information at 10 Gb/s (PRBS 2^9-1) was then added by a following Mach-Zehnder modulator (MZM), thus producing an optically IM/FSK labelled signal.

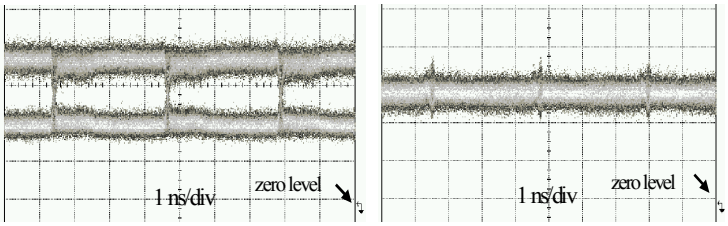

(a) *(b)*

Fig. 2.28. *(a) Eye-diagram of the residual intensity modulation after direct modulation of the DFB laser (b) eye-diagram after EAM compensation*

Just as in the IM/DPSK case, a limited IM extinction ratio was necessary for the FSK label detection, but a too low ER would in turn deteriorate the payload detection. Therefore, a compromise value had to be selected for the extinction ratio of the IM payload in the IM/FSK scheme.

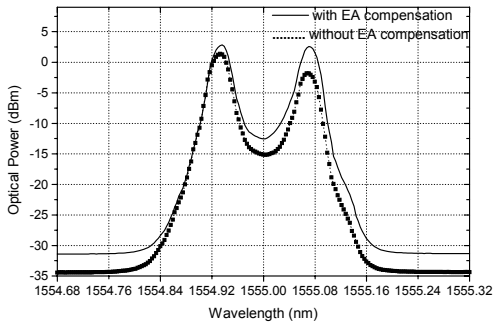

Fig.2.29. *Optical spectrum before/after EAM compensation*

In fig. 2.28 (b) it can be observed that this method, unfortunately was only able to partly compensate for the amplitude modulation inserted by the DFB laser. The rising edge of the intensity DFB modulation and the falling edge of the EAM did not exactly match, thus leaving a small ripple in the intensity of the FSK modulated signal. This ripple was not a problem for receiving the FSK label, but it was a detrimental when adding the IM payload on top of it. The ripple was small compared with the 312 Mb/s signal, but became quite

large (comparable with a whole bit period) when treating the 10 Gb/s IM payload signal. This meant that one every 32 eyes in the pattern became quite degraded and thus imposed a limit on the BER performance of the system. This problem could be accounted for partially by carefully synchronizing the two data streams, so that the top of the ripple occurred during the transition between two payload bits, thus minimizing its influence.

It should be noted that the laser used in the experiments was relatively old but worked satisfactorily in the mentioned scheme, except for the ripple. Some newer DFB lasers were tried, but they proved not to be useful for this way of operation because they clearly were not designed for this type of usage and then both the EAM and the DFB responses where impossible to match.

Using GCSR lasers

Single grating assisted coupler sampled reflector (GCSR) laser sources could represent a key component for the core node router design of IM/FSK labelled networks such as the STOLAS architecture, due to their agile wavelength tunability [81]. This tuneable laser is able to emit at 41 different channels, from 1529.55 to 1561.42 nm with a channel spacing of 100 GHz [82]. A GCSR laser consists of four sections, i.e. a gain block, a phase module, a coupler and a Bragg grating. The coupler acts as a coarse tuner, transferring power vertically between the two waveguides – one that runs forward to the gain block, and another one, above it, that runs backward into the phase and Bragg grating sections. The phase section is usually used for fine wavelength tuning, and can also be used for FSK modulation [83]. The structure and configuration of a GCSR laser is shown in fig. 2.30. Further analysis on device fabrication, tuning mechanisms, and performance of these lasers has been described in [57].

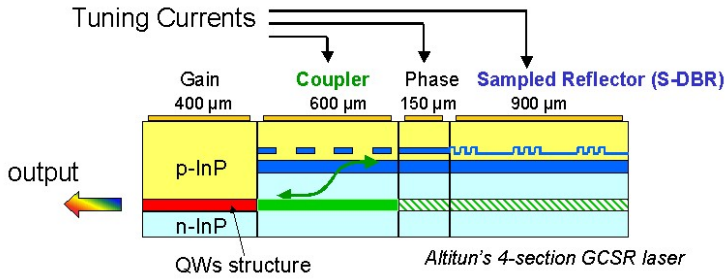

Fig. 2.30. *GCSR internal scheme. (Figure from [84]).*

Generation of FSK signals was investigated by using this type of laser, injecting directly the data flow into the phase section. A bias current was necessary in order to fit the working point of this section. The magnitude of the frequency deviation of the generated FSK signal was shown to be

dependent on the current applied to the phase section. Frequency deviation values up to 40 GHz were measured by applying a current not exceeding the maximum tolerable value of 10 mA, although performance was greatly dependent on the selected wavelength. For the experiments reported here, a frequency deviation of 20 GHz was selected.

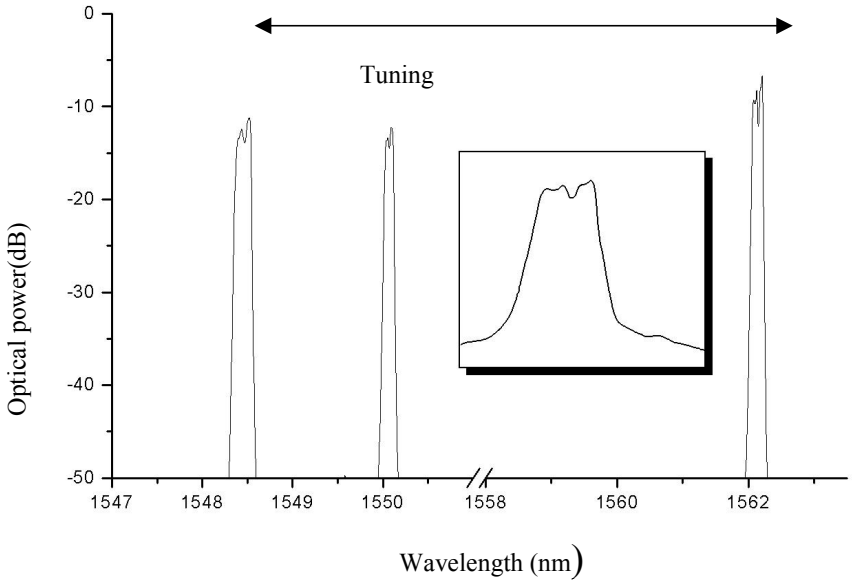

Fig. 2.31. *Wavelength-tunable FSK signal generation. The inset shows the poor FSK generation at specific wavelengths.*

Fig. 2.31 shows the measured optical spectrum of several channels while applying FSK modulation. From the figure, it can be observed that the GCSR lasers used in the experiments could be tuned over 32 nm in the 1529-1561 nm range. The inset shows the detailed measured spectral structure of the generated FSK signal, which was greatly dependent on the selected channel. As will be evident in later sections, the combination of channels needed for the experiments (especially when generating WDM IM/FSK signals) was unfortunately so that several times a much degraded FSK spectrum was obtained.

2.2.2 IM/FSK detection

For the direct detection of the FSK label, it is important that one of the tones in the FSK signal be sufficiently suppressed so that, even with the interference of the IM payload, it would still allow for correct detection. The filter used for the FSK detection, therefore, had to show a sufficiently high suppression ratio and at the same time have an edge that was sharp enough to distinguish between the two FSK tones.

Two schemes of detection were investigated. The first one applying an FBG based optical add-drop multiplexer (OADM), which showed an acceptable performance with regard to suppression and sharpness, but had the disadvantage of not being tunable amongst the different channels. The second scheme employed two cascaded filters, the first one of which was a tunable Fabry-Perot filter (FPF)

Fig. 2.32 (a) shows the measured transmission and reflection response of the OADM used in later experiments, while fig. 2.32 (b) shows the spectrum of the transmitted and received FSK signal. The suppression between the two FSK tones achieved with this scheme was 15 dB, which proved to be sufficient for FSK detection, even with the IM payload modulation imposed on the signal.

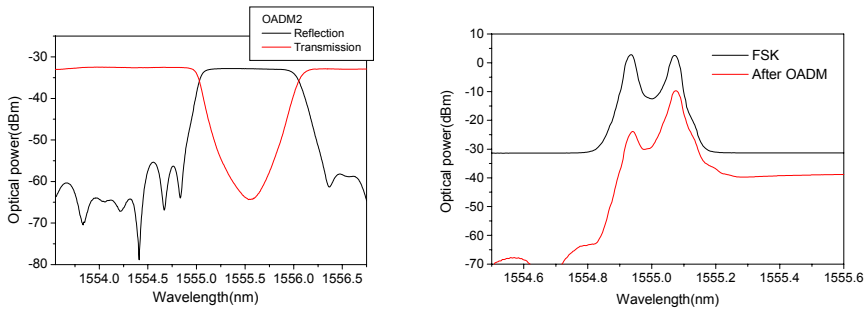

(a) *(b)*

Fig.2.32. *(a) Transmission and reflection of the OADM, (b) optical spectra of the FSK signal and demodulated FSK signal.*

A better performance was possible when using two cascaded filters. In this case an FBG and a tunable FPF. The enhanced performance of the two cascaded filters gave as result a suppression of 18 dB between the two FSK tones.

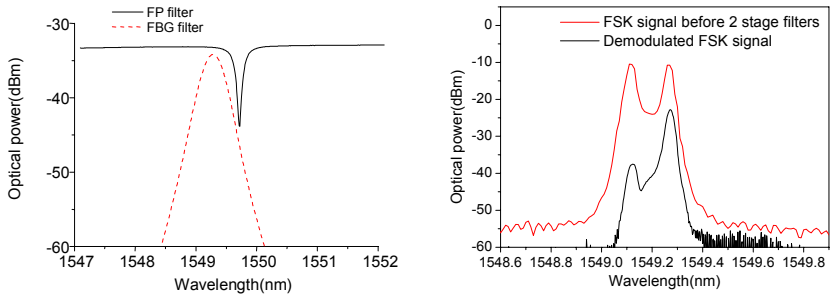

(a) *(b)*

Fig.2.33. *(a) Transmission of FBG and reflection of FP filters, (b) optical spectra of the FSK signal and demodulated FSK signal.*

Fig. 2.33 (a) shows the transmission response of the FBG (dotted line) and the reflection response of the FPF (solid line). It is to be noted that the sharpness of the edge of the FP filter proved to be higher than that of the OADM, and was highest when employing it in reflection. Fig. 2.33 (b) shows the spectrum of the transmitted and detected FSK signal in this detection scheme.

2.2.3 Back-to-back performance

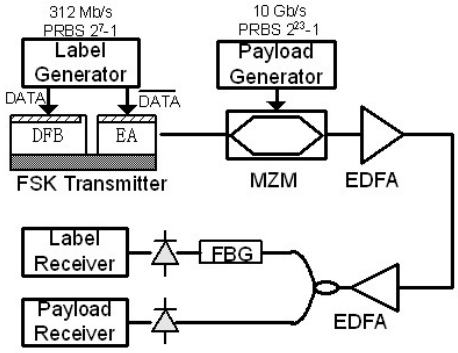

Fig. 2.34. *Experimental setup for back-to-back measurements of IM/FSK signals.*

In later experiments presented in this thesis, the selected method for FSK generation was the DFB/EAM source presented in Section 2.2.1. Its back-to-back performance was therefore measured through the setup shown in fig. 2.34. At the receiver node, the labelled signal was split using a 3 dB optical splitter. The output of one arm was directly detected by a photodiode and thus the optical payload was converted into the electrical domain. In the other arm, a single lobe of the FSK labelled signal was filtered out by a FBG, thus achieving FSK demodulation. The demodulated label was received by an electrical receiver with a 1.8 GHz bandwidth.

The drawback of the DFB/EAM method was measured and is shown schematically in fig. 2.35. The intensity modulation generated by the direct modulation of the DFB laser is shown on the left, and the IM generated with the negative data on the EAM is shown on the right. Together they should cancel each other out, thus giving a flat intensity response with a frequency modulation. In reality, the falling edge of the DFB induced modulation and the rising edge of the compensation introduced by the EAM did not exactly match, giving rise to a small ripple. This deteriorated one of every 32 of the IM payload eyes, thus reducing the performance of the system as a whole. It

is expected that if dedicated FSK laser sources were used in the transmission, this would improve the resulting BER performance.

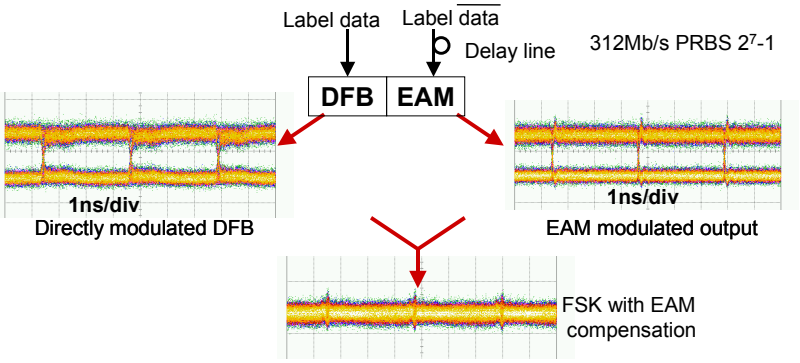

Fig.2.35. *FSK eye diagrams using the DFB/EAM method.*

Related to this problem, another aspect relevant for the design of the combined modulation format was the synchronization between the FSK and IM bits. Fig. 2.36 shows examples of the ripple effect when the FSK and IM bits were not perfectly synchronized and the degradation was at its worst. In this case the eye pattern was distorted and detection performance was greatly reduced. This effect would be accumulative in the case of label swapping through several nodes and thus the performance degradation would even be more severe.

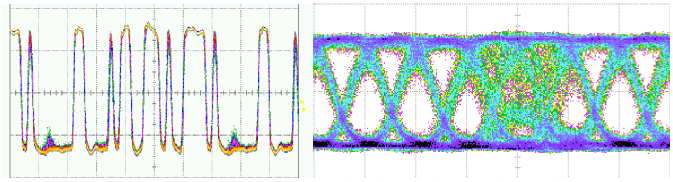

(a) *(b)*

Fig. 2.36. *Example of a detected 10 Gb/s (a) bit pattern and (b) eye diagram when the IM and FSK bit-sequences were not perfectly synchronized and the ripple effect was at its worst case.*

In fig. 2.37 the measured bit-pattern of the detected FSK label signal and its corresponding eye diagram are shown. As mentioned earlier, in the IM/FSK labelling scheme, some payload information is superimposed onto the label after the FSK demodulation. The received label eye diagram has a multi-level structure due to the intensity modulation of the payload, which can be observed in fig. 2.37 (b). The pattern dependence introduced by the 10 Gb/s IM payload on top of the 312 Mb/s label is clearly observable. In spite of that, the eye diagram remained open and the FSK label could be properly recovered. A degraded performance was also shown to be dependent on the

optimization of the receiver bandwidth. It was, in any case, clear that the modulation depth of the IM modulation is a crucial design parameter for a combined IM/FSK labelling system. Experimentally an ER of 3 to 6 dB allowed to detect the signals with an acceptable performance.

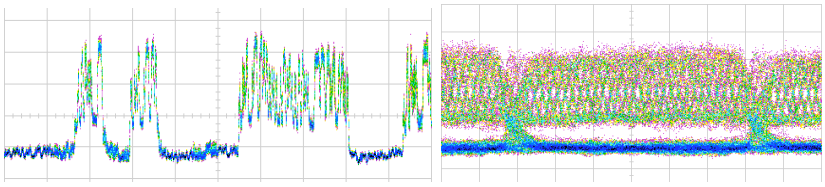

Fig.2.37. *(a) Received pulse pattern and (b) eye pattern of detected FSK modulation at 312 Mb/s, synchronized to a 10 Gb/s IM pattern.*

Fig. 2.38 shows the relation between the measured receiver sensitivities for a BER of 10^{-9}, of the payload and label when varying the modulation depth of the payload in the back-to-back case. As expected, reducing the ER of the payload enhanced the performance of the label, while making the sensitivity of the payload worse. A balanced sensitivity of the label and payload could be achieved with nearly 6 dB of IM extinction ratio.

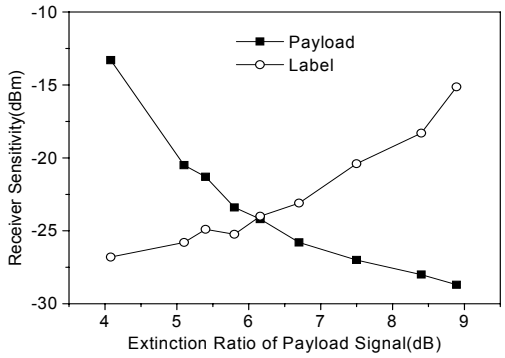

Fig. 2.38. *Payload and label receiver sensitivity versus extinction ratio of the payload.*

In an all-optical network, the performance of the label is far more important than that of the payload, because a single error in the label could mean that the whole packet was lost, hence having more dramatic consequences that an error in a payload bit. Therefore, the ER of the payload was generally selected so that the label performed better than the payload in the experiments. Fig. 2.39 shows the resulting BER curves for the back-to-back case of the IM/FSK combined modulation format with an IM ER of 5 dB and with an optimized electrical bandwidth at the label reciever. The receiver

sensitivity at a BER of 10^{-9} was -32.6 dBm for the FSK label and -24.2 dBm for the IM payload respectively. As mentioned earlier, this performance could be varied by changing the ER of the payload if it was viewed beneficial for the network to adjust the performance of the label with respect to the payload.

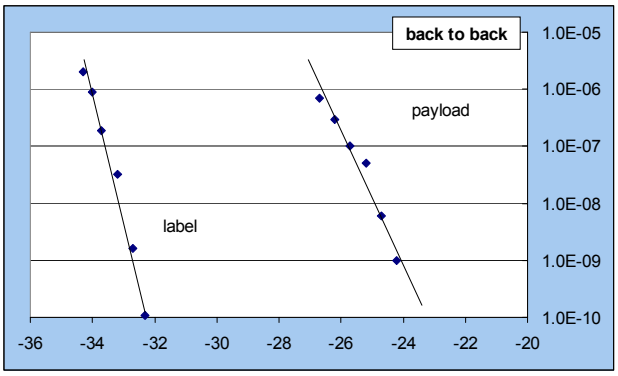

Fig. 239. *Measured back-to-back BER curves of the payload and label.*

2.3 CSS labelling

A novel method for optical subcarrier labelling was proposed in [85]. It was based on the carrier-suppression of the payload, which generated two sidebands onto which the optical label was modulated [86]. In this carrier-suppressed sideband (CSS) labelling scheme, the sideband label and the payload can be combined by using a directional coupler and separated from each other by means of an optical filter. The generated payload consisted of a 10 Gb/s IM modulated signal. For the label, two different bit-rates were implemented, at 156Mb/s and 1.25 Gb/s respectively.

A schematic diagram of the proposed optical label transmitter is shown in fig. 2.40. The output of a continuous-wave laser was first split into two light beams through an optical coupler. The payload information was then directly impressed upon one of them using an external intensity modulator. In the other arm, the light was first modulated by a dual-drive Mach-Zehnder modulator driven by a radio-frequency (RF) clock generator. The DC bias difference of this modulator was set to be equal to the swing voltage $V\pi$ while the RF clock signals driving the modulator arms had a π phase shift between them. In this way the output of the modulator consisted mostly of two sidebands while the carrier component was strongly suppressed [87].

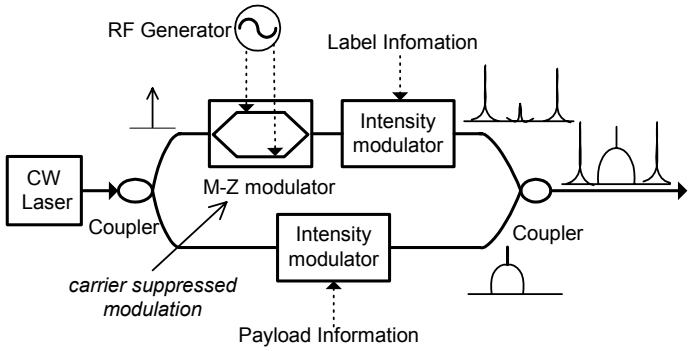

Fig. 2.40. *The proposed architecture of the optical label transmitter*

After the carrier suppression, the label information was impressed upon the two sidebands using a conventional intensity modulator. As the generated label did not have any optical carrier component in its spectrum, it could be directly multiplexed with the optical payload through an optical coupler. The spectra of the generated signals is shown in fig. 2.41. In the left hand side, it can be observed that the carrier component was strongly suppressed in the spectrum of the generated optical sidebands. The power ratio of carrier to sideband was measured to be below -32 dB, although it was heavily dependent on the input polarization state and RF voltage. Fig. 2.41 (b) shows the labelled signal with a label to payload power ratio of 5 dB.

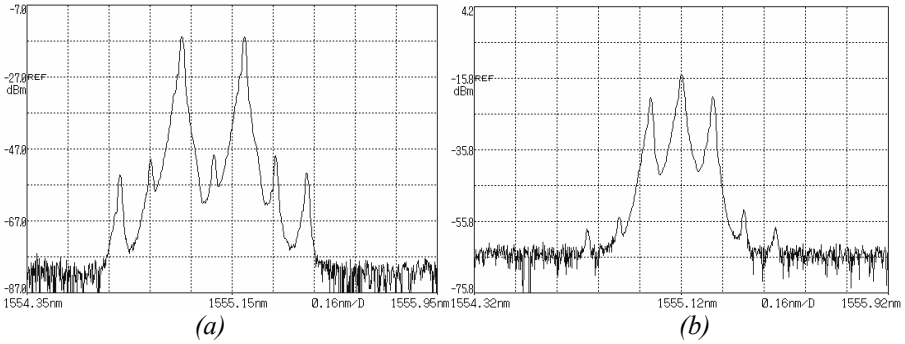

(a) *(b)*

Fig. 2.41. *Spectrum of (a) the generated double sidebands with the suppressed carrier (b) the generated signal consisting of payload and label*

At the receiver, two FBG based OADMs used as filters were employed for the extraction of the payload and label from the transmitted signals. The edge of the first filter's transmission function was located between the wavelengths of one sideband and the carrier. In this way, the sideband carrying the label information was dropped and inserted into the optical receiver. The carrier with the other sideband was then injected into the second OADM filter, the transmission edge of which was again located

between them. Thus the carrier containing the payload information was extracted by the second OADM filter and detected. Fig. 2.42 shows the spectra at different stages of the filtering process at the receiver.

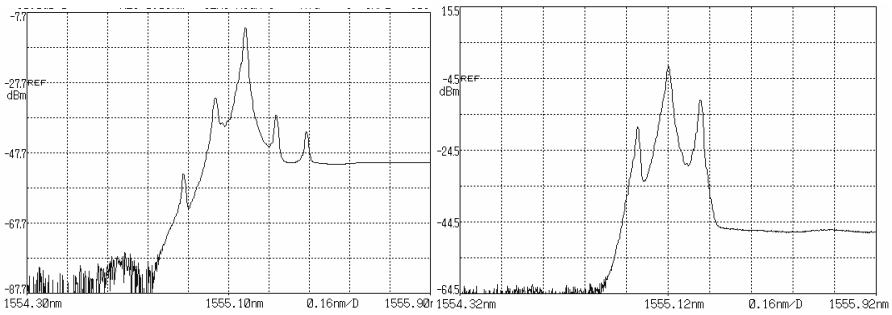

(a) *(b)*

Fig. 2.42. *Spectrum of (a) the extracted label after first OADM (b) the extracted payload with the residual label after second OADM.*

The main advantage of the proposed transmitter is that the label and payload signals can be controlled independently, allowing for an arbitrary label to payload power ratio, while adding a limited intermodulation distortion between them. Another advantage is that it does not require the use of RF mixers or optical notch filters, which reduce the system complexity.

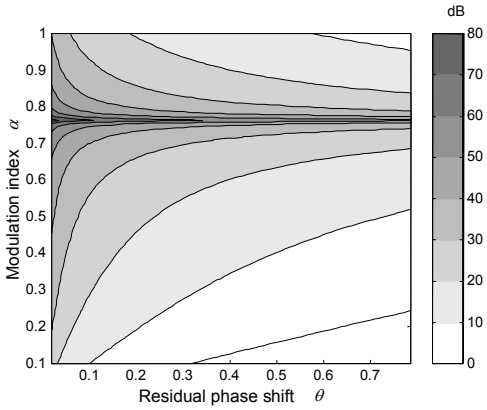

Fig. 2.43. *Contour plot of the carrier suppression ratio as a function of the residual phase shift and the modulation index.*

The modulation index $\alpha = V_m/V_\pi$ is the ratio between the amplitude of the RF signals V_m, and the voltage which is required in the MZM for a π-phase shift, V_π. When V_{bias} is the DC voltage that biases one of the arms, the residual phase $\theta = (\pi V_{bias}/V_\pi) - \pi$, indicates the disparity from the null point of the MZM. Fig. 2.43 shows the contour plot of the calculated suppression ratio as a function of the modulation index and residual phase shift. An optimum modulation index was found at 0.765 which is totally independent of residual

phase shift. Therefore even when the MZM was not working at its null point, a large suppression ratio of more than 80 dB still could be achieved by changing the RF voltage.

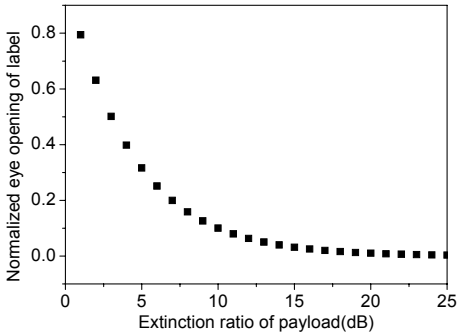

Fig. 2.44. *The extinction ratio of the payload versus the eye opening of the label which is normalized by the maximum optical power.*

Numerical calculations of the eye opening of the label as a function of the extinction ratio of the payload are shown in fig. 2.44. Clearly the eye opening of the label is decreased when increasing the payload extinction ratio. This indicates that also for this labelling method, a limited extinction ratio for the payload is required in order to detect the label.

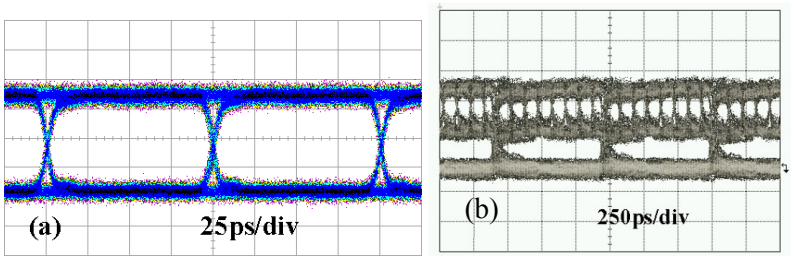

Fig. 2.45. *Measured eye diagrams for (a) 10 Gb/s back-to-back payload, (b) 1.25 Gb/s back-to-back label.*

Fig. 2.45 shows the eye diagrams of the signal at 10 Gb/s for the payload and 1.25 Gb/s for the label. Due to the intrinsic amplitude fluctuation of the intensity modulated payload, the received label eye diagram had a multi-level structure, that reflected the payload information at 10 Gb/s. Because the payload and the label were synchronized with each other, every eye of the label showed 8 small eyes.

The measured BER performances of the payload and the label for the back-to-back case and for the different label bit-rates, are shown in fig. 2.46. It can be observed that the performance is best when the label has a much

lower bit-rate and thus would have a narrower spectrum. The sensitivity of payload and label when the label bit-rate was 1.25 Gb/s was -28 dBm, while when the label bit-rate was 156 Mb/s, the payload sensitivity was -36 dBm and the label sensitivity was -34 dBm. It is believed that an optimized filtering scheme would enhance the performance of the first case.

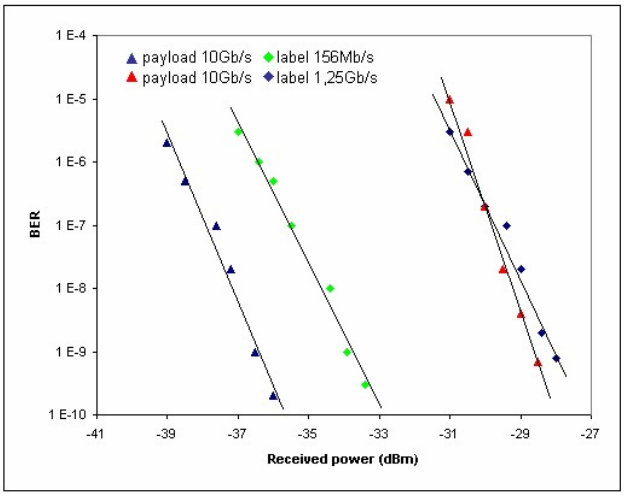

Fig. 2.46. *Measured back-to-back BER performance of the CSS scheme for various label bit-rates.*

On the negative side, the performance of the label when employing the CSS labelling method is lower than the one of the payload, specially at high bit-rates. This is the opposite of the desired response of a labelled signal, although the sensitivity still proved to be at a high level. Another drawback is that the upgrading of the payload bit-rate would mean that its spectrum would be broadened, which in turn would imply that the sidebands should be further apart. This would have an impact on the system, in the sense that filtering and RF generation should also be changed throughout the network.

2.4 Encoding methods

As shown in previous sections, the modulation crosstalk between IM payload and FSK label (or the DPSK label) degrades the performance of the label. This crosstalk is originated in the spectral overlap of the payload and the label [54]. Fig. 2.47 clearly demonstrates the modulation limitation of the IM/FSK scheme. Having to keep the modulation depth of the payload at a moderate level, might compromise the network performance and limit the network scalability.

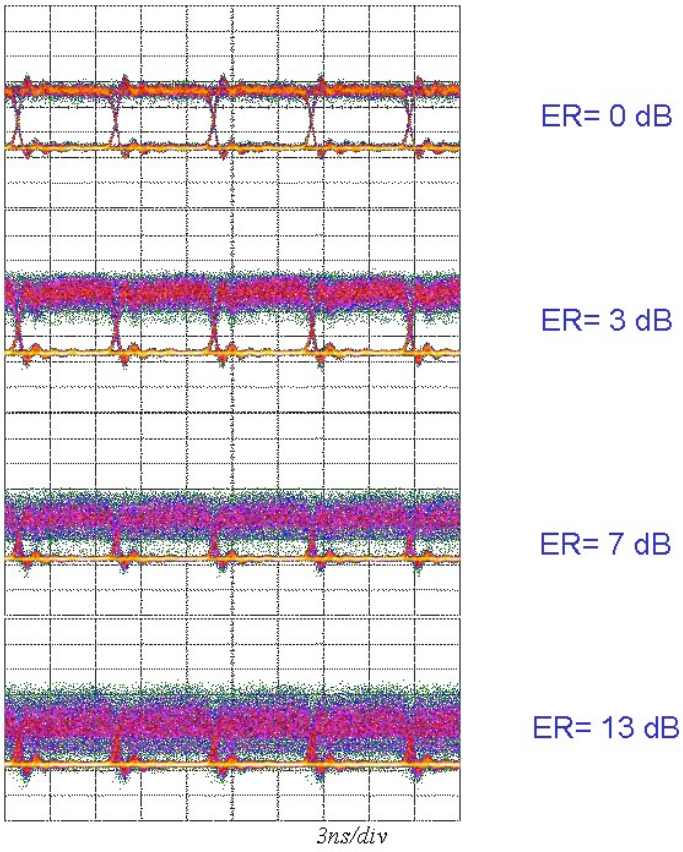

Fig. 2.47. *Eye-diagrams of detected 155Mb/s FSK labels in the presence of 10 Gb/s payloads with various extinction ratios.*

For improving the label receiving performance, four basic methods can be applied: 1) decreasing the modulation depth of payload, which in turn will degrade the performance of the payload; 2) improving the optical discriminating performance; 3) increasing the ratio of payload to label bit-rate, which taken a whole network design into consideration most likely would be fixed; or 4) reshaping the payload spectrum through DC-balanced coding, such as Manchester coding (MC) or 8B/10B coding. Fig. 2.48 shows the calculated spectra of DC-balanced codes compared to the NRZ format. The important difference is that the encoding methods present a limited (for 8B/10B) or zero (for MC) DC component. When modulating the label, this would be the part of the spectrum where most of its power will be located. Therefore, a spectral separation between payload and label is achieved.

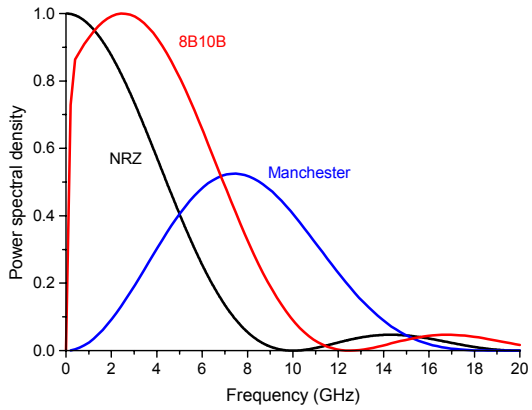

Fig. 2.48. *Calculated spectra of balanced codes compared to the NRZ format.*

The experimental results in this section will show that Manchester encoding is the most effective in improving the modulation performance of the optical labelling scheme. However, the Manchester code has a poor coding efficiency since it doubles the bandwidth requirements on the payload transmitter and receiver. 8B/10B on the other hand specifies no more than four sequential identical bits by encoding every 8 bits of data onto 10 bits of the encoded stream [89].

Compared to the 100% extra spectral bandwidth required for the Manchester code, it only reduces the bandwidth efficiency by 20%. In addition, the generation of 10 Gb/s 8B/10B code has been demonstrated through the proper configuration of an electrical multiplexer [90].

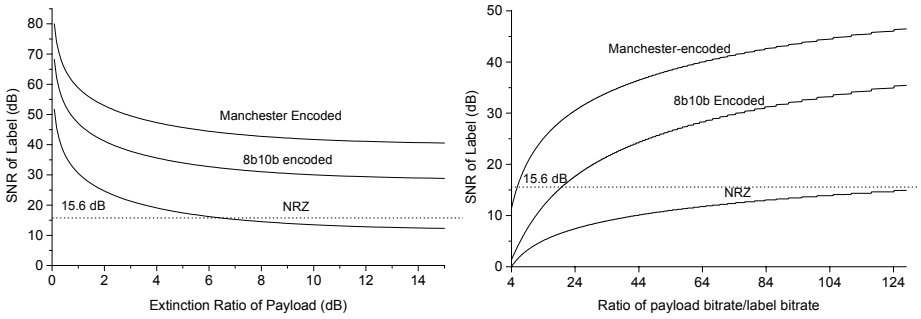

Fig. 2.49. *SNR performance of the FSK label in the presence of NRZ, Manchester and 8B/10B payloads, as a function of (a) the ER of the payload, (b) the ratio between payload and label bit-rate.*

Fig. 2.49 shows the SNR of the FSK label signal – if the power of the payload is treated as 'noise' for the label – when the payload is modulated in the NRZ format or encoded with MC and 8B/10B respectively. In fig. 2.49 (a) the payload to label bit-rate ratio was set to be 16 and the

extinction ratio of the payload was varied to verify the enhancement in performance due to coding. MC resulted in an improvement of more than 20 dB compared to the NRZ format. Fig. 2.49 (b) shows the results at different payload to label bit-rate ratios when the extinction ratio of the payload was set to 20 dB. The relative improvement of the method showed to be greater at lower bit-rates.

2.4.1 Manchester encoding versus NRZ

Manchester coding has been shown to offer several advantages, such as enabling a simple clock extraction operation [91]. Furthermore, its differential detection scheme exhibits a high-level intensity fluctuation tolerance [92], verifying itself as a promising coding system for high-speed burst mode transmission links [93]. In addition, Manchester coding greatly reduces low frequency components through spectrum shaping, hence having several applications in improving the modulation performance of network nodes [94], [95].

A comparison between MC and NRZ is shown in fig. 2.50. In the NRZ code, a logic ‘one’ is defined as the high level state, while a logic ‘zero’ is defined as the low level state. In MC, there is a transition at the middle of each bit period: a low-to-high transition represents ‘one’, and a high-to-low transition represents ‘zero’. Such an encoding may be alternatively viewed as encoding ‘1’ into ‘01’ and ‘0’ into ‘10’ at double the bit-rate.

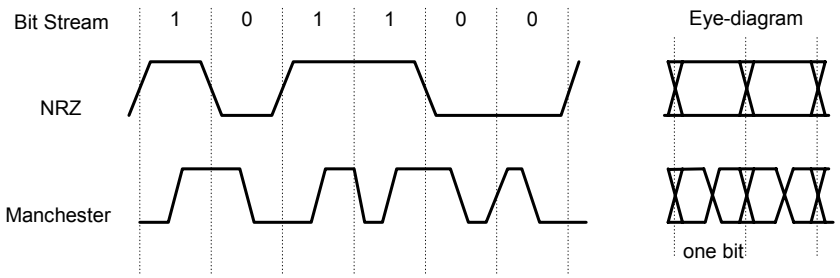

Fig. 2.50. *Waveform and eye-diagram of Manchester coding and NRZ.*

Fig. 2.51 shows the measured power spectra of a Manchester-coded and NRZ-coded random pattern signal at 10 Gb/s. It can be observed that compared to NRZ, MC distributes more power in the high frequency region and less power in the low frequency region. A strong clock frequency component can also be observed in the spectrum.

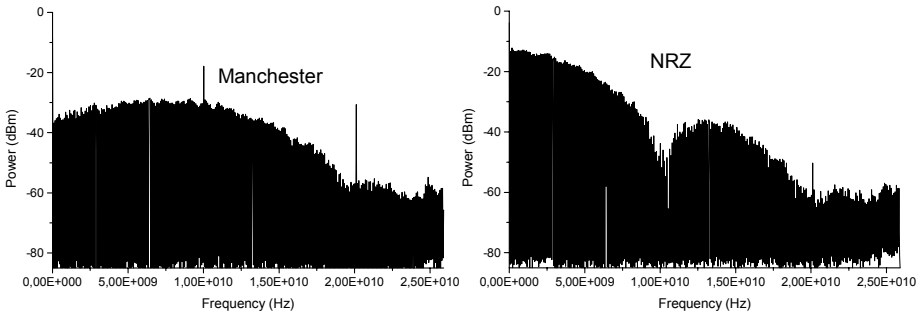

(a) *(b)*

Fig. 2.51. *Power spectrum of (a) Manchester encoding and (b) NRZ.*

2.4.2 Proposed method for Manchester generation

A typical implementation of Manchester coding and decoding is shown in fig. 2.52. To generate the Manchester code, an electrical logic component is usually employed to perform an exclusive-or (XOR) operation between an original NRZ and clock signal [91].

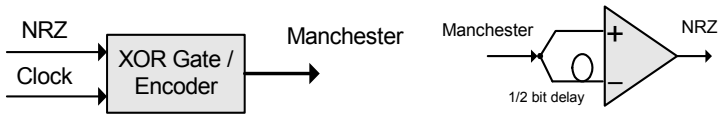

Fig. 2.52. *Manchester coding/decoding*

Since no clock rate conversion is needed in this operation, Manchester coding can work well at high bit rates. To decode the Manchester signal, a differential amplifier is usually employed to compare the energy received in each half time slot. The differential operation creates a power difference between consecutive half bits, thus the signal can be converted back to the NRZ format [93].

Although the potential of electrical XOR operation has been reported at bit rates as high as 40 Gb/s [91], a Manchester encoded optical transmitter operating above 10 Gb/s is still difficult and costly to implement due to the scarcity of high-speed electrical logic gates. A novel method to implement high speed Manchester coding with an electro-optical Mach-Zehnder modulator (MZM) was proposed in [96]. Unlike previous reported encoding methods [94], it does not require any electrical logic gate.

A Manchester code can be obtained through an XOR operation between an original NRZ signal and a clock signal. Consequently, there is always a transition, either rise or fall, at the middle of each bit period, which represents the '1' or '0' symbol respectively. The proposed method is based on a dual-drive MZM, which is driven by both a NRZ data and a clock signal. During each data bit, the clock signal will have a 'high' and a 'low' state. Thus, with the proper alignment, when the data signal is a '1', the two arms will experience a π phase shift in the first half of the bit, and the same phase shift in both arms in the second half of the bit. The output of the MZM will then be a '01' signal, and vice versa for a '0' data bit, as exemplified in fig. 2.54. Therefore an XOR operation directly in the optical domain was performed, and a Manchester-encoded optical signal could be generated while no electrical XOR gates were needed.

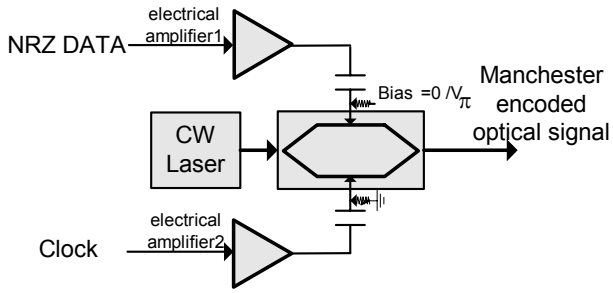

Fig. 2.53. *The proposed Manchester coding method.*

As shown in fig. 2.53, the MZM is configured to perform the logic operation between a NRZ data and a clock signal. As indicated by the measured output waveform in fig. 2.54, the symbols are finally transformed into transition edges at the middle of bit periods, thus achieving Manchester coding.

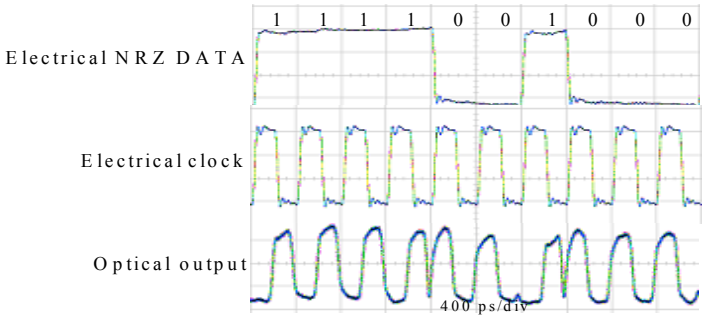

Fig. 2.54. *Demonstration of XOR operation between NRZ data and clock*

2.4.3 Experimental verification of Manchester coding

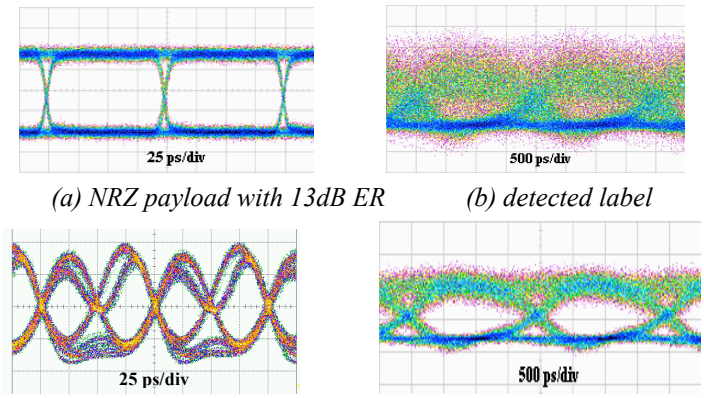

(a) NRZ payload with 13dB ER *(b) detected label*

(c) MC payload with 13dB ER *(d) detected label*

Fig. 2.55. *Eye-diagrams of extracted label in the presence of NRZ/MC payload.*

In order to experimentally verify the performance the IM/FSK labelling format in the presence of MC coding, a system was set up consisting of a 622 Mb/s optical FSK label with a tone spacing of 20 GHz and a 10 Gb/s IM payload. The transmitter was based on the DFB/EAM method, while the receiver was based on a FP filter, as described in previous sections.

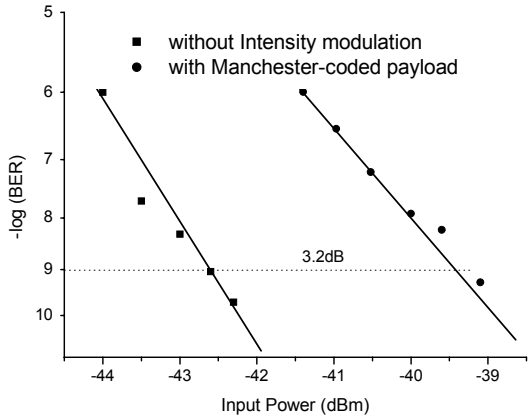

Fig. 2.56. *BER performance of the extracted label in the presence of MC payload.*

Fig. 2.55 shows the eye-diagrams of the detected label in the presence of NRZ- and Manchester-coded payloads. In the presence of a NRZ payload with an ER of 13 dB, the detected label was greatly distorted and could not be detected with an acceptable BER. Conversely, with the MC payload at the same ER, the detected label had a large eye-opening resulting in error-free

performance. The results of BER measurements shown in fig. 2.56 indicate that adding the FSK label to the MC payload resulted in a 3.2 dB power penalty, as opposed to 9.8 dB for the traditional NRZ modulated payload (see fig. 2.39).

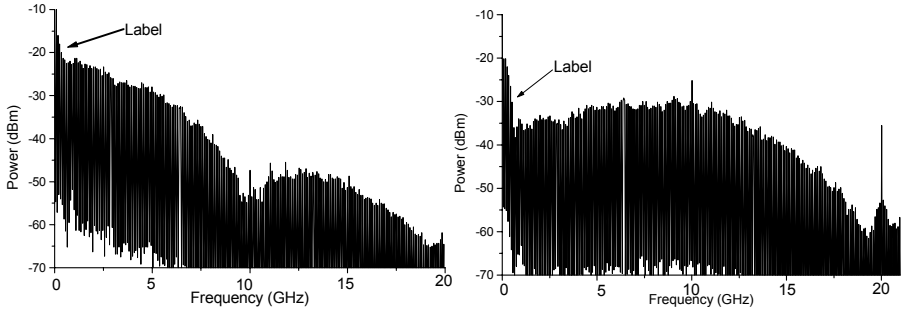

(a) *(b)*

Fig. 2.57. *RF power spectrum of extracted label in the presence of (a) NRZ payload and (b) MC payload with 13 dB of extinction ratio.*

In fig. 2.57 the measured RF power spectra of the extracted labels provide further information on the modulation performance. In the presence of the NRZ payload, much of the label power is loaded with cross-talk noise induced by the payload. Alternatively, with the MC payload, the label can be distinguished by nearly 20 dB, thus allowing a much better receiver performance (these figures should be compared to the ones in fig. 2.51, where the label is not present).

2.4.4 Experimental verification of 8B/10B coding

The performance of 8B/10B encoding applied to the orthogonal labelling scheme was also evaluated experimentally. The transmitters and receivers were similar to the ones used in the last section, but in this case the label bit-rate was set to 156 Mb/s, while its FSK tone spacing was kept at 20 GHz and the payload bit-rate was 10 Gb/s.

The 8B/10B code was directly generated through encoding a PRBS 2^9-1 signal by programming the data pattern generator, corresponding to a periodical data pattern of 1280 bits. As shown in fig. 2.58 (a), the low frequency components of the payload spectrum below 100 MHz were greatly suppressed through 8B/10B encoding. Thus through 8B/10B encoding, much less interference from the IM payload was observed in the electrical spectrum of the demodulated label, shown in fig. 2.58 (b).

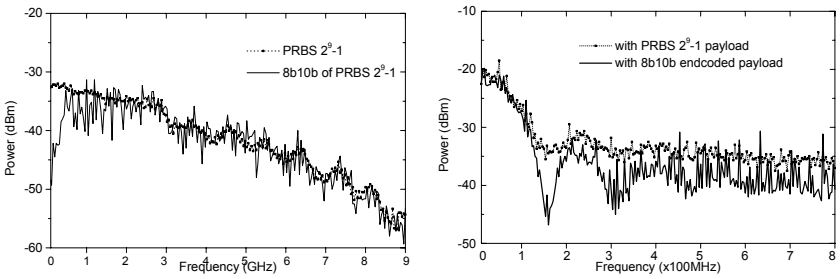

(a) *(b)*

Fig. 2.58. *(a) Power spectra of PRBS and 8B/10B encoded payloads (b) Power spectra of demodulated labels in the presence of PRBS and 8B/10B payloads.*

Fig. 2.59 shows the relation between the label receiver sensitivity and the ER of the payload. Through 8B/10B encoding, the degradation of the label receiver sensitivity with the increased ER is limited to a certain range. The insets show the eye-diagrams of the received label when the IM payload ER was equal to 10 dB, which further verify the performance improvement in the presence of 8B/10B encoding.

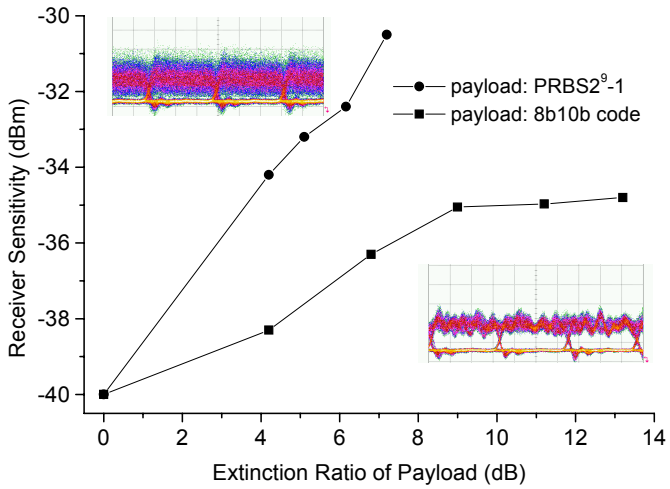

Fig. 2.59. *Label receiver sensitivity versus IM ER in the presence of PRBS and 8B/10B payloads.*

A further benefit of 8B/10B coding was found in the experiments where GCSR lasers were used to perform the FSK modulation. The used GCSR lasers exhibited a severe pattern-dependent modulation response when used to generate FSK signals, which was induced by their inherent non-uniform frequency response [97].

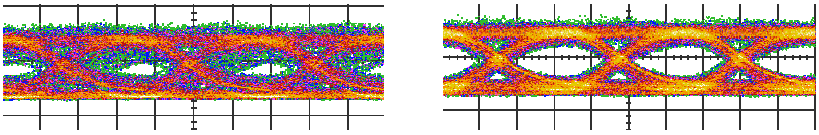

(a) (b)

Fig. 2.60. *Demodulated 156 Mb/s FSK eye-diagrams of a GCSR laser modulated by (a) a PRBS and (b) the same PRBS but 8B/10B coded.*

This problem could be overcome by using DC-balanced encoding. Fig. 2.60 shows the eye-diagrams of the demodulated FSK signal. When the GCSR lasers were frequency modulated by a PRBS data sequence, severe pattern-dependent intensity fluctuations could be observed in the received signals, as shown in fig. 2.60 (a). However, when 8B/10B encoding was applied, the eye-opening improvement in the received signals was clearly perceptible.

2.5 Chapter summary

In this chapter, the generation and detection of optical orthogonally labelled signals has been studied. Several methods of generating the orthogonal label have been presented, which included the IM/DPSK scheme, where the payload is intensity modulated and the label is differential-phase keying modulated; the IM/FSK scheme that also modulates the payload in intensity, while adding a frequency shift keyed label to the carrier; and finally, a carrier-suppressed sideband labelling scheme.

Numerical analysis of the IM/DPSK transmitter and receiver revealed that a theoretical maximum of 9.5 dB could be used for the extinction ratio of the IM payload, while the requirements on the laser linewidth were dependent on the bit-rate and most severe for low label bit-rates.

In experiments, the differential XOR operation was omitted in the transmitter throughout the thesis, because the signals under study were generated by pseudo-random bit sequences (PRBS), that become a shifted version of themselves when applying such a differential operation.

The demodulation of the DPSK label was performed in a Mach-Zehnder interferometer (MZI) with a one bit delay in one of the arms. After demodulation, the signal still showed the presence of the IM modulated payload, which would set a limit to the extinction ratio (ER) to be employed for the payload. Obviously, a degraded intensity ER would result in a higher payload penalty. On the other hand, the ER should not be too large, in order to being able to detect the phase modulated label. It proved therefore

essential to optimize the ER of the transmitter. To comply with this limitation induced by the label, as well as to satisfy the requirements for a proper detection of the payload, an ER in the range of 3 to 6 dB was applied in the following analysis

For the IM/DPSK labelling scheme, it was found that the system performance showed an improvement with increasing values of the ratio between the payload and label bit rate. The back-to-back sensitivity of a 10 Gb/s payload and a 2.5 Gb/s label was measured to be -25 and -29 dBm respectively, for a 3dB ER of the payload. When increasing the payload bit-rate to 40 Gb/s, it was found that the 2.5 Gb/s label automatically performed better, enhancing its sensitivity by about 2 dB for a given ER. The payload at the higher bit-rate had a poorer performance at a given extinction ratio.

An alternative approach to the IM/DPSK scheme was presented as the DPSK/IM scheme, where the payload was DPSK modulated at 40 Gb/s while the label was IM modulated at 2.5 Gb/s. In this case, the DPSK payload showed a B2B sensitivity of -32 dBm, while the IM label showed a sensitivity of -25 dBm

The transmitter and receiver of the IM/FSK scheme were also investigated. The generation of the FSK signal was realized and measured using three methods, while the payload in all cases was added by a chirp-free Mach-Zehnder modulator (MZM). The first method was based on two tunable ECLs, which proved to be less effective due to the appearance of large intensity ripples due to the non-matching raising and falling edges of the lasers.

A second and novel source for constant-amplitude FSK modulation, used a directly modulated DFB laser, where the corresponding unwanted intensity modulation was compensated by an EAM, which showed a much better result. However, small intensity ripples were still present at the output of the FSK source, due to the non-matching raising and falling edges of the DFB laser and EAM. When this signal was intensity modulated at a much higher bit-rate, this ripple would limit the performance of the payload. One way to limit the detrimental effect of the intensity ripple would be to carefully synchronize the payload and label data streams, so that the ripple would occur during the transition of two payload bits. Another simple way to overcome the problem would be to apply coding techniques that would allow for a higher ER of the payload, on which the ripple would have a much smaller impact.

The third method for FSK generation would be modulating the phase section of a GCSR laser. These lasers showed a wavelength dependent FSK response, which meant that at certain wavelengths, the desired 20 GHz

tone-spacing of the FSK modulation could not be met. The DFB/EAM method showed the best performance and a higher stability, and was therefore used in most of the experiments presented in the rest of this thesis.

The FSK detection was realized suppressing one of the tones by either a single filter or cascading two filters. The cascading method showed a 3 dB higher performance when detecting the remaining tone in a photo detector. The back-to-back receiver sensitivity at a BER of 10^{-9} was -32.6 dBm for the FSK label and -24.2 dBm for the IM payload respectively, at an ER of the payload of 5 dB.

A third introduced alternative to all-optical labelling, was the CSS scheme, that is based on the carrier suppression of the payload and labelling modulation of the sidebands. An advantage of the proposed transmitter is that the label and payload signals can be controlled independently, allowing for an arbitrary label to payload power ratio. On the other hand, an upgrade of the payload bit-rate would mean that the whole system should be changed accordingly with regard to the label, which is not the case for the other labelling schemes presented in this chapter. The back-to-back sensitivity of this scheme was measured to be -28.5 dBm for both payload and label when the payload was modulated at 10 Gb/s and the label at 1.25 Gb/s. When the label bit-rate was reduced to 156 Mb/s, the sensitivities were respectively -34 and -36 dBm for label and payload.

In both the IM/DPSK and the IM/FSK labelling schemes, one of the biggest drawbacks, is the large amount of cross-talk that the payload impresses on the label. This is due to the fact that both modulation methods use the same part of the spectrum as the highest energy transmission. A way of overcoming this problem (and therefore being able to enlarge the ER of the IM payload) is using encoding formats for the IM transmission.

Because the label bit rate typically would be much lower than the payload bit rate due to the small amount of control information, the label signal would be a narrow-band signal. When applying a coding technique to the payload that would shift the most significant part of its power spectrum to higher frequencies, the cross-talk will be significantly suppressed. Line coding techniques, such as Manchester-coding [95] or 8B/10B coding [74] have proven to generate such a spectral shift.

A novel method to implement high-speed Manchester coding (MC) was presented in [96]. The generated 10 Gb/s Manchester encoded signal showed error free performance, while applying the coding method to the IM/FSK scheme, showed a dramatically improvement in performance, by allowing the ER of the payload to be raised up to 13 dB. The drawback of MC is that it doubles the needed bandwidth of the signal.

An alternative coding method is 8B/10B, which only reduces the bandwidth efficiency by 20%. When this coding method was applied to an optical IM/FSK labelled signal consisting of a 10 Gb/s IM payload and a 156 Mb/s FSK label, a noticeable enhancement of the performance was achieved, which increased while enlarging the payload ER. This method also proved useful in reducing the pattern dependent modulation response of GCSR lasers.

The overall results of the labelling schemes with regard to their back-to-back performance are be summarized in Table 2.2. For a payload at 10 Gb/s both the IM/DPSK and the IM/FSK schemes show a sensitivity of around -25 dBm, while the sensitivity of the label in those cases was in the region of -30 dBm, and could even be enhanced to almost -40 dBm if Manchester coding was employed, at the cost of doubling the required bandwidth. The carrier-suppressed sideband (CSS) labelling scheme showed a better performance, although the method does not allow for an upgrade in payload bit-rate without major changes in the label part of the system.

Table 2.2. *Compared B2B results for the proposed all-optical orthogonal labelling schemes.*

Scheme	***Bit-rate***		***Sensitivity***		***ER payload***
	payload	***label***	***payload***	***label***	
IM/DPSK	*10 Gb/s*	*2.5 Gb/s*	*-25*	*-29*	*3*
IM/DPSK	*40 Gb/s*	*2.5 Gb/s*	*-21*	*-25*	*6*
DPSK/IM	*40 Gb/s*	*2.5 Gb/s*	*-25*	*-32*	*3*
IM/FSK	*10 Gb/s*	*312 Mb/s*	*-24.2*	*-32.6*	*5*
IM/FSK-MC	*10 Gb/s*	*622 Mb/s*	*-24.2*	*-39.5*	*13*
IM/FSK-8B/10B	*10 Gb/s*	*156 Mb/s*	*-24.2*	*-35*	*10*
CSS	*10 Gb/s*	*1.25 Gb/s*	*-28.5*	*-28.5*	*-*
CSS	*10 Gb/s*	*156 Mb/s*	*-36*	*-34*	*-*

These results show that the orthogonal modulation formats are a promising approach to optical labelling for ultra-high packet-rate routing and forwarding in the optical layer. At the same time, the limitation on the intensity modulated extinction ratio has to be carefully considered for the given network, as a sub-optimized value would have a detrimental effect on the network scalability.

Chapter 3

Transmission of orthogonally labelled signals

When transmitting an optical signal through a fiber, dispersion compensation has to be carefully tailored as to minimize the degradation of the signal, and power levels have to be optimized in order to reduce non-linearities while keeping an acceptable signal to noise ratio (SNR) [68]. For an orthogonally labelled signal, that consists of two superimposed modulation formats, this would be expected to be even more important.

For the IM/FSK scheme strict requirements for dispersion compensation for the payload are expected, due to the walk-off between the two FSK tones, given that a large tone spacing is used for the FSK modulation. For the IM/DPSK scheme self-phase modulation (SPM) would convert the intensity modulation (IM) into phase modulation (PM), while dispersion would lead to PM to IM conversion [98].

In this chapter, the performance of all-optical orthogonally labelled signals with regard to transmission over various fiber spans will be investigated. Various types of compensation schemes and compensation ratios will be considered, and various fiber types studied. The issues of optimum power levels and extinction ratio (ER) will also be addressed. The IM/DPSK labelling scheme will be firstly investigated, followed by results on the IM/FSK scheme. Finally, the CSS labelling method will also be validated with respect to transmission.

3.1 IM/DPSK transmission

In this section the single channel transmission properties of all-optically labelled signals using the IM/DPSK orthogonal modulation, will be

investigated. Both numerical and experimental results of transmission links of various distances will be presented. The interaction of dispersion and non-linearities in transmission fibers has been extensively studied [99], [100]. Dispersion management issues, such as the difference in performance of the various compensation schemes will here be presented for the orthogonal modulation methods. In this context, pre-compensation is defined as the scheme that employs a dispersion compensating fiber (DCF) before the standard single-mode fiber (SMF) span; post-compensation as the scheme that is designed with the DCF after the SMF; and hybrid compensation as the scheme where the compensation is split equally between the start and the end of the fiber.

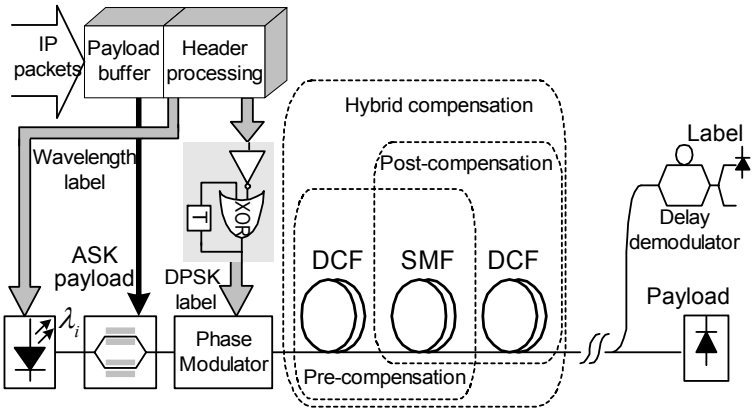

Fig. 3.1. *Transmission setup of two-level optical labelling system. (Figure from [102]).*

A schematic diagram of the system under study is shown in fig. 3.1, where the different types of dispersion compensation are indicated. The transmitter and receiver of the IM/DPSK labelled signal are equivalent to the ones described in the previous chapter.

3.1.1 Numerical analysis

For the numerical analysis, a system based on an intensity modulated payload at 10 Gb/s accompanied by a DPSK modulated label at 2.5 Gb/s transmitted over a single span, was considered. Fiber spans of varying length consisting of SMF compensated by DCF with different degrees of compensation have been numerically modelled. The attenuation of the SMF was 0.19 dB/km and its dispersion 16.5 ps/nm/km at 1550 nm. The DCF had an attenuation of 0.6 dB/km and a dispersion of -80 ps/nm/km. The degree of compensation was defined as the ratio of the dispersion accumulated in the DCF to the dispersion accumulated in the SMF. Fig. 3.2 show the results on eye-opening

penalty (EOP) performance of the payload – defined as the reduction in ER, measured in dB – in the post-, pre- and hybrid compensation schemes depending on SMF length, compensation ratio and input power. The figures indicate the maximum SMF length corresponding to a 2 dB EOP as a function of span average input power and degree of compensation.

In all three cases, the optimum compensation ratio was found to be less than 100%, which is believed to be due to the influence of the DPSK label on the signal (the 100% compensation was calculated for a pure IM signal). The hybrid and pre-compensation schemes showed a slightly higher tolerance to the change of the compensation ratio when the input power was of the order of 15 dBm. In all three cases, the power level could be varied between 0 and 20 dBm, while still being able to achieve an acceptable performance. The lowest penalty of the payload was obtained in the pre-compensation scheme, which indicates that, provided the input power is kept constant, the pre-compensation scheme would respond with the largest payload eye-opening.

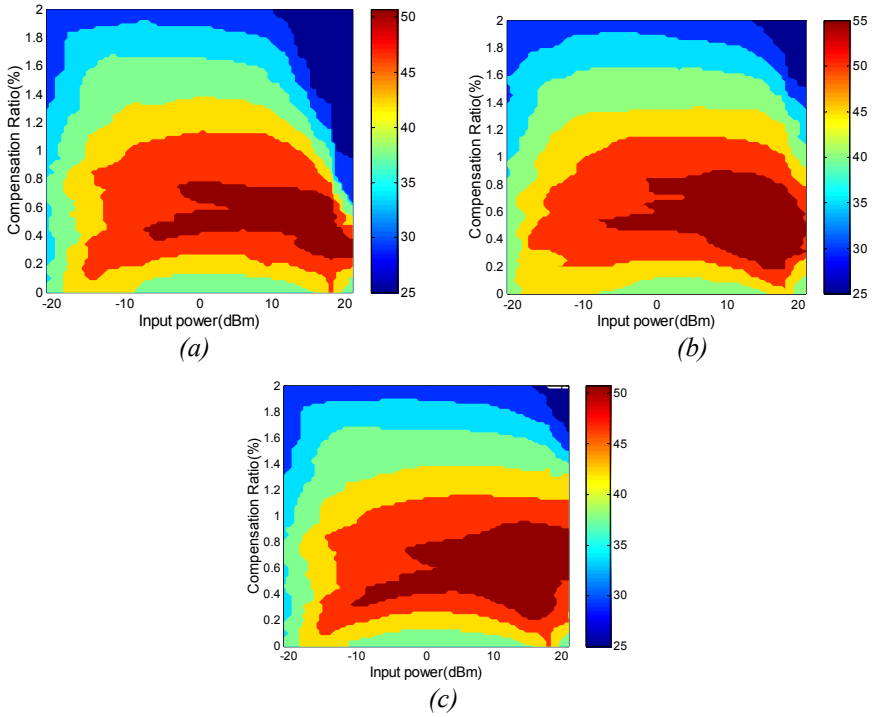

Fig. 3.2 *Maximum SMF length in km for a 2 dB EOP for the payload as a function of signal average input power and compensation ratio for (a) post-compensation, (b) pre-compensation and (c) hybrid compensation.*

Fig. 3.3 shows the EOP performance of the label for different compensation schemes. The transmission performance of the label was observed to be very

similar in all three cases. It is also found that, although the DCF could improve the eye opening of the payload, this would in turn always degrade the label performance. The reason for this is believed to be that a degraded payload extinction ratio would be beneficial for the label and vice versa, as discussed in Section 2.1.

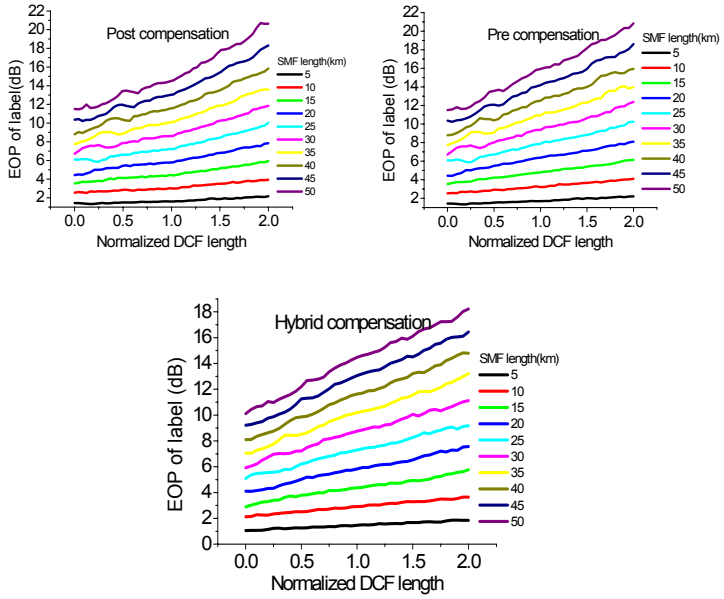

Fig. 3.3. *EOP for the label as a function of compensation ratio and SMF length for hybrid compensation. Results for post- and pre-compensation are included to illustrate their similarity.*

3.1.2 Performance with 10 Gb/s payloads

This subsection will present experimental results of the transmission of IM/DPSK labelled signals at a bit rate of 10 Gb/s for the payload and 2.5 Gb/s for the label for different types of fibers and compensation schemes. First transmission over a 50 km post-compensated SMF link will be validated, followed by transmission over a 80 km pre-compensated NZDSF link.

Transmission over 50 km of SMF with post-compensation

The experimental setup is shown in fig. 3.4. The signal source was a wavelength tunable external cavity laser (ECL) working at 1552.5 nm. The signal was first intensity modulated by a Mach-Zehnder modulator. The

DPSK label was then impressed by a phase modulator. The transmission span consisted of 50 km of SMF followed by 8.6 km of DCF. The dispersion of the SMF at 1552.5 nm was 17.1 ps/nm/km, and its attenuation 0.18 dB/km. The accumulated dispersion of the dispersion compensated fiber span was 3.92 ps/nm/km, and its total loss 15 dB. The input power to the fiber span was set to 6 dBm.

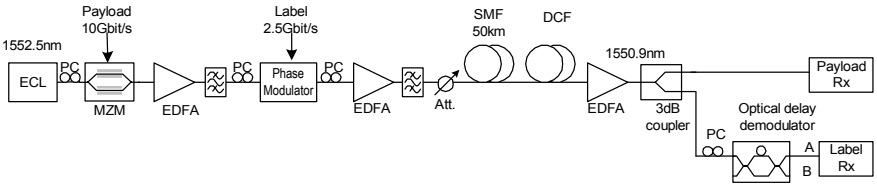

Fig. 3.4. *Experimental setup for the transmission of IM/DPSK signals over a post-compensated fiber-span.*

At the receiver, a fiber based one bit delay demodulator was used for the DPSK label. As expected, a trade off between the extinction ratio requirements for the payload and the label was observed, which was similar to that of Section 2.1. An ER of 3 dB was chosen for the IM payload, in order to have an enhanced label receiver sensitivity.

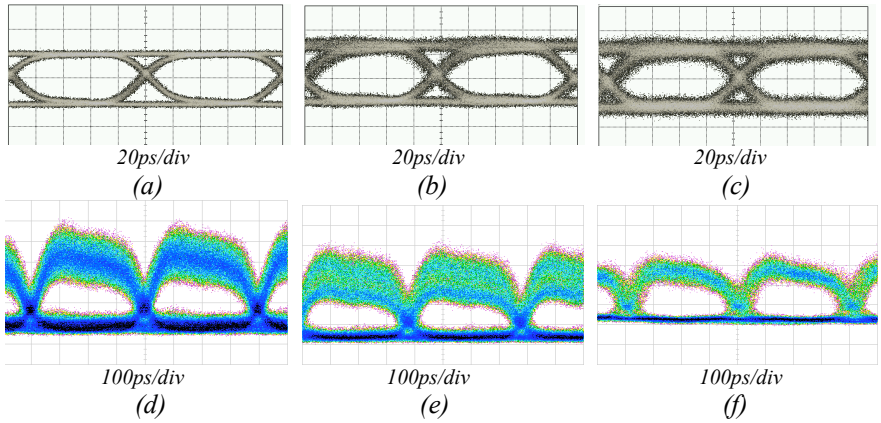

Fig. 3.5. *Measured eye diagrams for (a) original pure IM signal at 10 Gb/s, (b) back-to-back payload, (c) payload after transmission over 50 km of SMF, (d) back-to-back label at 2.5 Gb/s, (e) label after 50 km transmission, (f) pure DPSK signal after 50 km transmission.*

The eye diagrams for the original data and the transmitted signal are shown in fig. 3.5. Due to the intrinsic amplitude fluctuation of the intensity modulated payload, the received label eye diagram presented a multi-level structure as discussed in Section 2.1, which becomes apparent when comparing fig. 3.5 (e) which corresponds to the IM/DPSK signal after

transmission, and fig. 3.5 (f) that shows the pure DPSK signal after transmission.

The obtained BER curves are shown in fig. 3.6, compared to the cases where pure DPSK or IM signals were transmitted. The sensitivities for a BER of 10^{-9} after transmission, were -25 dBm for the label and -16 dBm for the payload. Compared to the IM/DPSK back-to-back performance shown in fig. 2.15, the power penalty after transmission for the label was below 1 dB. However, the payload experienced a relatively large penalty of up to 8 dB, due to the low extinction ratio at which it was modulated. A more optimized ER would be able to be found for transmission purposes, that would introduce a balanced and similar penalty for both payload and label. In any case, signals could be received with a BER in the range of 10^{-10}.

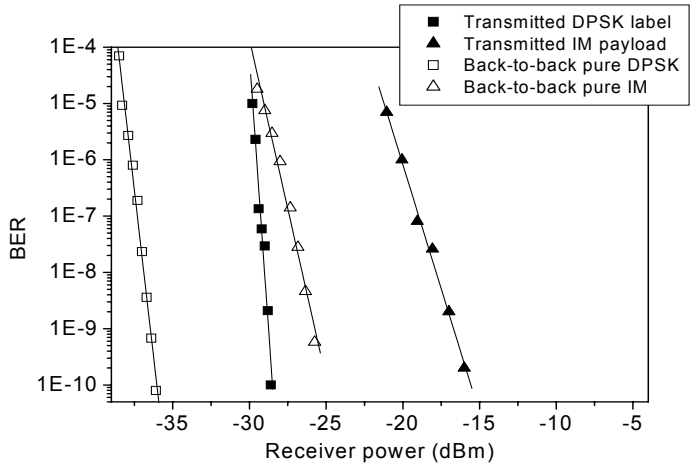

Fig. 3.6. *Measured BER performance for back-to-back (single modulation) and after transmission (orthogonal modulation).*

Transmission over 80 km of NZDSF with pre-compensation

The transmission system analysed next is mostly identical to the previous one, except that the selected compensation scheme is pre-compensation, and the fiber used for transmission is a non-zero dispersion shifted fiber (NZDSF). These fibers are designed to have a small dispersion close to 1550 nm in order to prevent large dispersion accumulation while preventing a phase matching condition for four-wave mixing (FWM) [103]. Other than the transmission link, the experimental setup is the same as in fig. 3.4. The ECL was lasing at 1555.7 nm. The transmission span consisted of 80 km NZDSF with dispersion of 4.8 ps/nm/km and dispersion slope of 0.044 ps/nm^2/km. A

matching length of DCF was used to fully compensate for the chromatic dispersion applied in a pre-compensating scheme. The ER of the payload was kept at 3 dB.

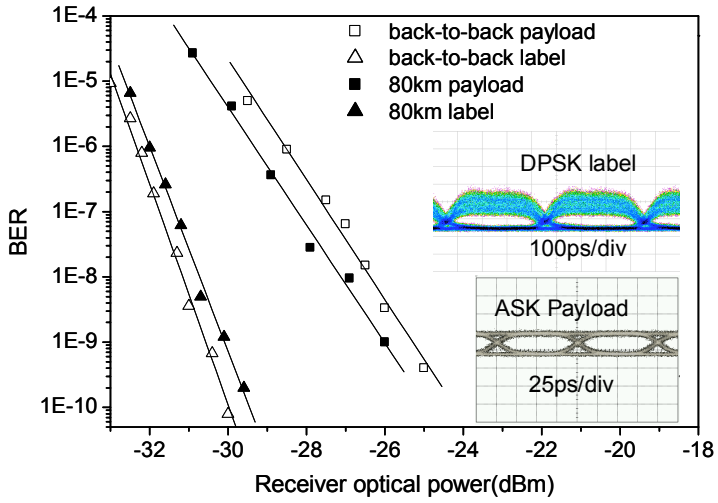

Fig. 3.7. *Measured BER performance for back-to-back and after 80 km NZDSF transmission and eye diagrams of the payload and label after transmission.*

The BER performance and the eye diagrams of the payload and label after transmission over 80 km NZDSF with a pre-compensation scheme are shown in fig. 3.7. Very clear and open eyes could be obtained for both payload and label after transmission, even with the persistent multi-level structure of the label. Both the payload and label could be received with a BER of less than 10^{-9} after the 80 km transmission link. The DPSK label experienced a very low power penalty of 0.5 dB due to transmission, which is comparable to the post-compensated SMF transmission discussed in the last section. The receiver sensitivity of the payload after transmission was observed to be even enhanced by 0.7 dB compared to the back-to-back case, which is believed to be due to a variation in the ER of the payload label.

The receiver sensitivities of the payload and the label as a function of span input power are shown in fig. 3.8. A larger input power was found to be beneficial for the payload, whereas an optimum point for the label detection was found at 8 dBm. This is believed to be due to the fact that a large input power increased the cross-talk originated from SPM and as a consequence would influence the DPSK label. Compared to our earlier experimental transmission of the IM/DPSK signal over 50 km of SMF, the employment of NZDSF provided a considerable improvement, specially for the payload.

Placing the DCF after the NZDSF in a post-compensation scheme and lead to 1.5 dB penalty for the payload sensitivity for an input power level of 6 dBm, while the same label sensitivity relatively to the pre-compensation scheme was maintained.

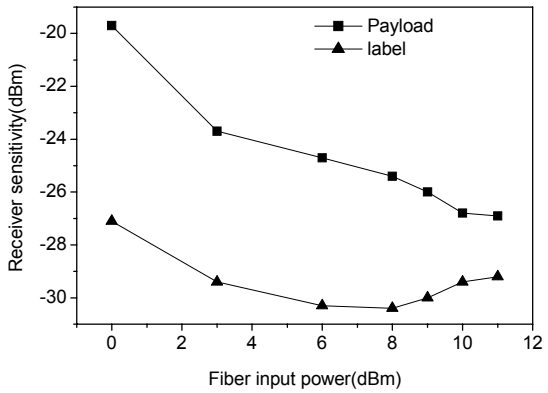

Fig. 3.8. *Measured receiver sensitivity as a function of the span input power for IM/DPSK at 10/2.5 Gb/s over an 80 km post-compensated NZDSF span.*

3.1.3 Performance with 40 Gb/s payloads

This subsection will present experimental results of the transmission of labelled signals at a bit rate of 40 Gb/s for the payload and 2.5 Gb/s for the label. The 8B/10B coding technique will be validated for the IM/DPSK labelling scheme in an SMF link of 40 km. After that, the alternative DPSK/IM labelling scheme will be validated for transmission over 50 km of SMF.

Transmission of a 40/2.5 Gb/s IM/DPSK signal over 40 km of SMF using 8B/10B coding

A transmission experiment was setup, in order to verify the effectiveness of encoding schemes used to relieve the extinction ratio requirements on the IM modulated payload, as well as to illustrate the possibility to upgrade the bit-rate of the payload in the system, without varying the system aspects regarding to the label. As discussed in the previous chapter, Manchester coding (MC) has advantages in clock-recovery and burst-mode data reception, however it doubles the bandwidth requirements on the payload transmitter and receiver, thus leaving only half of the bandwidth efficiency. Therefore 8B/10B was chosen as the coding technique for this system, because of its relatively high bandwidth efficiency (80%).

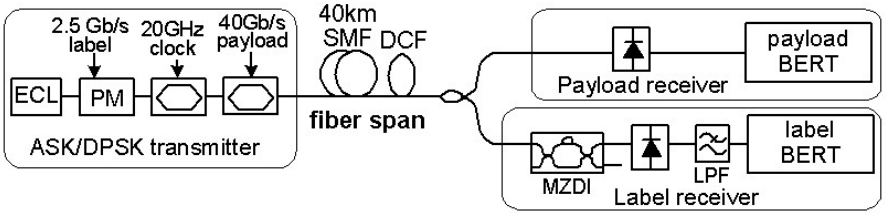

***Fig. 3.9**. Experimental setup used to verify the effectiveness of 8B/10B coding in an IM/DPSK transmission systems.*

The experimental setup is shown in fig. 3.9. The signal source was a wavelength tunable ECL working at 1550 nm. The 2.5 Gb/s DPSK signal was impressed through a phase modulator, that once again, did not make use of the pre-coder circuit for the DPSK format because the test signal was a 2^{23}-1 PRBS pattern. Two MZM in push-pull configuration were used to generate a RZ payload at 40 Gb/s. The first MZM generated a 40 GHz RZ pulse train with 33% duty cycle. The modulator was biased at the peak of its transmission curve and differentially driven at twice the switching voltage with an ac-coupled half-bit-rate (20 GHz) sine wave. The second MZM was driven by a 40 Gb/s 8B/10B encoded data-stream. The 8B/10B coding was directly generated through encoding a 2^7-1 PRBS by programming the data pattern generator, corresponding to a periodical data pattern of 160 bits. The configuration of the receiver was equivalent to the ones discussed earlier.

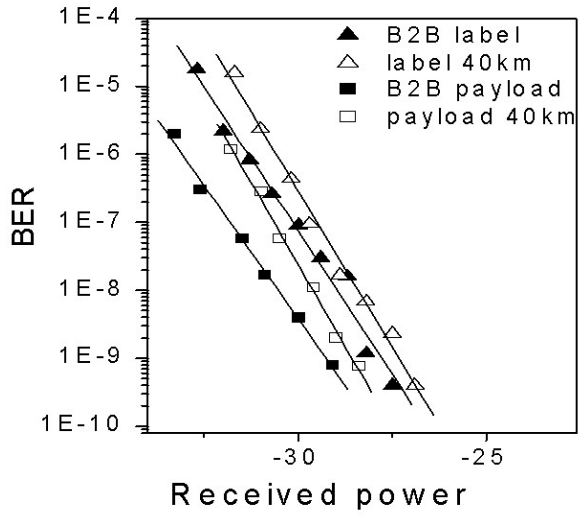

***Fig. 3.10.** Measured BER for payload and label in the back-to-back case and after 40 km transmission.*

The transmission span consisted of 40 km of SMF, with a matching length of DCF in a post-compensation scheme. The dispersion of the SMF and DCF was 16.9 ps/nm/km and -100 ps/nm/km, respectively. Fig. 3.10 presents the BER curves in the back-to-back case and after transmission, showing that the transmission penalties for the payload and label were less than 1 dB.

The measured sensitivities of the payload and label as a function of the payload ER are shown in fig. 3.11, where once again, the trade off between the ER requirements for the payload and the label are observed. Without 8B/10B encoding the balance point between the performance of label and payload was found close to 7 dB of IM extinction ratio. It should be noted that this optimum value could be decreased when a longer PRBS sequence was used for the payload due to the increased length of the continuous 'marks' and 'spaces'. When the payload was coded by a 2^7-1 PRBS sequence, proper DPSK label detection could not be achieved when the ER of the payload exceeded 8.6 dB. However, employing 8B/10B coding, the acceptable ER could be as high as 12 dB. Hence the limitation on the ER was overcome by employing 8B/10B coding for the payload and the system performance was significantly improved. The inset of fig. 3.11 shows the eye diagrams of the encoded signal at the point where payload and label showed a similar sensitivity, which was for about 10.5 dB of ER.

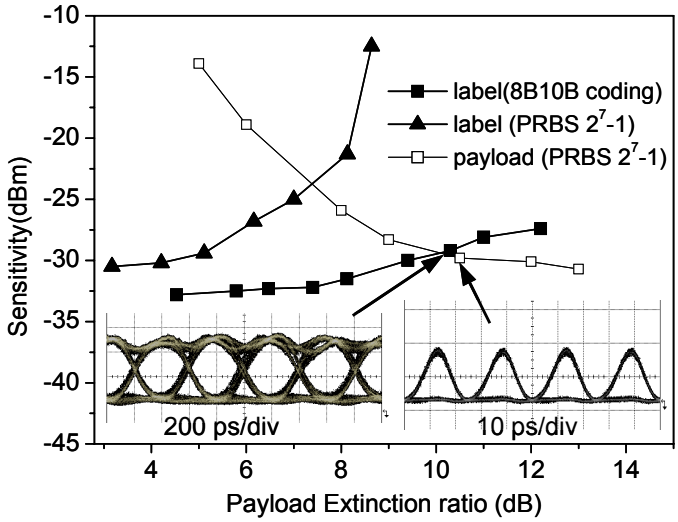

Fig. 3.11. *Measured receiver sensitivity for the payload and label vs. input extinction ratio of the payload and eye-diagrams at an ER of 10.5 dB.*

Transmission of a 40/2.5 Gb/s DPSK/IM signal over 50 km of SMF

Alternatively to the previous cases, orthogonal labelling can also be achieved through DPSK modulation simultaneously to IM modulation, but

interchanging the roles played by each modulation with regard to payload and label, as discussed in Section 2.1.2. In this transmission experiment the payload was DPSK modulated at 40 Gb/s, while the label was modulated on the intensity of the carrier at 2.5 Gb/s. The IM label insertion was performed by the use of a electro-absorption modulator (EAM).

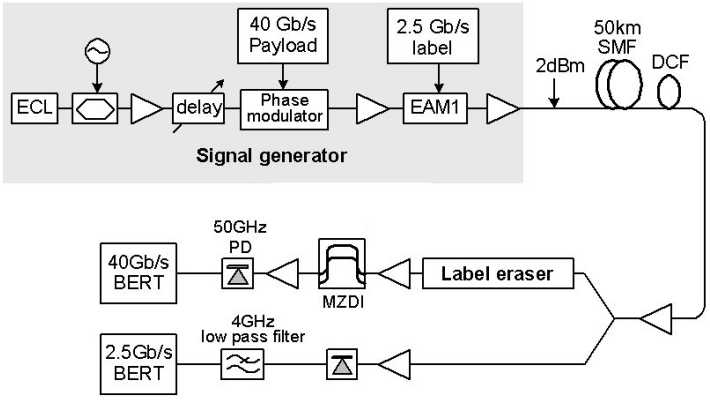

Fig. 3.12. *Experimental setup for the DPSK/IM orthogonal modulation scheme.*

The experimental setup is shown in fig. 3.12. The DPSK modulation was generated through a phase modulator driven by a 40 Gb/s PRBS data stream of length 2^{23}-1. The label information at 2.5 Gb/s (PRBS 2^{7}-1) was added by a following EAM, thus producing an optically DPSK/IM labelled signal.

The transmission span consisted of 50 km of SMF with a matching length of DCF in a post-compensation scheme. The dispersion of the SMF and DCF were 16.9 ps/nm/km and -100 ps/nm/km, respectively.

At the receiver, the signal was split, and the label was directly detected by a photodiode and filtered. The signal in the other arm underwent a label erasure process that will be described in detail in Section 6.1.5, in order to optimize the payload receiver. The payload was then fed to an integrated Mach-Zehnder interferometer with the appropriate delay in one arm to demodulate the DPSK signal, and finally detected by a 50 GHz photodiode. The integrated demodulator used in the experiment was a prototype produced at Research Center COM by Christian Mikkelsen and Haiyan Ou.

Fig. 3.13 shows the BER curves in the back-to-back case and after transmission over 50 km. The transmission penalty for the label was around 2 dB, while the payload showed a higher penalty of approximately 6 dB. It is envisaged that a better sensitivity performance would be achieved when using an optimized demodulator and if a balanced-receiver was applied to the payload.

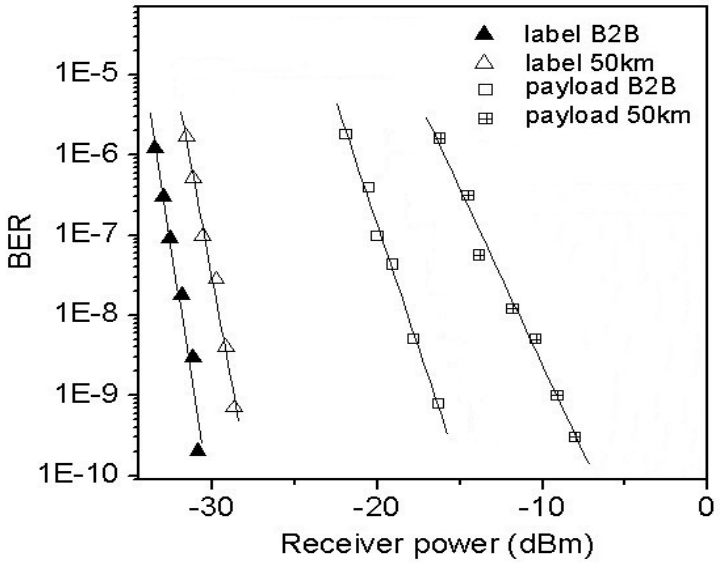

Fig. 3.13. *Measured BER results of transmission of DPSK/IM labelled signals.*

3.2 IM/FSK transmission

This section will deal with transmission of an FSK label over an IM payload. The optical FSK transmitter will be based on an integrated DFB laser in conjunction with an EAM as proposed in Section 2.2.1, while three different filtering configurations for the FSK receiver will be analyzed after transmission. These will be a fiber Bragg grating (FBG), an optical add-drop multiplexer (OADM) and a tunable Fabry-Perot filter (FPF). Transmission through different dispersion maps with various compensation schemes and fiber types will be investigated both numerically and experimentally for an the IM/FSK labelled signal. Cascadeability through multi-hop transmission will also be validated.

3.2.1 Numerical analysis

The analyzed simulation setup is shown in fig. 3.14. The DFB/EAM FSK transmitter was driven at 156 Mb/s, and its modulation depth was chosen to generate a spacing of 20 GHz. The 10 Gb/s payload data was then impressed on that signal by a MZM.

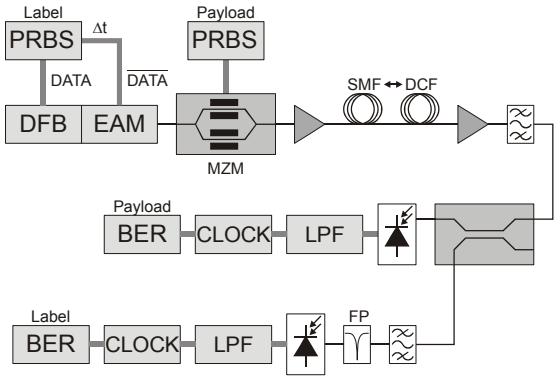

***Fig. 3.14**. Setup used for simulations on IM/FSK transmission (figure from [104]).*

After transmission, the signal was amplified and split equally between the payload and label receivers. The label signal was filtered by an optical band-pass filter that suppressed one of the frequency tones by 15 dB, while the noise figure of the amplifiers was set to 5 dB. The filters used for suppression of ASE as well as detection of FSK were modelled after commercially available components. The orthogonally modulated carrier was amplified and transmitted through 80 km of standard SMF, compensated by 12 km of DCF in various compensating schemes.

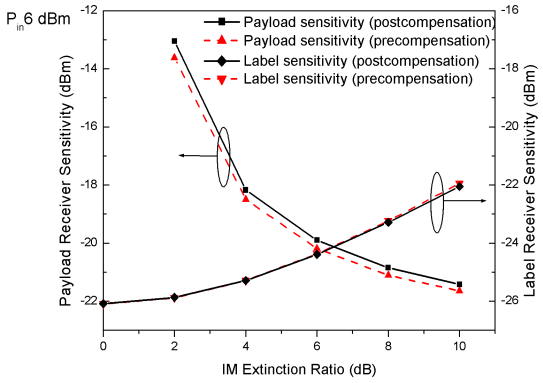

***Fig. 3.15.** Calculated influence of ER on payload and label receiver sensitivity for post- and precompensation.*

Fig. 3.15 shows the influence of the extinction ratio on the quality of the signal after transmission for a span input power of 6 dBm, by calculating the sensitivity for a BER of 10^{-9}. It shows that the performance was not greatly affected by transmission, as it compares well to the back-to-back results shown in fig. 2.38 of Section 2.2.3. The pre-compensation scheme showed a marginally better sensitivity for the payload.

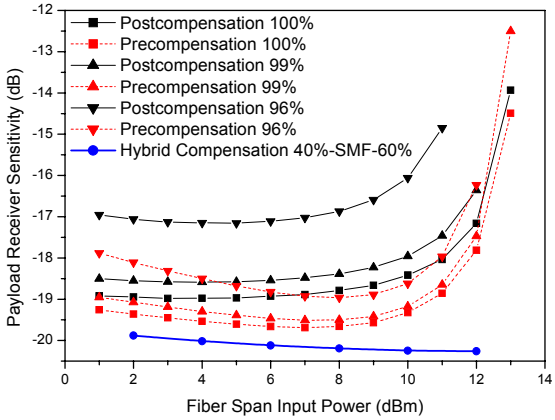

Fig. 3.16. *Calculated payload receiver sensitivity vs. input power for different compensation schemes.*

On the other hand, fig. 3.16 shows the dependence of the sensitivity of the payload on the span input power for different compensation schemes and compensation ratios. It can be observed that the compensation scheme had a significant influence on the payload sensitivity. A pre-compensated system achieved consistently better results for the payload than a post-compensated one. The difference in sensitivity between pre-compensation and post-compensation exceeded 2 dB in some cases. When the compensation ratio was reduced from full compensation, the performance was reduced (as opposed to the IM/DPSK modulation where under-compensating showed to have a positive influence on the performance of the system). Specially at high input power levels, the best results were achieved with a hybrid compensation scheme with 40% of the compensation before the SMF span.

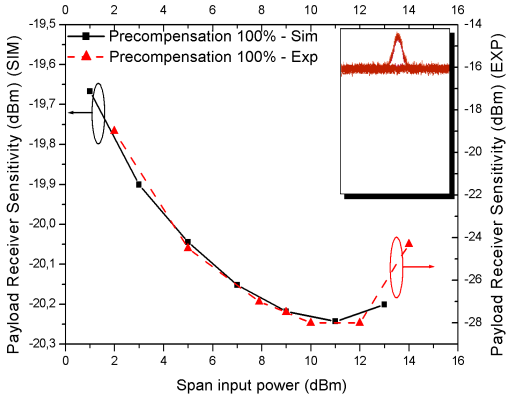

Fig. 3.17. *Comparison of laboratory and simulation results for 100% compensation. The inset shows the simulated intensity ripple of the FSK source.*

An optimum range of signal power launched into the fiber was found both in simulations and experiments. For the pre-compensating scheme, the payload receiver sensitivity had a minimum at approximately 8 dBm of input power. A lower input power did not provide a sufficiently strong signal to maintain the SNR, while excessive power caused the non-linear effects in the fiber to have a stronger impact on the signal. The label sensitivity was less influenced by the compensation scheme or by variations in input power. Simulations and laboratory experiments showed a very stable performance of the label signal, most likely due to the low bit-rate used for the FSK modulation.

The payload performance showed a qualitative agreement between simulations and experiments, as shown in fig. 3.17. The optimum power level of 11 dBm was also observable in the experimental results. The inset of fig. 3.17 shows the simulated residual ripple from the DFB/EAM FSK source, caused by the non-matched dynamic responses of the DFB and EAM that was discussed in Section 2.2.1.

3.2.2 Experimental results

This subsection presents the experimental results of transmission of IM/FSK labelled signals. Various types of compensation schemes and compensation ratios will be applied and compared. Different filtering schemes will also be validated for label detection. First, transmission over 88 km of hybrid-compensated SMF will be validated for this form of labelling. Next, various compensation schemes will be compared for a transmission link of 50 km of SMF. After that, various fiber types, compensation schemes and label bit-rates will be compared for transmission over 88 km links. Finally longer transmission spans will be demonstrated, employing different types of fibers.

Transmission over 88 km of SFM with hybrid compensation

In order to investigate the performance of the optical IM/FSK labelling scheme under transmission, a first transmission experiment was set up, consisting of an 88 km SMF transmission link, as shown in fig. 3.18.

Two pattern generators were used to generate a 2^{23}-1 PRBS payload pattern at 10 Gb/s and a 2^{7}-1 PRBS label pattern at 312 Mb/s. The label information was impressed upon the optical carrier at 1555.0 nm, through FSK modulation, while the payload information was added by using a MZM. The input power to the fiber was 10 dBm and the DCF was deployed in a hybrid dispersion compensation scheme, where its length was split equally before and after the transmission fiber.

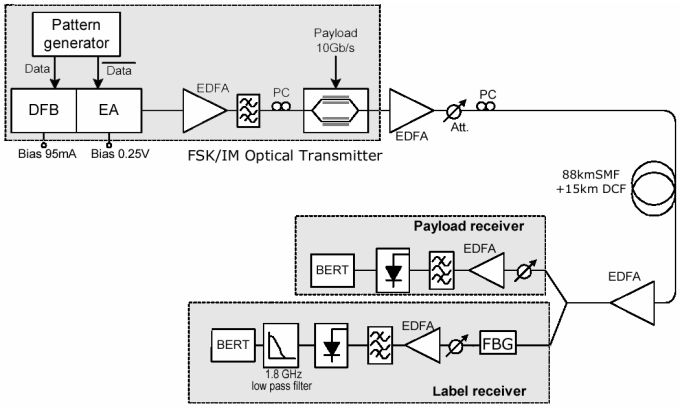

Fig. 3.18. *Experimental setup for the transmission of the orthogonally labelled IM/FSK signal.*

At the receiver the label was directly detected, while, an FBG was used to filter only a single tone of the FSK labelled signal, as described in Section 2.2.2. An electrical receiver with 1.8 GHz bandwidth was used for the detection of the demodulated-label data. The suppression ratio between the two optical tones after the FBG was measured to be 20 dB.

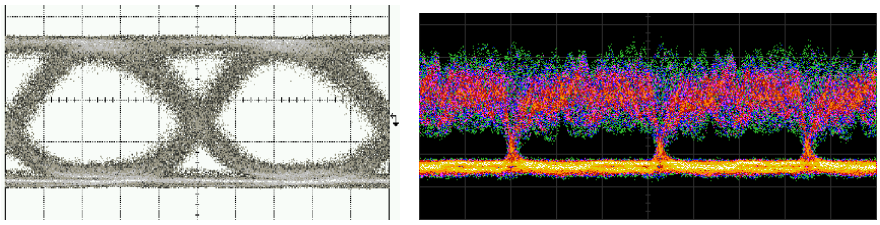

(a) 20 ps/div *(b) 1 ns/div*

Fig. 3.19. *Eye-diagrams of the received (a) payload and (b) label.*

Fig. 3.19 shows the eye-diagrams of the extracted payload and label after transmission. As indicated earlier, interference was introduced between the payload and label through intermodulation distortion, as shown in fig. 3.19 (b). A good trade-off between the label and payload performance after transmission could be achieved with nearly 6 dB of payload ER. Fig. 3.20 shows the BER curves of the signal for this ER. The transmission penalties for the label and payload were 2.2 dB and 1.2 dB respectively, which would validate the labelling scheme at the given settings with regard to transmission.

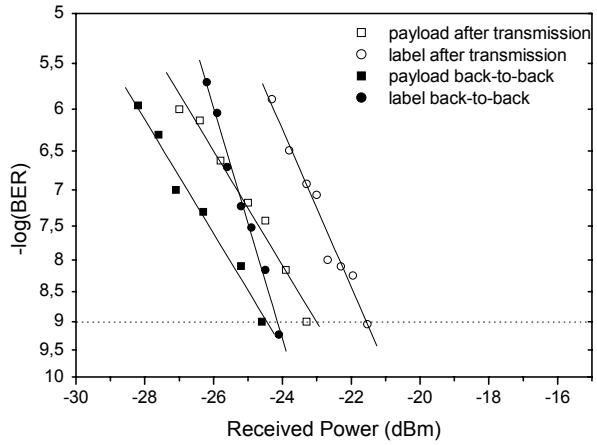

Fig. 3.20. *BER performance of the optically labelled signal after 88 km of transmission in SMF.*

Transmission over 50 km of SMF in various compensation schemes

With regard to varying the compensation schemes, the conclusions of the numerical analysis shown in Subsection 3.2.1 were supported through the experimental setup shown in fig. 3.21. The bit-rate was set to 312 Mb/s for the FSK label and to 10 Gb/s for the IM payload. The generation of the signals was equal to the ones discussed so far. FSK tone discrimination at the receiver was in this case achieved by the edge of the reflection of a fiber grating based OADM that also acted as a band-pass filter. The transmission span consisted of 50 km of SMF with a matching length of DCF. Both the pre-compensating the post-compensating schemes were evaluated.

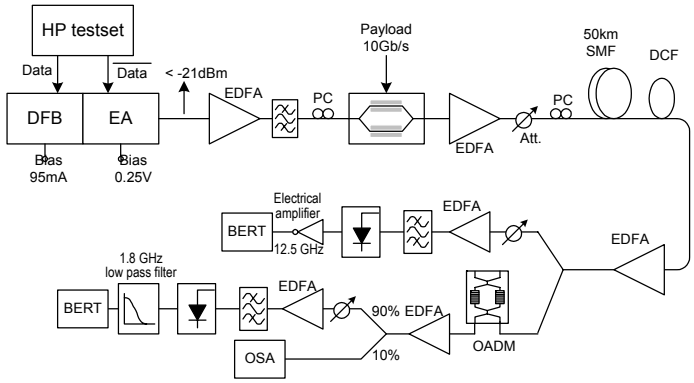

Fig. 3.21. *Experimental setup for the transmission of IM/FSK signals over a 50 km dispersion compensated span.*

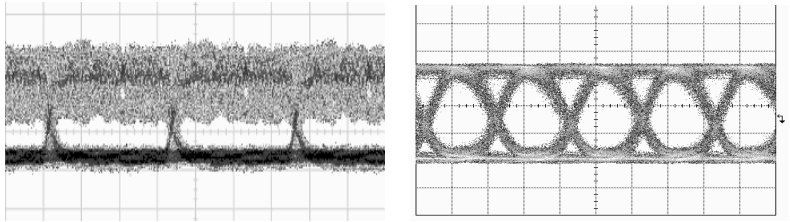

(a) 1 ns/div *(b) 50 ps/div*

Fig. 3.22. *Received eye-diagrams of (a) the FSK label at 312 Mb/s and (b) the IM payload at 10 Gb/s.*

Fig. 3.22 shows the eye diagrams of the received signals. As already discussed, in the FSK signal shown in fig. 3.22 (a), the 'one' level got greatly broadened by the influence of the intensity modulated signal. This broadening was directly dependent on the ER of the IM payload. The somewhat small label eye opening detected with a payload ER of 5 dB proved to be enough for label detection.

Fig. 3.23 shows the receiver sensitivity of the payload and label after transmission for the pre- and post-compensated schemes, as a function of the span input power. The results show a much better performance of the pre-compensating scheme, specially for the payload and at high power levels, which is in concordance with the numerical analysis. When the input power

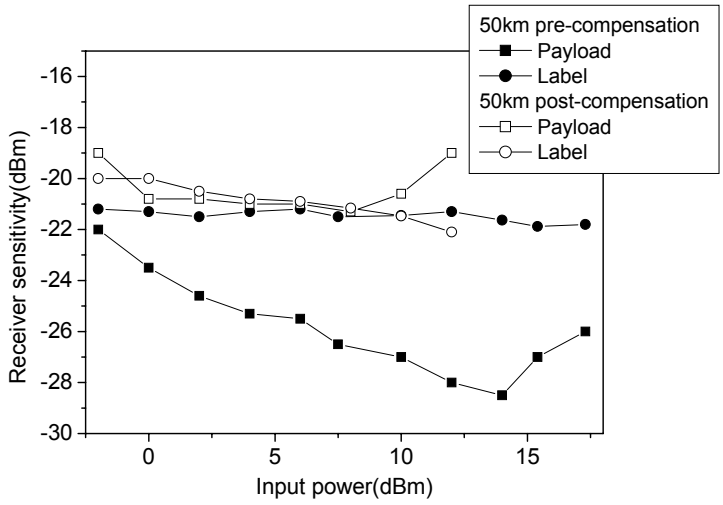

Fig. 3.23. *Receiver sensitivity of payload and label after transmission over 50 km of SMF for the pre- and post-compensating schemes.*

was set to 11.5 dBm, the difference in receiver sensitivity was as high as 9 dB. It is believed that the reason for this is that most of the non-linear effects occur in the first part of the fiber span, where the power is highest [106], [107], and the higher attenuation of the DCF would reduce the effective length and therefore the impact of nonlinearities [99]. The FSK label was much less affected by the compensating scheme. Pre-compensation showed a slightly better performance of about 1 dB for low levels of input power, while post-compensation appeared to perform better for power levels exceeding 10 dBm.

Fig. 3.24 shows the corresponding BER curves at an input power of 6 dBm. For the label (square marks), little difference is measured between the two schemes, both indicating roughly a 2 dB power penalty in their sensitivity compared to the back-to-back case at a BER of 10^{-9}. For the payload (triangles), on the other hand, the post-compensated transmission added 3.5 dB of penalty, while pre-compensation showed a far better performance. The reason for this enhanced performance (that also was observed in a less degree in the IM/DPSK transmission) is related to the different attenuation between SFM and DCF. As mentioned earlier, the higher attenuation of the DCF will reduce its effective length, which is where non-linearities are significant [99].

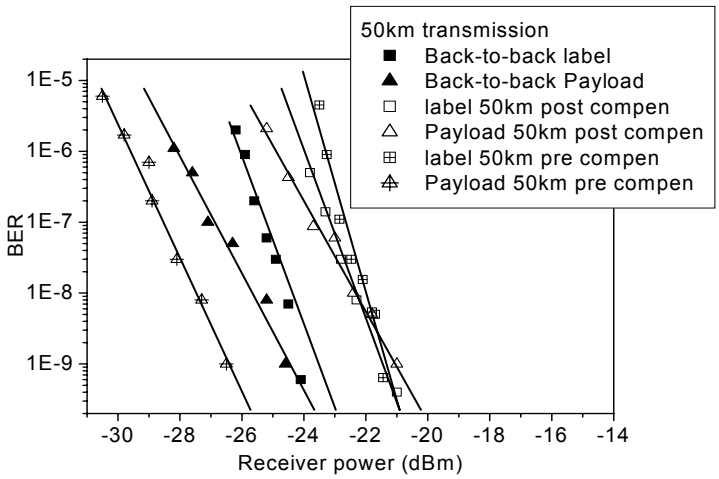

Fig. 3.24. *Bit error rates vs. received power for back to back, and 50 km transmission both with pre and post compensation.*

Transmission over 88 km for various fiber types, compensation schemes, compensation ratios and label bit-rates

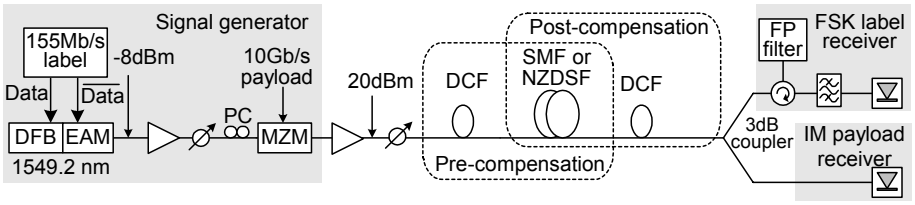

Fig. 3.25. *Experimental setup for the transmission of IM/FSK signals over 80 km of SMF or NZDSF.*

Besides the compensation scheme employed, the analysis performed in the last section for IM/DPSK labelling showed that the chosen type of fiber also has a strong impact on the performance of the system. In order to investigate this for the IM/FSK labelling scheme, the experimental system shown in fig. 3.25, was setup. It consisted of the same transmitter as in the previous sub-section, and a receiver that this time was based on a double optical filter stage that included a Fabry-Perot filter (FPF), which provided more than 15 dB of suppression ratio between the two FSK tones. The optical FSK label was sent at two different bit-rates, of 155 or 312 Mb/s, while the payload was kept at 10 Gb/s. The transmission link consisted of 80 km of either SMF or NZDSF with the appropriate compensation. The dispersion of the SMF, the NZDSF and the DCF were 16.9, 4.9 and -100 ps/nm/km, respectively.

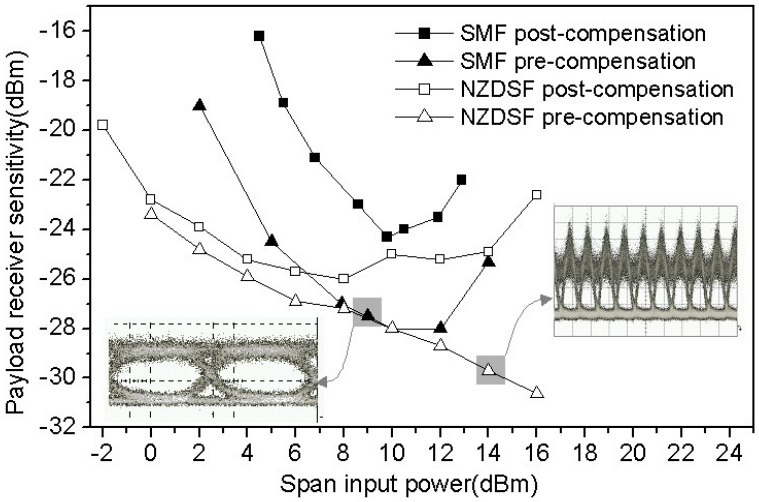

Fig. 3.26. *Receiver sensitivity of the payload as a function of span input power for different compensation schemes and fiber types.*

Fig. 3.26 shows how the position of the DCF, the fiber types and the span input power affected the payload performance through the 80 km transmission link. The performance is measured as the sensitivity for a BER of 10^{-9}, shown as a function of the span input power.

For the 10 Gb/s IM payload, an improved performance could be obtained in both fiber types by making use of pre-compensation. The NZDSF showed large tolerance to the span input power. At low power levels, the performance was degraded by the build-up of ASE noise from the amplifiers, but as the power was increased self-phase modulation in conjunction with dispersion degraded the payload. Between these two extremes an optimum input power at around 8 to 10 dBm was verified in most cases, although it also was observed that the payload sensitivity was still improving in the pre-compensated NZDSF case when the input power was further increased. However, these increased power levels resulted in intensity overshoots and distortion in the eye-diagram, which would likely be detrimental to later stages in the network. This effect is observable in fig. 3.27, which shows the eye-diagrams of the detected payload after NZDSF transmission at different power levels.

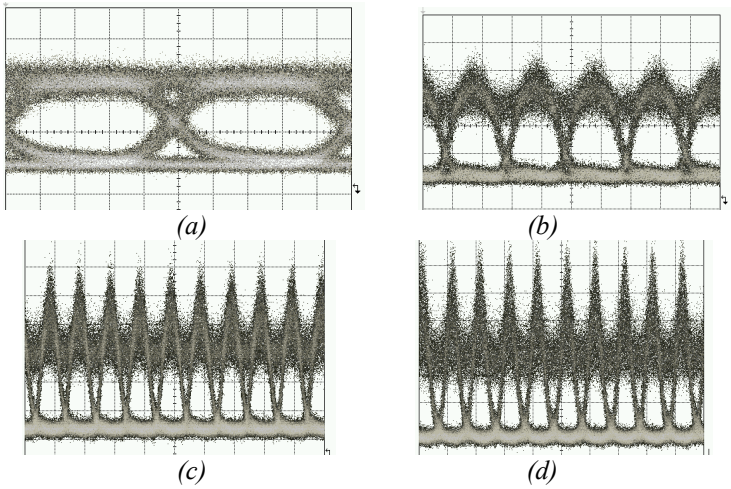

Fig. 3.27. *Influence of the span input power on the eye diagrams of a transmitted 10 Gb/s IM payload. (a) 9 dBm, (b) 12 dBm, (c) 14 dBm and (d) 17 dBm.*

Fig. 3.28 shows how the different types of compensation, the label bit-rates and the span input power affected the label performance after transmission over 80 km of SMF. It can be observed that for the label performance, almost constant sensitivity could be obtained when changing the input power and compensation schemes for both bit-rates, although the lower bit-rate performed better by almost 15 dB in all cases. The insets in fig. 3.28 show

the eye-diagrams of the detected label after transmission. Even with the superimposed payload information, the label-eyes were still open and allowed for error-free detection.

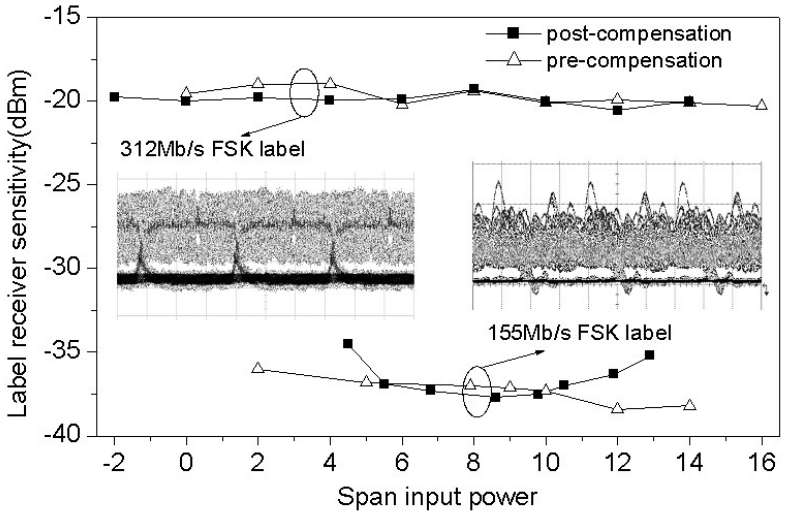

Fig. 3.28. *Receiver sensitivity of the label after transmission over 80 km of SMF, as a function of span input power for different compensation schemes and bit-rates.*

The system performance of the payload after transmission over SMF for different dispersion compensation schemes and ratios is shown in fig. 3.29. For the post compensation scheme, a slight under-compensation of about 2% improved the sensitivity by almost 5 dB at the minimum point corresponding

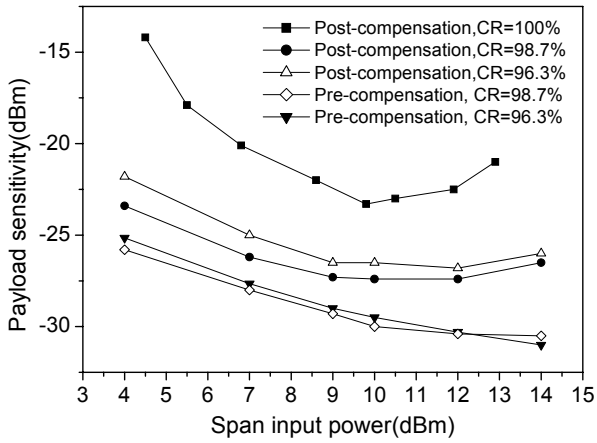

Fig. 3.29. *Receiver sensitivity of the payload as a function of span input power for different dispersion compensation schemes and ratios for SMF transmission.*

to an input power of 10 dBm. As the numerical results indicated, pre-compensation improved the performance of the IM payload considerably at all levels of input power, but even more at high power levels.

Fig. 3.30 shows the system performance of the label after transmission over SMF for different dispersion compensation schemes and ratios. It was found that 96% of compensation would result in roughly 1 dB penalty compared to full compensation. Post compensation achieved a better performance by about 1.5 dB at its best performance corresponding to an input power level of 9 dBm. However, all the measured sensitivities lay in a 3 dB range, showing a much smaller influence of compensation on the label than on the payload.

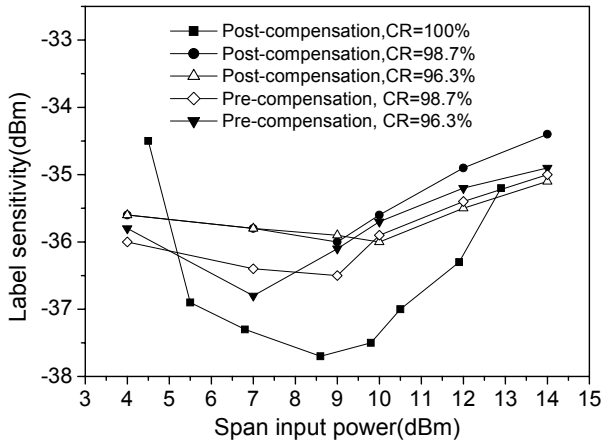

Fig. 3.30. *Receiver sensitivity of the label as a function of different dispersion compensation schemes and ratios.*

Transmission over 138 km of SMF and 160 km of NZDSF

In a real network, regular amplification of the signal is likely to take place for longer transmission links were no processing at a node would take place. Multi-span transmission of IM/FSK signals was also investigated over SMF and NZDSF. The longest reach of the SMF was 138 km, in the transmission link shown in fig. 3.31 (a), that included two pre-compensated spans and one post-compensated span, the length of which were 50, 44 and 44 km respectively. Between the spans, an amplifier was set to compensate for loss. The receiver sensitivity of the payload after transmission was measured to be -19.4 dBm, while the label showed a receiver sensitivity of -20.1 dBm, when the input payload ER was set to 4 dB.

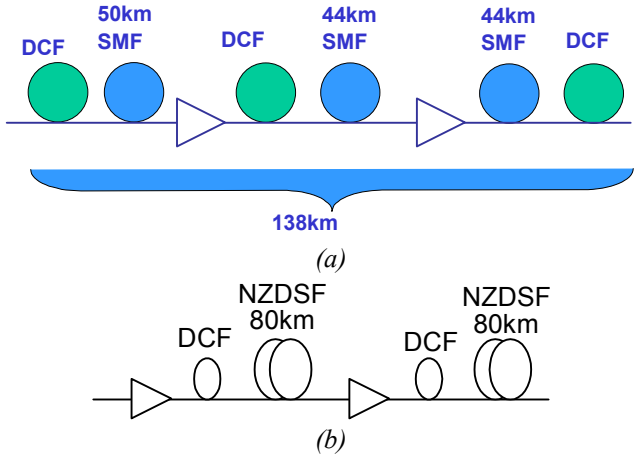

Fig. 3.31. *Transmission links over (a) 138km SMF, (b) 160km of NZDSF.*

For the NZDSF, the longest transmission achieved was 160 km, in a transmission link illustrated in fig. 3.31 (b), which consisted of two pre-compensated spans of 80 km each. The payload and label receiver sensitivities as a function of the input extinction ratio are shown in fig. 3.32 for the 160 km NZDSF transmission. It is noticeable that the point of equal sensitivity of the payload and label is shifted to a lower payload ER compared to the back-to-back case. The maximum tolerable ER for the payload in order to detect the label is also greatly reduced. It is envisaged that a too low extinction ratio could become a limiting factor for all-optical devices such as wavelength converters, label swappers and regenerators. Therefore network designers have to make a compromise in the choice of average distance between nodes when employing the IM/FSK labelling scheme. A scheme were the signal is not equally split between payload and label receiver, but favoured the label is believed to being able to contribute to partly alleviate this problem.

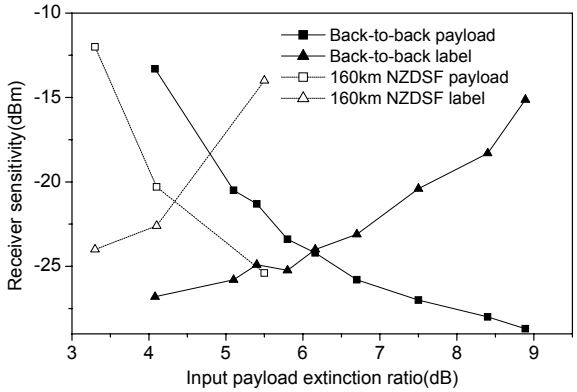

Fig. 3.32. *Receiver sensitivity versus payload extinction ratio for back-to-back and after 160 km transmission.*

3.2.3 Manchester-encoded transmission

The analysis performed in Section 2.4, showed that DC-balanced encoding of the payload could efficiently improve the modulation performance of the IM/FSK scheme. In order to confirm this improvement in a transmission link, an optical signal consisting of a 10 Gb/s Manchester-encoded IM payload and a 156 Mb/s FSK label was generated, and its performance evaluated after transmission over 80 km of compensated SMF.

The experimental setup is shown in fig. 3.33. After the DFB/EAM FSK source, a 20 Gb/s electrical 2:1 multiplexer (MUX) implemented the Manchester coding (MC) of the payload. When a 10 Gb/s payload data and its inverted data were simultaneously input into the MUX module with the same delay, the generated output signal consisted of the original data during the first half of the time slot, and a transit to the inverse data for the second half of the time slot, hence implementing MC in the electrical domain. This signal was then used to drive an intensity modulator with a nearly chirp-free performance. The generated signal was then transmitted over 80 km of SMF and 13 km of DCF with 3 dBm of input power.

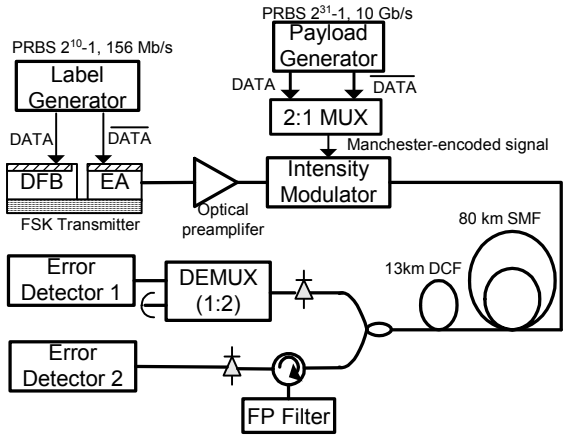

Fig. 3.33. *Experimental setup of a 10 Gb/s Manchester-encoded FSK-labelled optical signal transmission link.*

At the receiver node, the labelled signal was equally split, and in one arm was directly detected by a 20 GHz-bandwidth photodiode and decoded through an 1:2 electrical demultiplexer module. In the other arm, a Fabry-Perot filter with a 20 GHz full-width half-maximum bandwidth was used to achieve FSK demodulation by suppressing one tone by 8 dB.

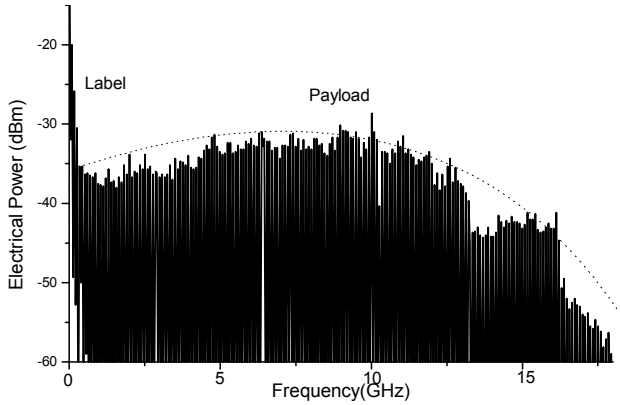

Fig. 3.34. *Electrical spectrum of the demodulated FSK label before the electrical filter.*

As discussed in Section 2.4.1, MC achieves a balanced intensity modulation of the payload by avoiding long strings of '1' or '0' bits, hence improving the performance of the label. In addition, since Manchester coding consequently allowed a high on-off extinction ratio of the IM payload, the payload could have a larger tolerance to the unwanted intensity ripples induced by the imperfect FSK generation. In this way, MC strengthened the robustness of the system.

Fig. 3.34 illustrates this performance improvement of the transmitted signal from a spectral point of view. As indicated by the dotted lines, MC reduced the spectral overlapping between the label and payload. Because of that, the received label had a SNR value – if the power of the payload is treated as 'noise' for the label – of about 20 dB, which resulted in a good performance when an appropriate electrical filter was used after detection.

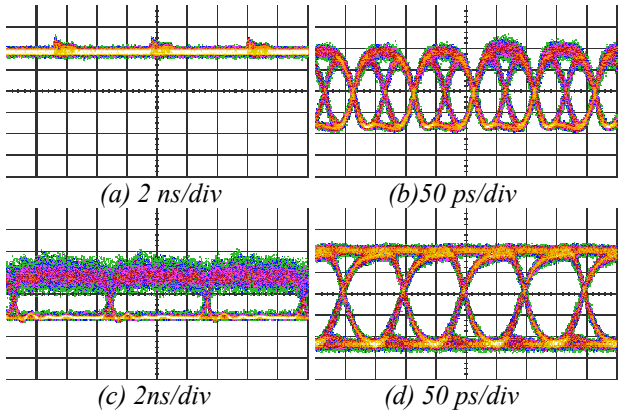

Fig. 3.35. *Eye-diagrams for an IM ER of 13 dB. (a) Intensity of the original FSK signal (b) FSK-labelled IM payload (c) demodulated label (d) decoded payload.*

Fig. 3.35 shows the eye-diagrams of the transmitted and received optical signals. As shown in fig. 3.35 (a), the generated FSK modulated signal had a nearly constant amplitude with some intensity ripples, due to the DFB/EAM source for FSK, as explained in Section 2.2.1. As the Manchester-encoded IM payload allowed an extinction ratio as high as 13 dB, the intensity ripples had a minor effect on the payload, as shown in fig. 3.35 (b). The received eye-diagrams of label and payload after transmission, shown in figs. 3.35 (c) and (d), present larger eye-openings than the non-coded IM/FSK signals presented earlier in this section.

BER measurements verified error-free transmission performance of both payload and label. The BER curves in fig. 3.36 (a) indicate that the penalty for FSK labelling the IM payload was only 0.5 dB at a BER of 10^{-9}, while the transmission penalty was about 0.7 dB. Conversely, fig. 3.36 (b) shows that for the label, the superimposed IM payload induced about 3.7 dB of penalty, while the transmission penalty was nearly 1 dB. It is believed that the label performance could be further improved through optimisation of the bandwidth of the electrical low-pass filter at the receiver.

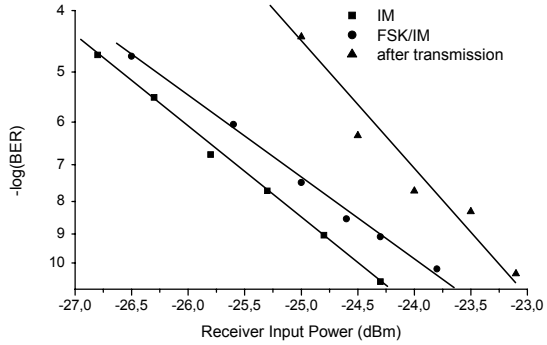

(a)

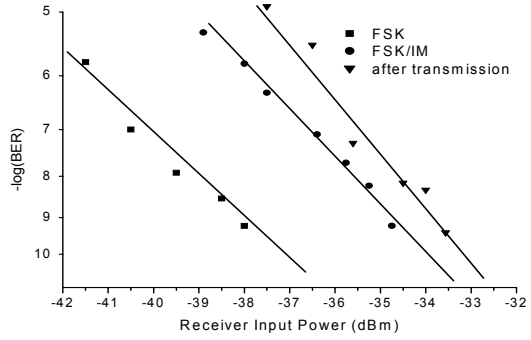

(b)

Fig. 3.36. *Measured BER performance of (a) payload and (b) label.*

3.3 CSS labelling transmission

The carrier-suppressed sideband (CSS) labelling method presented in Subsection 2.3 was validated in a transmission experiment over a 50 km span of SMF with corresponding compensation. The optically labelled signal consisted a 10 Gb/s payload and a 156 Mb/s label, generated in the way presented in the above mentioned subsection.

The experimental setup is shown in fig. 3.37. A dual-drive MZM with a 3 dB modulation bandwidth of 15 GHz and 3.5 dB of insertion loss, was configured to perform the carrier-suppressed modulation at the transmitter.

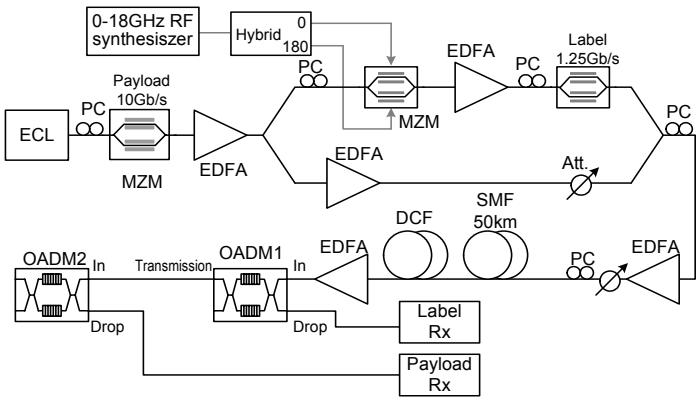

Fig. 3.37. *Experimental setup for the transmission of carrier suppressed sideband labelled signals.*

The DC bias difference of the two arms was exactly equal to the swing voltage V_π. An RF clock at 15 GHz was applied to a hybrid coupler, the two outputs of which had a π phase shift with respect to each other. These two outputs then drove the modulator to generate the two carrier-suppressed sidebands with a 30 GHz spacing. The other two MZ modulators functioned as intensity modulators to impress the 10 Gb/s payload and 156 Mb/s label information separately. The input extinction ratio of the payload was set to 4 dB, and an optical attenuator was inserted in the payload arm to adjust the payload to label power ratio. The generated signal at 1550 nm was then transmitted over 50 km SMF and a matching length of DCF.

At the end of the transmission link, two FBG-based OADM filters were used for the extraction of the payload and label from the transmitted signals. As explained in Section 2.3, the first OADM extracted one side-band carrying the label information, while the second OADM suppressed the other side-band leaving the payload for detection. Some residual label information

was still present in the payload due to the limited sharpness in the edge of the second OADM filter.

By changing the polarization state of the signal before the carrier-suppressing MZM and the input RF voltage, a suppression ratio of the carrier of up to 30 dB could be achieved, which ensured that no modulation distortion was added to the payload at the multiplexing stage. The payload to label power ratio could be adjusted by the attenuator, and was set to 5 dB.

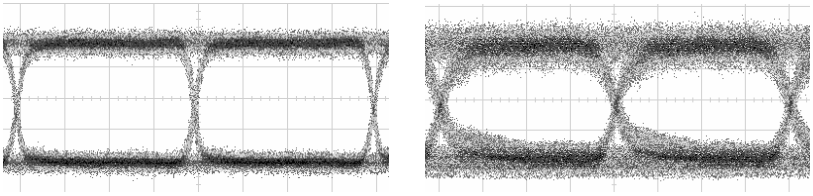

(a) 25ps/div *(b) 25ps/div*

Fig. 3.38. *Eye-diagrams of (a) original payload before multiplexing (b) extracted payload.*

The payload eye-diagrams before and after transmission are shown in fig. 3.38, which illustrates the degradation of the signal due to transmission and extraction. The BER curves shown in fig. 3.39 show that the penalties induced by the labelling and transmission are only about 0.3 dB for both label and payload.

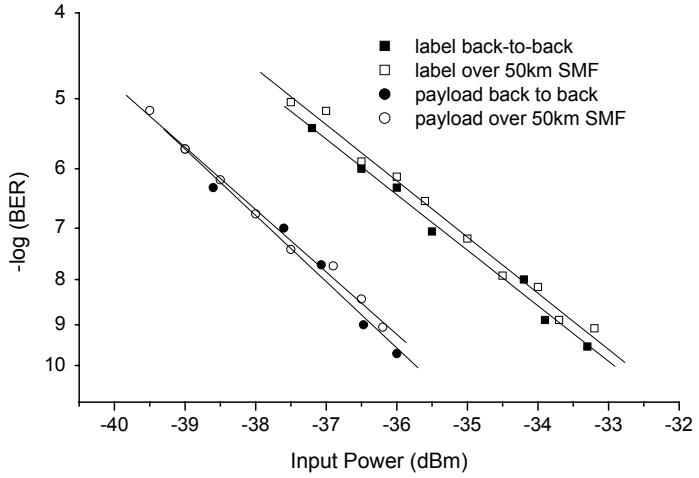

Fig. 3.39. *Measured BER curves after generation and transmission over 50 km of SFM, for a carrier suppressed sideband labelled signal consisting of a 10 Gb/s payload and a 156 Mb/s label.*

In order to asses the versatility of the labelling scheme with regard to bit-rate variations, a second transmission systems was built, consisting of the same 10 Gb/s payload, but accompanied this time by a 1.25 Gb/s label.

The experimental setup was the same as the one shown in fig. 3.37, and the transmission span was also identical. Because of the sharp edge of the OADMs, the achieved suppression of both the label with respect to the payload, and vice versa, was about 20 dB. It can be expected that an even larger suppression could be obtained if a narrow notch filter was deployed for payload and label separation.

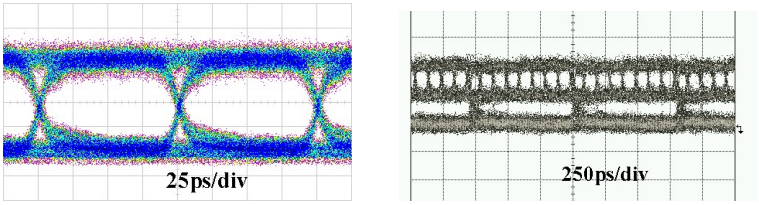

(a) *(b)*

Fig. 3.40. *Measured eye diagrams for (a) payload after 50 km transmission, (b) label after 50 km transmission.*

The eye diagrams for the transmitted signal are shown in fig. 3.40 and should be compared to the ones in the original eyes of the back-to-back case, shown in fig. 2.45 of Section 2.3, indicating that only a slight distortion was introduced by transmission.

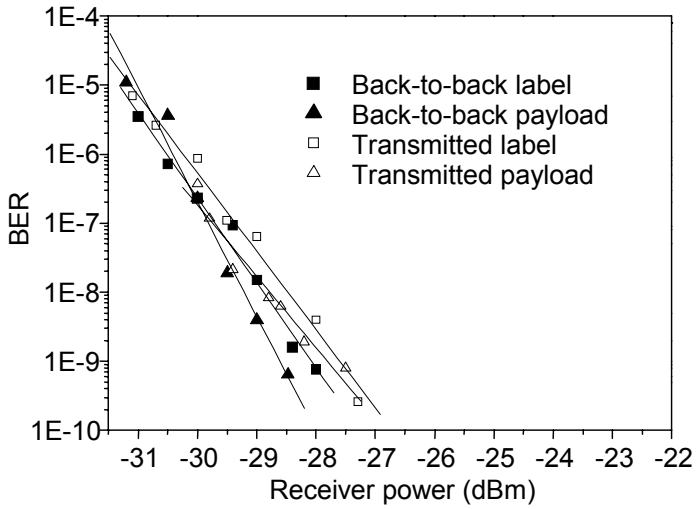

Fig. 3.41. *Measured BER performance for back-to-back and after 50 km transmission for a 10 Gb/s payload and a 1.25 Gb/s label.*

The measured BER performance of the 10 Gb/s payload and the 1.25 Gb/s label for back-to-back case and after 50 km of transmission are shown in fig. 3.41. As in the 156 Mb/s label case, error-free transmission of both the payload and the label can be achieved simultaneously, although the sensitivity was reduced by about 5 dB. After transmission, the label and the payload showed a low power penalty below 1 dB.

3.4 Chapter summary

In this chapter, the transmission of all-optical orthogonally labelled signals has been studied. Issues concerning dispersion schemes, dispersion ratios and input power levels have been investigated both numerically and experimentally. Compensation was performed according to three schemes: pre-compensation, where the compensation is located at the start of the transmission span; post-compensation, where it is located at the end; and hybrid-compensation, where it is split equally between the start and the end of the span. Various types of fibers have been assessed for the different labelling schemes. The results indicate that the transmission over hybrid compensated NZDSF could have the best performance.

For the whole of the chapter, the results are only comparable when they concern the same experimental setup, and have therefore been grouped in that way in the sections. For different experiments, the results are not directly comparable, as the detection scheme vary, the ER of the payload is modified, the filtering and amplifiers are diverse, and other parameters are changed. The focus has been set more on the demonstration of the feasibility of the transmission of the various labelling schemes, than on a comparison of their performance.

With regard to IM/DPSK labelling, numerical analysis were performed for a system with a 10 Gb/s payload and a 2.5 Gb/s label. For the payload, it was found that sub-compensating led to an enhancement in performance for all compensation schemes, while hybrid compensation showed the largest resilience tolerance to input power variations. The label, on the other hand, was always degraded by the use of dispersion compensating fibers, and its transmission properties were similar for the three schemes. The results suggested that the pre-compensation scheme would result in a smaller eye-opening penalty than post-compensation, which was later experimentally confirmed.

The labelling method was experimentally verified with regard to transmission over 50 km of SMF with post-compensation. This system showed a

sensitivity of -25 dBm for the label and -16 dBm for the payload. The received label eye diagram had the same multi-level structure, as was discussed in Chapter 2. Transmission over 80 km of NZDSF with pre-compensation showed a better performance, with less than 1 dB of transmission penalty. An optimum span input power was found around 8 dBm.

In order to be able to increase the ER of the payload while simultaneously ensuring DPSK reception, 8B/10B was employed on a 40 Gb/s IM payload and a 2.5 Gb/s DPSK label. The acceptable extinction ratio could be increased up to 12 dB resulting in a significant enhancement of the system performance.

The alternative DPSK/IM labelling scheme introduced in Section 2.1.2 was also experimentally validated with regard to transmission. Transmission over a 50 km SMF link of a 40 Gb/s DPSK modulated payload and a 2.5 Gb/s IM label, showed a transmission penalty of 2 dB for the label and 6 dB for the payload.

Simulations and experimental investigation of the transmission performance of IM/FSK orthogonally modulated signals using different compensation schemes, compensation ratios and fiber types, were also presented. The influence of span input power and extinction ratio on receiver sensitivity was evaluated. The numerical results for a 80 km fiber link revealed that also in the IM/FSK scheme, the pre-compensation scheme showed better performance for both the SMF span and a NZDSF span compared to post-compensation.

The labelling method was verified with regard to transmission on a system consisting of a 10 Gb/s IM payload with a 312 Mb/s FSK label. This signal was transmitted over 88 km of SMF in a hybrid-compensation scheme, after which the demodulation scheme for the label was based on a FBG. The penalty for this transmission was 2.2 dB for the label and 1.2 dB for the payload, and the sensitivities for a BER of 10^{-9}, -23.5 and -22.4 dBm, respectively.

An experimental comparison of the performance of the signal for the three compensating schemes was setup for a 50 km SMF transmission system, where the demodulation of the label was based on an OADM. For a 10 Gb/s payload and a 312 Mb/s label, the pre-compensating scheme showed a notoriously better result for the payload than the post-compensating scheme, while the label was little affected by the various schemes.

After that, the influence of the chosen fiber type was investigated over an 80 km fiber link with a label demodulation based on a FPF. An optimum of

the input power to the fiber of around 10 dBm for post-compensation and 14 dBm for pre-compensation was found when sending the signal over 80 km of SMF and NZDSF. This optimum reflected the trade-off between SNR and non-linearities in the fiber. The label showed again an almost constant label sensitivity with respect to span input power. A comparison on compensation ratios, confirmed some enhancement in performance by slight under-compensation.

Furthermore, transmission over 138 km of SMF and 160 km of NZDSF was achieved. For the 138 km SMF transmission the receiver sensitivities were measured to be -19.4 dBm for the payload and -20.1 dBm for the label, which translated into transmission penalties of 5.1 dB and 3.4 dB respectively. When using NZDSF, the maximum distance was raised to 160 km. However, an observed reduction of the optimum ER for the payload would need to be taken into account when designing such a system.

The enhanced performance of the IM/FSK labelling scheme when employing Manchester coding for the payload was assessed for transmission. A 10 Gb/s payload and a 156 Mb/s label were transmitted over 80 km of compensated SMF. The results showed that MC greatly enhanced the performance of the system at the cost of requiring twice the bandwidth for the payload.

Finally, the properties of the carrier-suppressed sideband labelling with regard to transmission were analyzed. A 50 km transmission system was setup for a signal consisting of a 10 Gb/s payload and a 156 Mb/s label, which resulted in less than 1 dB of power penalty for both payload and label. When increasing the label bit-rate to 1.25 Gb/s and using the same transmission link, the penalty remained below 1 dB, clearly demonstrating the feasibility of this scheme.

In conclusion, the experimental results suggest that an optimized transmission through network nodes would preserve the orthogonally modulated signals. The best choice for transmission dispersion design would be NZDSF in a hybrid- or pre-compensation scheme, while the optimum input power and payload ER have to be adjusted for each transmission link.

Chapter 4

WDM transmission of orthogonally labelled signals

The results presented in previous sections show that some trade-offs have to be made to provide the maximum receiver sensitivity for both the payload and the label. Obviously, in a WDM system these parameters and trade-offs also have to be taken into consideration. But on top of that, signals could be degraded through fiber non-linearities and the filtering schemes employed in multiplexing and demultiplexing of channels should be optimized in order to avoid further degradation [68].

In this chapter, the transmission of orthogonally labelled signals in a WDM environment will be studied. First, a numerically evaluation on the feasibility of WDM transmission of orthogonally labelled IM/FSK signals will be presented. The main addressed issues will be multiplexing, filtering and transmission impairments.

In the second section, the numerical results will be verified with regard to arrayed waveguide grating (AWG) detuning tolerance and wavelength channel spacing. After that, an 80 km eight-channel WDM transmission system will be implemented, in which one channel will be IM/FSK labelled and the other seven channels will be conventional intensity modulated at 10 Gb/s. This will be compared to a similar setup where the intensity of the signals will be Manchester encoded. In another implementation, a fully IM/FSK 3 channel transmission over 80 km of standard single-mode fiber (SMF) will be implemented using various types of sources which were presented in Section 2.2.1. Finally, a WDM transmission employing the IM/DPSK labelling format will also be validated in conjunction with 8B/10B coding of the payloads.

4.1 Numerical analysis

This first section presents numerical results on the limitations introduced by WDM systems with regard to orthogonally labelled IM/FSK signals. A first simulation will analyze the characteristics of multiplexers and demultiplexers used at transmitter and receiver. Then the limitations to filter detuning in the system are identified. Finally, an 8 channel WDM transmission systems is analyzed.

Multiplexing and demultiplexing

One of the parameters that would need to be optimized in a WDM IM/FSK system would be channel spacing [68]. The tolerable bandwidth of the filters used in multiplexing and demultiplexing would be related to this parameter. A back-to-back simulation was performed for a 10 Gb/s IM payload and a 156 Mb/s FSK label, varying the channel spacing from 50 to 100 GHz. The degradation of the signals was lower than 1 dB with respect to these parameters and ranges. Fig. 4.1 shows the payload and label receiver sensitivity as a function of channel spacing when filters of 40 GHz of bandwidth were used for de-multiplexing.

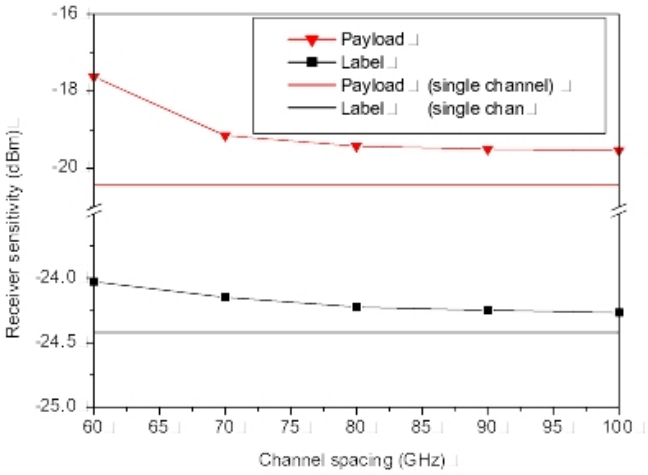

Fig. 4.1. *Back-to-back performance of two multiplexed channels compared to the performance of a single channel.*

It was found that the payload information could not acceptably be detected for a channel spacing of less than 60 GHz, given that for lower values of channel spacing, the intensity modulation side-lobes began to overlap introducing inter-channel cross-talk. On the other hand, the label did not have

this lower limit on channel spacing. Its receiver sensitivity was degraded by less than 1 dB, even in the case when the channel spacing was reduced to 50 GHz. The label performance only started to decrease for channel spacings of less than 20 GHz, which corresponded to the spacing of the FSK tones.

Filtering induced limitations

In an WDM optical network the labelled signal is likely to traverse several optical nodes from the source to the destination. Each WDM channel would be filtered out at each node for independent detection of the label. The retransmitted payload, would be filtered several times, so the degradation of the signal would accumulate from one node to the next.

In order to assess the potential degradation of the IM/FSK orthogonally labelled signal by filter cascading, a simulation using several filters was carried out. A 6 dBm IM/FSK signal was transmitted through ten first-order Gaussian tuneable optical band-pass filters, the bandwidth of which was varied between 40 and 60 GHz. The results are presented in fig. 4.2.

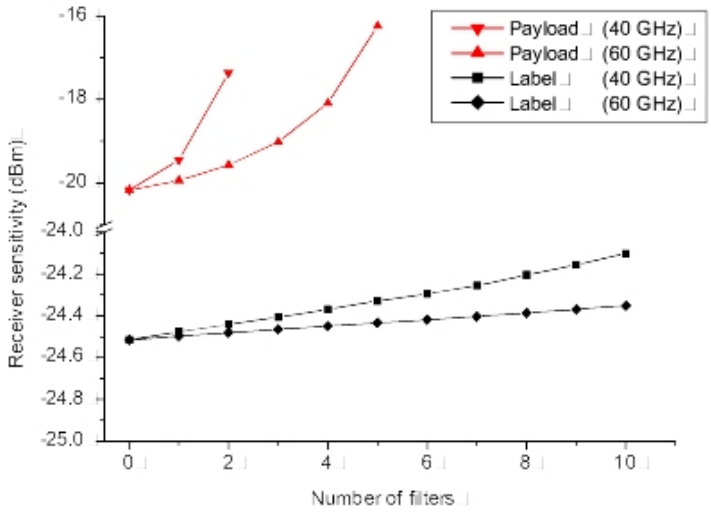

Fig. 4.2. *Payload and label receiver sensitivity vs. number of traversed filters with bandwidth of 40 and 60 GHz.*

For a 40 GHz filter bandwidth the payload could be detected with a BER value of less than 10^{-9} only after two filters. At this point the a receiver sensitivity penalty was 2.8 dB. When the bandwidth was increased to 60 GHz the payload could be adequately detected after five cascaded filters, after which, the penalty was 3.9 dB. The label was more tolerant to filtering and

could be received with a BER of less than 10^{-9} after all ten cascaded filters with a negligible penalty.

Furthermore, for the performance of a network, if some misalignment in the center frequency of the filters occurs, the amplitude of one of the FSK tones will experience a larger limitation than the other. The resulting imbalance would convert the FSK signal into an intensity modulation, and thus reduce the OSNR of the payload. Fig. 4.3 shows the numerical results with regard to payload and label receiver sensitivities as a function of filter detuning, when a single first order Gaussian filter with a 60 GHz bandwidth is employed.

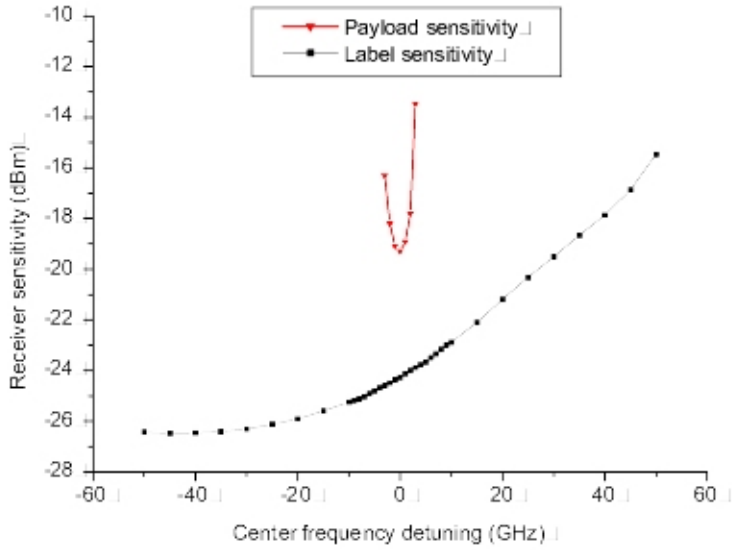

Fig. 4.3. *Payload and label receiver sensitivities vs. filter detuning.*

The results show that the payload could only tolerate a detuning in the range of 3 GHz, which puts a stringent requirement on the stability of the components in the system. The label was more tolerant to detuning. As the demodulation at the receiver was set to select the lower FSK tone, the performance was even enhanced when the misalignment of the filter was to the same side. A higher penalty was obviously observed when the detuning of the filter and the receiver each suppressed a different FSK tone.

If more than one filter were to be cascaded and all filters were detuned by the same amount, the influence would be even more pronounced. In the case of four cascaded filters, a detuning of only 1 GHz was found to be tolerable in order to be able to receive the payload with a BER of less than 10^{-9}. However, if the detuning in each filter would be random, the resulting signal

spectrum preserves a similar power in both FSK tones and thus, the power penalty with respect to the aligned filters is negligible.

WDM transmission

This section presents the numerical results of the transmission of eight IM/FSK channels in a WDM system. The output of eight IM/FSK transmitters with various channel spacings was multiplexed, amplified with a amplifier noise figure of 5 dB and transmitted through 80 km of fully pre-compensated SMF. The attenuation of the SMF was 0.19 dB/km and its dispersion 16.5 ps/nm/km at 1550 nm. The DCF had an attenuation of 0.6 dB/km and a dispersion of -80 ps/nm/km. After transmission, the signal was re-amplified, demultiplexed and detected. The multiplexer and demultiplexer consisted of 8 third order Bessel filters with a bandwidth of 40 GHz. The IM ER of all channels was set to 6 dB, while the average input power to the transmission link was varied from 3 to 15 dBm.

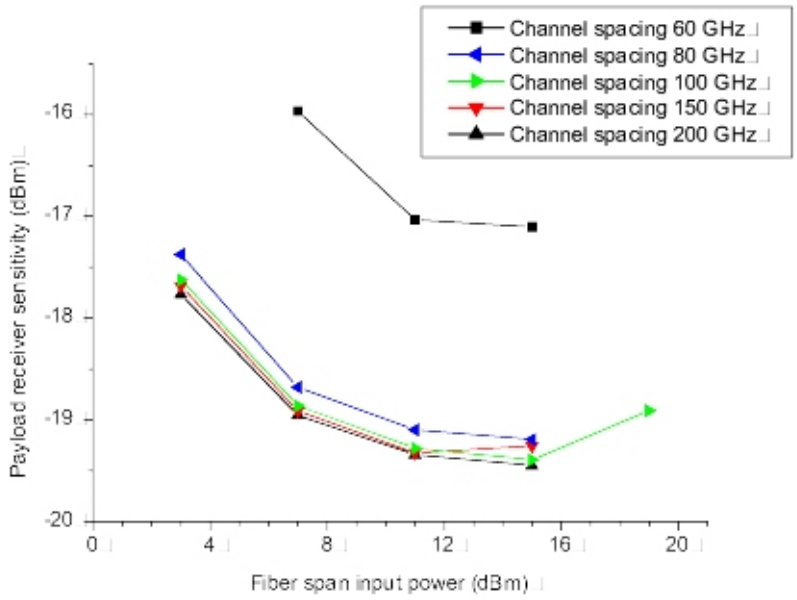

Fig. 4.4. *Payload receiver sensitivity vs. fiber span input power for various values of channel spacing.*

Fig. 4.4 shows the payload receiver sensitivity as a function of total input power to the fiber span, for various degrees of channel spacing. The results show that the transmission of 8 channels, spaced by 200 GHz, introduced a payload receiver sensitivity degradation of less than 1 dB compared to a single channel. The source of the penalty is most likely the filtering effect in

the multiplexer discussed in the previous subsection. The sensitivity curve had the same shape as in the case of single channel transmission, exhibiting a minimum for an input power of 15 dBm, which was 9 dBm higher than for simulations done for the single channel case. The shift in power optimum was caused by the fact, that in the WDM simulation the power of all channels was taken into account. The power of the individual channel at the sensitivity optimum was approximately 6 dBm, which then is in concordance with the single channel simulation results (see Section 3.2.1). As the channel spacing was reduced down to 80 GHz, the receiver penalty was negligible, and even for a channel spacing of 60 GHz, the sensitivity showed still to be within 2 dB.

4.2 Measured WDM system limitations

The previous section showed how filter detuning may strongly affect the system performance. In order to verify these numerical findings, in this section, the impact of channel spacing and AWG detuning on system performance will be experimentally investigated, followed by a first approach to the identification of channel-spacing limitations.

Arrayed-waveguide-grating (AWG) detuning tolerance

Arrayed-waveguide-gratings can be used to multiplex and demultiplex wavelength channels in WDM transmission systems [68]. As discussed in the previous section, in order to design an operational WDM network, the impact of laser frequency drift and optical filter stability should be taken into consideration. Compared with a conventional IM signal, the IM/FSK signal usually has a broadened spectrum due to the imposed FSK modulation. Therefore, imperfect alignment between the labelled channel and the AWG transfer function center frequency will cause an FSK to IM conversion that will induce crosstalk from the FSK label to the IM payload.

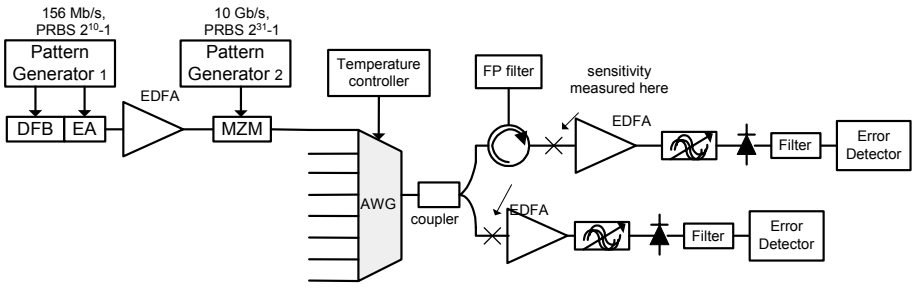

Fig. 4.5. *Experimental setup for measuring AWG detuning tolerance.*

The experimental setup for measuring the impact of AWG detuning on system performance is shown in fig. 4.5. A DFB/EAM source generated a 156 Mb/s FSK signal. An IM payload at 10 Gb/s was then imposed through intensity-modulating a MZM. The IM ER was set to 6 dB and the center wavelength of the signal was 1549.2 nm. This IM/FSK signal was first sent through a 8-channel AWG with a 3 dB bandwidth of 0.7 nm, was then split by an optical coupler and detected by a 10 GHz bandwidth receiver for the IM payload and a 600 MHz bandwidth receiver for the FSK label.

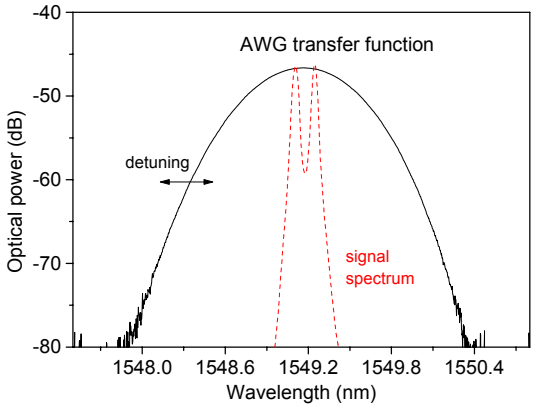

Fig. 4.6. *Measured AWG transfer function represented together with an IM/FSK signal spectrum.*

The channel spacing of the AWG was 200 GHz, and through temperature-control, the center wavelength of each channel could be detuned up to 100 GHz. The AWG used in the setup had a Gaussian shape with nearly 80 GHz of 3 dB bandwidth, as shown in fig. 4.6.

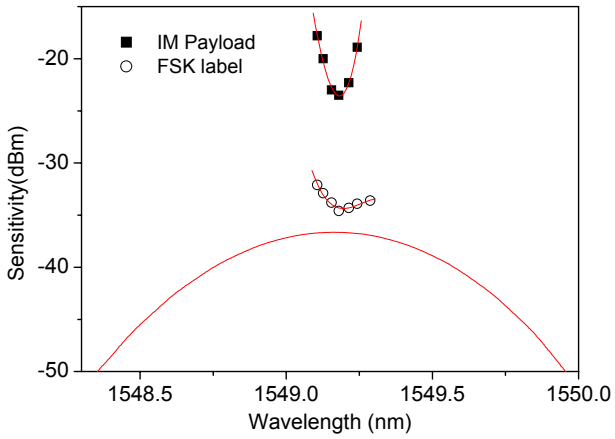

Fig. 4.7. *Measured sensitivity of detuned payload and label in the presence of AWG.*

The impact of filter detuning can be observed in fig. 4.7. The experimental results show a high level of similarity with the numerical results shown in fig. 4.3 for the payload. The label results appear to have a somewhat smaller degree of tolerance to the detuning of the AWG than predicted by the numerical results. This is believed to be due to the fact that the OSNR was worse for the experimental setup than in simulations.

The reduction in system performance is also observable in fig. 4.8, that shows the eye-diagrams of the received 10 Gb/s IM payload signal. When detuning the channel center wavelength, the two FSK tones of the IM/FSK signal at the output of the AWG would no longer be of equal amplitude, hence inducing intensity fluctuations on the signal and degrading the performance of the IM payload.

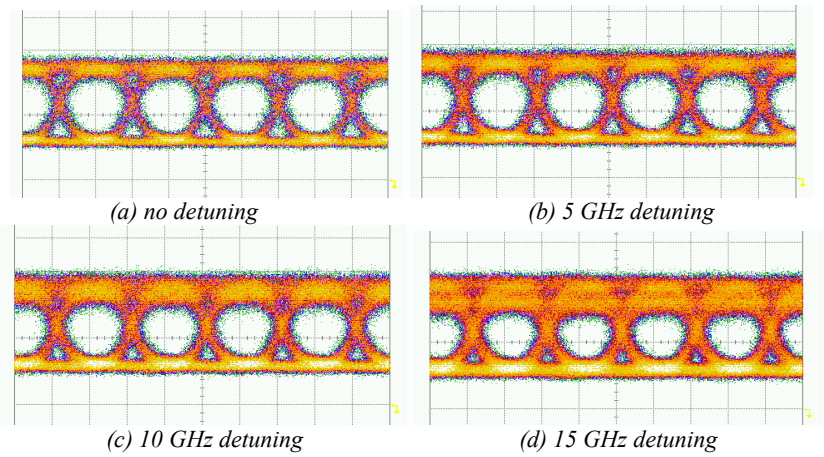

Fig. 4.8 *Eye-diagrams of the optical payload in the presence of AWG detuning. Horizontal scale is 50 ps/division.*

The filter detuning had a lower impact on the performance of the FSK label, where the power level of the tones could be increased or decreased during FSK demodulation. This is reflected in the lower slope of the sensitivity curve of the label, shown in fig. 4.7.

A more detailed plot of the measured receiver sensitivity induced by AWG detuning is shown in fig. 4.9. From it, it is observable that in order to induce at the most 1 dB of receiver power penalty for the IM payload, the center wavelength of the AWG should be kept within 0.08 nm (i.e. 10 GHz) of its original value. Given that the tone spacing of the FSK label was set to 20 GHz, this result is not surprising, as a 10 GHz detuning would mean centering the filter on one of the FSK tones, thus converting the label into amplitude interference.

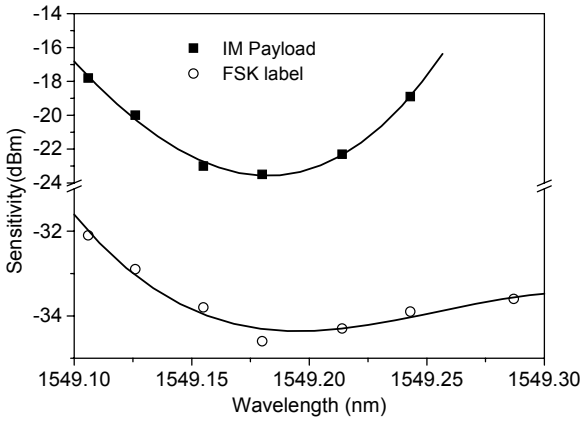

Fig. 4.9. *Receiver sensitivity for the IM payload and FSK label as a function of the AWG center wavelength.*

As the numerical results of the previous section indicated, when the IM/FSK signal is transmitted through a number of cascaded filters, the requirement on filter detuning would become more stringent than for a single filter. This would happen when the signal is re-transmitted from node to node in a labelled network. Fig. 4.10 shows the experimental setup used to investigate the IM/FSK signal performance under filter detuning at several network nodes. The same AWG as in the previous experiment was placed into a loop that included a dispersion-compensated 80 km SMF link.

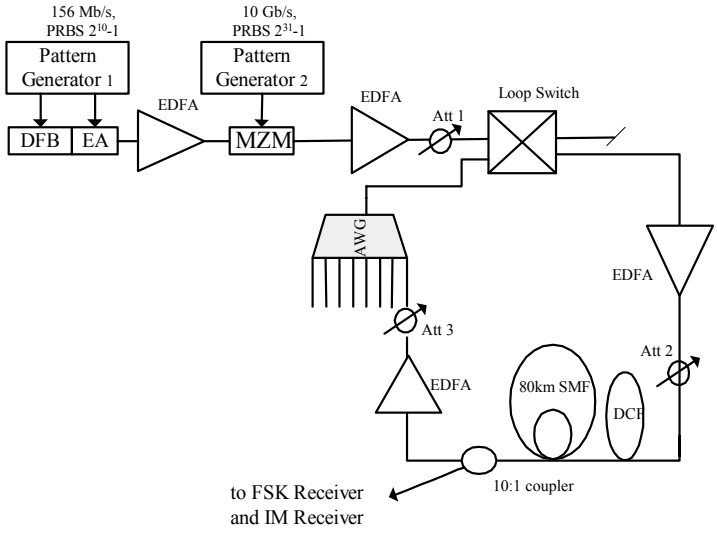

Fig. 4.10. *Experimental setup for the investigation of the performance of a detuned AWG in a re-circulating loop experiment.*

The experiment would replicate the situation of re-transmitting the IM/FSK signal through several network nodes that would be 80 km apart. No label swapping was performed, as the focus was set on the impact of cascaded filter detuning.

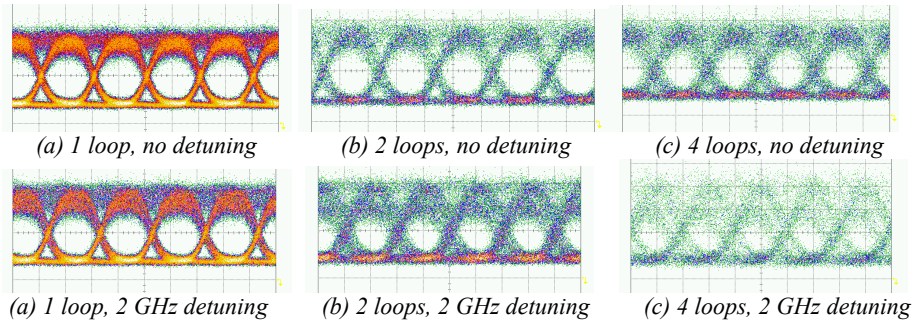

Fig. 4.11. *AWG detuning performance in a loop experiment (50 ps/div).*

As expected, and shown in fig. 4.11, the IM/FSK signal tolerance to AWG detuning was further reduced in a cascaded AWG transmission link. When the IM/FSK signal was sent through 4 AWGs, the maximum acceptable frequency detuning was 2 GHz in order to ensure error-free performance. In a real network, this limit would only exist if the detuning was equal in the filters of all nodes. In practice, the detuning of filters would probably happen in a random way and the detrimental effect of each one would mostly be cancelled out by the average of all detuned filters in the system. This would result in higher losses, but not in label to amplitude conversion. The stringent requirement on AWG detuning could also be relaxed through using a flat-top pass-band AWGs or by reducing the FSK tone spacing of the optical label.

Channel spacing

The allowable spacing of the IM/FSK signal to a neighbouring channel was investigated, in order to verify the performance of the IM/FSK labelling method in a conventional WDM system.

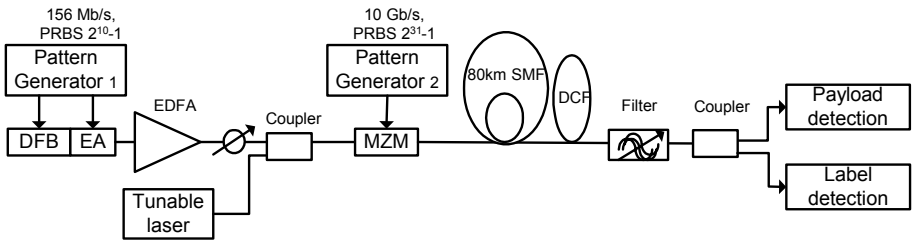

Fig. 4.12. *Experimental setup for measuring the impact of channel spacing.*

In the experimental setup shown in fig. 4.12, the 156 Mb/s FSK signal generated by a DFB/EAM source, was multiplexed with the output of a tunable laser, through a 3 dB coupler. The 10 Gb/s payload data generated by a PRBS source with a sequence length of 2^{31}-1, was then imposed on both channels by a low-chirp intensity modulator set to induce 6 dB of ER on the intensity modulation. After the modulator, the signals were transmitted through 80 km of SMF, which would de-correlate the signals with respect to the intensity modulation. At the receiver end, an optical tunable filter was used to demultiplex the wavelength channels for detection.

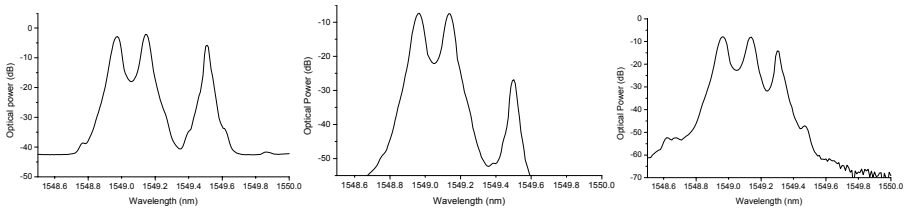

(a) *(b)* *(c)*

Fig. 4.13. *Spectra of multiplexed/demultiplexed IM/FSK signals. (a) Multiplexed channels with 50 GHz spacing. (b) Demultiplexed channels with 50 GHz spacing. (c) Demultiplexed channel with 30 GHz spacing.*

Obviously, the allowable channel spacing was mainly determined by the spectral bandwidth of the IM/FSK signal and by the bandwidth of the optical filter. In the experiment, the 3 dB bandwidth of the filter was around 0.5 nm. Through adjustment of the center wavelength of the optical filter, a demultiplexed channel-suppression ratio of 20 dB could be obtained for a 50 GHz channel spacing, while only 5 dB was obtained for a 30 GHz channel spacing, as indicated in fig. 4.13. With 30 GHz of channel spacing, the broad spectrum of the IM/FSK signal also overlapped with that of the neighbouring channel, which induced the severe interference noise observed in fig. 4.14. The IM/FSK label method should therefore be applied to WDM systems with a channel spacing of 50 GHz or more at the given bit-rate, which is in concordance with the previously presented numerical results.

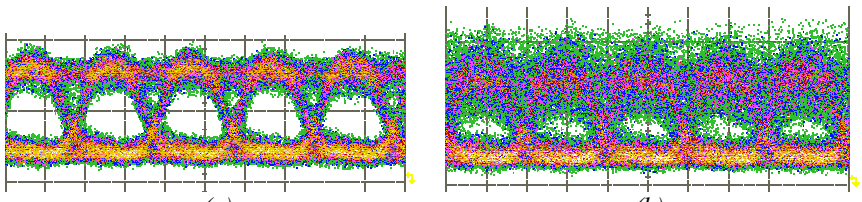

(a) *(b)*

Fig. 4.14. *Measured eye-diagrams for the IM payload with a channel spacing of (a) 50 GHz and (b) 30 GHz (50 ps/div).*

Fig. 4.15 shows the measured BER curves for a channel spacing of 50 GHz. The pure IM channel had obviously a clearer intensity waveform and a narrower spectral bandwidth. Compared to the IM/FSK signal, its receiver sensitivity presented a 6 dB improvement. The whole system performance was not noticeably changed when the channel spacing was increased beyond 50 GHz.

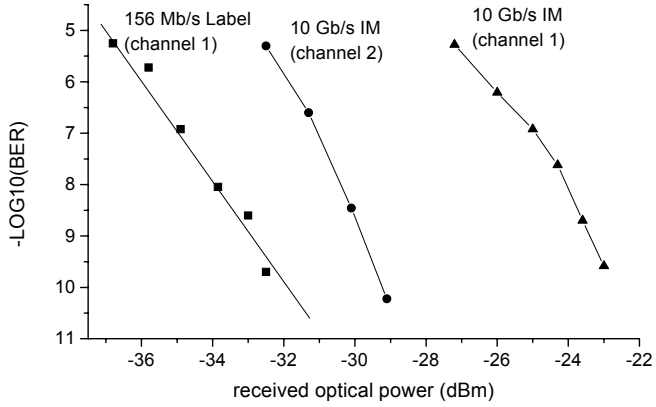

Fig. 4.15. *Measured BER curves for 50 GHz channel spacing. Channel 1 is orthogonally modulated while channel 2 is only intensity modulated.*

In this experiment, only one channel was modulated in the IM/FSK format while the other was kept in the conventional IM format, due to the availability of a single FSK source. If neighbouring channels were all in the IM/FSK format, it is estimated that the crosstalk between the channels would be increased due to the broadened spectral width. Considering the spectral bandwidth of the optical IM/FSK signal, the FSK tone spacing may be further optimized for a 50 GHz channel spacing WDM system, while upgrading to a 100 GHz WDM system would not present too much of a technical challenge.

4.3 WDM transmission of IM/FSK labelled signals

In this section, the experimental results on an eight-channel WDM system with a 200 GHz channel spacing in which one channel is IM/FSK labelled will be reported. After that, the benefits of encoding the intensity modulated data stream will be validated for such a WDM transmission system. Finally, a three-channel IM/FSK system with a 100 GHz channel spacing will be studied.

One IM/FSK channel with seven IM channels

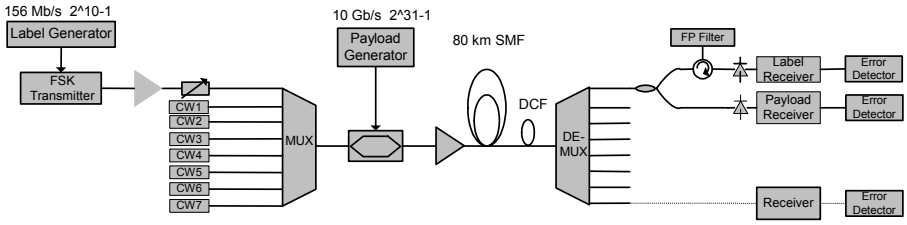

Fig. 4.16. *A WDM transmission system consisting of one IM/FSK channel and seven IM channels.*

As shown in fig. 4.16, the FSK signal generated by a DFB/EAM laser was multiplexed with the outputs of seven CW DFB lasers in an 8-channel AWG. The payload data was generated by a PRBS source with a sequence length of 2^{31}-1, imposed simultaneously on the eight channels by a low-chirp intensity modulator set to give 6 dB of ER on the intensity modulation. After the modulator, the signals were transmitted through a dispersion-compensated 80 km standard fiber link, which de-correlated the signals in the time domain, as full compensation was only achieved for a single wavelength. At the receiver, another AWG was used to demultiplex the wavelength channels, that were finally detected for BER measurements.

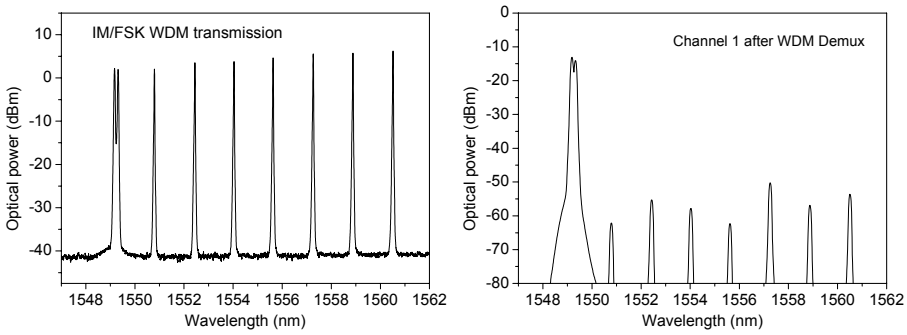

(a) *(b)*

Fig. 4.17. *Spectra of the (a) multiplexed and (b) demultiplexed channels.*

As indicated by fig. 4.17 (a), the eight channels covered the wavelength range between 1549.3 nm and 1560.6 nm, with a 1.6 nm (200 GHz) channel spacing. The IM/FSK signal was modulated on the first channel around a center wavelength of 1549.3 nm. The effective channel suppression ratio at the output of the wavelength demultiplexer was more than 40 dB, as shown in fig. 4.17 (b).

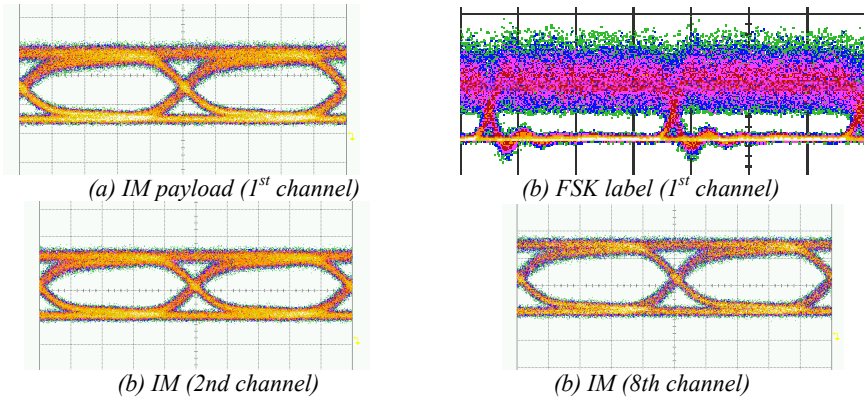

(a) IM payload (1st channel) *(b) FSK label (1st channel)*

(b) IM (2nd channel) *(b) IM (8th channel)*

Fig. 4.18. *Eye-diagrams of the received signals.*

The relatively high value of the channel spacing compared to the spectral bandwidth of the signal, resulted in the wavelength multiplexing and demultiplexing processes adding little degradation to the whole system. The transmission over 80 km of fiber also induced negligible degradation to the system performance. Fig. 4.18 presents the eye-diagrams of different wavelength channels, while fig. 4.19 shows the BER curves of the corresponding wavelength channels. Both figures confirm the numerical results of channel spacing obtained in the previous section.

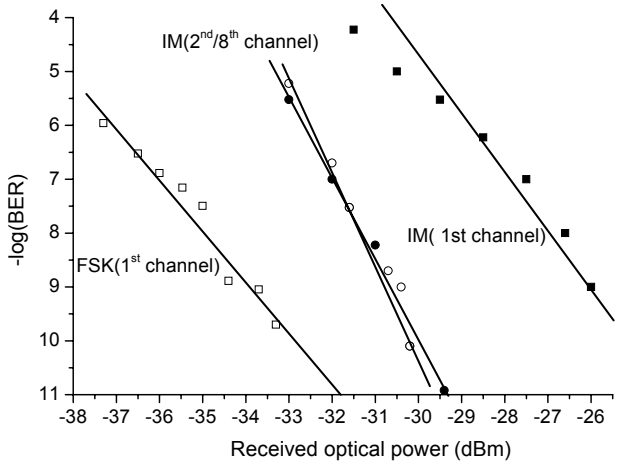

Fig. 4.19. *Measured BER curves of the different wavelength channels.*

A limitation to the realistic nature of this experiment is given by the fact that all channels were intensity modulated at the same time by the same intensity modulator. Most of the fiber-induced non-linear effects will occur in the first part of the fiber where the power is highest [107]. Even if the total span including the DCF compensation would induce a shift amongst channels that was greater than the duration of one bit, the alignment of the channels at the

start of the system would render the effects of fiber non-linearities to be less realistic. On the other hand, the concordance of the experimental results with the numerical analysis would indicate that this would not have a drastic effect on the system performance.

Manchester-encoded WDM transmission

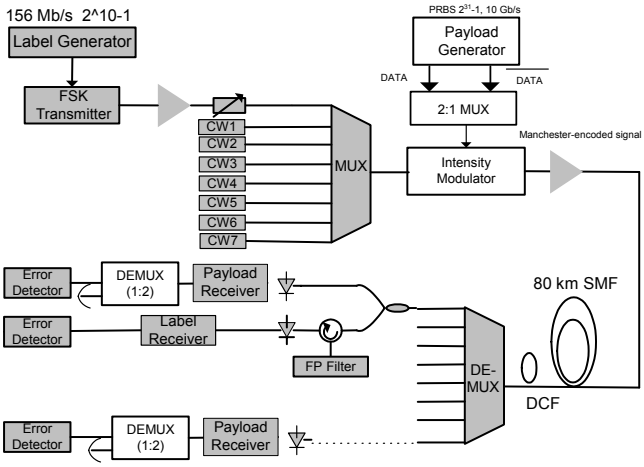

Fig. 4.20. *Manchester encoded WDM transmission system.*

It has already been discussed that through the use of Manchester coding (MC), IM/FSK signals can operate with a higher IM extinction ratio without degrading FSK receiver performance. For a 200 GHz channel spacing WDM transmission system where the payload is modulated at 10 Gb/s, the broadened spectrum induced by the Manchester code will not introduce a noticeable channel crosstalk. Thus Manchester encoding could effectively be applied to enhance the WDM system performance.

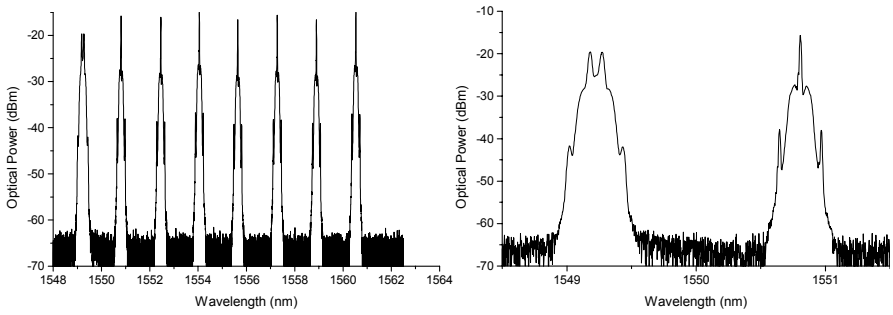

Fig. 4.21. *Spectra of multiplexed channels, (a) full range. (b) detail of the MC channel and a IM channel.*

The experimental setup shown in fig. 4.20 is equivalent to the setup illustrated in fig. 4.16, except for a 20 Gb/s multiplexer and demultiplexer added to apply Manchester encoding with the help of the conjugate data output of the pattern generator. The spectra of the multiplexed channels are shown in fig. 4.21 (a), while fig. 4.21 (b) gives the detailed structure of the Manchester encoded IM/FSK channel at 1549.3 nm next to a pure IM channel. The lack of channel-space induced limitations, is evident from these images.

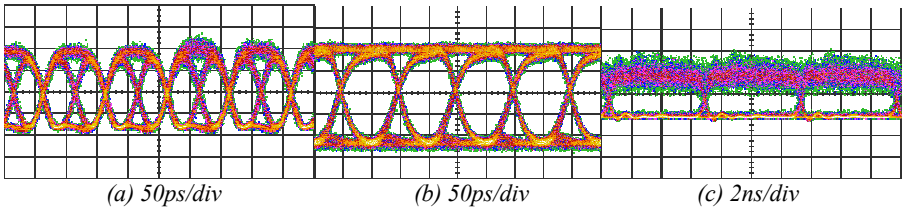

Fig. 4.22. *Eye-diagrams of (a) Manchester-encoded IM signal (b) decoded IM signal (c) demodulated FSK label.*

Because of the MC, the IM extinction ratio of all the channels could be adjusted up to 13 dB. With such a high extinction ratio, the IM payload was much insensitive to the residual intensity ripples introduced by the imperfect FSK source. Therefore, the IM receiver sensitivity of the IM/FSK channel was roughly the same as those of the other seven channels, and thus, only the results related to the IM/FSK channel are reported.

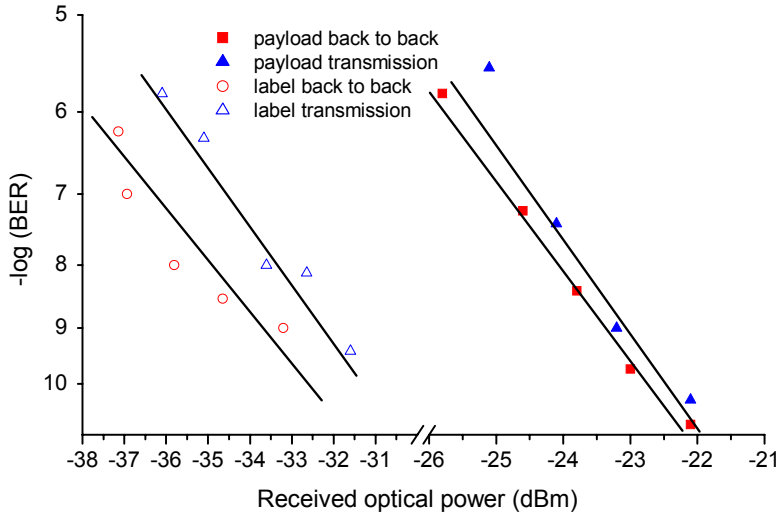

Fig. 4.23. *Measured BER curves of the IM/FSK channel in a WDM transmission before and after transmission.*

Fig. 4.22 shows the eye-diagrams of the Manchester-encoded payload signal, the decoded payload signal and the demodulated FSK label. A much higher ER than in fig. 4.18 was achieved, which translated into an enhanced system performance. Fig. 4.23 shows the measured BER curves for the IM/FSK channel in the back-to-back case and after transmission. The results indicate that the 80 km transmission only introduced a modest receiver sensitivity degradation. The power penalty at a BER of 10^{-9} was only 1.5 dB for the label and less than 1 dB for the payload.

Three-channel IM/FSK signal transmission

A three-channel IM/FSK signal transmission system was implemented, as shown in fig. 4.24. Two GCSR lasers and one DFB/EAM source were used to generate three IM/FSK signals at various wavelengths. The channel spacing was selected to be 100 GHz (0.8 nm), and thus the select wavelengths for the channels were 1548.5 nm (GCSR), 1549.3 nm (DFB/EAM) and 1550.1 nm (GCSR) respectively.

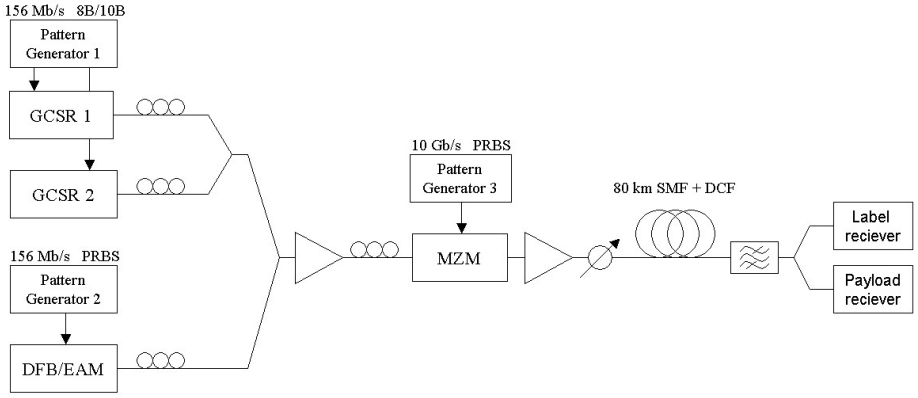

Fig. 4.24. *Experimental setup of the three-channel IM/FSK signal transmission system.*

As discussed in Section 2.4.4, the effect of the non-uniform frequency modulation response of the GCSR lasers, can be reduced by applying 8B/10B encoding to the label data (PRBS 2^9-1), before it modulates the two GCSR lasers. The DFB/EAM source was frequency-modulated by a PRBS with a length of 2^{10}-1. The output signals of the three lasers were multiplexed using two optical couplers, and then intensity modulated by a low-chirp Mach-Zehnder modulator with a 6 dB extinction ratio. The generated multi-wavelength IM/FSK signal was amplified to an average power of 10 dBm, and then injected into a fully compensated 80 km SMF link. At the receiver end, a tunable optical filter was used to demultiplex the wavelength

channels. The demultiplexed channel was finally detected for BER measurements. It should be noted that the 3 dB electrical bandwidth of the label receiver had an optimized value of 117 MHz in this experiment. Therefore, the label receiver performance of channel 2 is greatly improved, compared to the experiments reported in former sections.

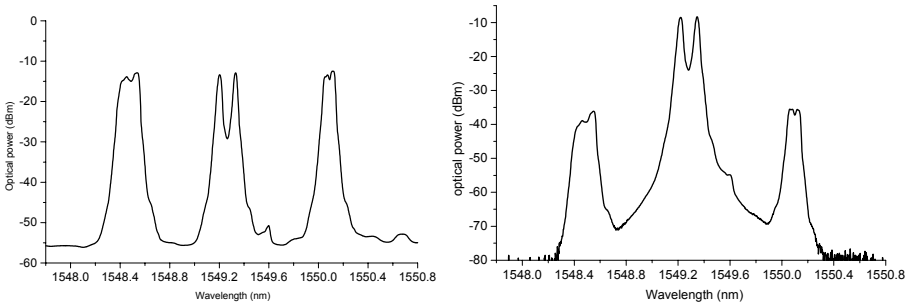

Fig. 4.25. *Spectra of multiplexed and demultiplexed channels.*

As shown in fig. 4.25, the optical filter can effectively demultiplex the wavelength channels with a channel suppression ratio of around 30 dB. The eye-diagrams of the received signals for each channel are shown in fig. 4.26. The frequency modulation efficiency of the GCSR lasers was wavelength dependent, as discussed in Section 2.2.1, which is why channel 3 showed a poor frequency modulation efficiency. For this reason, its label eye-opening was smaller than the one of the other channels. In spite of that, both the payload and the label of all three channels could be detected with a BER of less than 10^{-9}.

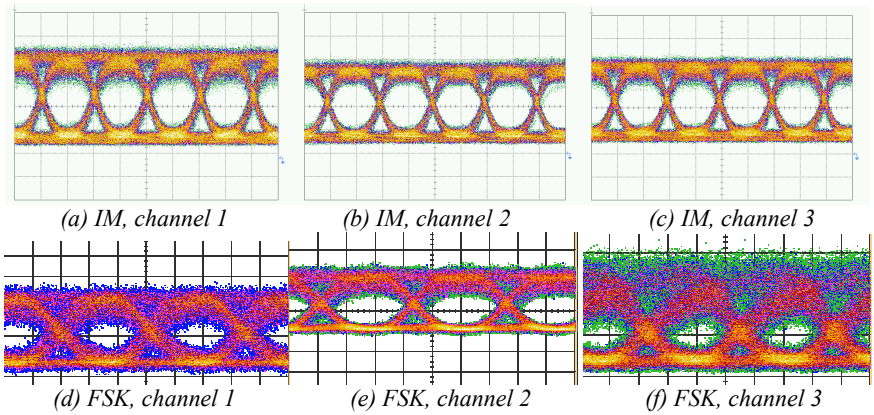

Fig.4.26. *Eye-diagrams of the received signals for the three channels.*

The BER curves for the transmitted signals and the back-to-back case are shown in fig. 4.27, from which it can be concluded that the power penalty introduced by transmission was within acceptable limits. Among the three

wavelength channels, channel 2 (generated with the DFB/EAM source) had the best FSK modulation performance due to its higher FM efficiency and showed practically no penalty due to transmission. The other two channels had better IM performance as they generated much less residual intensity ripples when they were frequency modulated. They showed a transmission penalty of 4 dB on the payload and a slight improvement on the label performance, which is believed to be due to a reduction of the ER of the payload during transmission.

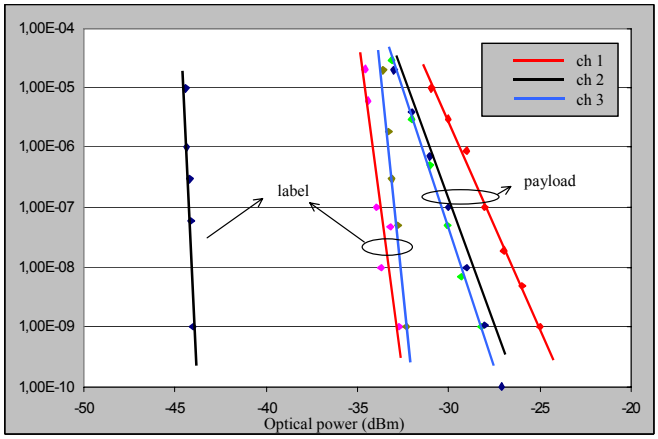

(a) back-to-back

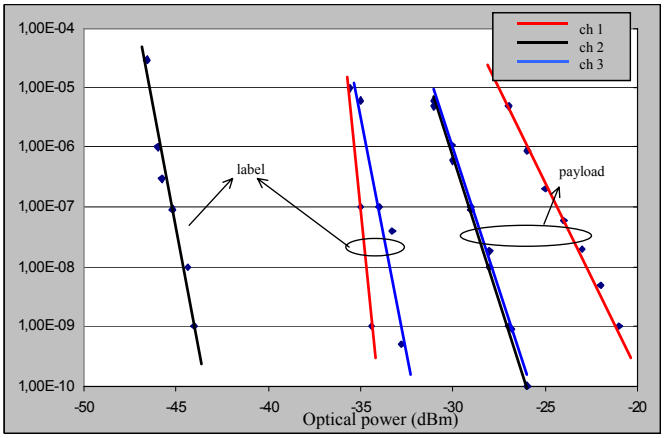

(b) after transmission

Fig. 4.27. *Measured BER curves for the three wavelength channels.*

These results confirm that the IM/FSK orthogonal labelling method with a payload bit-rate of 10 Gb/s and a moderate label bit-rate of 156 Mb/s (which would be enough for its purpose) is suitable for WDM systems. The limits of such a system would mostly be the same as a single IM/FSK system, provided the channel spacing is kept to 100 GHz. During the experimental

measurements, and even for channel spacings as low as 50 GHz the performance of the system could be optimized to a satisfactory level.

4.4 WDM transmission of IM/DPSK labelled signals

The performance of the IM/DPSK labelled scheme in a WDM transmission was verified in a four channel system at bit-rates of 40 Gb/s for the IM payload and 2.5 Gb/s for the FSK label. The payload was 8B/10B coded to enhance the performance of the system (see Section 2.4), thus its ER could be set as high as 12 dB.

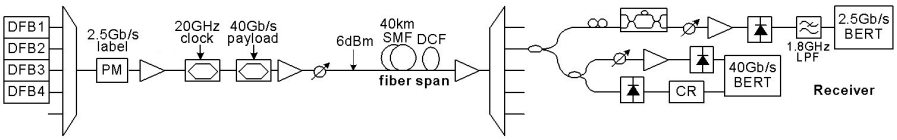

***Fig. 4.28**. Setup for the transmission over 40 km SMF of 4×40 Gb/s IM/DPSK labelled signals.*

The experimental setup is shown in fig. 4.28. Four DFB lasers were tuned to the carrier frequencies of the four channels with a channel spacing of 200 GHz, and multiplexed. The label DPSK modulation at 2.5 Gb/s and the payload RZ-IM modulation at 40 Gb/s RZ were added to the four carriers simultaneously by external modulators, and the signals were amplified to an average power of 6 dBm. The four IM/DPSK signals were transmitted through 40 km of post-compensated SMF and demultiplexed before reception. Both arms of the receiver were identical to the ones described earlier for IM/DPSK labelled signals.

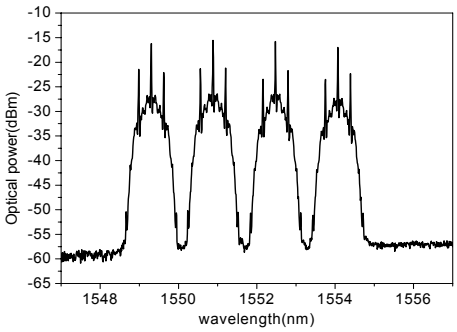

***Fig. 4.29**. Spectrum of the four IM/DPSK channels after transmission..*

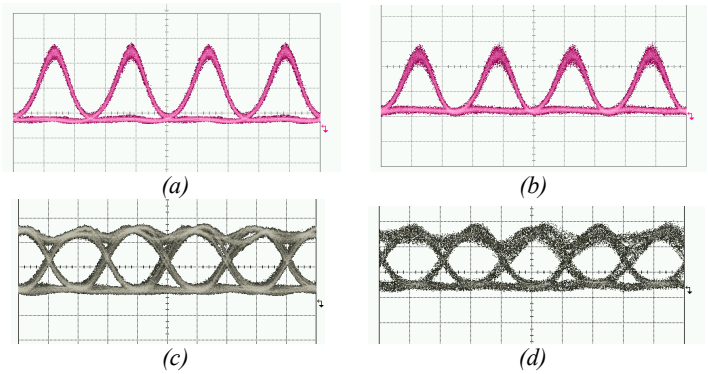

Fig. 4.30. *Eye diagrams of channel 2 (a) 40 Gb/s payload back-to-back (b) 40 Gb/s payload after 40 km(c) 2.5 Gb/s label back-to-back (d) 2.5 Gb/s label after 40 km*

Fig. 4.29 shows the spectra of the four IM/DPSK channels, which presented a limited spectral bandwidth which proved enough for WDM transmission at the given channel spacing. The eye-diagrams for channel 2 at various points in the system are shown in fig. 4.30. These indicate that the WDM transmission had very little detrimental effect on the signal.

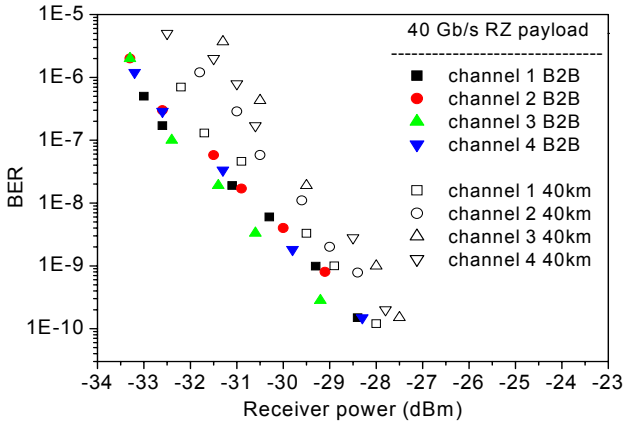

Fig. 4.31. *Payload BER results for the transmission over 40 km SMF of 4×40 Gb/s IM/DPSK labelled signals.*

The measured BER results for all four channels for the payload are shown in fig. 4.31 and for the label label in fig. 4.32. The results show that for the payload the transmission penalty was lower than 1 dB, while for the label it was lower than 1.5 dB. Bearing in mind that the system performance was enhanced by the 8B/10B encoding, even for these high bit-rates, the results validate the IM/DPSK orthogonally labelled format for WDM systems.

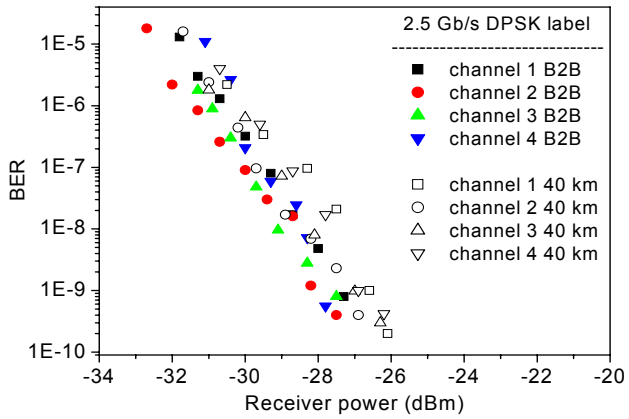

Fig. 4.32. *Label BER results for the transmission over 40 km SMF of 4×40 Gb/s IM/DPSK labelled signals.*

4.5 Chapter summary

In this chapter, issues concerning WDM systems for all-optical orthogonally labelled signals have been addressed. Most of the analysis was performed for the IM/SMF scheme, because WDM induced limitations such as filtering were believed to be higher for such a system. Both numerical and experimental results confirmed this assumption. An experimental validation of the IM/DPSK scheme in a four channel WDM system was also performed.

For an IM/FSK modulated signal, simulations showed that in a multi-channel system where channels would be multiplexed and demultiplexed in consecutive network nodes, the filtering effects must be taken carefully into account. If a too narrow optical filtering scheme was to suppress some parts of the spectrum, a significant impact on the payload receiver sensitivity would be observed. The bandwidth of the optical filters employed in the multiplexer, should be at least 40 GHz and the channel spacing should exceed 60 GHz for payloads modulated at 10 Gb/s.

Moreover, the stability of the optical components of the system proved to be of a crucial importance. A 3 GHz detuning between the center frequency of a filter and a labelled channel was shown to noticeably degrade the performance of the system, due to FSK to IM conversion.

During the transmission of eight labelled channels, the payload receiver sensitivity exhibited some dependence on channels spacing. No inter-channel

cross-talk was observed when the separation between the center frequencies of the WDM channels was greater than 100 GHz. However, if the spacing was reduced below 100 GHz, the spectra of the signals showed some overlap and a given channel could not be demultiplexed without receiver sensitivity penalty. Practically no non-linear interaction was numerically observed between the intensity-modulated channels.

The numerical results indicated that the factors that most influence the performance of the system, besides the ER of the payload modulation, were the bandwidth of the filters and their de-tunability. A misaligned filter, encountered during the transmission of IM/FSK signal, would drastically reduce the orthogonal independence of the modulation formats.

The conclusion of the simulations were confirmed experimentally. The detuning tolerance of an AWG and the impact of wavelength channel spacing, showed a high consistency with the numerical results.

Several approaches for measuring the performance of IM/FSK signals in a point-to-point WDM transmission system were evaluated. It was shown that IM/FSK channels can be added to pure IM channels, which would be a method to progressively upgrade WDM networks to optical labelling. A similar experiment, confirmed, as previously observed, that DC-balanced encoding techniques are able to enhance the network performance by relaxing the extinction ratio requirements for the IM payload.

A three-channel IM/FSK transmission system was implemented with a channel spacing of 100 GHz in which BERs of 10^{-9}, were achieved. The performance of the IM/FSK channels proved to be highly dependent on the performance of the FSK sources, with regard to FSK tone-spacing and IM stability before IM modulation.

An experimental investigation on the WDM transmission of IM/DPSK signals was also performed for a four-channel system with a 200 GHz channel spacing, showing penalties of around 1 dB after transmission over a compensated 80 km link.

These results confirm that the IM/FSK and IM/DPSK orthogonal labelling methods are suitable for WDM systems. The limits of such system would mostly be the same as a single IM/FSK transmission, provided the channel spacing is kept to 100 GHz or more.

It can therefore be concluded that the orthogonal modulation schemes can be feasibly used in practice to upgrade WDM transmission networks and that the main limiting factor of the whole system would be the performance of the sources and the stability of the employed filtering schemes.

Chapter 5

All-optical wavelength conversion

Wavelength conversion (WC) is an important technique in future all-optical switched networks for several reasons. As discussed in Chapter 1, the optical wavelengths could be deployed as extra labels to build up an appropriate optical path in the transmission fiber link and should therefore be able to be swapped in the intermediate network nodes [9]. Another reason for the importance of WC is that the very large bandwidth of standard telecommunications fibres can potentially be utilized by wavelength division multiplexing (WDM) techniques [68]. Channels could be wished to be routed to a common output, usually making it necessary to convert the wavelength of the signal [93].

WC can be done using several different techniques making use of passive or active components [109]. Wavelength conversion can be achieved by using non-linearities in passive optical fibres [110], [111], [112], [114], in which the non-linear response time can be as low as a few femtoseconds [98], providing ultra-fast all-optical wavelength conversion.

WC can also be achieved by the use of active components, such as electro-absorption modulators (EAM) [115] or semiconductor optical amplifiers (SOA) [116]. However, the operating speed of the later is still limited by its gain recovery time and the relatively slow carrier lifetime [117]. In order to increase their response, a combination of SOAs can be used in a Mach-Zehnder interferometer (MZI) [119], [120]. This is a versatile way of performing WC in the sense that it can be integrated with other network node functionalities such as label swapping, which will be discussed in detail in Chapter 6.

In this chapter, the principles of wavelength conversion are investigated for HNLF, SOA and SOAs in MZI. The techniques are first applied to intensity modulated (IM) signals in order to confirm their validity, and then be applied to wavelength conversion of labelled signals.

In the first section WC is experimentally investigated in highly non-linear fibers (HNLF). The effects of cross-phase modulation (XPM) and four wave mixing (FWM) are employed in order to achieve wavelength conversion. After that, WC in active components is investigated. WC in a single SOA is implemented at 40Gb/s in Section 5.2.

Given its importance as network elements and as wavelength converters [121], [122], [111], Mach-Zehnder interferometers with active SOAs (SOA-MZI) deserve a more in depth analysis of its performance and limitations for wavelength conversion of labelled signals. Therefore, Section 5.3.1 is devoted to the numerical analysis of WC in SOA-MZIs. Different setup options are analyzed and limits to the device design are obtained for 40 Gb/s IM signals. Finally, these SOA-MZI devices are used experimentally to wavelength convert labelled signals.

5.1 WC in HNLF

In this section, WC based on XPM in a HNLF followed by an optical filter [124], [110], [111], is investigated experimentally. FWM in a HNLF is then used to attempt to create a multi-wavelength IM/FSK signal generator useful for multicasting. Finally, in Section 5.1.3, the same technique is used for the WC of IM/DPSK signals.

5.1.1 XPM in HNLF of 40 Gb/s signals

The proposed wavelength converter technique is shown schematically in fig. 5.1. It uses the XPM in a HNLF followed by a optical filter by combining the incoming data (also called pump) with a continuous-wave (CW) signal [110], [125]. Because of XPM in the fibre, the intensity modulated data imposes a phase modulation on the CW signal, which generates optical sidebands on the spectrum of the CW signal. When the pump signal carries a ‘mark’, the sidebands will appear, while a ‘space’ in the pump signal will not produce any sideband. These sidebands can then be converted to amplitude modulation by suppressing the original CW signal and filtering out one sideband by an optical band-pass filter.

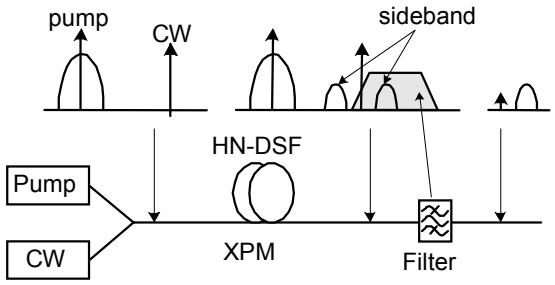

Fig. 5.1. *Schematic representation of the principle behind CW by XPM in a HNLF. The spectra are shown in the upper half of the figure, while the setup is depicted in the lower half.*

The numerical results were based on 1 km of HNLF with a non-linear coefficient of 5.1 $W^{-1}km^{-1}$. The data was a return to zero (RZ) signal at 40 Gb/s, with a power level of 20 dBm. The probe was 400 GHz apart and had a power level of 16 dBm. Fig. 5.2 shows the calculated spectra of the signal before and after the HNLF in the absence of noise, illustrating how the CW wave is phase modulated after passing through the HNLF. Other tones at equal spacings appear due to FWM in the fiber. By removing the CW wave with an optical notch filter and placing a band-pass filter after the HNLF with a central pass frequency centered on one of the optical sidebands, one can obtain a signal that is amplitude modulated with the carrier frequency of the optical sideband [124], [110].

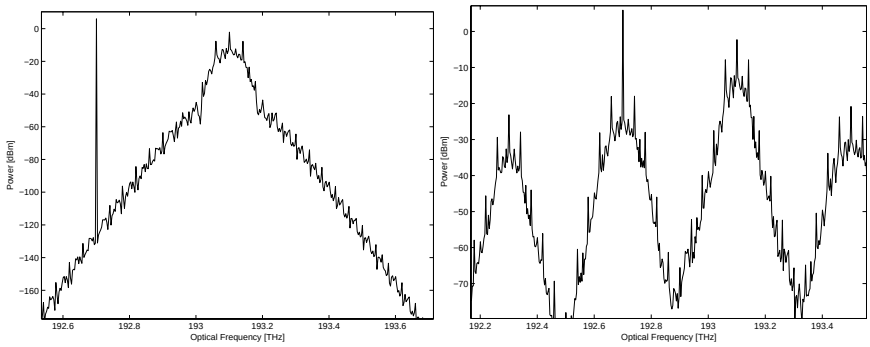

Fig.5.2*. The optical spectrum (a) before and (b) after the HNLF.*

The experimental setup is shown in fig. 5.3 for the case where OADMs are used for filtering. An external-cavity laser emitting at 1558.8 nm was modulated with 40 Gb/s data through a double MZM stage, and then amplified up to 16 dBm. A second laser emitting CW light at 1555.2 was used as CW source with a power level of 9 dBm. These two signals were coupled together and injected into 1 km of HNLF – with a non-linear

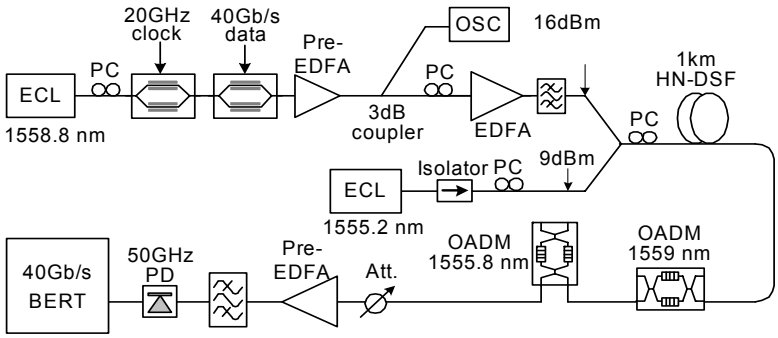

Fig. 5.3. *Experimental setup for validating the CW technique of filtered XPM in a HNLF in the case of filtering by FBG in OADMs.*

coefficient of 10.9 $W^{-1}km^{-1}$ and 0.87 dB/km losses – where the XPM took place. At the output of the fiber, the first OADM was used to filter out the original data channel plus the undesired tones that appear due to FWM in the fiber. A second OADM was then fine-tuned in order to filter out just one sideband of the phase-modulated signal at the CW wavelength. Both OADM were based on fiber Bragg gratings (FBG) and had a 3 dB bandwidth of 1 nm.

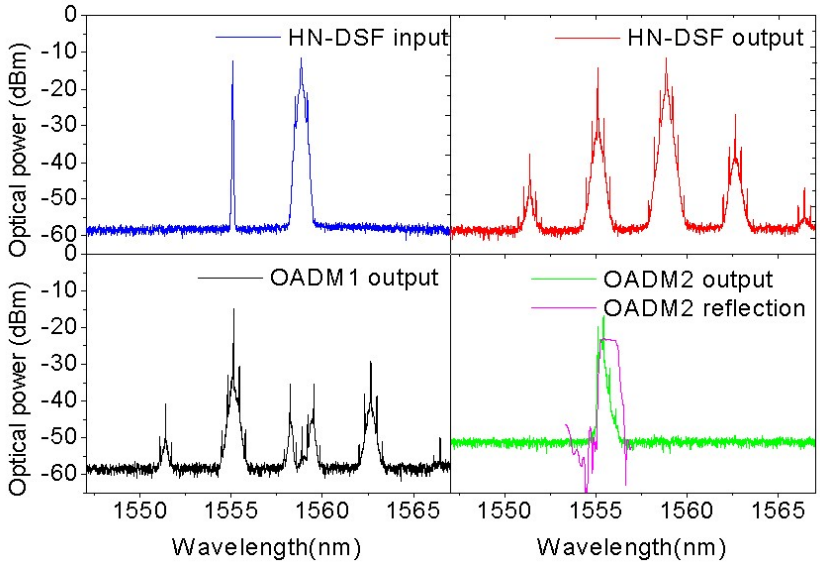

Fig. 5.4. *Spectra of the signals at various points of the WC process. (a) Original signals at the input of the HNLF, (b) output of the HNLF, (c) output of the first OADM with suppressed neighbouring tones and (d) response of the second OADM and its output, with the sideband WC data.*

Fig. 5.4 shows the spectra of the signals at the different parts of the WC process. It can be observed how the XPM process in the HNLF affected the CW signal modulating its phase, which broadened its spectrum. The first OADM reduced the power of the original data channel by more than 25 dB. Finally, the second OADM had to be carefully fine-tuned in order to achieve the desired demodulation of the phase information into amplitude modulation.

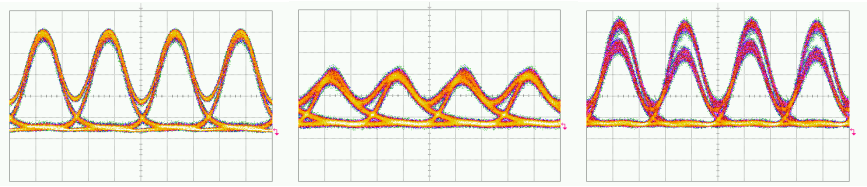

(a) *(b)* *(c)*

***Fig. 5.5**. Eye-diagrams of (a) 40 Gb/s original signal, (b) converted signal at 1555.181nm and (c) converted signal at 1555. 255nm*

The two useable side-lobes of the converted signal were located at 1555.18 nm and 1555.25 nm respectively, around the original CW wavelength. Fig. 5.5 shows the eye-diagrams of the original signal and of the filtered side-lobes of the converted signal. The OADM used to filter out these side-lobes had a non symmetrical response, as shown in the purple line of fig. 5.4 (d). For this reason, the eye-diagram of one of the converted side-lobes has a much better performance than the other, even though patterning effects where present in the response of the later.

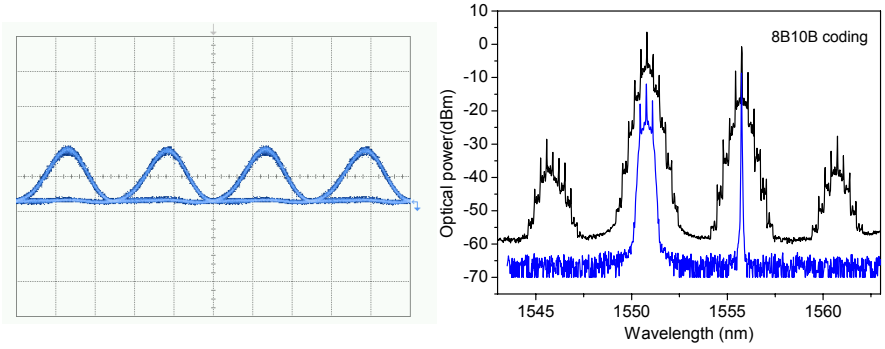

(a) *(b)*

***Fig. 5.6**. (a) Eye-diagram original 40 Gb/s data and (b) spectra of the signals before (blue) and after (black) the HNLF.*

It should be clear from this discussion, that the performance of this method of WC is highly dependent on the effectiveness of the filtering process involved

in selecting the side-lobe produced by the XPM. In order to further investigate the filtering effects on the signal, different filtering techniques were applied to the converted signal, and compared to the WC results obtained by using the FWM process and a Kerr switch in the same HNLF.

Fig. 5.6. shows the eye-diagram of the original 40 Gb/s data used in this case, plus the spectra of the signals before and after the HNLF. It should be noted that these spectra are not exactly the same as in the previous experiment, as the data source is located close 1551 nm in this case.

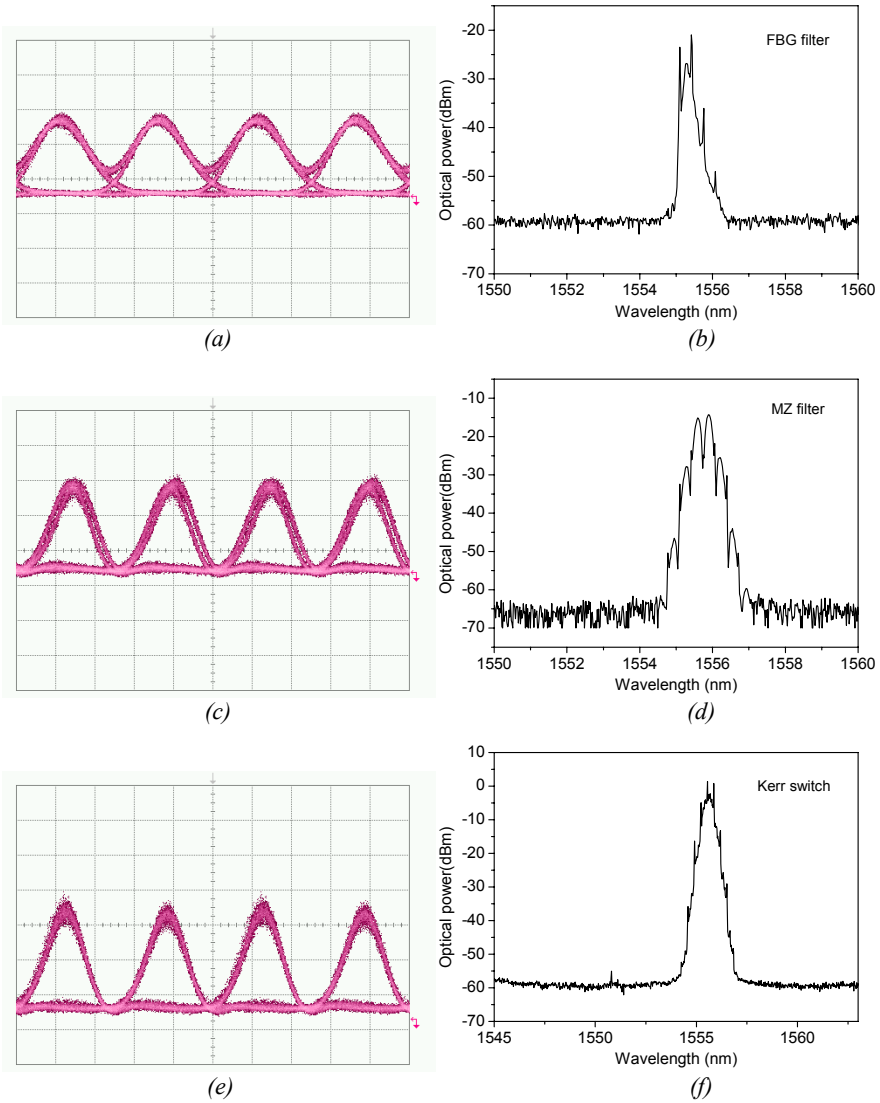

Fig. 5.7*. Eye-diagrams and spectra of the signal after filtering by a (top) FBG, (middle) MZ filter and (bottom) polarization effects in a Kerr switch.*

Fig. 5.7 shows the eye-diagrams and spectra for the two filtering methods and the Kerr switch. At the top the FBG of an OADM were used to filter out the side-lobes of the phase modulated CW light, in the same way as described in the last experiment. The ER of the converted signal was 12 dB in this case. The middle of fig. 5.7 shows the resulting eye-diagram and spectrum after using a MZ filter in a similar way. The ER of the converted signal was 13 dB in this case. Finally, the bottom of fig. 5.7 shows the results of conversion through a Kerr switch, which is based on a polarization beam splitter (PBS). In the absence of data signal, there is no output at the wavelength of the CW probe light, because the polarization of the probe after transmission along the HNLF is adjusted to be vertical to the port of the PBS used. In the presence of the pump, XPM induces a polarization rotation, which allows part of the probe to pass through the PBS. In this way, the original data is copied onto the probe. The ER achieved through this method was 9 dB.

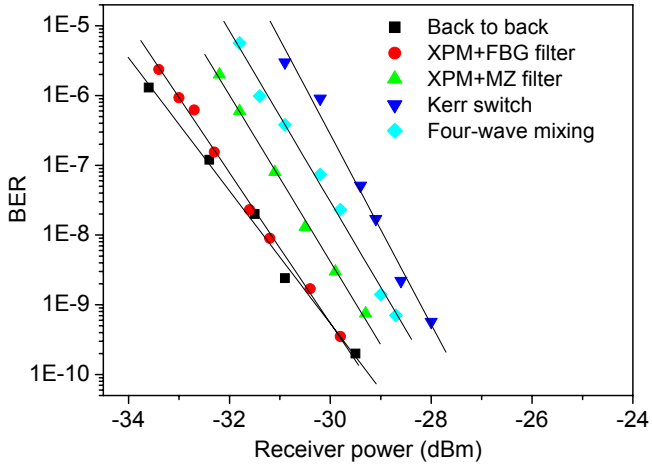

Fig. 5.8. *BER curves for the various filtering techniques used for WC through XPM in HNLF compared to FWM in the same fiber.*

As a summary, fig. 5.8 presents the BER curves for the different filtering methods. At a BER of 10^{-9}, the sensitivity penalties compared to the back-to-back case were 0.2 dB for XPM filtered by a FBG, 0.8 dB for XPM filtered by a MZ filter, 2.1 dB for the Kerr-switch method and 1.6 dB for FWM in the HNLF, showed here for comparison. Any of these methods was therefore acceptable for wavelength conversion of 40 Gb/s signals, although the FBG filtering in OADMs showed the best performance.

5.1.2 Multi-wavelength IM/FSK signal generation

The WC of an incoming signal to several simultaneous output wavelengths could have an application in multicasting within an optical network. There

are several methods to generate multi-wavelength IM/FSK signals. One method is to use several FSK laser sources with different wavelengths, another method is to utilize all-optical WC processes where only one FSK laser source is necessary [126]. In this section the second method will be addressed using FWM in a HNLF as WC method, in order to create 7 replicas of a IM/FSK labelled signal.

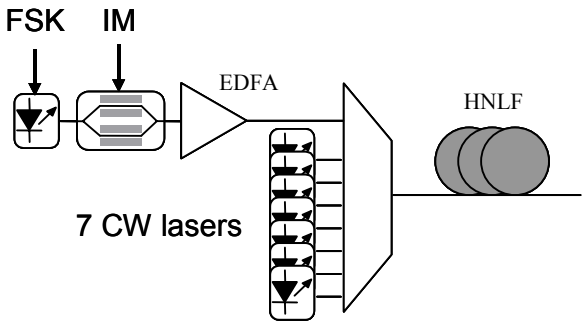

Fig. 5.9. *Experimental setup for generating multi-wavelength IM/FSK signals.*

The proposed method of generating a multi-channel IM/FSK signal used a single FSK pump in conjunction with seven CW sources injected into a HNLF, as shown in the experimental setup in fig. 5.9. The FWM process took place in 300 meters of HNLF. One FSK laser source based on the DFB/EAM method presented in Section 2.2.1, generated the pumping light. The generated light carried a 156 Mb/s FSK label and a 10 Gb/s IM payload at 1549.2 nm. It was then amplified to an average power of 20 dBm and injected into the HNLF with seven other CW light channels. As shown in fig. 5.10, the FWM mixing products reproduced the FSK label from the IM/FSK pumping light, although the conversion efficiency was around -25 dB. One important characteristic of this method, is that the FSK tone spacing of the converted light would be doubled compared to that of the incoming signal used as pump. Optical filters such as AWGs would be needed to extract the converted IM/FSK signals for further system use.

One important challenge to this method, was found in the fact that, in spite of the acceptable conversion efficiency of the FWM process through the HNLF, the power of the converted FSK channels remained low. This meant that an effective way to suppress the pump and residual CW channels, as well as to amplify the low power FSK channels without excessive noise addition would be required in order to be able to use the multi-channel FSK source in a systems. This is not as easy task, as the filtering involved should be sharp enough to filter out the FSK pump without degrading the right-most converted channel, should, at the same time, provide a suppression ratio large enough to suppress the strong FSK pump and 7 CW sources without

degrading the converted signals, and should finally be wide enough to let all 7 converted channels get through for re-transmission. It is believed that a more careful system design would increase the efficiency of the process.

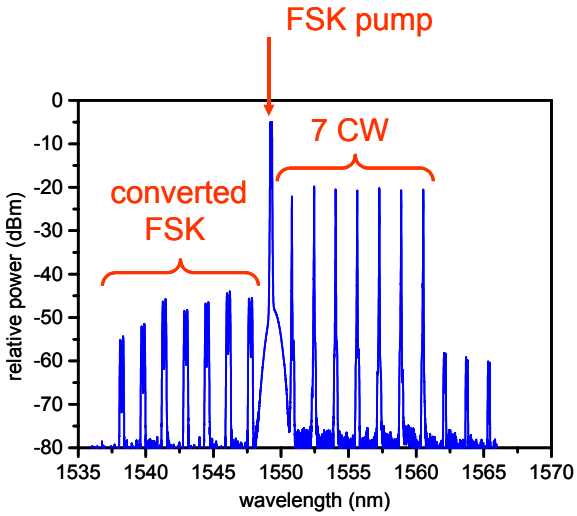

Fig. 5.10. *Spectra of multiple IM/FSK signals generated through FWM in HNLF.*

5.1.3 IM/DPSK WC by FWM in HNLF

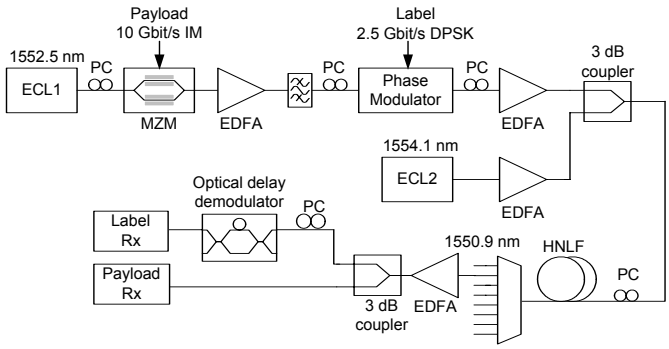

Fig.5.11. *Experiment setup for WC of IM/DPSK signals through FWM in a HNLF.*

In order to realize wavelength conversion (WC) of a IM/DPSK modulated signal while preserving the DPSK label, XPM based WC cannot be applied, and instead some transparent wavelength conversion scheme must be considered. Reported FWM wavelength conversion experiments [127], [129] indicate that using HNLF can result in large spectral and dynamic ranges. Therefore wavelength conversion using HNLF can be chosen as a good

candidate to transparent wavelength conversion for the combined IM/DPSK signal. This section presents the experimental investigation of this WC method for a IM/DPSK optically labelled signals consisting of a 10 Gb/s payload and a 2.5 Gb/s label.

The experimental setup is shown in fig. 5.11. The CW light sources were external cavity lasers lasing at 1552.5 nm (ECL1) and 1554.1 nm (ECL2), respectively. The IM/DPSK signal was generated by external modulators on ECL1. The labelled signal was then amplified and aligned with respect to polarization, before being combined with the CW signal emitted by ECL2. The FWM process took place in a 500 m-long HNLF with a non-linear coefficient of 10.6 $w^{-1}km^{-1}$. The zero dispersion wavelength of the HNLF was 1553.6 nm and the dispersion slope 0.022 $ps/nm^2/km$. A commercial AWG with a channel spacing of 200 GHz was used to filter out the converted signal. Fig. 5.12 shows the optical spectra at the output of the HNLF and the converted signal after the AWG. By optimizing the states of polarization of the pump and signal and the input power level, a conversion efficiency of the FWM process of -15 dB could be achieved.

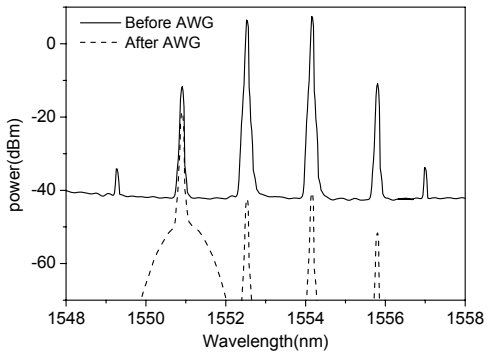

Fig.5.12. *Optical spectra at the output of 500 m HNLF (solid line) and the filtered converted signal after the AWG (dotted line).*

The original (back-to-back) eye diagrams of the payload and the label are shown in fig. 5.13 (a) and (c). While the its wavelength converted counterparts are shown in fig. 5.13 (b) and (d). Because the FWM effect in fibers can be exploited to achieve all-optical reshaping [127], it could be predicted that the extinction ratio of the converted IM signal would be enhanced due to this reshaping property. This was experimentally verified. For an initial ER of 3 dB of the IM signal, the ER of the converted signal was measured to be 3.5 dB. Therefore an even lower ER was needed at the source, in order to let the label performance still to outperform the payloads. According to the previous discussion of the optimisation of the input

extinction ratio, an ER of less than 3 dB should be selected. In our experiment the extinction ratio of the pump signal was set to 2.8 dB.

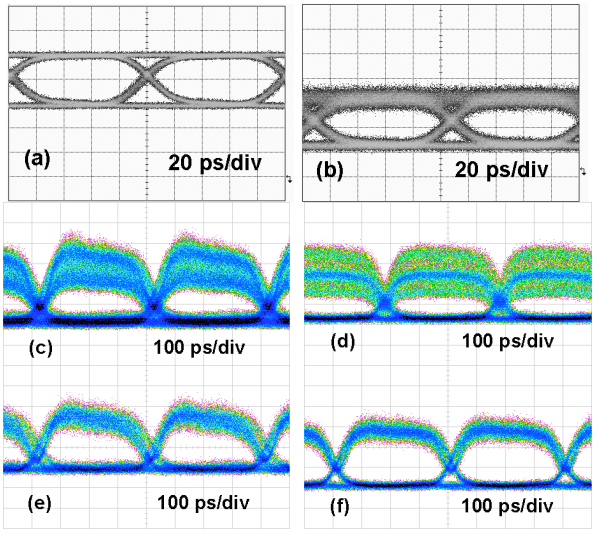

Fig.5.13. *Measured eye diagrams of (a) back-to-back payload, (b) converted payload, (c) back-to-back label, (d) converted label, (e) back-to-back DPSK signal without IM modulation, (f) converted DPSK signal without IM modulation.*

After FWM wavelength conversion, the phase information of the pump signal was efficiently replicated onto the new wavelength. The converted label showed a clear multi-level structure, and had reduced amplitude fluctuation in the 'marks' as compared to the back-to-back label, as shown in fig. 5.13 (c) and (d). It is believed that this also could be attributed to the reshaping of the signal. In order to confirm this, the conversion of a pure DPSK signal was performed. The eye-diagrams can be seen in fig. 5.13 (e) and (f), where the same reshaping of the 'mark' level is observable.

The BER curves for the experiment are presented in fig. 5.14. The penalty for conversion for the label was measured to be 1.6 dB. For the payload, the stringent requirements on its ER, translated into a power penalty of about 5 dB for the converted signal. The BER performance of the pure DPSK and IM signals were also measured. In this case the power penalty for conversion of the DPSK signal was within 1 dB and a very low receiver sensitivity of -36.5 dBm was obtained, indicating that the penalty for adding the IM payload to the label was around 8 dB. Comparing the BER of the converted payload of the labelled signal with the pure IM signal, the penalty for adding the label could be measured to be around 3 dB.

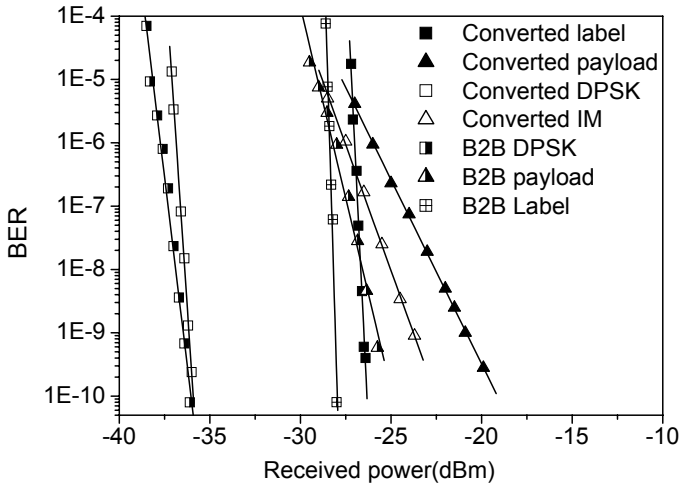

Fig. 5.14. *Measured BER performance for the payload and the label back-to-back and after FWM wavelength conversion.*

5.2 WC at 40 Gb/s in SOA

Another approach to wavelength conversion (WC) is the use the gain saturation effects of active devices such as SOAs, which would produce cross-gain modulation (XGM). As explained in [130], when a bias current is applied, inverting in the carrier population occurs. If then an input data signal is coupled into the SOA along with CW light at different wavelengths, as the data signal propagates through the SOA, it will modulate the carrier density, and therefore the gain. A lower gain will occur when a 'mark' travels through the SOA than when a 'space' is present, because the 'mark' saturates the gain. The CW-light experiences this change in the gain in the way that a lower gain will occur when the data stream is present with a 'mark'. Thus, a copy of the original data with inverted polarity will be obtained at the output of the SOA and at the wavelength of the CW light.

This technique was used in the experiment presented in fig. 5.15, for wavelength-converting a 40 Gb/s IM signal. A laser emitting at 1550 nm was intensity modulated by a 40 Gb/s PRBS pattern and amplified to 16 dBm. A second laser source emitted at 1555.8 nm with a power level of 9 dB. These two signals were coupled and injected into an SOA where the XGM process took place. At the output of the SOA, a FBG suppressed the original data channel and an OADM selected the converted data for detection. The SOA in the setup was developed under the SCOOP program and kindly lent for this

experiment. It had a length of 1400 μm and was driven with a current of 750 mA.

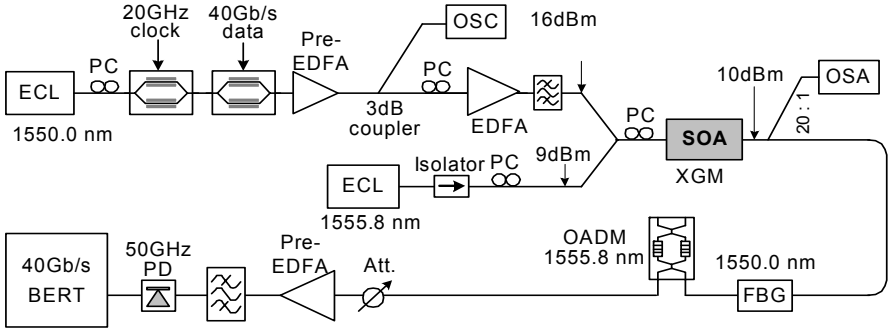

Fig. 5.15. *Experimental setup for WC of a 40 Gb/s signal through XGM in SOA.*

Fig. 5.16 shows the spectra of the signals at various points in the system. The black line shows the spectrum of the coupled signals injected into the SOA, where the signal at 1555.8 nm clearly has no modulation. The red line shows the spectrum of the signals at the output of the SOA, where the probe signal now has acquired modulation through XGM in the SOA, and the original data signal is still present. Finally, the blue line shows the wavelength converted signal after filtering.

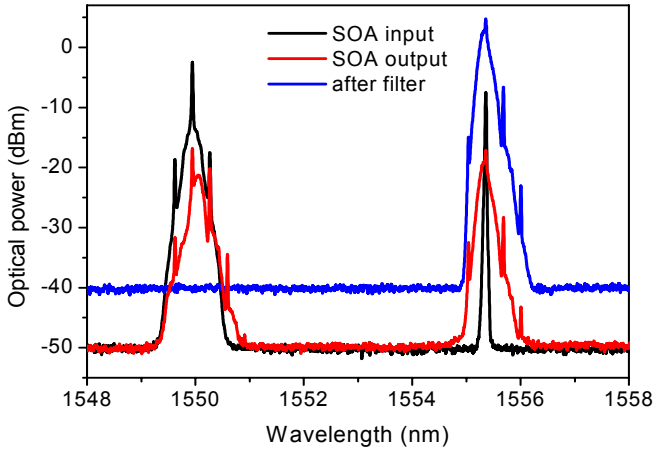

Fig. 5.16 *Spectra of the signals at various points in the system: (black) input signals to the SOA, (red) output of the SOA with evident XGM and (blue) filtered WC signal.*

The eye diagrams of the original and converted signals are shown in fig. 5.17. The RZ original signal has been inverted and appear to resemble more a NRZ signal, which is due to the limited gain recovery time of the SOA plus some filtering distortion.

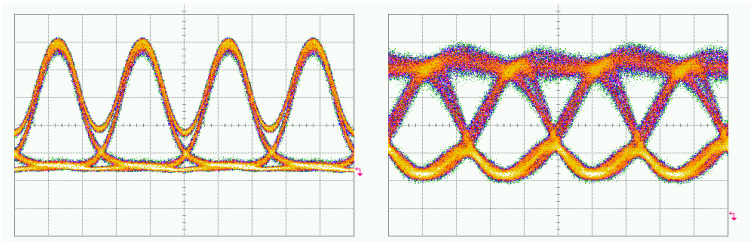

(a) *(b)*

Fig. 5.17. *Eye-diagrams of (a) 40 Gb/s original signal (b) converted signal.*

The measured BER are presented in fig. 5.18. The conversion penalty compared to the back-to-back case was 5 dB, partially due to the large insertion losses to the device.

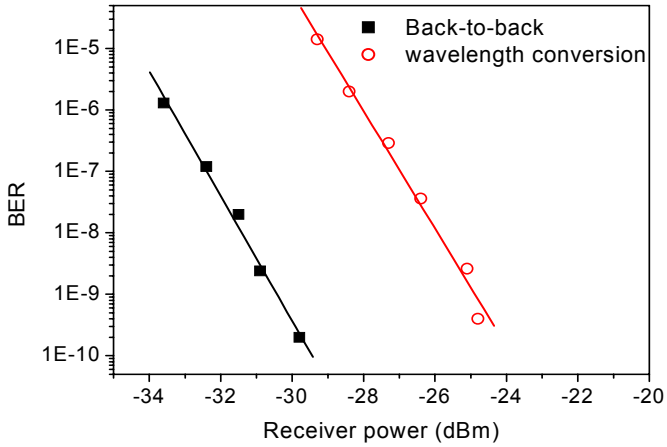

Fig. 5.18. *BER curves for WC of a 40 Gb/s signal through XGM in an SOA.*

It should be noted that this WC is only applied for an IM signal. For an orthogonally modulated signal, the information present in the angular modulation would be lost. In this sense, this WC technique could be viewed as an orthogonal label eraser, and indeed will be used as such in Section 6.1.1.

5.3 WC in SOA-MZI

A more advanced way to implement WC in active devices, would be to use a Mach-Zehnder interferometer with active SOAs in each arm (SOA-MZI). SOA-MZIs exploits the cross-phase modulation (XPM) effects in SOAs inside an integrated Mach-Zehnder interferometer (MZI). As shown schematically in fig. 5.19, in the MZI the CW will travel through both SOAs, while the data signal is launched into one of the two SOAs, where it will

modulate the carrier density and thereby also the refractive index. This will cause a phase modulation of the CW-light propagating in this SOA according to the bit pattern of the input data signals. At the output of the interferometer, the CW-light from the two SOAs interfere either constructively or destructively depending on cosine to the phase difference between the light from the two SOAs and is thus controlled by the input data signal. This leads to a wavelength converted output signal [131]. If the phase offset between the passive branches is set to zero and the two incorporated SOAs are identical, an output signal with high extinction ratio will be achieved [130]. The devices' inherent non-linear transfer function also allows regeneration of optical signals through compression of the optical noise amplitude [132].

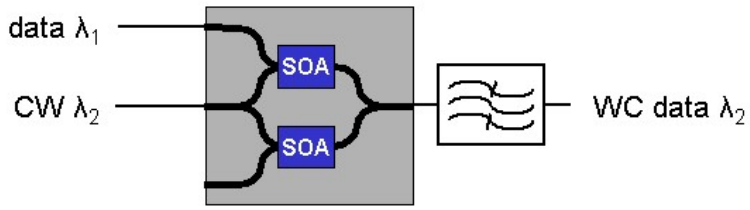

Fig. 5.19. *Schematic diagram of an SOA-MZI used for WC.*

Through adjusting injection current to each SOA, the optical signal at one output port can be constructively or destructively combined when no modulating signal is present. Consequently, the wavelength converter may have two logical output modes, i.e. the inverted and non-inverted mode [132].

This approach will reduce some of the limitations of the cross gain modulation process in a single SOA [30], such as a chirped output signal and an accumulation of the extinction ratio degradation.

5.3.1 Numerical analysis

This section presents numerical results of wavelength conversion using SOA-MZIs for networks based on time-serial labelled signals at bit-rates of 40 Gb/s, such as the one proposed in [134]. The simulations are based on specifications of commercially available SOAs and SOA-MZIs [135] and are carried out using VPI's transmission line laser models (TLLM). Further details on this type of simulations is found in [139]. Some specifications for SOAs and the incoming signal characteristics are presented. The aim is not to perform an in depth study and optimization of the device, but rather to corroborate previous published results and analysis [132], [130], [136], [138]

Various configuration schemes can be applied to the SOA-MZI wavelength converter [130]. A single SOA-MZI can be dual-arm or single-arm driven (also called standard configuration) by the modulating signals. Furthermore, it can be configured to operate with either co-propagating or counter-propagating probe and modulating signals. The combinations of these operating modes mainly result in four basic configuration schemes, shown in fig. 5.20. The counter-propagating schemes usually have a much smaller modulation bandwidth than their co-propagating counterparts, and are much more dependent on the SOA chip length [139], thus limiting the bit-rate for its functionality.

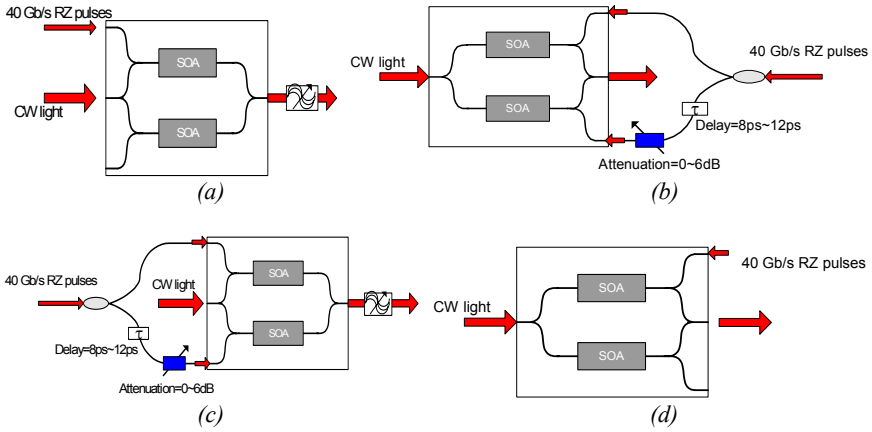

Fig. 5.20. *The four modes of operation of SOA-MZI wavelength converters: (a) standard co-propagating, (b) differential counter-propagating, (c) differential co-propagating and (d) standard counter-propagating modes.*

As shown in fig. 5.20 (b) and (c), in the differential schemes, the driving signal in one arm requires a correct timing delay and power attenuation to achieve the best switching performance. With a 40 Gb/s 33%-duty-cycle RZ signal as input, the timing delay usually ranges between 8~12 ps to keep the output signal in RZ format, while the optimum attenuation value is dependent on the SOAs' gain characteristics [139]. The simulation results showed that the attenuation generally ranges between 0~6 dB. The faster the gain recovery time is, the larger the attenuation value is required to be (see fig. 5.27).

Fig. 5.21 shows the calculated optical eye-opening penalty and fig. 5.22 the eye diagrams of the SOA-MZIs with different values of gain recovery time, comparing the results for the standard configuration and the differential mode of operation in the co-propagating scheme. Through the differential driving mode, the requirement on the SOA gain response can be much relaxed. As shown in fig. 5.21, the eye-opening penalty is kept below 2 dB even with

100 ps SOAs. Fig. 5.22 shows that the output in the differential mode also kept its waveform as the gain recovery time increases. Although pattern effects are observed with slow SOAs, the eye opening of the output signal is generally acceptable as long as the gain recovery time is limited below 100 ps.

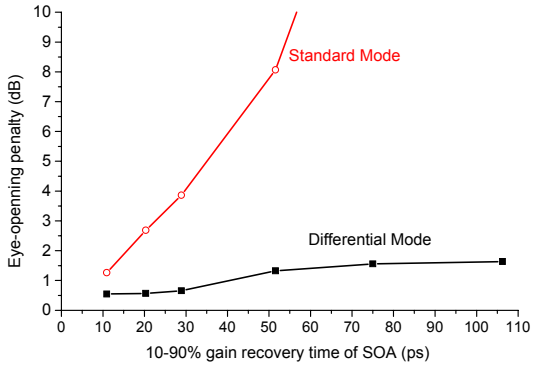

Fig. 5.21. *Calculated optical eye-opening penalty for different modes of operation.*

For the standard mode, on the other hand, with the gain recovery time increased beyond 30 ps, the output of the SOA-MZI were NRZ-like eye-diagrams and exhibited severe inter-symbolic interference (ISI).

Gain recovery time	10 ps	20 ps	30 ps	50 ps	100 ps
Single-arm driven	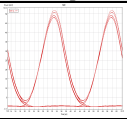	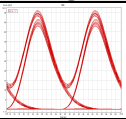	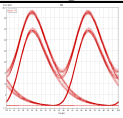	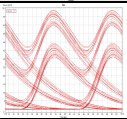	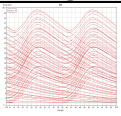
Differential driven	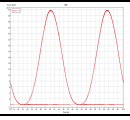	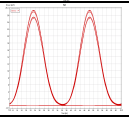	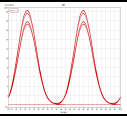	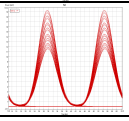	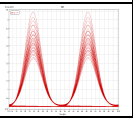

Fig. 5.22. *Eye-diagrams of a 40 Gb/s RZ signal for different SOA gain recovery times.*

The counter-propagation scheme is somewhat simpler to implement due to its filter free configuration. However, the switching performance of the SOA-MZI in this scheme proved to be very sensitive to the SOA chip length, which is in concordance with [132]. Fig. 5.23 shows the eye opening penalty (EOP) results for a simulation where the recovery time was set to 30 ps. As the SOA chip length was changed, other parameters as the injection current and confinement factor were changed accordingly to keep the SOA gain recovery time constant. The results show that when the SOA chip length was increased beyond 700 μm, the distortion on the signal induced over 3 dB of EOP. Compared with the co-propagating case, this scheme had the same

requirement on the SOA gain recovery time but has further requirements on the chip length, implying more challenges to fabrication.

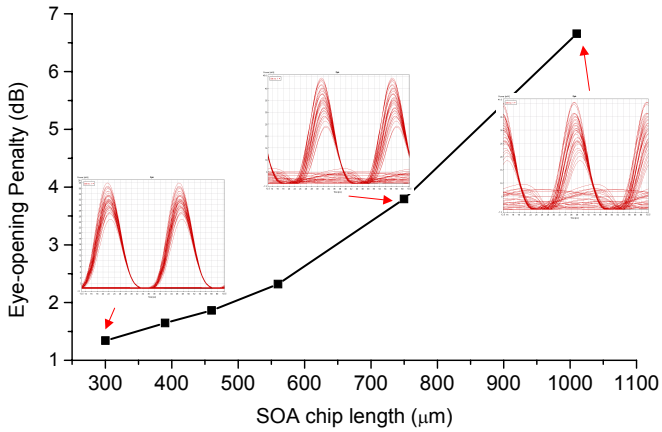

Fig. 5.23. *Eye-opening penalty vs. SOA-chip length in the differential counter-propagating mode. The SOA gain recovery time was 30 ps and the bit-rate 40 Gb/s.*

In light of the above results, it can be concluded that among the four configuration schemes, the differential driving scheme with co-propagating signals has the best modulation performance and greatly relaxes the requirements on the SOA gain response, as previously shown in [132]. The single-arm driving scheme with counter-propagating signals imposes the most stringent requirements on the SOA structures and gain response, in order to achieve wavelength conversion at 40 Gb/s. Consequently, only the co-propagating schemes will be further analyzed.

Single arm driven with co-propagating signals

In this section, along with varying the injection current and chip length, the simulations were set to vary the confinement factor, defined as the fraction of power contained in the core of the device [68].

Fig. 5.24 shows the frequency response of the device for different injection currents as a function of confinement factor and chip length. To achieve a good performance of a 40 Gb/s RZ modulated signal, the 3 dB modulation bandwidth is usually required to be larger than 70% of the operating bit-rate [70], i.e. 28 GHz in this case. The optimization of the modulation bandwidth has previously been extensively studied [140], [136], [138]. With a relatively low injection current as shown in fig. 5.24 (a), the 28 GHz limit requires the use of SOA-chips with length longer than 2 mm and confinement factor

larger than 0.6. By doubling the injection current, the requirements can be much relaxed, as shown in fig. 5.24 (b).

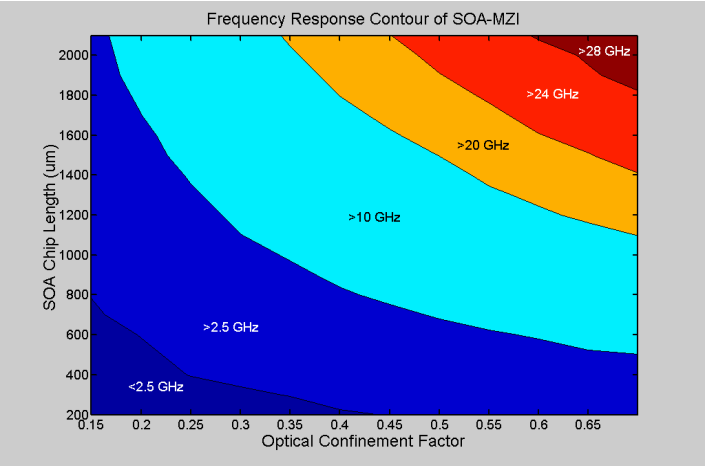

(a)

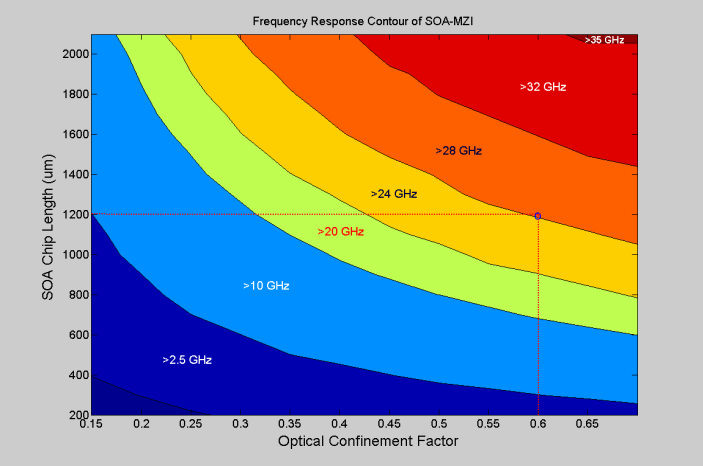

(b)

Fig. 5.24. *Frequency response contour of an SOA –MZI with co-propagation scheme with an injection current of (a) 15 times and (b) 30 times the transparency current.*

As indicated by fig. 5.24 (b), an SOA-MZI with a 1.2 mm length and a 0.6 confinement factor would achieve a modulation bandwidth of 28 GHz. Fig. 5.25 shows the performance of an SOA-MZI under these characteristics, when the incoming signals are in the NRZ or RZ format with an 8 ps rise time (defined as 10% to 90% of the peak value). All the eye-diagrams exhibited large eye-openings with slight pattern-effects. However, for the RZ signal, the pulses were broadened up to around 12 ps, due to the limited bandwidth. To further reduce the pulse broadening effects, higher bandwidth would be required.

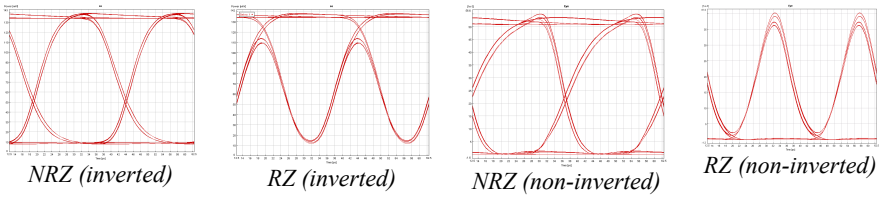

Fig. 5.25. *Output eye-diagrams of an SOA-MZI with 28 GHz modulation bandwidth.*

Differential-arm driven with co-propagating signals

When a single pump pulse differentially drives the SOA-MZI, the phases of the two branches are affected as shown in at the top of fig. 5.26 by the blue and red lines. Due to the limited gain recovery time, both phase-change profiles would have long trailing edges. However, through proper delay and attenuation, the profile of the overall phase difference can be tailored to have a more sharp edge, hence resulting in an improved performance, as shown at the bottom of fig. 5.26.

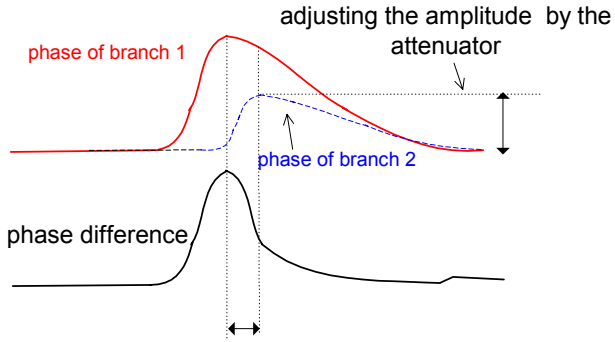

Fig. 5.26. *Principle of the differential driving operation.*

The optimum attenuation value in the differential driving scheme is strongly related to the gain recovery time of the SOA-MZI. As shown in fig. 5.27, the larger the gain recovery time is, the smaller the attenuation value the scheme requires. As the gain recovery time of the SOA was varied from 10 ps to 100 ps, the optimum attenuation value was changed from 4 dB to 1 dB. In the simulations, the relative timing delay was set to be around 8 ps to keep the output signal in a 33%-duty-cycle RZ format.

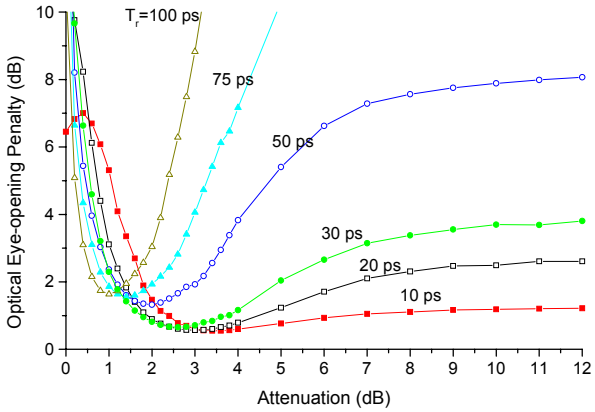

Fig. 5.27. *Optical eye-opening penalty versus power attenuation value for various SOA recovery times.*

As shown in fig. 5.28, improper attenuation values will induce pulse broadening and pattern effects. For a 30 ps gain recovery time, the attenuation value corresponding to the optimum eye-opening was found to be around 3 dB.

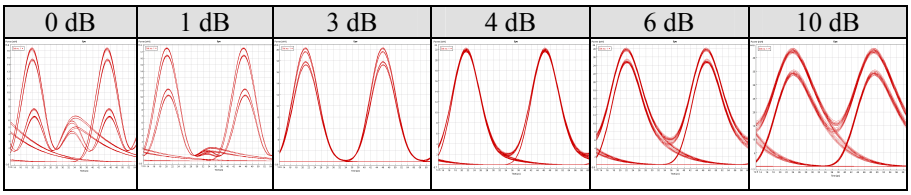

Fig. 5.28. *Eye-diagrams vs. power attenuation for a gain recovery time of 30 ps.*

The relative timing delay can be adjusted to further reduce the pattern effects induced by a slow gain recovery time. Fig. 5.29 shows the simulated eye-diagrams with an SOA with a recovery time of 100 ps. As the timing delay was increased from 8 ps to 16 ps, and the attenuation was changed accordingly, the pattern effects could be reduced. However, due to the pulse broadening, the actual eye opening at the same average power level was not improved.

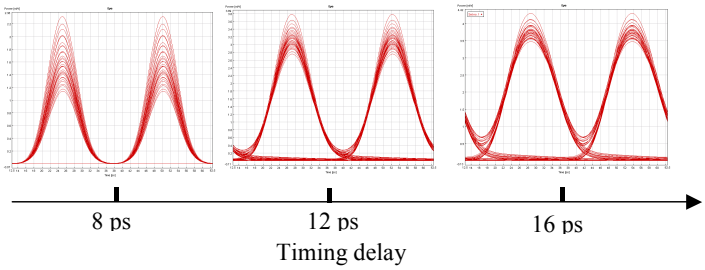

Fig. 5.29. *Increased timing delay to reduce distortion.*

Performance in the presence of noise

In an optical node, several optical modules and subsystems would generate noise and distort the signal waveform, hence degrading the network performance. Taking into account that generally, SOA-MZIs generate small chirp, and assuming a perfect timing synchronization between the modules included in an all-optical node, the major signal impairments include optical signal to noise ratio (OSNR) degradation and waveform distortion.

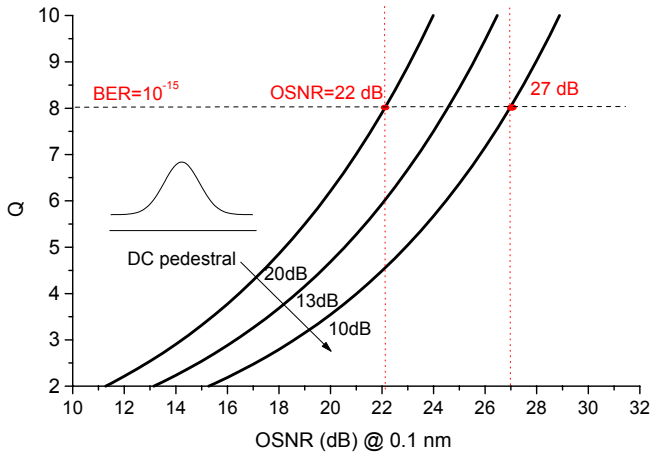

Fig.5.30. *OSNR performance of the 40 Gb/s RZ signal with an optimized optical receiver*

The OSNR performance of a 40 Gb/s RZ signal with a DC pedestal, due to noise or a finite switching on-off ratio, was calculated, as shown in fig. 5.30. In the calculation, the optical signal was assumed to have a Gaussian shape with 33% duty cycle and the bandwidth of the optical receiver was optimized for the best receiver performance. As indicated in fig. 5.30, the OSNR performance was sensitive to the degree of suppression of the DC-pedestal. For a RZ signal with 20 dB of suppression, the OSNR was required to be no less than 22 dB to achieve a BER level at 10^{-15}, while for a suppression ratio of 10 dB the OSNR requirement was increased to 27 dB.

In the next generation all-optical networks, the signals would be sent in packet formats [134]. Up to now, the SOA-MZI performance has been investigated with continuous modulating data and CW probe signals. A numerical analysis was therefore performed in order to investigate the SOA-MZI performance with 40 Gb/s optical packets.

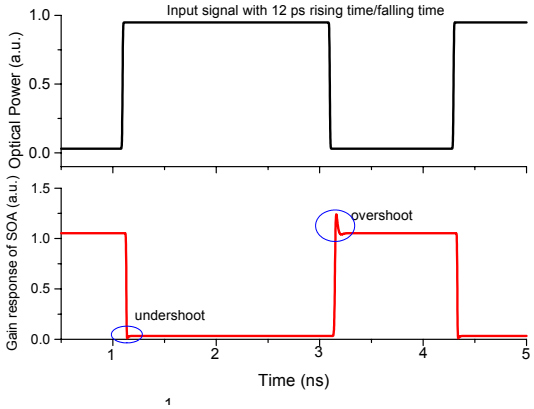

Fig. 5.31. *Gain response of an SOA with 10 ps of gain recovery time, to an optical rectangular pulse with 10 ps rise/fall time.*

Fig. 5.31 shows the gain response of the SOA to an optical rectangular pulse. The duration of the optical square pulse was set as 2 ns. If the input pulse had a rise and falling time that was shorter than the gain recovery time, overshoots and undershoots were observed at its gain response. However, the duration of such an overshoot/undershoot was very short for SOAs with fast gain recovery time. If the input pulse had a rise and falling time that was larger than the gain recovery time, the SOA could respond to it smoothly.

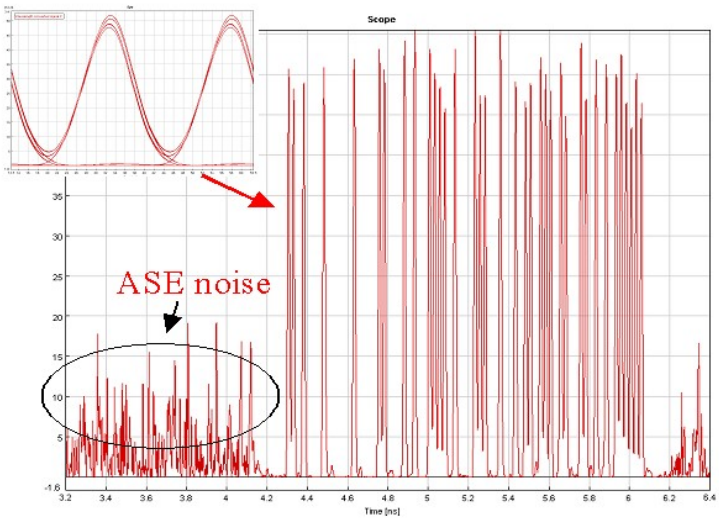

Fig. 5.32. *Converted signal consisting of packets, in the presence of ASE noise*

Fig. 5.32 shows the simulation results for wavelength conversion of packets in the presence of ASE noise. The recovery time of the SOAs was set to 10 ps. The figure presents the whole packet, and a detail of the eye diagram

as an inset, showing that a good eye opening was achieved. During the guard band period between packets, neither modulating signal nor probe signal was injected into the SOA-MZIs, therefore, the ASE noise generated in the SOAs was dominating. Such ASE noise may potentially degrade some network operations. One possible way to reduce its influence, would be to arrange the probe block to be switched instantly in the wavelength tuning process and remain in that state until the next packet arrives. In this way, the probe signal would always be present to saturate the SOAs and the ASE noise would be greatly suppressed.

5.3.2 Experimental results

This section presents an experimental assessment of the performance of SOA-MZIs as wavelength converters for labelled signals. Experimental results are presented for an emulated payload data at 10 Gb/s in the standard configuration. During the wavelength conversion at a node, an orthogonal FSK label would be erased, preparing the signal for the insertion of a new label. In this chapter, it is the wavelength conversion that is the focus of the attention, leaving label swapping for the next chapter. Therefore, only the results of wavelength conversion of intensity modulated signals will be analyzed, which also would be the employed format in time-serial labelled networks [141].

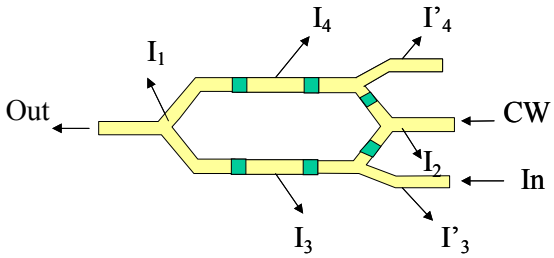

Fig. 5.33. *Schematic of the SOA-MZI wavelength converter used for experiments, in a co-propagating operation mode. The green squares represent the SOAs.*

The experimental results were obtained using an integrated three-port SOA-MZI wavelength converter that had six SOAs incorporated as shown in fig. 5.33, that was kindly borrowed from the University of Eindhoven, and its characteristics published in [50]. Because of dissimilar characteristics in the SOAs and coupling ratios, the non-inverting and inverting modes of operation showed different responses. This operating modes could be achieves by changing the current settings of the SOAs. The experimental setup is shown in fig. 5.34. The data signal was IM modulated at 10 Gb/s on a 1549.3 nm carrier. The probe was a continuous wave (CW) signal operating at 1552.4 nm, which corresponded to the peak transmission of the Optical

Band Pass Filter (OBPF) located at the output of the wavelength converter. The purpose of this OBPF with a bandwidth of 0.73 nm, was to suppress the original data wavelength.

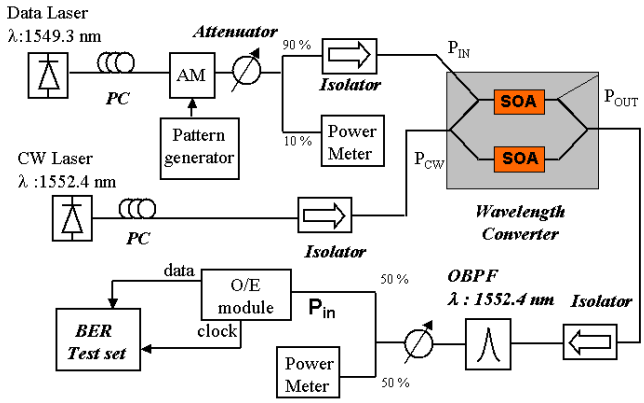

Fig. 5.34. *Experimental setup for IM wavelength conversion in an SOA-MZI.*

As numerically predicted in the previous subsection, the counter-propagating operation was less effective than the co-propagating mode of operation, due to a limited modulation bandwidth that reduced the conversion speed to values lower than for co-directional coupling [116], [143]. Nevertheless, the counter-propagating scheme was measured for a non-inverting current setting at 2.5 Gb/s. By optimizing the system carefully, the penalty was minimized to 1 dB.

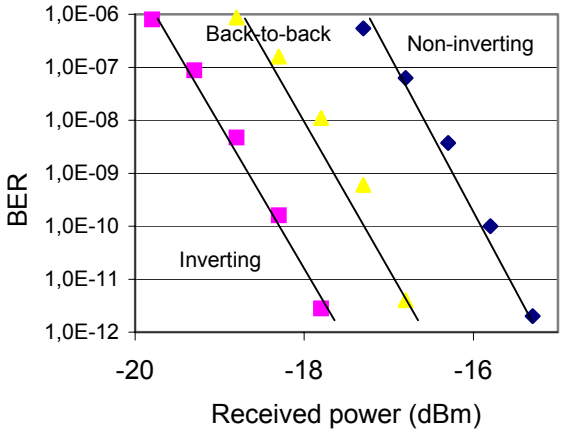

Fig. 5.35. *BER curves for inverting, non-inverting operation and the back-to-back system at 10 Gb/s.*

For the co-propagating mode, the power penalty for the wavelength conversion was measured at 2.5 Gb/s and at 10 Gb/s. The penalty at 2.5 Gb/s was 1 dB for the inverting operation and 1.5 dB for the non-inverting operation. For wavelength conversion at 10 Gb/s in a co-propagating scheme, the BER curves for inverting, non-inverting operation and the back-to-back system are shown in fig. 5.35. For non-inverting operation a 1 dB power penalty was observed, but for the inverting operation even a regenerative effect of 1 dB was measured. The 1dB sensitivity improvement for the inverting operation verified the regenerative effect of the MZI wavelength converter [132]. For the non-inverting operation the 1 dB penalty was most likely caused by the lower extinction ratio of the converted signal.

Because the data signals in a network do not always exhibit the exact same power level when they reach the WC unit, an important parameter to characterize is the dynamic range of the wavelength converter. It was found that the 3 dB dynamic range at 2.5 Gb/s was 3.9 dB for the non-inverting co-propagating mode, while being 2.6 dB for the inverting mode. Despite of that, for the device under study, the inverting operation was still preferable above the non-inverting, due to its larger regenerative effect.

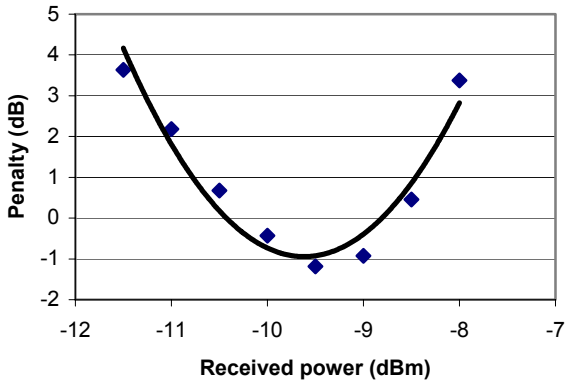

Fig. 5.35. *The dynamic range of the SOA-MZI wavelength converter in the inverting co-propagating operating mode at 10 Gb/s.*

Still in the co-propagating operation mode and for a bit-rate of 10 Gb/s, the results of the dynamic range measurements are shown in fig. 5.34. The 3 dB dynamic range in this case was found to be 3.7 dB for the inverting mode and 1.7 dB for the non-inverting mode of operation. These results are in agreement with other results published in the literature [143]. For orthogonally labelled signals, the wavelength conversion process should also ensure that the ER of the intensity modulation is kept within certain limits, in order to properly detect the label, as commented in previous sections. This will have special relevance when using wavelength conversion in conjunction with label swapping, which will be addressed in the next chapter.

5.4 Chapter summary

In this chapter, the issues concerning wavelength conversion (WC) of optically labelled signals have been studied. WC has been achieved in passive and active devices for bit-rates of 40 Gb/s.

WC in a highly non-linear fiber (HNLF) was used in a setup that exploited cross-phase modulation (XPM) by introducing the data signal along with a CW signal at the desired wavelength to convert to. If the incoming data is combined with a continuous-wave (CW) signal and sent through a highly non-linear fibre, the data imposes a phase modulation onto the CW light through XPM. This phase modulation generates optical sidebands on the CW signal, which can be converted to amplitude modulation by suppressing the original CW signal and filtering out one sideband with the appropriate optical band-pass filter.

This approach proved to be much dependent on the effectiveness of the applied filtering method. Therefore, several filtering methods were compared. The results showed that the most effective method due to the sharpness of the edges of the FBG involved was the use of optical add-drop multiplexers (OADM), that almost showed no conversion penalty. Using a Mach-Zehnder filter also induced less than 1 dB of penalty, while a scheme based on the polarization effect of XPM and a Kerr switch induced 2.1 dB of penalty. Using the same settings for a FWM wavelength conversion showed a penalty of 1.6 dB. This type of WC has the advantage of being transparent to the bit-rate and highly effective at high bit-rates, as the processes involved are all-optical.

FWM as also contemplated for the simultaneous replication of a IM/FSK labelled signal onto several channels, although the conversion efficiency and therefore the filtering issues proved to be severely limiting. Nevertheless, the benefit of FWM compared to XPM in HNLF is that the labelling information contained in the angular modulations of orthogonally labelled signals is not lost in the conversion process. To verify this, a WC of a IM/DPSK labelled signal through FWM in HNLF was implemented. The conversion penalty for the label compared to the back-to-back case was 1.6 dB. However, the regenerating character of the WC process forced to reduced even further the ER of the intensity modulation, which was the cause of a higher penalty on the payload of 5 dB.

Wavelength conversion in active devices occupied the rest of the chapter. An IM 40 Gb/s wavelength conversion was achieved by XGM in SOA with 5 dB of penalty, which were partly due to the large insertion losses into the device.

An alternative method for WC in active devices, was employing Mach-Zehnder interferometers with SOAs in each arm (SOA-MZI). These devices were investigated both numerically and experimentally.

Various configuration schemes of SOA-MZI were simulated and discussed. The results showed that the co-propagating schemes performed better than the counter-propagating schemes, as the counter-propagating signals, required the use of short length SOA chips for high switching performance. Furthermore, it was shown that the differential driven mode of operation relaxed the requirements on the SOAs involved and improved the performance, at the cost of having an extra delay and attenuator to optimize. This optimum attenuation value was affected by the timing delay and the SOA gain characteristics. The requirements on the SOA for an SOA-MZI designed for WC of 40 Gb/s signals are summarized in Table 5.1.

Table 5.1. *Comparison of the SOA-MZI configuration schemes for 40 Gb/s wavelength conversion.*

Scheme	Signal format	Requirements on SOA
Single arm, co-propagating	NRZ, RZ	Gain recovery time < 30ps
Single arm, counter-propagating	NRZ, RZ	Gain recovery time < 30ps Chip length < 500 μm
Differential, co-propagating	RZ	Gain recovery time < 100ps
Differential, counter-propagating	RZ	Gain recovery time < 100ps Chip length < 500 μm

The performance of the SOA-MZI was also analyzed with respect to the noise level of the incoming signals and the noise generated in the device. According to fig. 5.30, the OSNR level of the output signal should be no less than 30 dB with a 3dB~6dB margin requirement in order to achieve a BER of 10^{-15}. For a packet based network, the ASE noise generated at the SOAs when no switching signal is present at the input could prove detrimental to the system if not taken into account.

Finally, WC was experimentally verified in an SOA-MZI at 10 Gb/s, supporting the numerical conclusions. The regenerative effect of the SOA-MZI was clearly observed and the dynamic range of the device under study measured to be around 3 dB.

In conclusion, it has been demonstrated that WC in passive HNLF is suitable for optical labelled signals at high bit-rates, as long as the filters involved are sharp and stable enough. In active devices, the design has to match the

requirements of the bit-rate of the signal, but offers a higher versatility and a looser requirement on filter stability.

However, ER of the payload could be enhanced in some of the presented WC processes. Thereby, the label performance in the orthogonally modulated signal would be reduced. This could be a constraint to WC or at least it could set a limit on the amount of nodes where WC can be applied without renewing the label.

Another limitation to the presented wavelength converters, is that signals transversing them necessarily have to be converted to a new wavelength. The only WC that did not show this limit was the counter-propagating scheme in an SOA-MZI, but the limitations of this scheme compared to its co-propagating counterpart render it unviable. For a network node that means that if the same wavelength has to be used for the input and output signals, either the converter has to be surpassed, or a double converter scheme has to be employed, in which an intermediate wavelength is employed. This solution can in fact be combined with the swapping of the label, as will be proposed in Chapter 6.

Chapter 6

All-optical label swapping

Label swapping is one of the essential all-optical network node functionalities. The information carried by the label should serve for networking purposes, and should be able to be dynamically altered at each intermediate node [145].

Label swapping is closely related to wavelength conversion. Given that the chosen wavelength can be used for routing purposes, the wavelength of the signal can be viewed as a second label. In this sense wavelength conversion can be regarded as a coarse label-swapping technique, that should be assessed along with the swapping of the label carrying bit-information.

The present chapter presents the investigation on several label swapping techniques from a systems point of view. Label swapping of IM/DPSK labelled signals will be addressed first, by label erasure and insertion in active and passive devices. The second section will employ SOA-MZIs, electroabsorption modulators (EAM) and a combination of both for IM/FSK label swapping. After that the very simple label swapping method for CSS labelling will be briefly commented, and finally a numerical analysis will be carried out for the insertion of time-serial IM labels employing SOA-MZI.

6.1 IM/DPSK label swapping

This section presents experimental validation of label swapping techniques for orthogonally labelled IM/DPSK signals. Both active and passive components for label erasure will be investigated. The benefit of combining wavelength conversion with the label swapping process will be analysed. The payload bit-rates used in the experiments will vary between 10 and 40 Gb/s. Label swapping for the alternative DPSK/IM format will briefly be

discussed. The SOA and the EAM used in the experiments of this section were kindly provided by GIGA-Intel.

6.1.1 DPSK label erasure by XGM in SOA

SOAs working as wavelength converters making use of XGM, only respond to intensity variations of the control signal, in which case, all phase information or frequency information will be erased in the process [146]. The schematic of the label erasure part of the experimental setup is shown in fig. 6.1. The transmitter and receiver, omitted in this figure, are the same as the ones presented in Section 2.1, generating an IM/DPSK signal. Its center wavelength was 1552.5 nm and its bit-rates was set to 10 Gb/s for the payload and 2.5 Gb/s for the label. As discussed earlier, the intensity modulation had to have a limited extinction ratio of 3 to 4 dB, in order to correctly detect the label.

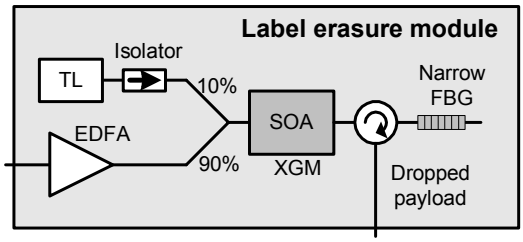

Fig. 6.1. *Experimental setup for DPSK label erasure based on an SOA.*

The DPSK label should be erased by an intensity-sensitive wavelength converter that copies the payload information onto a new wavelength while omitting the phase information of the label. In this approach the erasing of the DPSK label was done by cross-gain modulation (XGM) based on wavelength conversion in an SOA, described in Section 5.2. The new carrier was generated by a wavelength tunable external cavity laser (TL) working at 1550.0 nm. A narrow fiber Bragg grating was deployed directly after the SOA to overcome pattern dependence and to remove frequency chirp [148]. Finally, the payload at the output of the label-eraser module, was directly detected.

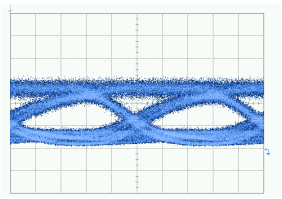

Fig. 6.2. *Measured eye diagram of the payload after label erasure.*

Fig. 6.2 shows the eye diagram of the detected payload after label erasure, which is open although it shows some pattern effects. The BER curves of the label erasing process compared to the back-to-back performance are shown in fig. 6.3. For a BER of 10^{-9}, the penalty for label erasing in the SOA was found to be 2.5 dB.

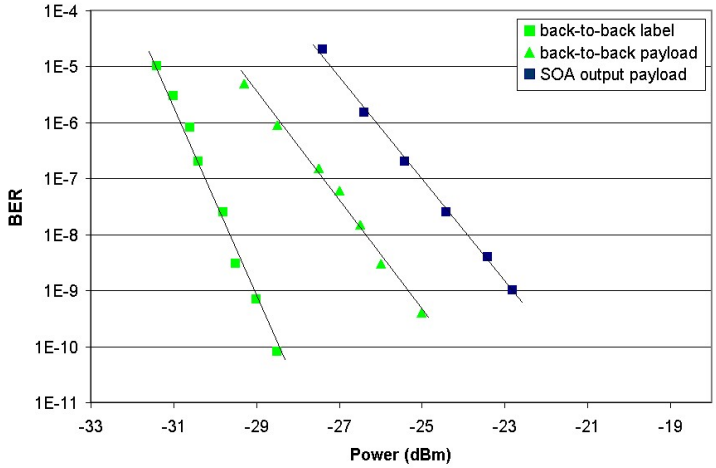

Fig. 6.3. *Measured BER curves of the label erasure through XGM in SOA.*

6.1.2 DPSK label insertion by XAM in an EAM

For the IM/DPSK labelling format, label insertion can be done by modulating the phase of the carrier directly on the payload IM bit-stream, by a phase modulator. Another approach would be to wavelength convert the incoming signal while adding the phase modulation, thus adding flexibility to the node. Because the chirp induced by EAM-based wavelength conversion is negligible [149], the phase of the probe and pump signals are not affected in the wavelength conversion process. Therefore the DPSK label can be inserted by phase-modulating a new carrier-wave and then copying the payload onto it through cross-absorption modulation in an EAM.

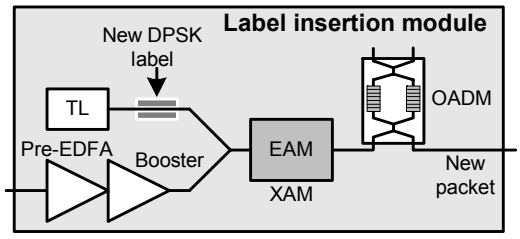

Fig. 6.4. *Experimental setup of DPSK label insertion based on XAM in an EAM.*

The schematic diagram of this approach is shown in fig. 6.4. The incoming signal was intensity modulated at 10 Gb/s and centered at 1550.0 nm. In the label-insertion module, a tunable external-cavity laser (TL) emitting at 1555.0 nm, was phase modulated with a new DPSK label at 2.5 Gb/s. These two signals were combined and injected into an EAM. The absorption coefficient of this device is dependent on the carrier density, which in turn is dependent on the incoming optical field [150]. With an intensity modulated optical signal present at the input, the carrier density follows the intensity variations of the data signal, which will vary the absorption experienced by the accompanying phase modulated signal of constant intensity [152]. The result is that the XAM process in the EAM copies the intensity modulated data stream onto the phase modulated carrier [153], thus achieving label insertion. An OADM would then be used to select the signal for re-transmission.

At the receiver, the IM/DPSK signal was split in two, in order to detect the IM payload and the DPSK label separately. The DPSK label was demodulated using a one bit delay fiber interferometer before direct detection.

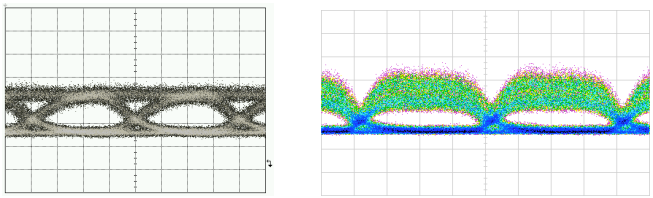

(a) *(b)*

Fig. 6.5. *Eye diagrams after label insertion (a) payload, (b) label.*

Fig. 6.5 shows the eye diagrams of the payload and the label after wavelength conversion and insertion of the new DPSK label. Very clear and open eyes can be obtained for both the payload and the label after wavelength conversion and label insertion. The label eye diagram in fig. 6.5 (b) has the multi-level structure of the ‘mark’ level that has been encountered before, while the payload eye diagram, shown in fig. 6.5 (a) showed some regeneration with respect to ER and noise in the ‘0’ level.

Fig. 6.6 shows the BER curves for the label insertion process. It is noticeable that the performance of the converted payload was enhanced by 1 dB due to the regeneration of the extinction ratio.

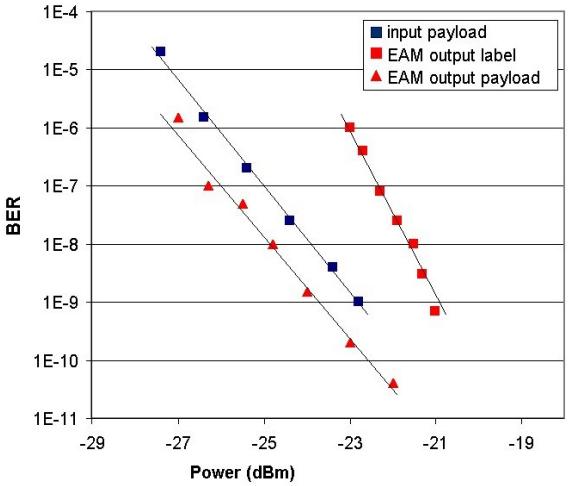

Fig. 6.6. *Measured BER curves for label insertion through XAM in an EAM.*

6.1.3 DPSK label swapping combining SOA and EAM

In a network node, the labelled signal is likely to have to be wavelength converted along with having its label swapped. One limiting factor of most wavelength conversion processes is the inability to "convert" the signal to the same wavelength it had at the input (leaving the carrier wavelength unaltered, that is). This would impose severe restrictions to the performance of the network as a whole, because of the possible output channels for a node one would not be able to use, thus increasing the blocking probability [155]. Another challenge for the optical node is the need of fast tunable filters that would select the optical channel to be re-transmitted, while suppressing the other unwanted wavelengths that might be present at the output of the node [156]. A way to overcome both of these problems would be to combine the label erasing process with a wavelength conversion to an intermediate wavelength chosen to be different from the channels used in the labelled network. The label insertion process could then be combined with yet another wavelength conversion, that this time would select the carrier wavelength according to the wanted channel at the output of the node. In this way the same channel can be used as input and output, and the filtering can be fixed to suppress only the intermediate wavelength used between label erasing and label insertion.

Hence, combining the previously presented label erasure and label insertion methods would be a promising solution for label swapping in IM/DPSK network nodes. The schematic diagram of the proposed method is presented in fig. 6.7, and consists of combining the label erasure module and the label insertion module described in the two last subsections.

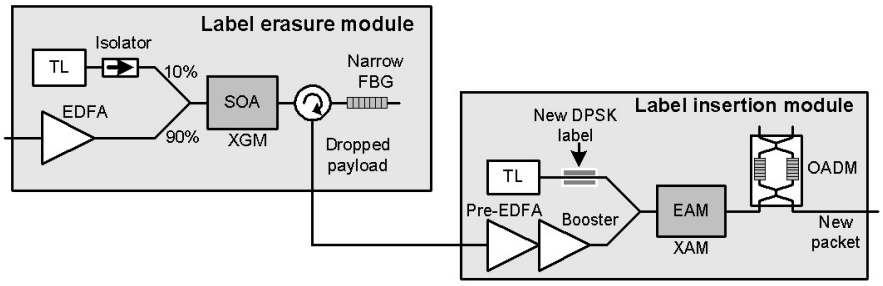

Fig. 6.7. *Label swapping process for IM/DPSK labelled signals with fixed filtering and possibility of re-usage of the wavelength channel.*

The BER curves of this label swapping process with wavelength conversion is shown in fig. 6.8. The results marked in green belong to the back-to-back performance of the payload and label. The extinction ratio of the IM was chosen so that the label would out-perform the payload by 4 dB. The results marked in blue are for the payload after the label was erased in an SOA and the signal was converted to the intermediate wavelength. Finally, the results marked in red are for the cascaded label erasure and new label insertion and when the signal was re-converted to the desired output wavelength. For a BER of 10^{-9}, the overall penalty of the system was 1.6 dB for the payload, but was as high as 8 dB for the label. The reason for this worsened performance for the label was the enhancement of the ER that the payload experienced in the process. As discussed in Section 2.1, the performance of the label is much dependent on the ER of the payload. Therefore, an improvement on the ER of the payload would in turn mean a degradation on the performance of the label. Careful optimisation would ensure that the IM ER would be kept at a constant level, thus drastically reducing the penalty of the label.

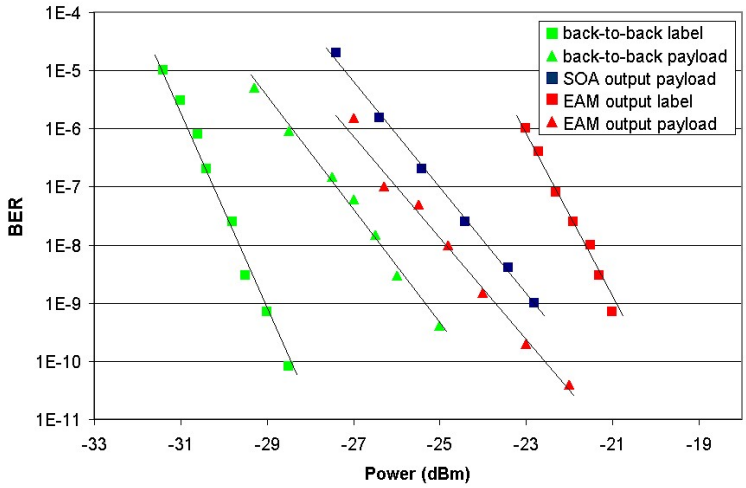

Fig. 6.8*. BER performance of the label swapping process for IM/DPSK signals.*

6.1.4 DPSK label swapping in HNLF

In Section 5.1.1 it was observed that a highly non-linear fiber (HNLF) could be employed for wavelength conversion by using the effects of cross-phase modulation (XPM) on the accompanying CW carrier. This effect is only dependent on the intensity of the data signal. Thus, an IM/DPSK labelled signal would lose its phase information while being wavelength converted by this method. The remaining payload after label erasure, could then be phase modulated in order to add a new label to the signal.

This section presents the results of this method of label swapping for IM/DPSK labelled signals. The filtering method employed was the Kerr-switch analyzed in Section 5.1.1. It is based on a polarization beam splitter (PBS) that, for proper alignment, blocks the incoming signal in the absence of a pump. XPM would induce a polarization rotation in the signal, which would allow part of the CW to pass through the PBS. The IM payload data was copied onto the new carrier through this method, while the DPSK information was lost.

The experimental setup is shown in fig. 6.9. The signal source was a DFB laser at 1550.9 nm. The DPSK label information at 2.5 Gb/s (PRBS 2^{23}-1) was added to the laser source by a phase modulator. The payload information was the added by two external dual-drive Mach-Zehnder modulators (MZM) driven by a 40 Gb/s 8B/10B encoded data-stream, that provided an extinction ratio of 12 dB.

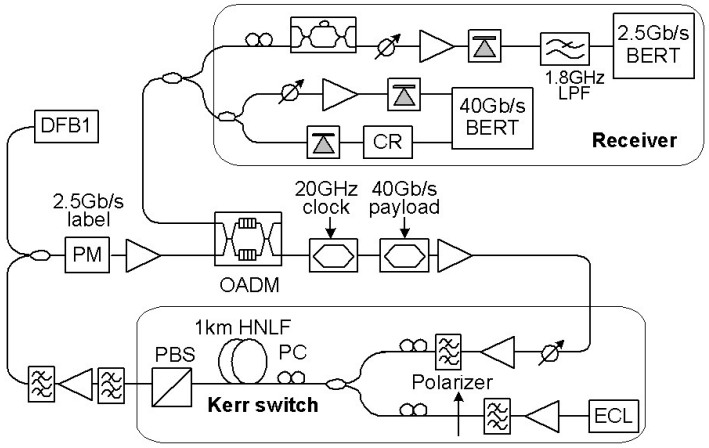

Fig. 6.9. *Experimental setup for label swapping of IM/DPSK signals through a HNLF and a Kerr-switch.*

The optically labelled signal was input to the highly non-linear fiber (HNLF) for wavelength conversion and label erasure. A tunable external cavity laser at 1555.8 nm was used as CW input for the Kerr switch. The label-erased payload at the new wavelength then was re-injected to the phase modulator in order to insert the new label. An optical add-drop multiplexer was used to extract the signal after label swapping. At the receiver, the DPSK label demodulation was provided by a MZI with 8 cm length difference between its two arms. A low-pass filter with 1.8 GHz bandwidth was applied in the DPSK receiver to flatten the optical power distribution within one label bit and to remove the amplitude fluctuation induced by the intensity modulated payload.

It should be noted that in the Kerr-switch, even if the DPSK label information is erased during the wavelength conversion process, an additional phase term of each pulse at 40 Gb/s is added to the converted signal. However most of this phase noise could be removed by the differential DPSK demodulation and by passing through a 1.8 GHz low-pass filter in the DPSK label receiver.

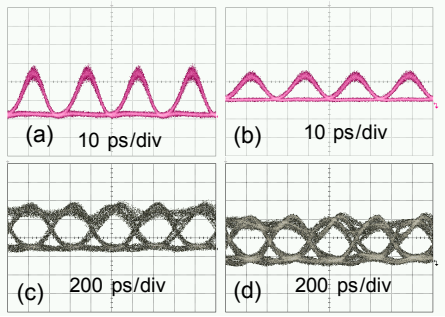

***Fig. 6.10**. Received eye-diagrams for the 40 Gb/s payload (above) and 2.5 Gb/s label (below). (a) and (c) before label swapping; (b) and (d) after label swapping.*

The detected eye-diagrams for the 40 Gb/s payload before and after label updating are shown in fig. 6.10 (a) and (c), respectively. Fig. 6.10 (b) and (d) show the eye-diagrams of the DPSK label. Very clear and open eyes could be obtained for both the payload and label after label swapping. Because of the residual phase shift introduced by the Kerr switch, the payload ER after the wavelength conversion was slightly degraded to 9 dB to ensure the label detection.

Fig. 6.11 shows the BER curves for the label swapped signal compared to the non-swapped signal. The penalties for a BER of 10^{-9} were 4 dB for the payload and 0.3 dB for the label. The higher degradation of the payload was due to the reduction of its ER in order to preserve the performance of the label.

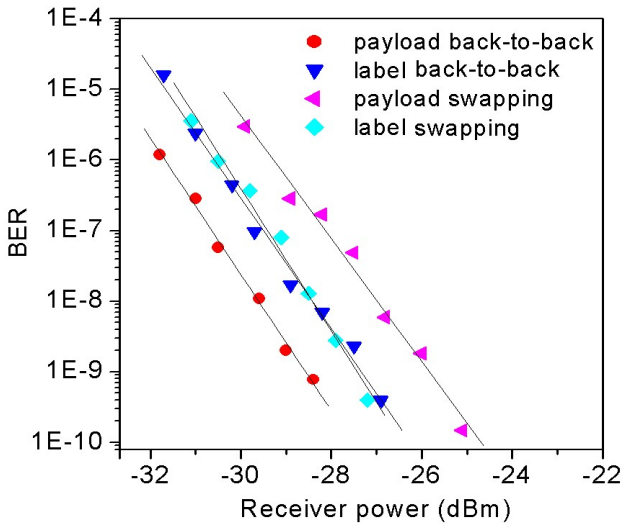

Fig. 6.11. *Measured BER for the IM payload and the DPSK label with and without label swapping.*

6.1.5 DPSK/IM label swapping

An alternative way of employing intensity and phase modulation orthogonally, would be to modulate the label in the intensity and the payload in the phase of the carrier, as described in Section 2.1.2. This section presents a method of erasing the IM label at 2.5 Gb/s while keeping the DPSK payload information at 40 Gb/s for further use in the network. The method is similar to the one used in the DFB/EAM FSK source described in Section 2.2.1, in the sense that it makes use of the inverted intensity data to drive an electro-absorption modulator (EAM) in order to remove the intensity modulation.

The setup for the experiment is shown in fig. 6.12. The signal generator was described in detail in Section 2.1.2. It consisted of a laser source emitting at 1550 nm, that was phase modulated at 40 Gb/s in order to encode the payload information. After that, an EAM was used to modulate the 2.5 Gb/s intensity label while keeping the phase untouched [158].

At the receiver, the labelled signal was split using a 3 dB optical coupler. The output of one arm was used for label detection by filtering and direct detection by a photodiode.

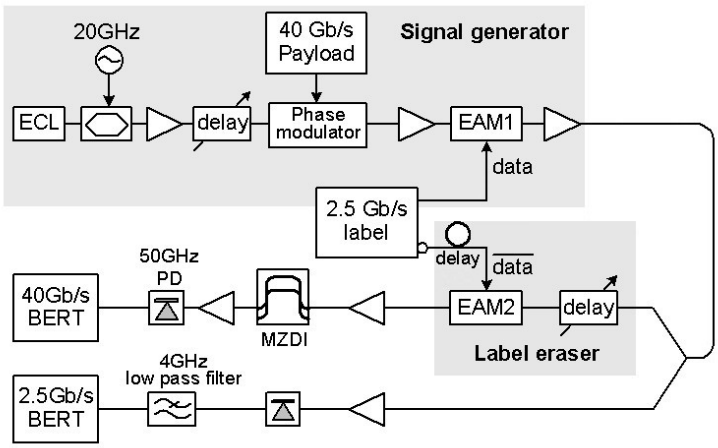

Fig. 6.12. *Experimental setup for label erasure in the DPSK/IM format.*

From the second output of the splitter, the labelled signal was input to another EAM driven by the inverted label data with suitable delay and amplitude for label erasure. In a real system this would be performed with the detected label, but in the present setup, the original data source was used. In this way, the signal exhibited an almost flat intensity, while the phase containing the payload information still was modulated. This was feasible because the chirp induced by the EAM was negligible, as shown in [149].

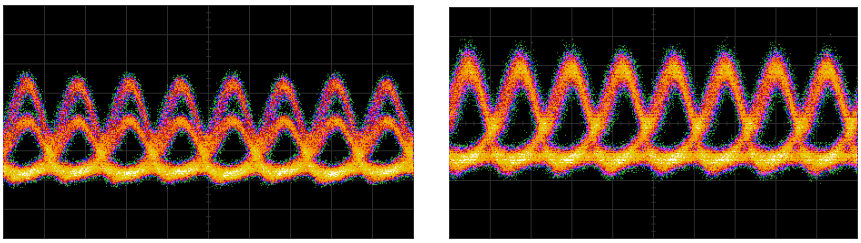

(a) *(b)*

Fig. 6.13. *Eye diagrams of the payload (a) without label erasure, (b) with label erasure.*

Fig. 6.13 shows the eye-diagrams of the demodulated payload before and after the label erasure process. The figure illustrates clearly why the detection of the payload was much enhanced when the intensity modulated label was removed from the data stream. After label erasure, a good eye pattern of the demodulated payload was received. The received IM label eye diagrams were not affected by this process and were therefore identical to the ones presented in fig. 2.17 of Section 2.1.2.

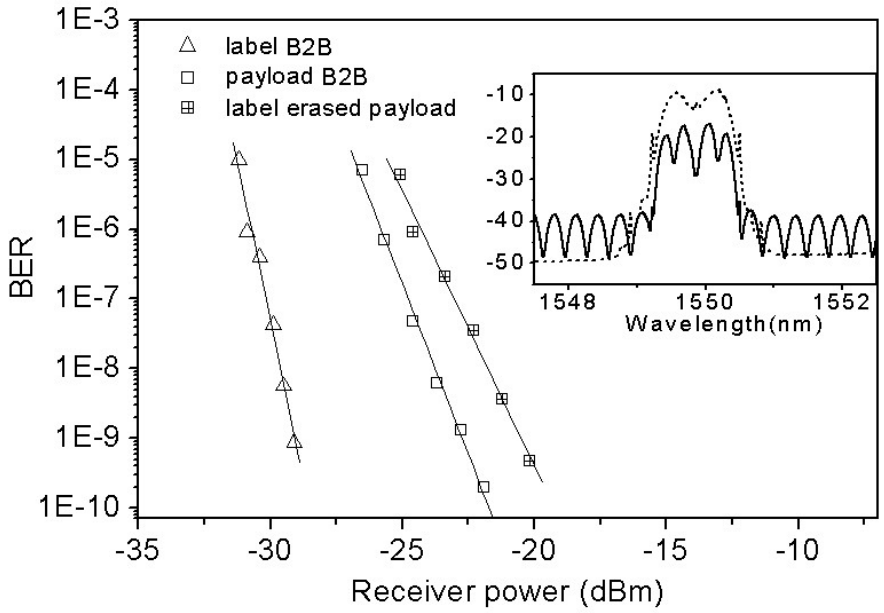

Fig. 6.14. *Measured BER results for the payload and label. The inset figure shows the optical spectra of the labelled RZ-DPSK signal (dashed line) and after label erasure and demodulation (solid line).*

Fig. 6.14 shows the BER curves in the back-to-back case and after label erasure. This method requires the erasure of the label in order to properly detect the payload. Therefore, a DPSK payload signal without labelling was measured, in order to compute the penalty of labelling and erasing that label. This penalty was found to be 2.3 dB. The inset figure shows the optical spectra for the labelled payload and the payload after label erasure and demodulation.

6.2 IM/FSK label swapping

Fig. 6.15 shows the schematic diagram of an SOA-MZI wavelength converter based label processing node, as suggested by [50] for the STOLAS network concept. A small part of the incoming optical power would be fed to the label processing circuit, that would define a new label through a look-up table. The new wavelength would be set by a tunable laser diode, and the incoming intensity-modulated payload data would be transferred to this new wavelength by an SOA-MZI, in the way described in Section 5.3. In the wavelength conversion process the old FSK information would be erased while the payload data would be copied onto the new wavelength. The new FSK label would be inserted by frequency detuning on the incorporated tunable laser.

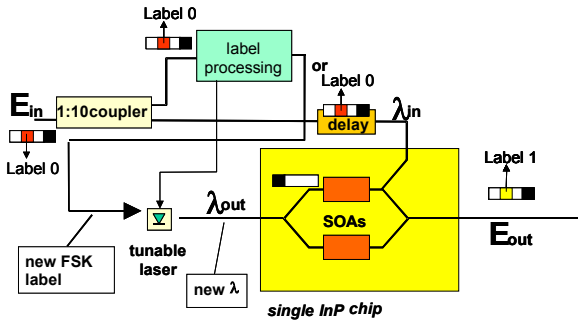

Fig. 6.15. Schematic diagram for a label swapping node with an SOA-MZI based wavelength converter for orthogonal IM/FSK labelling .(Figure from [50]).

This section will describe and compare label swapping techniques for IM/FSK labelled signals, based on SOA and/or EAM. Experimental results are presented for a payload data at 10 Gb/s and an FSK label at 312 Mb/s.

6.2.1 FSK label erasure in SOA-MZI

As shown in Section 5.3, an SOA-MZI, can effectively be used as wavelength converter. In the XPM process involved, the signal at the new wavelength only acquires de intensity of the payload, while the frequency or phase information will be lost. In this way, wavelength conversion in SOA-MZIs can be combined with the label erasure of the FSK label.

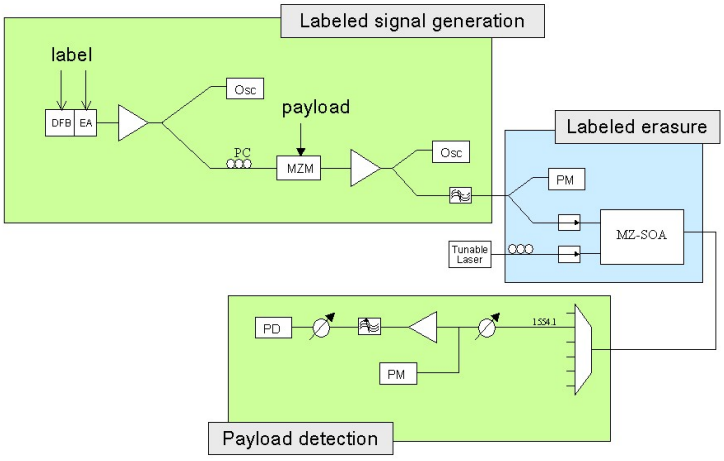

Fig. 6.16. Experimental set-up for FSK label erasure using an SOA-MZI wavelength converter.

The experimental set-up for label erasure is depicted in fig. 6.16. The optical FSK modulation was generated by a DFB/EAM source at 1549.3 nm, that later was intensity modulated. This produced a labelled signal with an IM payload rate of 10 Gb/s and an FSK label rate of 312 Mb/s, which was set to a power level of -9 dBm. The CW source was a tunable ECL emitting at 1554.1 nm with a power level of 0 dBm. These two signals were injected into the SOA-MZI, where the wavelength conversion would take place, thus erasing the FSK label. At the output of the SOA-MZI, an AWG based multiplexer was used to filter out the converted signal.

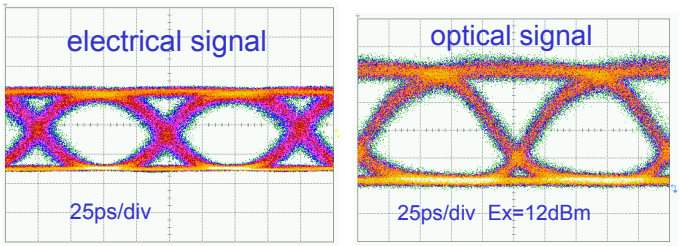

Fig. 6.17. *Received eye diagrams of the label erased payload.*

The output payload eye diagram after label removal is shown in fig. 6.17. For an input payload extinction ratio of 4.5 dB, the output signal had an extinction ratio of 12.9 dB, resulting in an increased receiver sensitivity of 2 dB compared to the back-to-back case, clearly demonstrating the 2R regenerating capabilities of the SOA-MZI.

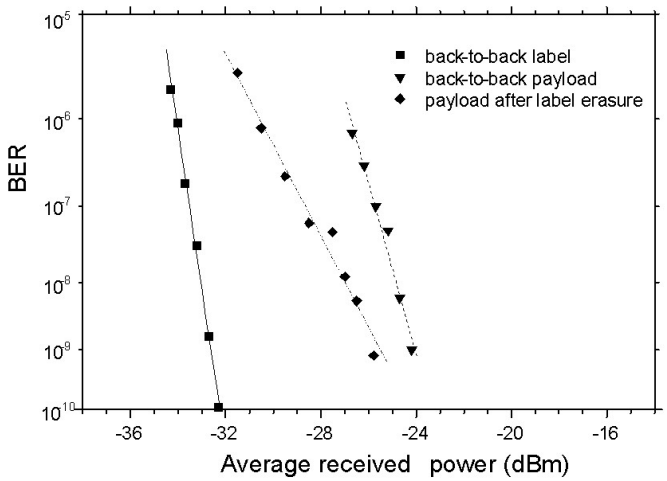

Fig. 6.18. *BER curve for an IM payload at 10 Gb/s after label erasure in an SOA-MZI wavelength converter.*

Fig. 6.18 shows the BER curves for the label erasure compared to the back-to-back configuration of the IM/FSK signal. The receiver sensitivities at a BER of 10^{-9} were -32.6 dBm for the label and -24.2 dBm for the payload respectively. The label erasure process enhanced the performance of the payload by 1.7 dB, because of the increased ER of the output signal. As it was discussed in Section 2.2.1, this ER would probably be too high if a new FSK label had to be impressed on top of the IM signal. The settings for the SOA-MZI should therefore be adjusted in order to have a more moderate ER, unless the node was an edge node were the payload was to be directly detected or re-transmitted without re-labelling.

6.2.2 FSK label insertion in SOA-MZI

The same SOA-MZI wavelength converter can be used as a label insertion circuit, if the new FSK label is modulated on the new carrier before it is inserted into the device. Compared to the last scheme, it only means using an FSK modulated signal instead of a CW signal at the input of the SOA-MZI converter. The signal output of the SOA-MZI would then consist of the original payload data, converted to the FSK signal wavelength, with the superimposed FSK label modulation. The experimental set-up is shown in fig. 6.19.

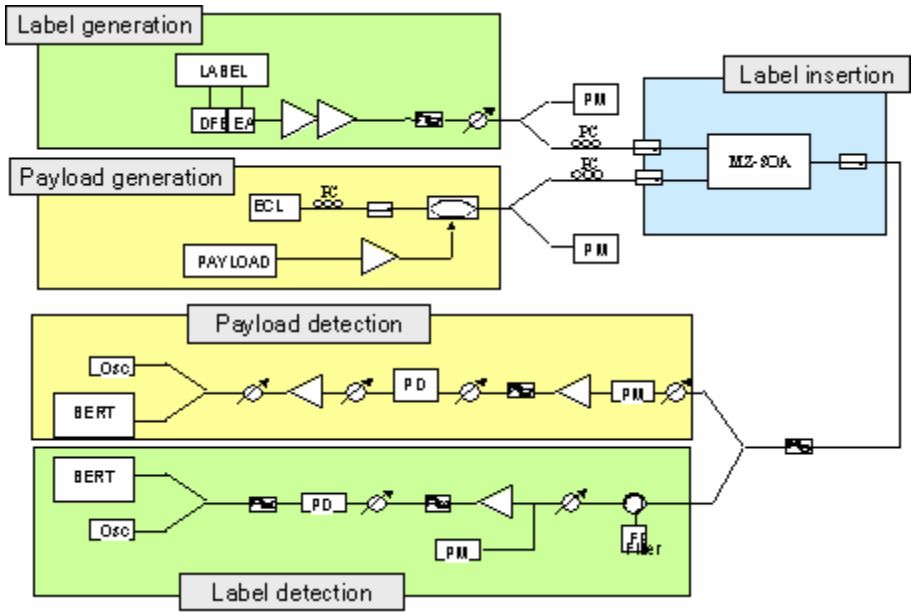

Fig. 6.19. *Experimental set-up for FSK label insertion using an SOA-MZI.*

The eye diagrams of the payload and the detected label after label insertion are shown in fig. 6.20. As mentioned in the last subsection, a high regeneration in the SOA-MZI would lead to degradation of the label, due to the fact that for a proper detection of the FSK signal, a certain power level in the 'zero' bits should be present. The ER of the input signal was measured to be 5.1 dB and an ER of 4 dB was achieved at the output of the SOA-MZI adjusting the current settings to a sub-optimum configuration.

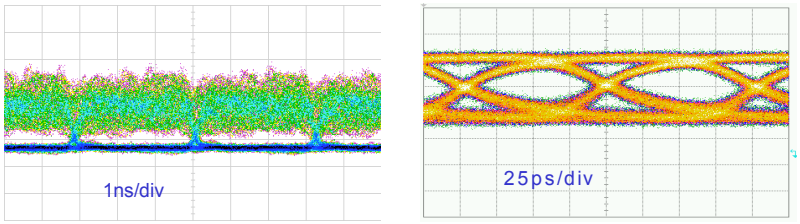

(a) *(b)*

Fig. 6.20. *Received eye diagrams of (a) label and (b) payload after label insertion.*

Fig. 6.21 presents the optical spectrum of the setup. From fig. 6.21 (a) it can be observed that there was not a substantial spectral broadening due to the label insertion. This indicates that the chirp introduced by the SOA-MZI had therefore no effect on the performance, which is in accordance with the chirp measurements and simulations results presented in [50].

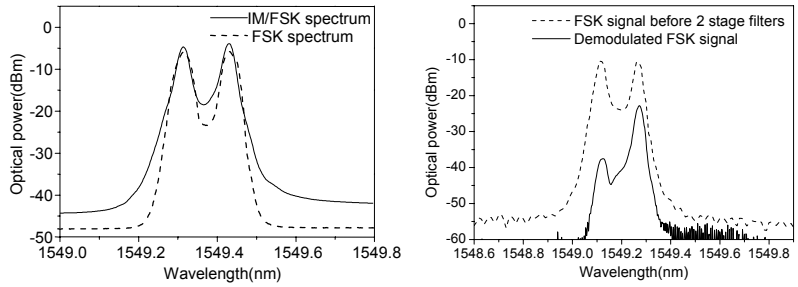

(a) *(b)*

Fig. 6.21. *(a) Optical spectra of the pure FSK and the IM/FSK signal, (b) optical spectra of the FSK signal and demodulated FSK signal.*

The resulting BER curves are presented in fig. 6.22, compared to the back-to-back case. For a BER of 10^{-9}, the receiver sensitivity was -31 dBm for the label, and -23.5 dBm for the payload. No substantial degradation of the receiver sensitivity was observed in the label insertion process. The BER of the inserted label had a different slope than the back-to-back FSK label (that did not traverse the SOA-MZI module), indicating that the dominant source of noise might have varied in this case [159].

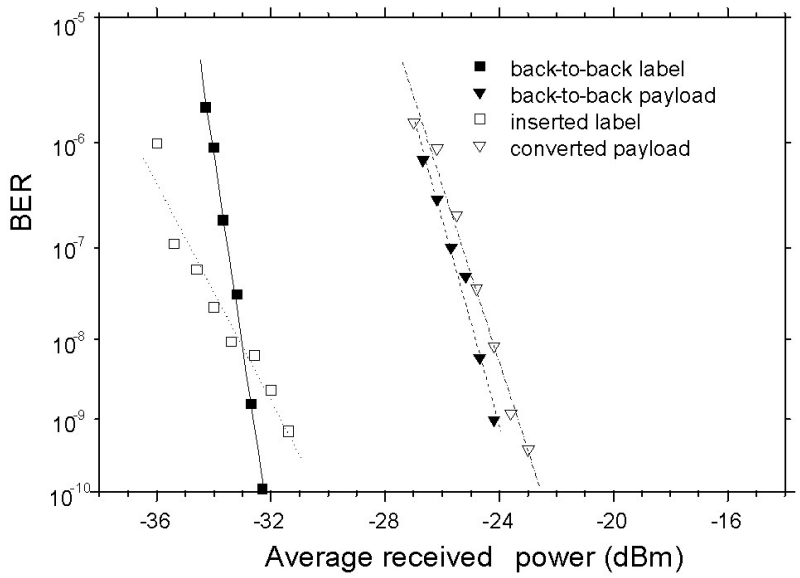

Fig. 6.22. *Measured BER curves of the payload and label after label insertion.*

6.2.3 FSK label insertion in EAM

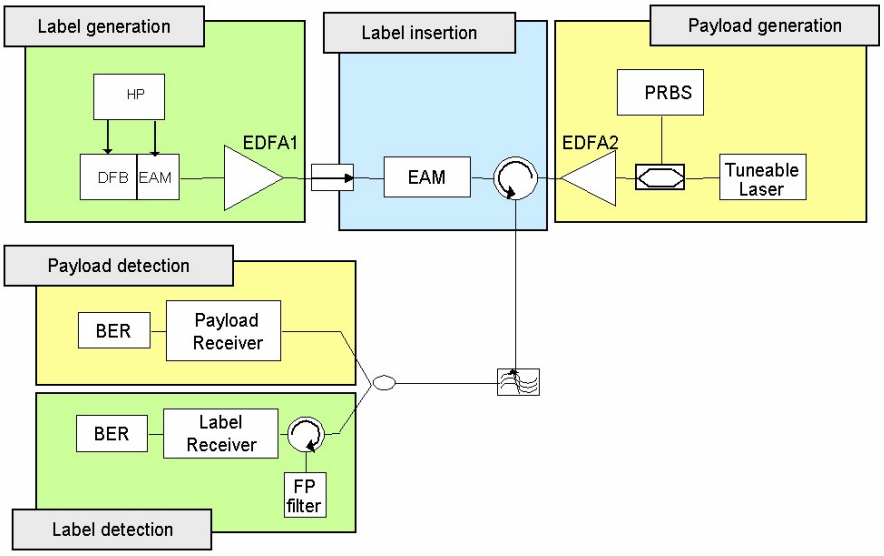

Fig. 6.23. *Experimental set-up for FSK label insertion using an EAM.*

Cross-absorption modulation (XAM) in an EAM can also be employed for FSK label insertion. As discussed in Section 6.1.2, the chirp induced by

EAM-based wavelength conversion is negligible, thus the angular modulation of the probe and pump signals are not affected in the wavelength conversion process [149].

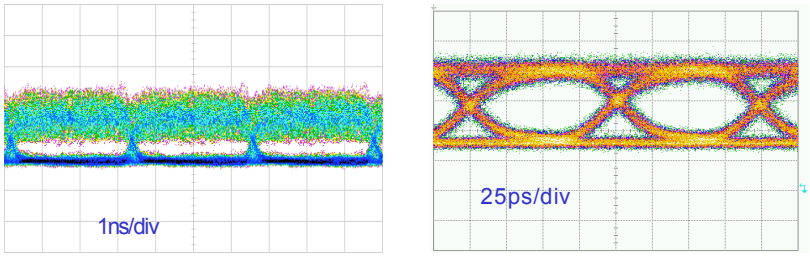

Fig. 6.24. *Received eye diagrams of (a) the label and (b) the payload after label insertion.*

The experimental set-up for FSK label insertion based on this technique, is shown in fig. 6.23. A DFB/EAM source generated an FSK modulated signal at 312 Mb/s based on a PRBS with a pattern length of 2^7-1. At the same time, a CW light beam generated by a tunable laser working at 1554.1 nm was intensity-modulated in a MZ-modulator at 10 Gb/s with a PRBS with pattern length of 2^9-1. These two signals were injected into an EAM in counter propagation, where wavelength conversion, performed through XAM, copied the IM information onto the FSK signal. The EAM needed high levels of power as input, so the optical power of the IM payload was set to 23.5 dBm, while the label was set to 12.5 dBm. After wavelength conversion, the original payload carrier was filtered out through an optical filter with a bandwidth of 1.6 nm, after which the signal was split for payload and label detection.

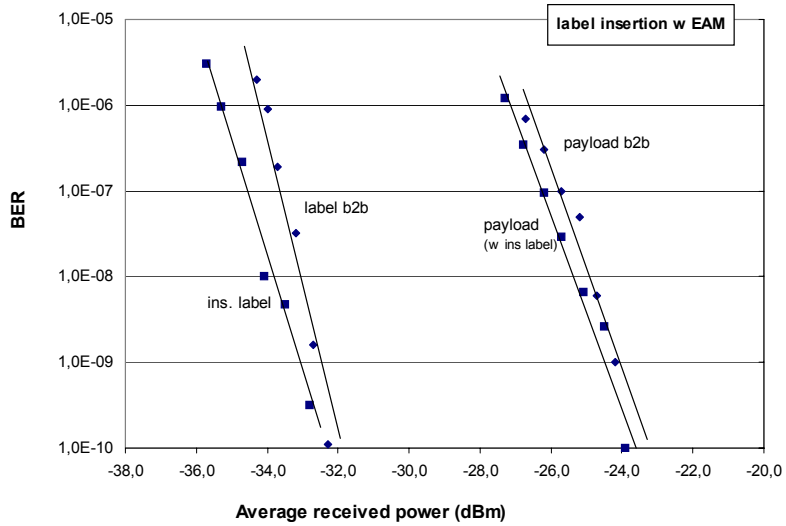

Fig. 6.25. *BER versus input power for label insertion in the IM/FSK labelling scheme.*

Fig. 6.24 shows the received eye diagrams of the payload and label after label insertion, clearly showing that the IM information was successfully duplicated onto the new carrier with the new FSK label. The input ER was adjusted to 4.5 dB, while at the output the ER was measured to be 4 dB.

BER measurements are shown in fig. 6.25, indicating an enhancement in performance of both payload and label of around 1 dB for a BER of 10^{-9}. The drawback of this label insertion scheme is the high levels of power needed to make the method effective.

6.2.4 FSK label swapping in SOA-MZI

Based on the experience gained through the experiments of Sections 6.2.1 and 6.2.2, the label erasure and insertion processes could be combined in one single operation, by employing an SOA-MZI. The schematic diagram of the method is presented in fig. 6.26. An IM/FSK labelled signal is inserted in the data input of the SOA-MZI, while the new FSK label is modulated on to the new carrier wavelength and inserted into the CW input of the SOA-MZI. The wavelength conversion process in the device will copy the IM payload onto this new labelled signal. An appropriate band-pass filter at the output of the wavelength converter would ensure that the output of the system is the new FSK label at the new wavelength with the IM payload impressed on top of it. In this way, the whole label swapping is performed with the help of one single device, provided that the new FSK signal is available at a different wavelength than the old FSK label to be erased.

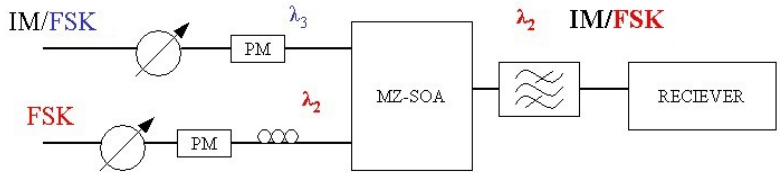

Fig. 6.26. *Principle of IM/FSK label swapping employing a single SOA-MZI.*

Although, a counter-propagation mode of operation could be used for being able to re-use the same wavelength for the input and output signals, the SOA-MZI under study showed insufficient performance for data rates above 5 Gb/s for this mode of operation. This result is in accordance with the numerical investigation performed in Section 5.3.1.

Fig. 6.27 shows the experimental setup. A GCSR laser was FSK modulated with a PRBS signal at 312 Mb/s. Its output was then intensity modulated at

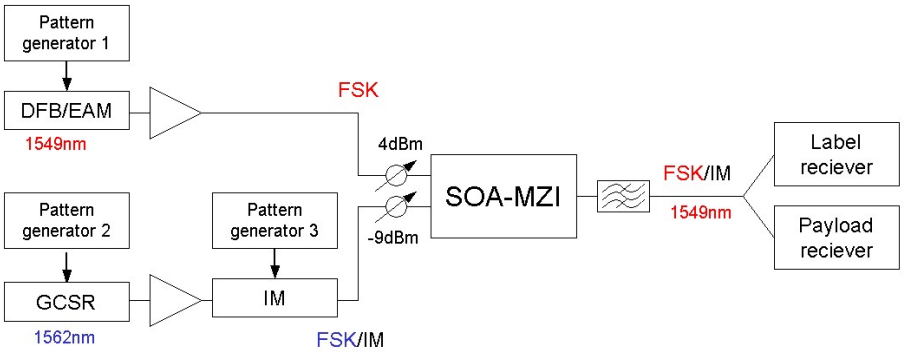

Fig. 6.27. *Experimental setup for label swapping in SOA-MZI.*

10 Gb/s by a chirp-free MZ modulator. This IM/FSK signal at 1562.1 nm was set to -9 dBm and input to the SOA-MZI as the data input. A pure FSK signal was generated by a DFB/EAM source at 1549.0 nm and amplified to 4 dBm, before being input to the CW arm of the wavelength converter. The device proved to be extremely sensitive to polarization and power levels, but after careful optimization and filtering, the IM payload impressed onto the new FSK label at 1549.0 nm was present at the output and ready for detection.

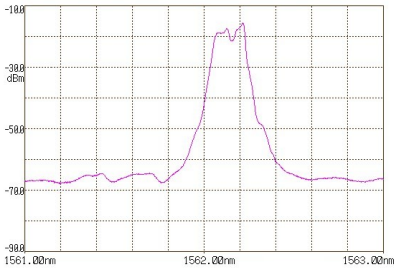

(a)

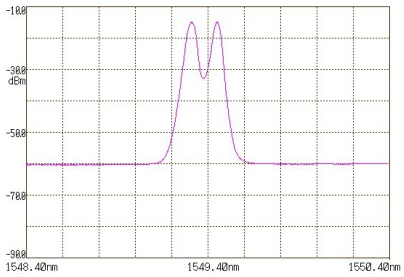

(b)

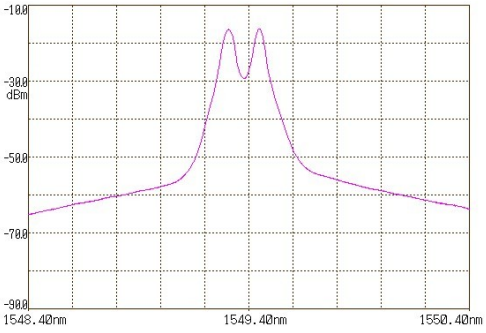

(c)

Fig. 6.28. *Spectra of label swapping in SOA-MZI. (a) "old" IM/FSK signal, (b) new label to be inserted and (c) output signal with the "old" payload and the new label.*

Fig. 6.28 shows the spectra of the input and output signals. The FSK modulation of the GCSR laser at the selected wavelength in fig. 6.28 (a) was degraded because of the wavelength dependence of the performance of these lasers, but the impact of this to the system was negligible, given that this was the FSK label to be erased. The DFB/EAM source in fig. 6.28 (b) on the other hand, presented a remarkable FSK spectrum with the desired tone spacing of 20 GHz. At the output, the imposed IM payload broadened this spectrum as shown in fig. 6.28 (c).

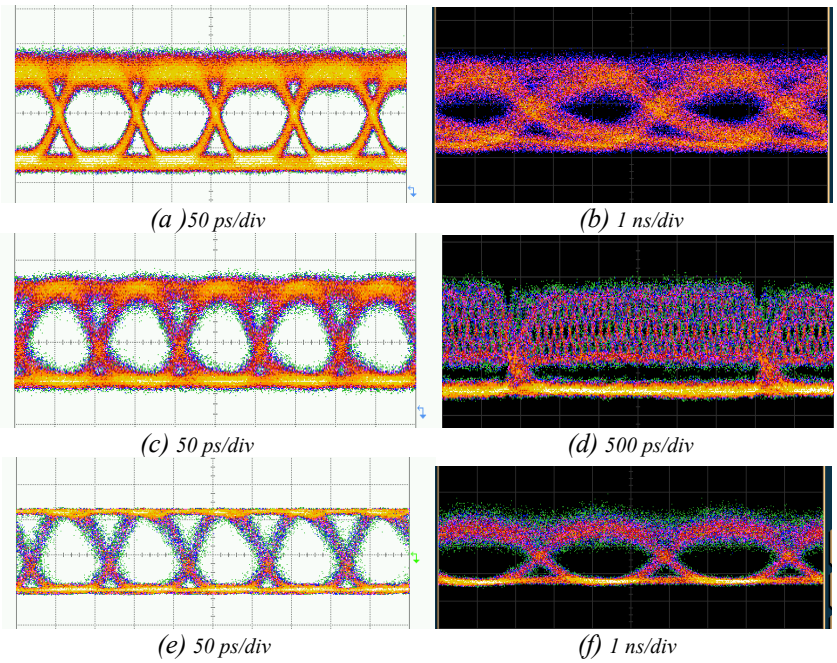

Fig. 6.29. *Eye diagrams of label swapping in SOA-MZI. (a) input IM payload, (b) detected input FSK label, (c) optical output IM payload, (d) optical output FSK label, (e) detected electrical IM payload and (f) detected electrical FSK label.*

Fig. 6.29 shows the eye-diagrams of the signals at various points in the system. The payload eye-diagrams are shown at the left and the label at the right with dark background. At the top of the figure, the input signals are shown. It is clear that the detected (and thus electrically filtered) FSK label at the input was not optimized, but given that this was the label to be erased, this did not have a real impact on the measured performance of the system as a whole. The middle of fig. 6.29 shows the output of the SOA-MZI. The IM payload has been slightly degraded by the more efficient new FSK label. For the demodulated label, the pattern dependence introduced by the 10 Gb/s IM payload is very clear. However, the eye diagram remains open and the FSK label is properly recovered. The bottom of fig. 6.29 shows the benefit of electronic filtering at the receiver. The presented eye-diagrams correspond to

the same signals as the middle of the figure, but in this case the electrical and filtered signals are shown. This indicates that careful optimization of the electrical bandwidth at the receivers may significantly enhance the performance of the system as a whole.

In the setup, various combinations of input wavelengths were tested. The regenerating effect of the SOA-MZI depended on power level, current settings and polarization, which as a result gave a variety of ER values at the output. Fig. 6.30 shows the dependence of the BER on the received power for two such combinations of input wavelengths compared to the back-to-back performance of the signal. The sensitivity for the back-to-back case at a BER of 10^{-9}, was -32 dBm for the label and -24 dB for the payload. The other two results presented correspond to swapping to a higher wavelength (1549.3 to 1551.1 nm) and swapping to a lower wavelength (1550.1 to 1549.3 nm). The performance proved again to be highly dependent on the IM ER in the sense that when the payload performed best, the label was degraded and vice versa.

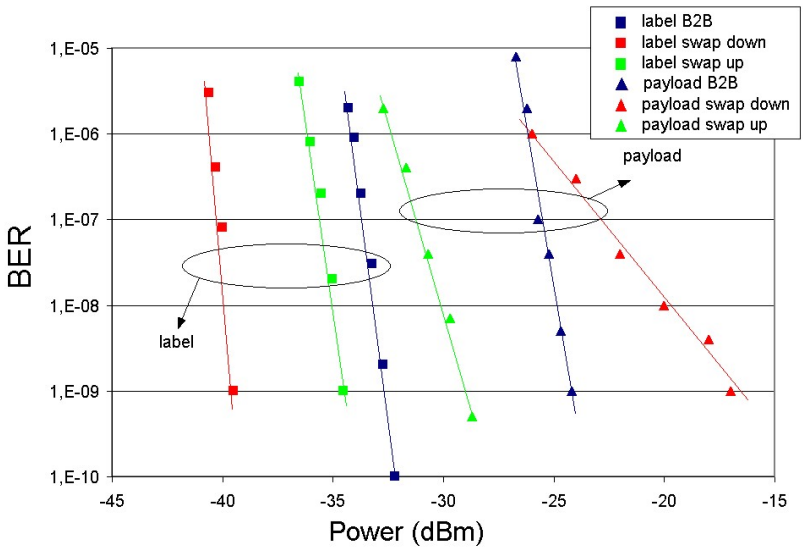

Fig. 6.30. *BER curves for label swapping in SOA-MZI for IM/FSK signals for various label swapping settings.*

6.2.5 FSK label swapping combining SOA-MZI and EAM

Swapping the FSK label in an SOA-MZI in co-propagation as described in the last subsection, had the drawback that the same wavelength could not be used for the input and output signals. As mentioned earlier, for a network node, that would mean that one of the possible channels of the output could not be used, which would have a strong detrimental effect on the network

performance as a whole [161]. A way of overcoming this problem would be to erase the incoming label by converting the signal to an intermediate wavelength different from the ones used as channels in the network, and then use a second wavelength converter to select the desired channel and insert the new FSK label. A second benefit from this approach is that fast tunable filtering is avoided as discussed in Section 5.3.1. This approach can be achieved by first erasing the FSK label and converting the wavelength in an SOA-MZI as presented in Section 6.2.1, and subsequently impressing a new FSK label through a second wavelength conversion process in an EAM as discussed in Section 6.2.3.

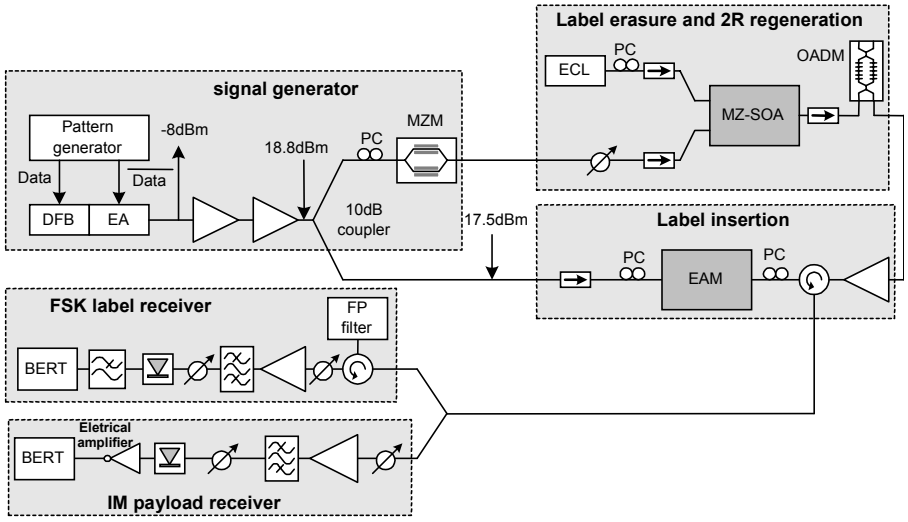

Fig. 6.31. *Experimental set-up of cascaded FSK label erasure and insertion.*

Fig. 6.31 shows the set-up for this label swapping technique. A DFB/EAM source emitting at 1549.3 nm was used for both the label to be erased, and the new label to be inserted, thus proving the capability of re-usage of the same wavelength. The difference in paths from the original signal source and the re-insertion of a label ensured that the two signals were de-correlated and thus could be regarded as two different label sources. The labels consisted of PRBS signals at 312 Mb/s. The payload information at 10 Gb/s was added by a Mach-Zehnder modulator to one of the FSK label signals, thus producing an optically IM/FSK labelled signal. The CW input was provided by a tunable ECL emitting at 1554.1 nm, which was regarded as the intermediate wavelength. At the output of the SOA-MZI, only the payload was present, as discussed in Section 6.2.1. This payload was amplified and fed into an EAM where FSK label insertion took place through XAM, as discussed in Section 6.2.3.

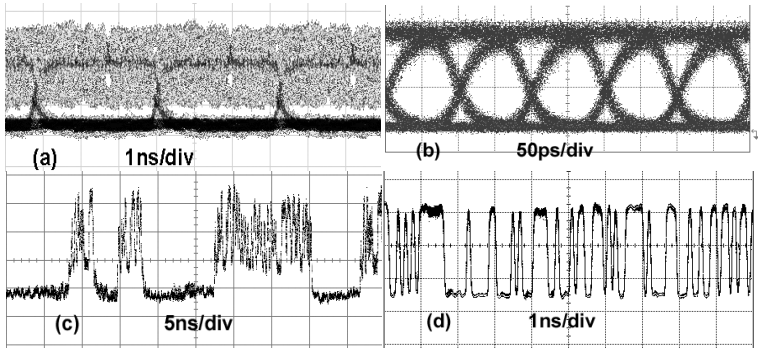

Fig. 6.32. *(a) Received eye diagram of FSK label; (b) eye diagram of the IM payload; (c) received pattern of the label; (d) received pattern of the payload.*

The eye-diagrams and patterns of the updated FSK label and IM payload are shown in fig. 6.32. The FSK signal presented a considerable intensity jitter at its topmost level. Even if the intensity of the payload at its 'one' levels showed a fairly constant behaviour, the filtering of one of the FSK tones would at the same time degrade the IM spectra located around that tone, thus producing the intensity jitter. This did not have a detrimental effect on the FSK performance, as the label eye opening is defined at the lower part of the intensity ripples.

Another advantage of label swapping based on cascaded SOA-MZI and EAM is that the ER of the payload could be adjusted by the non-linear absorption of the EAM. The ER of the input signal was measured to be 5.1 dB, while an ER of 4 dB was achieved at the output of the swapping system.

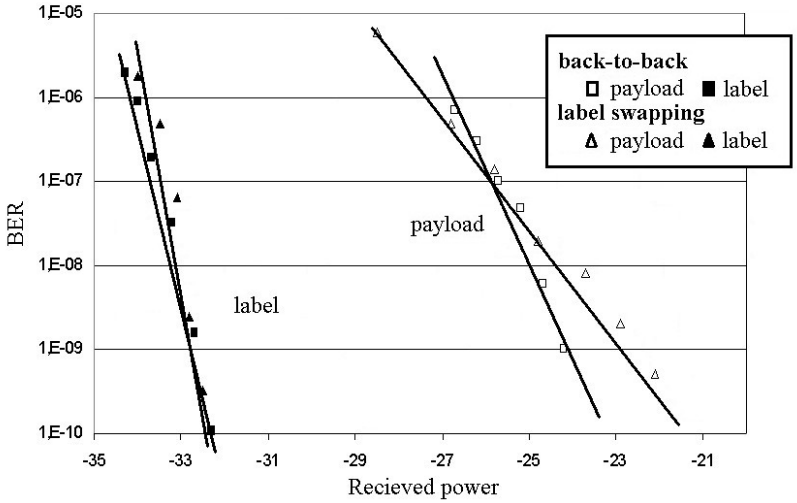

Fig. 6.33. *BER curves for label swapping combining SOA-MZI and EAM.*

The results for the BER measurements for the FSK and IM signals after a complete label swapping are shown in fig. 6.33. For a BER of 10^{-9}, the sensitivity was -33 dBm for the label and -23 dBm for the payload. For the back-to-back case, the sensitivities were -33 dBm for the label and -24 dB for the payload, hence it is observed that there is no substantial observed power penalty for either payload nor label by this method of IM/FSK label swapping.

6.3 CSS label swapping

One of the main benefits of carrier-suppressed sideband (CSS) labelling, is that the swapping process is very simple and almost identical to the generation of the signal. This is due to the fact that the sidebands are always obtained from the carrier itself that carries the payload information.

The basic concept behind optical label swapping for CSS labelled signals is illustrated in fig. 6.34. The incoming label is separated from the payload through optical filtering and input to the label processing module. The pure payload is then amplified and split into two parts by a 3 dB splitter. In the first arm, the payload carrier is suppressed in the way described in Section 2.3, in order to extract the two sidebands. The new label is then modulated on these sidebands and combined with the second branch by another 3 dB coupler. Thus the new label is added on the payload and the label swapping process is accomplished.

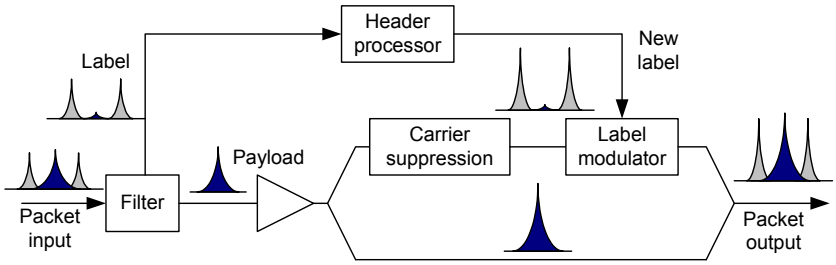

Fig. 6.34. *Schematic diagram of an optical sideband labelling node.*

The advantages of this scheme include that the modulation and detection of the payload and the label can be achieved independently, and no additional tunable lasers are necessary at the label-swapping node. Because the sidebands are directly generated from the payload carrier, the possibility of overlapping between the payload and label when using an external laser is totally prevented.

The label-swapping process relies entirely on the filtering of the payload and the generation of new sidebands where the new label will be modulated. This process is the same as the generation of the signal. Therefore, no additional penalty will be incurred when swapping the label, as the penalty will be the same as when generating the signal, as long as the 'old' label is sufficiently suppressed. The results are therefore equivalent to the ones presented in Section 2.3, where the generation of the signal was discussed.

6.4 Time-serial IM label insertion in SOA-MZI

Time-serial labelling is a way of overcoming the problem of synchronization between payload and label that other techniques may present. In the time-serial labelled network node presented in [134] for the LASAGNE project, the label would be extracted by the optical XOR operation performed in an SOA-MZI [30], between the intensity modulated packet and an all-optically extracted clock [63]. The details of this process fall outside the scope of this thesis, but can be consulted in [139] and [141].

This section presents numerical results of label insertion and wavelength conversion using SOA-MZIs for intensity modulated (IM) time-serial labelled signals consisting of a 40 Gb/s payloads and a 10 Gb/s labels. A solution is proposed to combine these functionalities in order to simplify an all-optical label swapping node. The simulations are based on specifications of commercially available SOAs and SOA-MZIs [135].

6.4.1 Label insertion

Label insertion of time-serial labels, could be realized simply by the use of a coupler. However, this coupler would introduce a residual phase-shift which would not be desirable for the system. On top of that, with just a coupler, it would be difficult to adjust and balance the power levels of the payload and label. Because of that, in the proposed all-optical node [134], all-optical XOR logic gates based on SOA-MZIs are the choice for optical label insertion. This scheme allows for control on the amplitude of both label and payload, thus making it easier to ensure a constant amplitude in the packet at the output of the node. Another benefit, is that the employed model could be combined with all-optical processing in the SOA-MZI module [130].

The schematic of the SOA-MZI and an illustration detailing the principle of operation as an XOR gate are shown in fig. 6.35, and explained in detail in [130]. The two input data streams and the CW-light are coupled into the

MZI, where the data signals are launched into the two SOAs. At the output of the interferometer, the CW-light from the two SOAs interferes either constructively or destructively depending on cosine of the phase difference between the light from each SOAs, and is thus controlled by the input data signals. This leads to a wavelength converted output signal that corresponds to a logic XOR of the two input data signals, as indicated by fig. 6.35 (b). This XOR logic gate also allows for reshaping the level of power levels of label and payload by conveniently adjusting the current into the different SOAs.

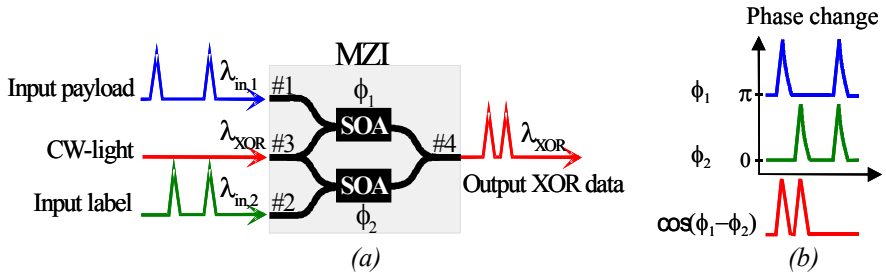

Fig. 6.35. *(a) Optical XOR gate based on SOA-MZI. (b) Phase change and the output of the XOR gate. (Figure from [130]).*

The simulations presented in Section 5.3.1, showed that the analyzed SOA-MZIs could be used for 40 Gb/s wavelength conversion in the single-arm configuration, and thus could be employed in the proposed labelling insertion scheme, provided a fast enough SOA recovery time (<30 ps) was available. In order to evaluate the performance of the label insertion scheme, the static transfer function was calculated for the constructive output of the SOA-MZI.

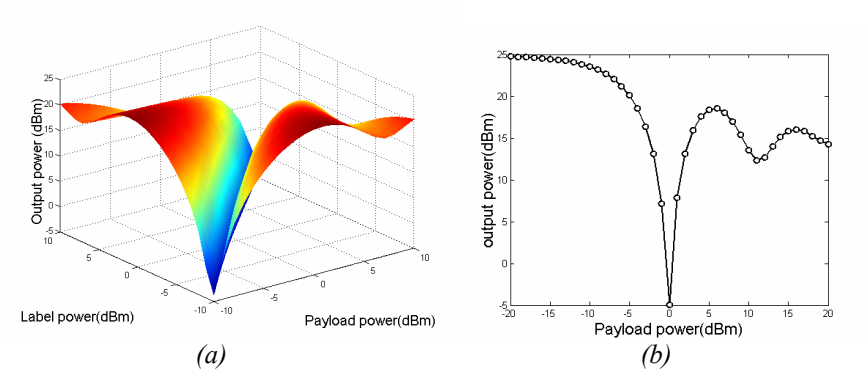

Fig. 6.36. *(a) Static transfer function for logic XOR from the constructive output. (b) Transfer function for the payload when the label power is 0 dBm.*

Fig. 6.36 (a) shows the power level at the output as a function of the label and payload power levels when the CW input was set to 0 dBm, and the current to the SOA was 600 mA. Fig. 6.36 (b) shows the detailed curve for the payload, when the power level of the label and the CW signal both were 0 dBm. A minimum transmission dip appears clearly at certain combinations of input payload and label power, which indicates that at these input power levels, the cross-phase modulation process gives a π phase difference between the two arms, and so the interference of the CW light at the output of the interferometer would be destructive. Very high output power levels could be obtained when the payload power was either less than -15 dBm or larger than 4 dBm as indicated by fig. 6.36 (b).

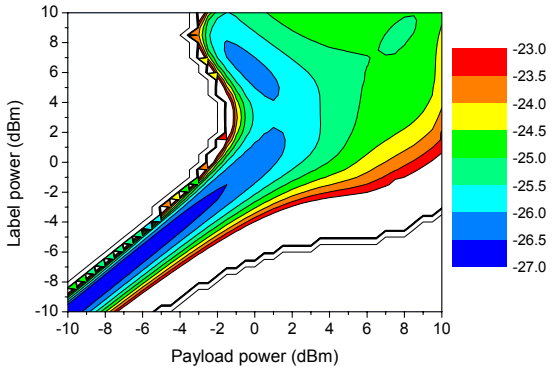

Fig. 6.37. *Receiver sensitivity as a function of payload and label power levels.*

When the input signals contain data packets, the response of the system may vary. Numerical results were obtained for a simulation of a payload at 40 Gb/s consisting of a PRBS of length 2^7-1, and a label at 10 Gb/s consisting of 4 bits. At the output, the BER was measured for the whole packet and the sensitivity for a BER of 10^{-9} was calculated. Fig. 6.37 shows the power resilience of the payload and label. The colour bar on the right shows the receiver sensitivity in dBm. Assuming an acceptable power penalty of 1 dB, the payload and label power levels should be lower than 0 dBm, and the power difference between them should be less than 1.5 dB.

The time jitter between the payload and label would also be an important parameter for this label insertion module. For a simple setup where the payload and label were progressively misaligned in the temporal domain, and assuming an acceptable sensitivity penalty of 1 dB, numerical results indicate that the timing jitter between the signals should be less than 7.8 ps for the above mentioned packet format.

6.4.2 Combined label insertion and wavelength conversion

The above proposed configuration schemes operate with co-propagating modulating data and CW signals. With co-propagating signals, the potential of SOA-MZI operation speed can be fully exploited. However, it is necessary to place a filter at the output port to filter out the modulating signals. As the wavelength of CW signal changes fast in several nanoseconds, the center wavelength of the filter has to be aligned with the wavelength of CW signal at the same speed, as discussed earlier. The all-optical processing approach adopted in [134] would also require the filter to be controllable in the optical domain. Such an optical filter would be hard to design and fabricate.

A further problem of employing SOA-MZI as building blocks for an all-optical network [134], is related to the fact that in the co-propagating mode of operation, the wavelength converter can not re-use the same wavelength for the output, as was mentioned in Section 6.2.4.

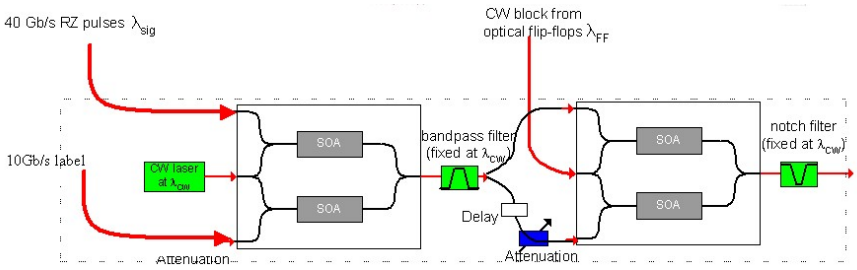

Fig. 6.38. *Combined label insertion and wavelength conversion by two cascaded SOA-MZIs and a CW laser.*

One way to overcome the difficulties listed above, would be to configure the SOA-MZI in the counter-propagating mode. However, such a scheme, though simple, presents a much smaller modulation bandwidth than the co-propagation scheme, as the results of Section 5.3 indicated. Another solution would be to construct a combined label insertion and wavelength converter module using two cascaded SOA-MZIs and one CW laser, as shown in fig. 6.38.

The incoming 40 Gb/s payload pulses would modulate the upper arm of the first SOA-MZI, while the 10 Gb/s would be inserted in the lower arm. This standard-driven SOA-MZI stage, would transfer the new labelled signal onto a fixed intermediate wavelength set by an internal CW laser. This signal would easily be filtered by a fixed filter, and injected into the second differential-driven SOA-MZI as the modulating signal, given that the results

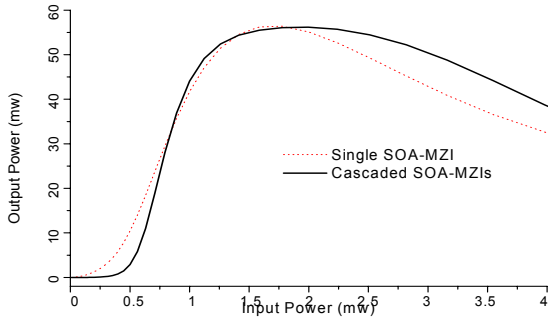

Fig. 6.39. *Transfer function of cascading SOA-MZIs.*

of Section 5.3.1 indicated that the differential driven scheme was the most effective. The second SOA-MZI would receive the appropriate CW signal generated by the part of the optical node that decides on the output wavelength (in the node proposed by [134] it would be optical flip-flops as presented in [162]), and would transfer the modulating data onto it. At the output, a notch filter would be used to filter out the light generated by the fixed intermediate wavelength. In this way, the incoming pulses of both payload and label would be finally converted onto the wavelength set by the decision making part of the node. This configuration avoids the need of tuneable filtering and allows for re-transmission on the same wavelength as the incoming packet, as well as allowing for an independent control on the power levels of payload and label.

	Single stage	Cascading
Single-arm driven	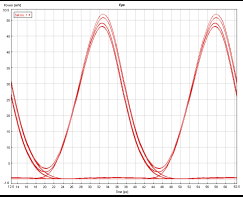	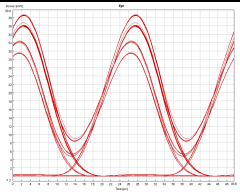
Differential driven	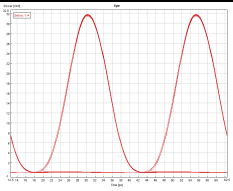	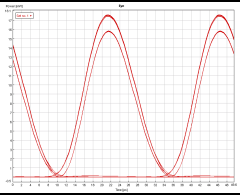

Fig. 6.40. *Degraded modulation performance induced by the cascaded configuration.*

Fig. 6.39 shows the calculated transfer function of two cascaded SOA-MZIs (solid line). Compared to the single stage scheme (dotted line). The transfer function of the cascading scheme presented a more steep transfer function,

implying a more effective reshaping capability, however, the overall modulation bandwidth would be somewhat degraded by the cascading operation. Fig. 6.40 shows the eye-diagrams of the output signals of the SOA-MZIs with single- and cascaded stages. The gain recovery time of the SOA was set to 10 ps, and in the differential driving scheme, the timing delay was set to 8 ps. In can be observed that, particularly in the single-arm driven case, cascading SOA-MZIs broaden the pulse width of the output signal.

6.5 Chapter summary

In this chapter, the issues regarding label swapping for optically labelled signals have been studied. The label swapping process was in many cases related to wavelength conversion (WC), that either was used to erase or insert the label. This showed in many cases beneficial to overcome the problem of not being able to re-use the same wavelength when wavelength conversion in a single stage was used. IM/DPSK labelling and IM/FSK labelling were experimentally investigated in the first place. After that, the label swapping process for carrier-suppressed sideband labelling and time-serial labelling were briefly discussed.

Label swapping for the IM/DPSK signal was realized in active devices by label erasure in an SOA with a penalty of 2.5 dB, and label insertion in an EAM, which could enhance the performance of the payload. Combining both processes, rendered a labelling swapping system. However, the sensitivity of the new label was reduced mostly due to the regeneration of the ER of the payload, which caused a higher intermodulation cross-talk.

The erasure of the DPSK label could also be performed in passive devices by realizing WC in a HNLF through XPM, in the same way as was presented in Section 5.1.1. The new DPSK label could then be impressed on the lightwave by a phase modulator. This technique was almost penalty-free for the label, when a 4 dB penalty was introduced in the payload.

For the alternative DPSK/IM labelling method, label erasure was performed by injecting the conjugated data stream of the detected 2.5 Gb/s IM label into an EAM that thus removed the intensity modulation from the 40 Gb/s DPSK payload. This process of labelling the signal and removing the label generated a penalty of 2.3 dB.

For IM/FSK labelled signals, label erasure was first realized employing an SOA-MZI as wavelength converter. The wavelength process was only dependent on the intensity of the signal, and thus the FSK information was erased. The setup also demonstrated the regenerative capabilities of the device. The same device was then used for FSK label insertion, by

modulating the CW input of the converter with the new label. This process showed no substantial power penalty. Combining these two approaches, became the basis for IM/FSK label swapping in a single device, and was experimentally tested for several combinations of wavelengths. The performance showed a high dependence on the input power levels and polarization states. The results were equally dependent on the degree of regeneration on the ER of the IM payload, which, if too high, would degrade the performance of the label.

An alternative FSK label insertion was performed in an EAM, which showed an enhancement in performance of both payload and label of around 1 dB. However, the high levels of power needed to make this label insertion method effective made it less suitable for real networks. Nevertheless, label swapping of the IM/FSK signal was performed using an SOA-MZI for label erasure and an EAM for label insertion. Because of the possibility of controlling the ER of the payload in a more accurate way through the two stages, the overall penalty for the label swapping was 1 dB for the payload and inappreciable for the label.

The SOA-MZIs were also contemplated for insertion of intensity modulated time-serial labels. The benefits of employing these devices are that the power level and regeneration of the payload and label can be controlled separately, and that the IM time-serial label possibly would not have to be separated from the payload, as the XOR operation of the old label and a bit pattern chosen to give as result the new label could be performed, as shown in [130], which would simplify the optical node.

A numerical analysis of the label insertion was performed based on the specifications of commercially available SOAs and SOA-MZIs. The results indicate that the power levels of payload and label should be similar and lower than 0 dBm, and that the time delay between payload and label should be smaller than 7.8 ps.

As in other cases when combining label insertion with wavelength conversion, a single SOA-MZI module, though effective, would not be suitable. This is because of the need for fast tunable filtering at the output, which would not allow for an output signal at neither the label nor the payload wavelengths, thus severely limiting the performance of the node. A double stage wavelength conversion and label insertion module was therefore proposed and briefly discussed.

In conclusion, the methods for orthogonal optical label swapping were satisfactory in performance as long as the process involved was able to maintain the same ER for the payload. Otherwise, the degradation of either the payload or the orthogonal label would be severe when crossing several

nodes in a network. It was shown that CSS labelling employs the same techniques for generation and detection as for label swapping, and is therefore a simple technique to implement. Finally, for most optical labelling swapping nodes, the versatility of combining wavelength conversion with label swapping proved to be the most attractive solution, partly, because a complicated scheme of fast tunable filtering is avoided, and the network is not limited in terms of possible channels to be chosen as output. The presented techniques can therefore be regarded as promising methods for optical label swapping for all-optical labelled networks.

Chapter 7

Experimental integration of network functionalities

Optical labelling is designed to work in all-optical networks in a transparent way. Both the wavelength label and the orthogonal label would be swapped at the intermediate nodes in order to build an appropriate optical path in the transmission fiber link. The payload on the other hand, would be kept in the optical domain.

The various features that have been studied in this thesis so far, are aimed to work together as optical labelling sub-systems in such an all-optical network. The process would start with creating an optically labelled signal and transmitting it through a certain length of fiber, where it would reach a network node. In this node, the label would be extracted for processing, the signal would be wavelength converted and a new optical label would be re-inserted, thus having the new optically labelled signal present at the output of the node at the desired wavelength. At the nodes output, the signal should have the required quality to be re-sent over another length of fiber. This process would take place a certain number of times in the network before final detection in an edge node.

All these functionalities should also be operable in a WDM environment. Although, at some intermediate nodes, it is possible that only some of the features could be necessary. A switch could have wavelength conversion but no label processing, for example.

In previous chapter it has been shown that these optical features, necessary in the optical network, have a satisfactory performance at least for a BER of 10^{-9}, when measured one at a time. However, the quality of the signal at each stage should be high enough for the next block in the system to be operable.

In this chapter, system experiments are presented for all the functionalities that an optically labelled network should perform, from the point of view of the physical layer. The focus will be on the performance of the system, not in building a real network. In that sense, most of the time, real packets will not be generated, instead continuous signals will be employed. The signals will carry no real processable information, but will consist of PRBS sequences. The aim in each case is a proof of concept of the labelling format and the applied techniques for labelling handling in the node from a systems point of view.

Various bit-rates and several of the studied techniques will be employed. Generally the setup will include a signal generator, a fiber link, a label swapper/wavelength converter node, a second fiber link and a final receiver. Experiments will be presented for IM/DPSK, IM/FSK and time-serial labelling. In the last case optical packets will be created and handled.

7.1 IM/DPSK WDM transmission and label swapping

This section presents the experimental results of a WDM transmission and label swapping system for IM/DPSK labelled signals. The technique of 8B/10B encoding the payload was carried out, showing the significant reduction of the cross-talk between the IM payload and the DPSK label, which was presented in Section 2.4. The system consisted of 4 channels where each payload was IM modulated at 40 Gb/s and each label was DPSK modulated at 2.5 Gb/s. These signals were transmitted over a 40 km compensated fiber link before one of them was selected for label swapping.

The experimental setup of WDM transmission and label swapping is shown in fig. 7.1. The WDM source included four distributed feedback (DFB) lasers that were combined in a WDM multiplexer with a frequency spacing of 200 GHz. The wavelengths of the lasers were 1549.3 nm, 1550.9 nm, 1552.5 nm, and 1554.1 nm, respectively, in compliance with the 200 GHz ITU-standardized wavelength proposal. The payload data was 8B/10B encoded as described in Section 2.4. It was therefore possible to have an initial extinction ratio of the payload of 12 dB.

The transmission span consisted of 40 km of standard SMF with a matching length of DCF in a post-compensation scheme. The dispersion at 1550 nm of the SMF and DCF were about 16.9 ps/nm/km and -100 ps/nm/km, respectively.

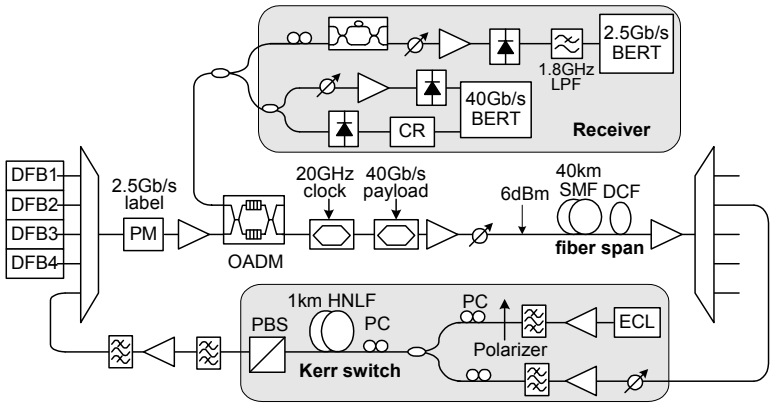

Fig. 7.1. *Experimental setup for WDM transmission and label swapping of IM/DPSK signals.*

After this transmission span the optically labelled WDM signal was demultiplexed and channel 2 at 1550.9 nm was selected for label swapping. The signal emerging from the demultiplexer was amplified to 20 dBm and input to a HNLF for wavelength conversion and label erasure based on optical Kerr switch, as explained in Section 5.1.1. An ECL at 1555.8 nm with a power level of 15 dBm served as the CW input for the wavelength converter. In this way, the input IM/DPSK signal at 1550.9 nm was converted to a pure IM payload signal at 1555.8 nm. This label-erased signal was multiplexed with the 4 DFB lasers and re-injected to the phase modulator for insertion of a new label. An optical add-drop multiplexer was then used to extract the signal at 1555.8 nm after transmission and label swapping.

As mentioned in Section 5.1.1, an additional phase term of each pulse at 40 Gb/s is added to the converted signal during the label erasing process. However, for the slower DPSK label, this fast varying term could be regarded as phase noise and could be electrically filtered out by a 1.8 GHz low-pass filter at detection after the differential demodulation.

Fig. 7.2 (a) shows the optical spectrum for the initial fully IM/DPSK modulated WDM signals. Fig. 7.2 (b) shows the spectra of the input (grey line) and the output (black line) of the HNLF. Fig. 7.2 (c) shows the reinserted label swapped signal as a new WDM channel. Finally, fig. 7.2 (d) shows the spectrum of the received signal after transmission, label swapping and selection from the OADM, ready for detection. The selected channel spacing proved enough for no inter-channel cross-talk to occur.

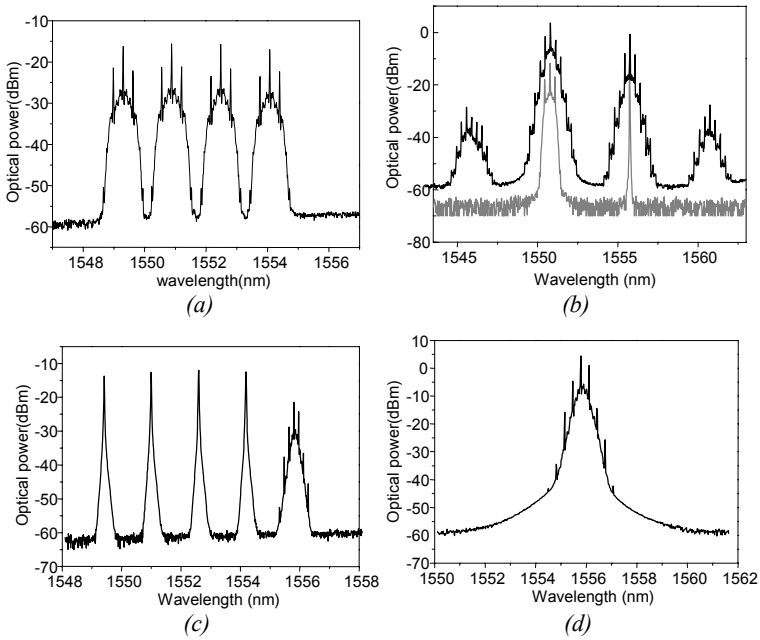

Fig. 7.2. *Measured optical spectra for (a) initial 4×40 Gb/s IM/DPSK signals, (b) the input (grey line) and the output (black line) of HNLF, (c) the reinserted channel to the WDM signal after wavelength conversion and label swapping, and (d) the received signal after transmission and label swapping and filtering, ready for detection.*

The detected eye-diagrams for the 40 Gb/s payload for the back-to-back case, after transmission and label updating are shown in the top part of fig. 7.3. At the bottom of the figure, the eye-diagrams of the DPSK label are shown. Very clear and open eyes could be obtained for both the payload and label after transmission and label swapping. Because of the residual phase shift introduced by the Kerr switch, the payload ER after the wavelength conversion was slightly degraded to 9 dB to ensure the label detection.

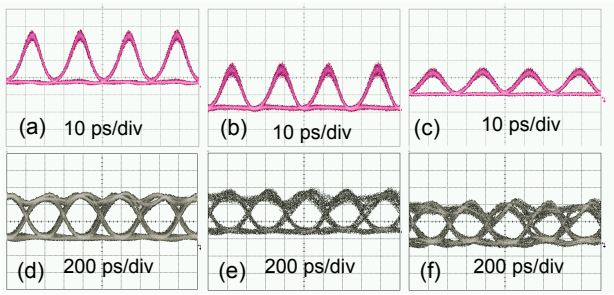

Fig. 7.3*. Received eye-diagrams for the 40 Gb/s payload (above) and 2.5 Gb/s label (below). Back-to-back at the left, after transmission over 40 km fiber in the middle, and after transmission and swapping at the right.*

A BER of less than 10^{-9}, could be achieved for all four channels after 40 km transmission. The receiver penalties of the payload were less than 1 dB, and the penalties of the label were less than 1.5 dB. Successfully transmission and label updating was demonstrated on channel 2, as shown in fig. 7.4. The cascaded transmission and label swapping resulted in 3.3 dB power penalty for the payload and 0.3 dB penalty for the label. The small penalty of the renewed label was not surprising, as this label was generated shortly before the receiver, but it shows that no residual phase was left in the signal. The penalty of the payload was mainly caused by the reduction on the ER after label swapping and the filtering process. It is envisaged that the performance of the payload could be further improved if a chirp-free wavelength converter was applied to the label erasure.

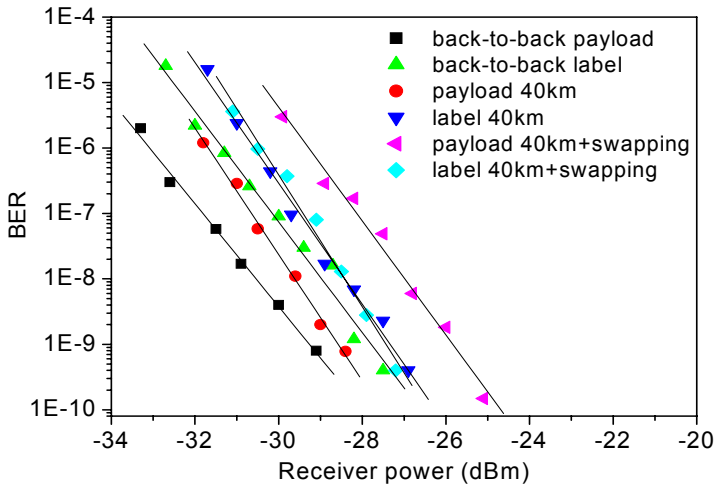

Fig. 7.4. *Measured BER performance for WDM transmission and label swapping for a IM/DPSK signal.*

7.2 IM/FSK system experiments

While studying the IM/FSK orthogonal labelling format, several techniques were shown for the generation of the signal. In Section 2.2.1, a DFB/EAM source was presented and GCSR lasers were studied. Both types of sources will be used in this section. For the label swapping methods it was encountered that a single SOA-MZI could be used as a single stage wavelength converter and label swapping module. This method was put to use in a system experiment that transmitted the IM/FSK signal, label swapped and wavelength converted it, and re-sent it through a second transmission link. The results of this experiment will be presented in the first subsection.

A drawback of this single stage approach was identified to be that the incoming signal could not be converted to the same wavelength at the output port. This problem was solved by the next method in a double conversion technique. The signal was converted to an intermediate wavelength in an SOA-MZI that erased the old label, while an EAM was then used for label insertion and wavelength conversion to the desired wavelength. This double wavelength conversion approach was also implemented between two transmission links.

Finally, the WDM capabilities of the IM/FSK signal in transmission and a label swapping node will be roughly assessed by sending the nearest channel along with the signal to be label-swapped and wavelength converted.

7.2.1 Transmission and SOA-MZI label swapping

A first node prototype of an all-optical switching network based on IM/FSK labelling will be based on label swapping and wavelength conversion in a single SOA-MZI, as described in Section 6.2.4. The experimental setup is illustrated in fig. 7.5. At the edge router, generation of an optical 156 Mb/s FSK modulated signal was obtained by a DFB/EAM source emitting at 1549.3 nm. The optical FSK modulated signal, with a tone spacing of 20 GHz, was then fed into an optical Mach-Zehnder intensity modulator operated at 10 Gb/s, resulting in a combined IM/FSK signal. The extinction ratio of the IM was adjusted to 6 dB. The combined IM/FSK optically labelled signal was amplified and launched into a dispersion compensated fiber link composed of 40 km of SMF followed by 7 km of DCF before reaching a label swapping node.

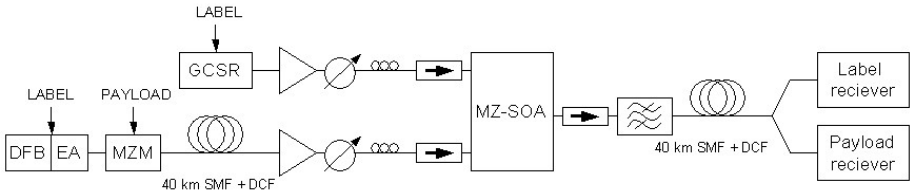

Fig. 7.5. *Experimental setup for IM/FSK label generation, transmission, label swapping in a single SOA-MZI wavelength converter and re-transmission.*

This node was implemented using an SOA-MZI with a frequency modulated GCSR laser emitting at 1550.1 nm and with a tone spacing of 10 GHz, as input. Through the wavelength conversion process, the old FSK label was erased while the new FSK label was inserted, as explained in Section 6.2.4.

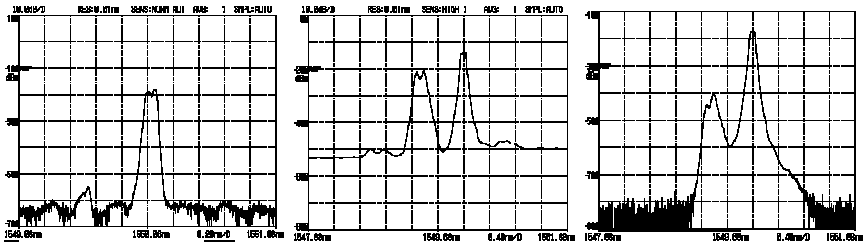

(a) *(b)* *(c)*

Fig. 7.6. *Spectra of the signal at the swapping node: (a) pure FSK signal at 1550.1 nm (new label); (b) output of SOA-MZI; (c) filtered output (IM/FSK signal at 1550.1 nm)*

Fig. 7.6 shows the spectra of the signals at the label-swapping node. Due to the co-propagating operation of the SOA-MZI, the spectra of the new converted signal as well as the residual old signal are observable. As the two types of laser sources used in the experiment had different FM efficiencies, the two FSK signals show different modulation depths, hence the different spectral widths observed in the figure. An optical band-pass filter was used to remove the original, non-desired wavelength, before launching the signal again into another 40 km long dispersion compensated fiber link compensated by 7 km of DCF.

After transmission, both payload and label were detected as shown in fig. 7.7. The eye diagram of the detected label at the receiver in fig. 7.7 (b) shows the degradation due to the smaller tone spacing of the new label generated by the GCSR laser, plus the cross-talk from the residual signal after wavelength conversion as shown in fig. 7.6 (c). In any case, the eye was open enough for adequate detection.

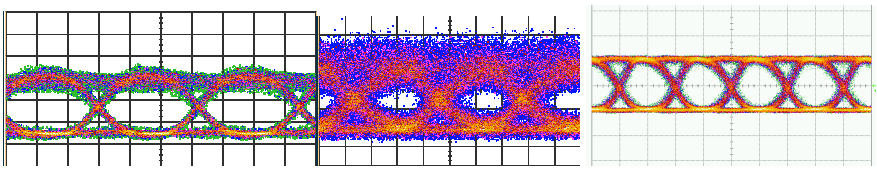

(a) 2 ns/div *(b) 2 ns/div* *(c) 50 ps/div*

Fig. 7.7. *Eye-diagrams of the signal (a) detected label at the swapping node (old label); (b) detected label at the receiver node; (c) detected payload at the receiver node.*

Fig. 7.8 shows the measured BER performance as a function of the average received optical power. For the IM receiver, the sensitivity at a BER of 10^{-9}, was measured to be -28 dBm. Which means that, only a 0.5 dB power penalty was measured for the IM payload after the 2 hop transmission with label swapping. Because the label is generated by two different FSK sources, it is not sensible to compare the FSK performance before and after label

swapping. However, the FSK modulated signal suffered a higher power penalty of approximately 2 dB due to transmission over the second span. This is attributed to imperfect dispersion compensation at this wavelength, which is critical with tone spacing as large as 10 GHz [165], as well as cross-talk from the IM payload due to non-linear coupling in the fibers.

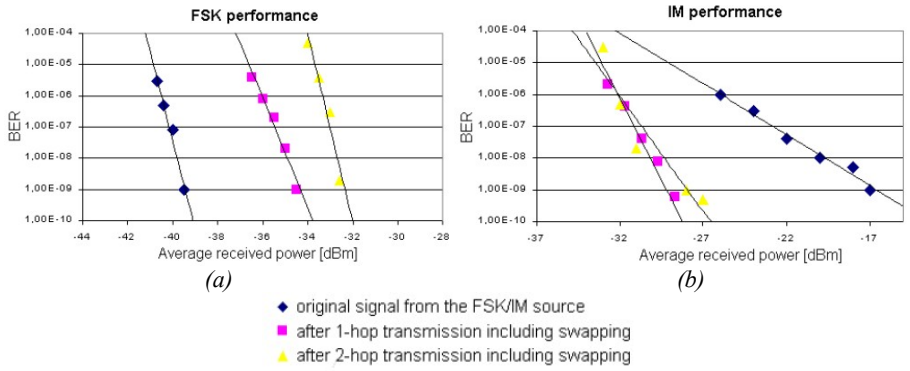

Fig. 7.8. *BER curves for (a) label and (b) payload, for back-to-back (blue), after transmission and label swapping (purple) and at the end of the whole system (yellow).*

Although the FSK performance suffers an average of 2 dB of power penalty in each span, including the wavelength conversion stage, this degradation would not affect the global network performance because a new label would be re-inserted at each node. The IM performance demonstrates the regeneration effect due to the interferometric behaviour of the SOA-MZI wavelength converter [166]. Therefore, a high level of scalability would be possible by using the combined scheme.

7.2.2 Transmission and SOA-MZI/EAM label swapping

The double wavelength conversion technique that employed an SOA-MZI for label erasure and an EAM for label insertion, was shown in Section 6.2.5 to be more flexible by being able to re-use the wavelength of the incoming signal. This subsection shows the results of this labelling technique when used between two transmission links.

The experimental set-up is shown in fig. 7.9. The FSK modulated label at 312 Mb/s (2^7-1 PRBS) was generated using the DFB/EAM technique described earlier. The payload information at 10 Gb/s (PRBS 2^9-1) was then added by an EAM, thus producing an optically IM/FSK labelled signal. The extinction ratio of the payload was set at 4.3 dB, as no coding method was used. This ensured that with the regenerating effect with respect to IM ER in

the label-swapper, the final ER had the required level for re-transmission and detection of both label and payload.

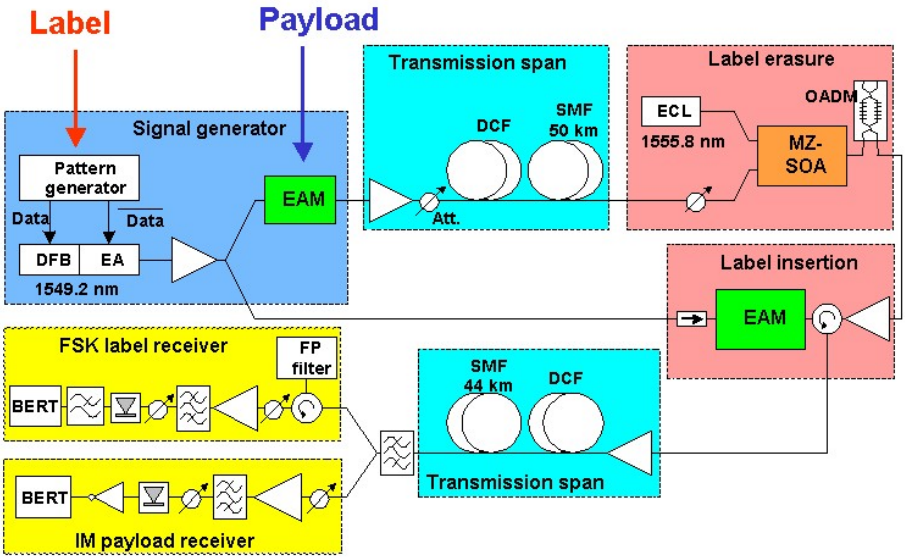

Fig. 7.9. *Experimental set-up for two-hop transmission with label swapping in a double SOA-MZI / EAM stage.*

The first transmission hop consisted of 50 km of SMF with a matching length of DCF. The dispersion was 16.9 ps/nm/km for the SMF and -100 ps/nm/km for the DCF. In Section 3.2, the pre-compensation scheme was identified as having a better performance than a post-compensation scheme. Hence pre-compensated fiber spans were chosen for both fiber links. After the first transmission the optically labelled signal was input to the SOA-MZI for label erasure and 2R regeneration. A tunable external cavity laser at 1555.8 nm was used as CW input for the SOA-MZI. Very good label erasure and 2R regeneration could be observed at this stage. Due to its non-linear transfer function, the extinction ratio of the converted signal was greatly improved to 12.9 dB, which lead to a 2 dB enhancement for the receiver sensitivity. The regenerated payload was then fed into an EAM as the pump signal for the label insertion process, where the ER of the label-renewed signal was adapted to the required value for re-transmission. The original FSK signal was split into two parts in order to use one of them as the second label source for the label insertion module, thus validating the re-usage of the same wavelength after the label-swapping node.

As mentioned earlier, a limited extinction ratio is mandatory in the orthogonal labelling scheme. This relatively low extinction ratio could easily

be accomplished by adjusting the reverse bias of the EAM. The ER of the output signal of the label swapper was set to 4.9 dB through this method.

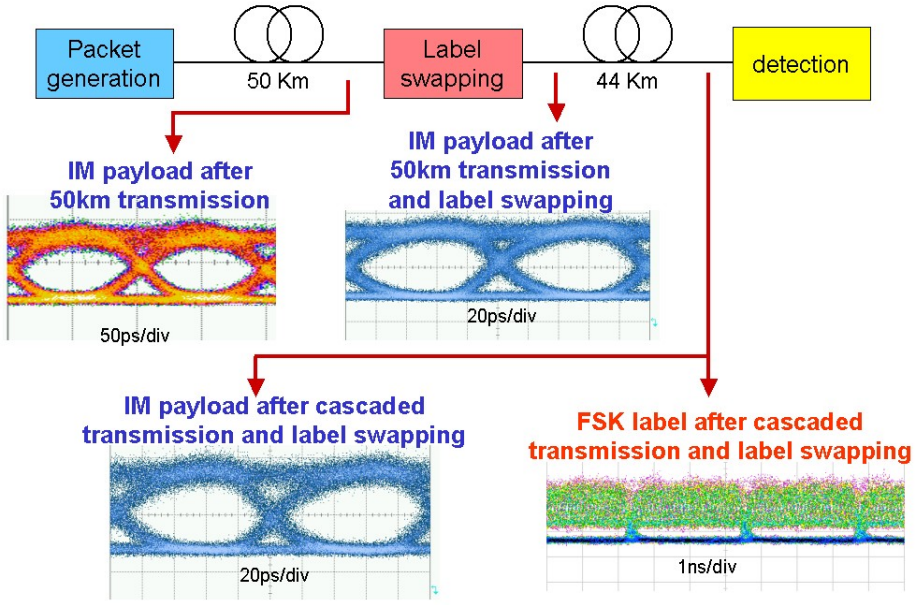

Fig. 7.10. *Eye diagrams of the signal at various points in the system.*

The second hop consisted of 44 km of SMF with the corresponding DCF. At the receiver, the frequency discrimination for FSK demodulation was achieved by two optical filter stages providing more than 15 dB suppression ratio between the two FSK tones.

Fig. 7.10 shows the eye diagrams at various points in the system. Some distortion was observable both due to transmission and label swapping. However, the eyes were kept open through out the system and the detection was successfully achieved. For the label at the end of the second transmission, it is clear that some payload information is superimposed onto the label after the FSK demodulation, however the eye was again still open and allowed for proper detection.

Fig. 7.11 shows the BER curves in the back-to-back case, after the first hop, after the label swapper and after the second hop. The cascaded transmission and label swapping resulted in 1.9 dB power penalty for the payload and 1.8 dB penalty for the label, thus validating this labelling scheme and label-swapping technique for network application.

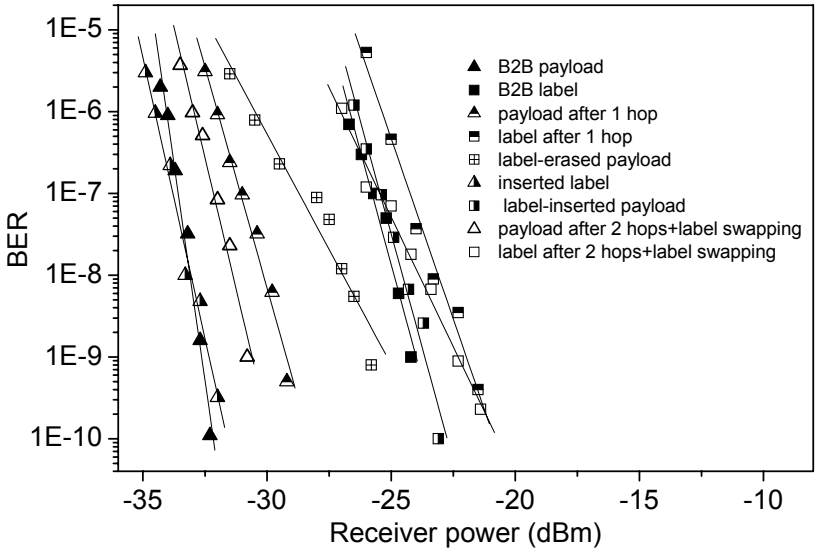

Fig.7.11. *Measured BER results for the payload and label after cascaded transmission and label swapping.*

7.2.3 Two channel network system experiment

In Chapter 4, the influence of neighbouring channels in a WDM IM/FSK optically labelled transmission system was addressed. It was shown that, for a sufficient channel spacing, the influence (if any) could be reduced to the channels located closest in the spectral domain. In Chapter 5, the approach of label erasure and insertion combined with wavelength conversion in a single SOA-MZI was studied and found simple and effective, as long as the input and output wavelengths did not coincide. This findings, combined with the analysis on transmission of IM/FSK signals performed in Chapter 3, will serve as base for the experiment presented in this sub-section.

Two IM/FSK channels were first transmitted over a 40 km transmission fiber link. Then one channel was dropped and label-swapped at the swapping node before being re-combined with the original non-swapped channel and being both re-transmitted over another 40 km fiber span, after which the swapped channel was dropped again for detection, where its performance was measured.

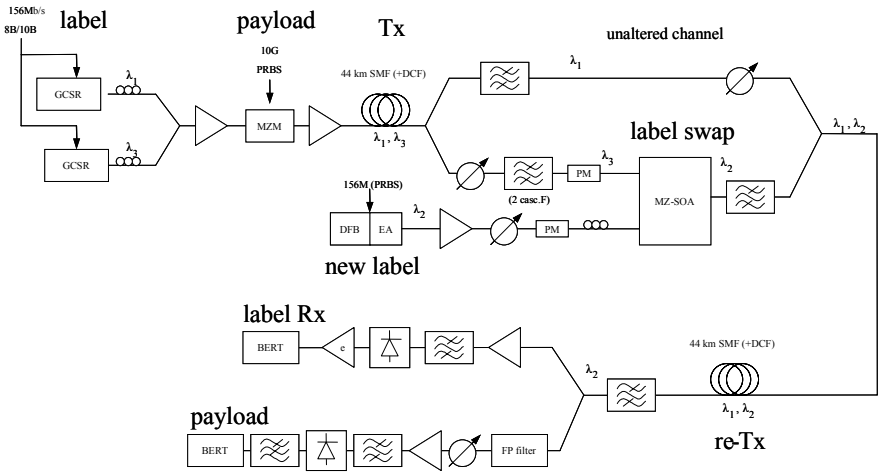

Fig. 7.12. *Experimental setup for a 2 channel WDM transmission system with a label-swapping node.*

The system setup is shown in fig. 7.12. The three channels were emitted at 1548.5 nm, 1549.3 nm and 1550.1 nm, respectively. The IM/FSK signals were generated at the transmitter node at wavelengths corresponding to channel 1 (1548.5 nm) and channel 3 (1550.1 nm) by GCSR laser sources at 156 Mb/s. The payload information at 10 Gb/s was impressed on both these signals simultaneously by a MZ modulator. These two channels were transmitted over a dispersion compensated 44 km SMF span before reaching the label-swapping node. At the swapping node, the IM/FSK signal at channel 3 was label-swapped, and its wavelength changed to that of channel 2 (1549.3 nm). This signal was generated by a DFB/EAM source. The IM/FSK signals at channel 1 and channel 2 were then combined in a coupler and re-transmitted over another 44 km SMF span before being detected.

Fig. 7.13 shows the measured spectra of IM/FSK signals at different points in the system. In all cases, the signals had a sufficiently large OSNR to ensure acceptable BER performance. Fig. 7.13 (a) shows the original channels generated by the GCSR sources. These sources are wavelength tunable, but their FSK response is highly sensitive to the chosen wavelength. Because the DFB/EAM source was fixed with regard to wavelength for the FSK operation, it was necessary to situate the other two channels around it. This meant that the GCSR sources were both working at a sub-optimum wavelength with regard to their FSK performance. This is the reason why the spectra of fig. 7.13 (a) shows two IM/FSK signals with a somewhat small tone spacing and modulation depth.

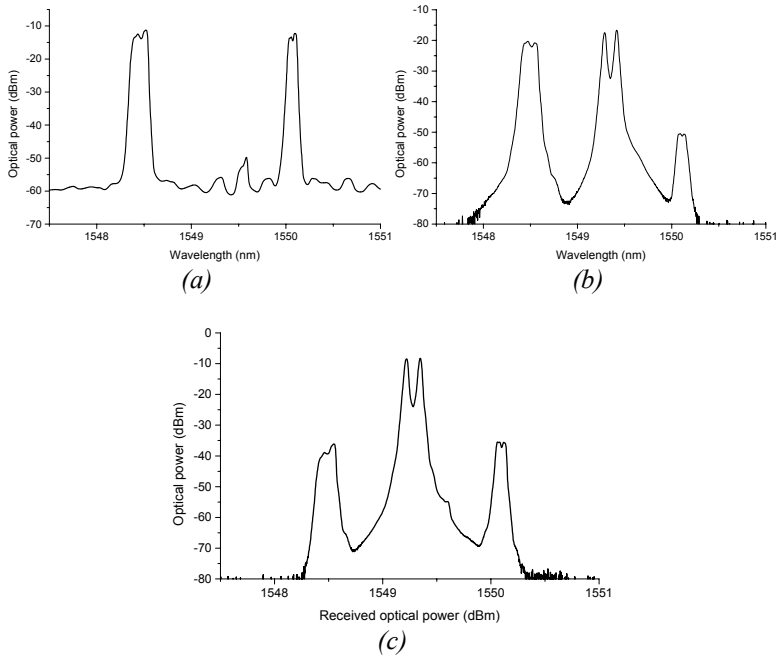

Fig. 7.13. *Spectra of the IM/FSK signals. (a) Channel 1 and channel 3 at the source. (b) Output of the label-swapping node. (c) Demultiplexed channel 2 at the receiving node.*

Fig. 7.13 (b) shows the re-combined signals after the label-swapping module. Channel 3 was wavelength converted into channel 2, that was using the more effective DFB/EAM source for label generation, which is the reason for the clearer FSK tones observable in channel 2. A residual tone at the old wavelength is still present, but suppressed by more than 30 dB. Finally, fig. 7.13 (c) shows the spectrum after filtering before the receiver. The filtered channels experience a suppression of almost 30 dB compared to channel 2 that was selected for detection.

Fig. 7.14 shows the measured eye-diagrams of the different IM/FSK signals. The payload of channel 1 is shown in fig. 7.14 (a), which is the unaltered signal in the intermediate node. Fig. 7.14 (b) shows the payload of channel 3 at the label swapping node, that was wavelength converted into channel 2, which is shown in fig. 7.14 (c). The FSK label of this new channel after re-transmission is shown in fig. 7.14 (d).

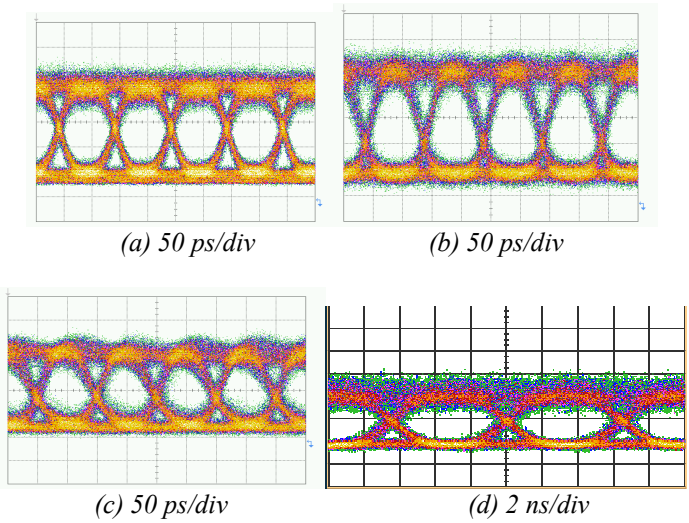

(a) 50 ps/div *(b) 50 ps/div*

(c) 50 ps/div *(d) 2 ns/div*

Fig. 7.14. *Eye-diagrams of IM/FSK signals: (a) IM payload of channel 1 at the receiver; (b) IM payload of channel 3 at the swapping node; (c) IM payload of channel 2 at the receiver; (d) FSK label of channel 2 at the receiver.*

As already explained, in the entire transmission link, channel 1 is kept unaltered while channel 3 is terminated at the swapping node. Only channel 2 experiences both the label-swapping and WDM transmission process. For this reason, only channel 2 is given a detailed analysis through BER measurements. In fig. 7.15, the performance of the FSK label and IM payload of channel 2 are compared with that of the back-to-back case, measured with the same source in order to make the comparison realistic. It can be

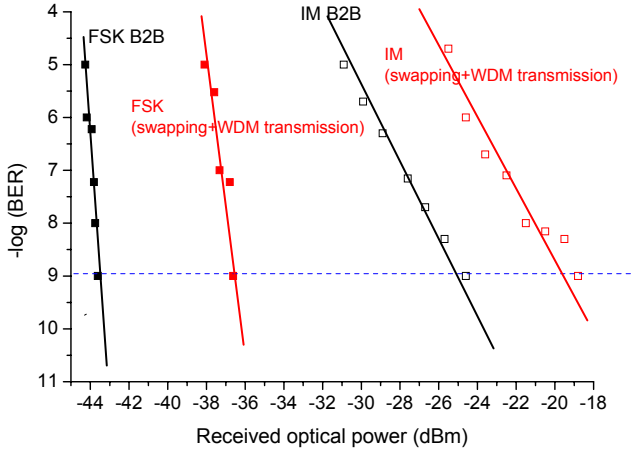

Fig. 7.15. *Measured BER curves of channel 2 compared to the back-to-back case.*

observed that WDM transmission and label-swapping introduce nearly 7 dB of power penalty to the FSK label, and 5 dB of power penalty to the IM payload. Those large penalty values are attributed to the relatively poor quality of the FSK sources used in the present experiment. Better sources, as expected to be provided in a commercial network, would alleviate this limitation. It would therefore be important to optimize the IM/FSK transmitter and the SOA-MZI to further improve the system performance.

7.3 Time-serial labelling system experiment

As a final approach to network node functionalities, a time-serial labelling scheme will be adopted. This section will present experimental investigation of the functionality of a network node with two-hop transmission and all-optical packet switching and wavelength conversion for an optically serial-bit labelled packet consisting of a 10 Gb/s label and a 40 Gb/s payload. Propagation over two transmission spans consisting each of 44 km standard SMF separated by a network node including packet switching and wavelength conversion functionalities will be implemented.

In the proposed all-optical packed switched network in [134] the incoming payload at 40 Gb/s would be assigned a 10 Gb/s label, which would both be intensity modulated signals in the return to zero format. The nodes would perform routing and forwarding operations based on the information retrieved from the optical label. This would generate a gating signal to control the converted wavelength and the time-slot of the switched packet [14].

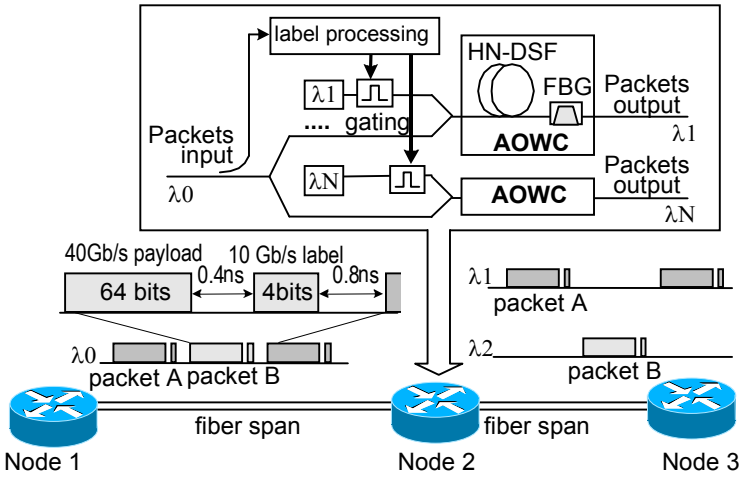

Fig. 7.16 *System architecture for packet switching and wavelength conversion.*

In the experiment, the packet length was 2.4 ns which included a payload of 64 bits at 40 Gb/s, a guard band of 0.4 ns between payload and label and a label of 4 bits at 10 Gb/s. The guard band between two packets was 0.8 ns, as illustrated in fig. 7.16.

The all-optical wavelength converter (AOWC) used XPM in a highly non-linear fibre followed by an optical filter [110], as explained in Section 5.1.1. If the incoming data is combined with a CW signal and sent through a highly non-linear fibre, the data imposes a phase modulation onto the CW light through XPM. This phase modulation generates optical sidebands on the CW signal, which can be converted to amplitude modulation by suppressing the original CW signal and filtering out one sideband in an optical band-pass filter.

In the experiment, a gating XPM scheme was implemented, by replacing the CW signal with an optical gating signal, where XPM occurs effectively during the gating period, when the gating signal is at its 'high' state, as shown in fig. 7.17.

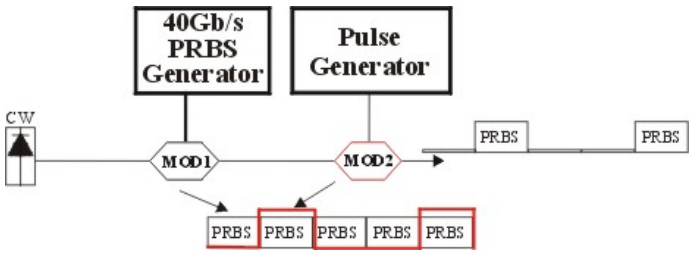

Fig. 7.17 *Principle of optical wavelength switching through the use of a gating signal as input to the HNLF wavelength converter.*

In this way, the gating signal – that would be controlled by the label information – would select the appropriate packets for wavelength conversion, thus realising packet switching in the time domain at the same time. For a full operational node, several of these AOWC could select the appropriate packets at the appropriate wavelengths for each output fiber of the node.

The experimental setup is shown in fig. 7.18. The packet generator consisted of an external-cavity laser (ECL) emitting at 1558.8 nm, and two external dual-drive Mach-Zehnder modulators. The first modulator generated a 40 GHz RZ pulse train with 33% duty cycle. The second modulator was driven by a packet stream consisting of two alternated 40 Gb/s packets, named types I and II, from here on. The payload data was 64 bits of random data, while the labels of packet I and II were set to 1001 and 1110, respectively. In order to allow for the clock recovery (CR) each label bit (at

10 Gb/s) was in practice made up of 4 bits at 40 Gb/s. The guardbands were then coded as 16 and 32 zero bits respectively.

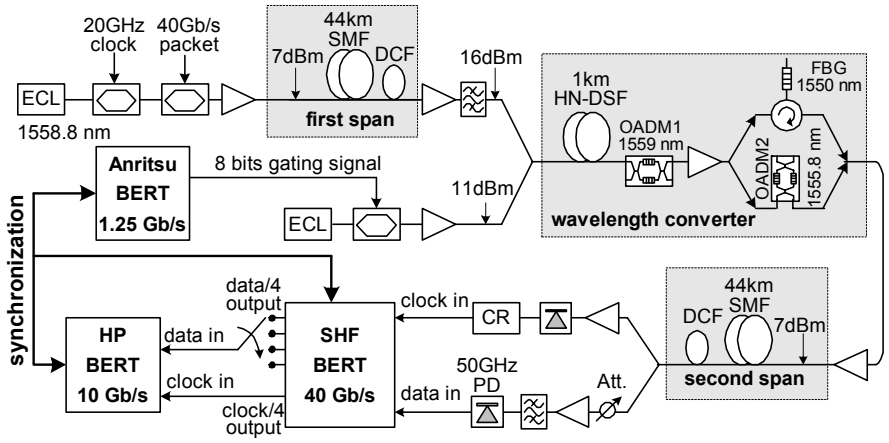

Fig. 7.18. *Setup of the time-serial labelling switching node experiment.*

The first transmission hop consisted of 44 km of SMF with a matching length of DCF in a post-compensation scheme. After this first transmission span the optically labelled signal was input to 1 km of highly non-linear fibre (HNLF) for the packet switching and wavelength conversion. A tuneable ECL was used as the probe for the AOWC. The probe signal was a gating signal generated by an intensity modulator driven by a 1.25 Gb/s data stream, as shown in fig. 7.17. This gating signal consisted of 8 bits which had four continuous ones and four zeros. Packet switching was then realized at the four continuous ones, the duration of which were equal to one packet length. Synchronisation of the incoming packets and the gating signal was achieved by changing the initial position of the four ones in the gating signal. In the proposed network, the gating signal would be obtained all-optically by an all-optical n-bit XOR gate and a series of optical flip-flops [168].

The OADM1 connected immediately after the HNLF was used to suppress the pump signal. In a real network, the gating signal would be lasing constantly, but varying between the selected output wavelengths between packets. In the experiment this was performed by changing the probe wavelength between 1550.9 and 1555.2 and measuring the output for each case. In order not to change the setup and making the measurements more reliable, the system was made capable of handling both wavelength conversions. After the HNLF, the PM to IM conversion took place at the steep edge of a FBG with a centre wavelength at 1550 nm and an OADM2 at 1555.8 nm. The performance of the AOWC was evaluated to be penalty free for conversion of a 40 Gb/s signal (PRBS 2^{31}-1) from 1559.0 nm to

1555.9 nm. After the switching node, the emerging signal was re-sent through a second transmission hop consisting of 44 km of SMF and a matching length of DCF.

At the receiver node, the labelled packet was split using a 3 dB optical coupler. The output of one arm was amplified and detected by a photodiode in order to provide clock recovery. The other arm was input to the pre-amplified receiver for BER analysis.

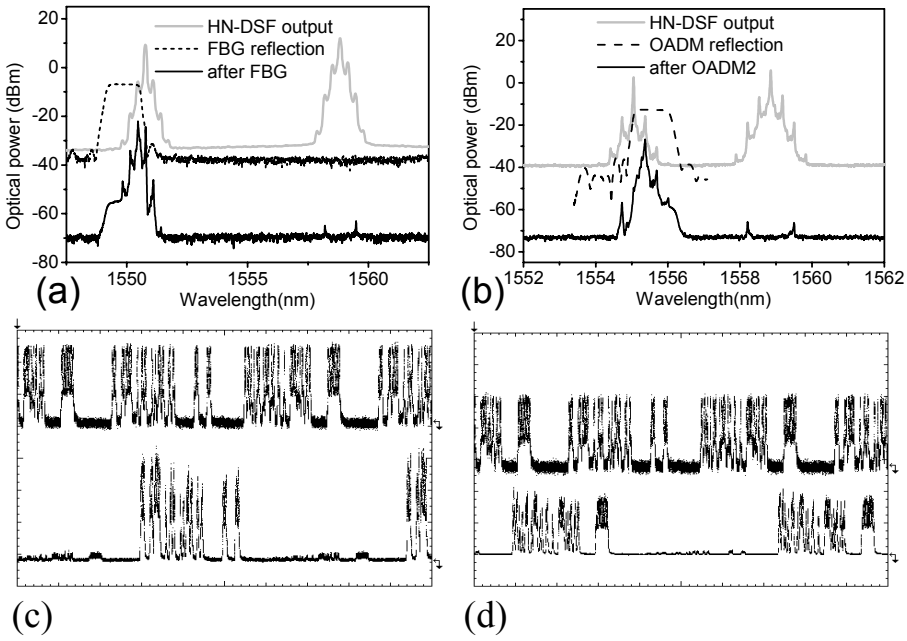

Fig. 7.19. *Optical spectra and waveform of packet switching and wavelength conversion for (a) and (c) from 1559nm to 1550.9 nm, (b) and (d) from 1559nm to 1555.2nm.*

The optical spectra after wavelength conversion are shown in fig. 7.19 (a) and (b), while fig. 7.19 (c) and (d) show the waveform of the initial packets (upper) and switched packets (lower). For the original stream, the packets are visible with their alternating labels in front of them. The lower part of the figure shows the selected packet after switching and wavelength conversion. Some amplitude distortion was visible in the packet, but the label and payload information was still clearly observable. The result is that packets of type I were switched to 1550.9 nm while packets of type II were switched to 1555.2 nm. The switching extinction ratio (defined as the ratio between the minimum power of the transmitted ones and the maximum power of the blocked packet) was higher than 12 dB.

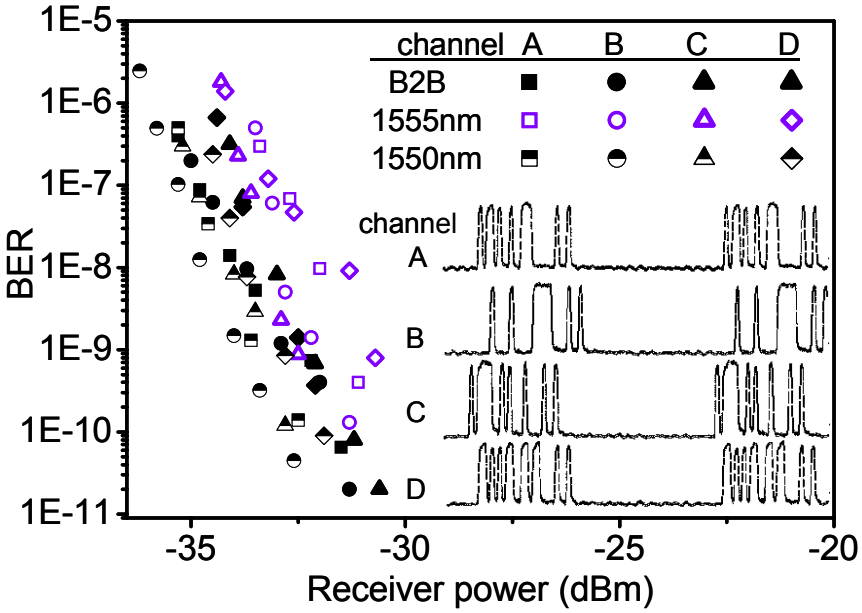

Fig. 7.20. *Measured BER results for the original packets and after 2-hop transmission, packet switching and wavelength conversion. The inset figure shows the waveform of demultiplexed four channels at 1550.9 nm.*

The 40 Gb/s BER analyzer used in this experiment was only able to test PRBS sequences, not user-defined patterns. In order to test the BER performance, the 40 Gb/s packets were detected by a 50 GHz photo diode and electrically demultiplexed to 4 tributaries at 10 Gb/s. These 4 channels at 10 Gb/s were then input to a 10 Gb/s test-set which did allow programmable data patterns to be analyzed. Thus, the BER of the 40 Gb/s packet could be presented by 4 signal channels at 10 Gb/s. Fig. 7.20 shows the BER curves in the back-to-back case and after two-hop transmission, packet switching and wavelength conversion. The maximum power penalty for a BER of 10^{-9}, was less than 1.5 dB for the converted packet II at 1555.2 nm. The BER of the converted packet I at 1550.9 nm was even slightly better than the back-to-back case. This can be explained by the fact that two packets generate errors in the back-to-back case while only one packet contributes to the bit error rate after wavelength conversion. Also, the data sequences of packets of type I and II were, different and pattern induced errors could have an effect in the measurements. The inset figures shows the waveform of the 4 demultiplexed channels for the signal converted to 1550.9 nm. All 4 channels had very clear waveforms resulting in error-free detection.

7.4 Chapter summary

In this chapter, the complete system functionalities of network nodes have been experimentally investigated with respect to different labelling schemes and in conjunction with transmission, thus setting up a system validation of optical labelling for all-optical networks. For some of the experiments, transmission of several wavelength cannels was added to the system validation. The optical IM/DPSK, IM/FSK and time-serial labelling schemes have been studied in each section.

Firstly, a WDM transmission and label swapping for 4 IM/DPSK channels consisting of a 40 Gb/s payload and a 2.5 Gb/s label was presented. The overall penalty of 40 km of transmission and label swapping was of 3.3 dB for the IM payload and 0.3 dB for the DPSK label.

For the IM/FSK labelling scheme, firstly, label erasure and insertion was simultaneously achieved in a single wavelength conversion stage for a 10 Gb/s IM payload and a 156 Mb/s FSK label. Successful transmission of the combined IM/FSK signal over two hops of 40 km length, consisting each of a dispersion compensated SMF link, showed a 2 dB penalty for the label and a 0.5 dB penalty for the payload, which had been regenerated at the SOA-MZI wavelength converter.

For overcoming the problem of filtering and validating the possibility of re-using the same wavelength for the output signal as for the input, a second network system experiment was setup for the IM/FSK scheme, in which label removal was accomplished in an SOA-MZI, while the FSK label insertion was achieved in an EAM. The power penalty of the cascaded transmission over 50 and 44 km of SMF, and the intermediate label swapping, was shown to be below 2 dB for both payload and label. The sensitivities after transmission, swapping and re-transmission were -31 dBm for the label and -22 dBm for the payload for this system.

A 2 channel IM/FSK system with a channel spacing of 100 GHz, was also implemented. The signals were sent over a 44 km transmission link, after which just one of them underwent label swapping and wavelength conversion. The label-swapped signal was then re-combined with the other original signal, and re-sent over a second 44 km transmission link. The system achieved a BER performance of less than 10^{-9}, but with the rather high penalties of 7 dB for the label and 5 dB for the payload. The origin of the penalty showed to be mostly the limited performance of the FSK sources.

Finally, a packet switched network systems experiment was setup for time-serial labelled packets. The IM signal consisted of 10 Gb/s optical labels

followed by 40 Gb/s payloads, which were sent over a transmission span of 44 km. After transmission, packet switching and gating-controlled all-optical wavelength conversion, based on a HNLF were performed. The selected switched packets (half of the original ones) were then re-sent over a second 44 km span. The power penalty of the cascaded transmission, packet switching and wavelength conversion was shown to be below 1.5 dB.

The results confirm the potential of optical labelling schemes for all-optical networks. The orthogonal labelling schemes would not suffer from a higher penalty on the performance of the label, given that it will be swapped at each node. The payload on the other hand will be likely to transverse several nodes and its performance and signal degradation has to be kept within acceptable limits. For the IM/FSK scheme the quality of the FSK sources proved to be one of the most important factors in order to improve the performance of the system.

The results further demonstrate the potential for the realization of compact label swapping devices based on integrated SOA-MZI wavelength converters, assisted by agile tunable lasers. Such a compact label swapping modules would be a desirable key building block for future core networks.

In conclusion, the successful experimental duplication of the system functionalities of a network node validate labelling and specially orthogonal labelling as a promising solution for all optical packet switched networks.

Chapter 8

Summary and conclusions

In order to utilize the enormous transport capacities made available by wave division multiplexing (WDM) in a more flexible and efficient way, future optical networks are moving towards optical packet switching [172]. The use of optical labels to route and forward Internet protocol (IP) data without having to detect the payload is therefore a promising solution to overcome an eventual electronics bottleneck [21], [5]. In addition to the optical wavelength that can serve as an optical label in multi-protocol lambda switching (MPλS) schemes [8], a second level of optical label is still necessary for provisioning, maintaining, and restoring switched light-paths. All-optical label switching will therefore be used to route and forward packets in future high-speed networks independently of IP packet length and payload bit rate. Labels will be received and swapped at every node in a core network, while the payload information will be transparently forwarded with possible wavelength conversion [12].

Several label-coding techniques have been reported, such as serial-bit labelling [134] or sub-carrier multiplexing [15]. Orthogonal modulation has been suggested as a novel method to perform optical label switching operations in order to increase the throughput of IP over WDM networks, combining intensity modulation (IM) with differential phase shift keying (DPSK) or frequency shift keying (FSK) on a single carrier [48].

In this thesis all-optical labelling has been studied with respect to its different functionalities, leading up to duplicating the system characteristics of a network node in an experimental setup, for various types of labelling methods. The investigation has been divided isolating the effects of the various system aspects. The analysis started with the generation of the signals and a study of their single channel and WDM transmission properties. This was followed by the system functionalities that would be expected of an all-optical node, which are wavelength conversion and all-optical label swapping. These investigations were assembled and summarized in an evaluation of complete systems experiments in which labelled channels were

generated, transmitted, wavelength converted, label-swapped and re-transmitted before detection. These complete systems experiments confirmed the potential use of the orthogonal labelling methods for all-optical networks.

For the IM/DPSK labelling method, the transmitter requires a differential XOR operation of the data. This was however omitted in the experiments throughout the thesis, because a pseudo-random bit sequence (PRBS) becomes a shifted version of itself under this operation (see Appendix A). The demodulation of the DPSK label was performed in a Mach-Zehnder interferometer (MZI) with a one bit delay in one of the arms.

After demodulation, the signal still showed the presence of the IM modulated payload, which would set a limit to the extinction ratio (ER) to be employed for the payload. This limit was numerically found to be of 9.5 dB, while in experiments a more conservative value of 3 to 6 dB was employed. For the performance of the system, it proved essential to optimize this value.

It was further found that the system performance showed an improvement with increasing values of the ratio between the payload and label bit-rate, although a low label bit-rate would set a strong requirement on the laser linewidth.

Transmission experiments suggested that pre-compensation scheme would result in a lower eye-opening penalty than post-compensation and that a slight under-compensation would be beneficial for the performance. Transmission over 80 km of non-zero dispersion shifted fiber (NZDSF) with pre-compensation showed less than 1 dB of transmission penalty, while an optimum span input power was found around 8 dBm. These results were not degraded by the WDM transmission of four channels with a 200 GHz spacing.

A wavelength conversion (WC) of a IM/DPSK labelled signal through four-wave mixing (FWM) in a highly non-linear fiber (HNLF) was implemented, which kept the label information at the new wavelength. The conversion penalty for the label compared to the back-to-back case was 1.6 dB. However, the regenerating character of the WC process forced to reduced even further the ER of the intensity modulation.

Label swapping for the IM/DPSK signal was realized in active devices by label erasure in a semiconductor optical amplifier (SOA) with a penalty of 2.5 dB, and label insertion in an electro-absorption modulator (EAM), which could enhance the performance of the payload. Combining both processes, rendered a labelling swapping system. However, the sensitivity of the new

label was reduced mostly due to the regeneration of the ER of the payload, which caused a higher intermodulation cross-talk.
The erasure of the DPSK label could also be performed in passive devices by realizing WC in a HNLF through cross-phase modulation (XPM). The new DPSK label could then be inserted using a new phase modulator. This technique was almost penalty-free for the label, when a 4 dB penalty was introduced in the payload.

Finally, the WDM transmission and label swapping for 4 IM/DPSK channels consisting of a 40 Gb/s payload and a 2.5 Gb/s label was presented. The overall penalty of 40 km of transmission and label swapping was 3.3 dB for the IM payload and 0.3 dB for the DPSK label.

The experimental results suggest that the orthogonal IM/DPSK modulation scheme could be a promising candidate for optical labelling in future IP-over-WDM networks, although a slow DPSK label would impose rigorous requirements on the linewidth of the source. Additionally, the temperature and mechanical stabilization of the 1-bit delay MZI used for DPSK demodulation would become a challenge.

This led to an alternative approach, presented as the DPSK/IM scheme, where the payload was DPSK modulated while the label was IM modulated. This scheme showed a slightly higher transmission penalty, but reduced the requirements on the laser linewidth, as the DPSK bit-rate was much higher (40 Gb/s in experiments). The label erasure was performed by injecting the inverted data stream of the detected IM label into an EAM that thus removed the intensity modulation from the DPSK payload. The process of labelling the signal and removing the label caused a 2.3 dB penalty.

For the IM/FSK labelling scheme, a novel source for constant-amplitude FSK modulation was presented. It used a directly modulated DFB laser, and compensated the corresponding unwanted intensity modulation by an integrated EAM. However, small intensity ripples were still present at the output of the FSK source, due to the non-matching raising and falling edges of the DFB laser and the EAM. When this signal was intensity modulated at a much higher bit-rate, this ripple would limit the performance of the payload. One way to limit the detrimental effect of the intensity ripple would be to carefully synchronize the payload and label data streams, so that the ripple would occur mostly during the transition of two payload bits, another way to overcome the problem would be to employ coding methods that would allow for a higher IM extinction ratio.

Another method for FSK generation is modulating the phase section of a GCSR laser, which proved to be highly tunable, but showed a wavelength dependent FSK response. The payload was in all cases added by a chirp-free

Mach-Zehnder modulator (MZM), while the FSK detection was realized suppressing one of the tones and directly detecting the resulting intensity modulated signal.

An experimental comparison of the performance of the IM/FSK signal for three compensating schemes presented a much better result for the payload under the pre-compensating scheme, while the label was little affected by the various schemes. A slight under compensation proved to be favourable. Furthermore, transmission over 138 km of single mode fiber (SMF) and 160 km of NZDSF was achieved. However, an observed reduction of the optimum ER for the payload would need to be taken into account when designing longer system.

For an IM/FSK modulated signal in a WDM system, the stability of the optical components of the system proved to be of a crucial importance. A slight detuning between the center frequency of a filter and a labelled channel was shown to noticeably degrade the performance of the system, due to FSK to IM conversion. The performance of the IM/FSK channels proved to be highly dependent on the performance of the FSK sources.

For IM/FSK labelled signals, label erasure was realized employing an SOA-MZI as wavelength converter. The wavelength process was only dependent on the intensity of the signal, and thus the FSK information was erased. The same device was then used for FSK label insertion, by modulating the CW input of the converter with the new label, which showed no substantial power penalty. Combinating these two approaches, became the basis for IM/FSK label swapping in a single device, which combined with two transmission spans showed a 2 dB penalty for the label and a 0.5 dB penalty for the payload.

An alternative FSK label insertion was performed in an EAM, which showed an enhancement in performance of both payload and label of around 1 dB. However, the high levels of power needed to make this label insertion method effective made it less attractive. Nevertheless, label swapping of the IM/FSK signal was performed using an SOA-MZI for label erasure and an EAM for label insertion. Because of the possibility of controlling the ER of the payload in a more accurate way through the two stages, the overall penalty for a two hop transmission and label swapping was below 2 dB for both payload and label.

In both the IM/DPSK and the IM/FSK labelling schemes, one of the biggest drawbacks, is the great amount of cross-talk that the payload impresses on the label. A way of overcoming this problem (and therefore being able to enlarge the ER of the IM payload) is using encoding formats for the IM transmission. When applying a coding technique to the payload that would

shift the most significant part of its power spectrum to higher values, the cross-talk will be suppressed significantly. Both Manchester-coding and 8B/10B coding were used to generate such a spectral shift.

A novel method to implement high-speed Manchester coding (MC) was presented in [96]. The generated Manchester encoded signal showed an error free performance, while applying the coding method for the IM/FSK scheme, showed a dramatically improvement in performance, by allowing the ER of the payload to be raised up to 13 dB. The drawback of MC is that it doubles the required signal bandwidth. Alternatively, 8B/10B coding only reduces the bandwidth efficiency by 20%. A noticeable enhancement of the performance was achieved when applying this coding to the payload of both IM/FSK or IM/DPSK labelled signals. This method also proved useful in reducing the pattern dependent modulation response of GCSR lasers.

Given that most labelling methods employ WC in the label swapping process, WC was implemented in passive and active devices for bit-rates of 40 Gb/s, regardless of labelling method. WC in a HNLF was used in a setup that exploited XPM created sidebands in conjunction with the appropriate optical band-pass filter. This approach proved to be much dependent on the effectiveness of the applied filtering method, although it has the advantage of being transparent to the bit-rate and highly effective at high bit-rates, as the processes involved are all-optical.

An 40 Gb/s IM wavelength conversion was also achieved by XGM in an SOA. An alternative method for WC in active devices, was employing an SOA-MZI. These devices were investigated both numerically and experimentally. Various configuration schemes of SOA-MZI were analyzed. The results showed that the co-propagating differentially driven mode of operation relaxed the requirements on the SOAs involved and improved the performance, at the cost of having an extra delay and attenuator to optimize.

The SOA-MZIs were also employed for insertion of intensity modulated time-serial labels. For this time-serial labelled scheme, a packet switched network systems experiment was setup. After transmission, packet switching and gating-controlled all-optical wavelength conversion, based on a HNLF were performed. The selected switched packets were then re-sent over a second span, showing and overall power penalty of less than 1.5 dB.

A last introduced alternative to for all-optical labelling, was the CSS scheme, that is based on the carrier suppression of the payload and labelling modulation of the sidebands. The system is easy to implement and showed less than 1 dB in transmission penalty over 50 km of SMF. An advantage of the proposed transmitter is that the label and payload signals can be

controlled independently, allowing for an arbitrary label to payload power ratio.
On the other hand, the performance of the label when employing the CSS labelling method is lower than the one of the payload, specially at high bit-rates. This is the opposite of the desired response of a labelled signal, although the sensitivity still showed to be of a high level. Another drawback is that the upgrading of the payload bit-rate would mean that its spectrum would be broadened, which in turn would imply that the sidebands should be further apart. This would have an impact on the system, in the sense that filtering and sideband detection should also be changed throughout the network.

In general, the results show that orthogonal labelling is a promising approach to ultra-high packet-rate routing and forwarding in the optical layer. At the same time, the limitation on the intensity modulated extinction ratio has to be carefully chosen for the given network, as a sub-optimized value it would have a detrimental effect for the network scalability.

For the IM/FSK scheme the quality of the FSK sources proved to be one of the most important factors in order to improve the performance of the system, while for the IM/DPSK the requirements for the laser linewidth and the stability of the receiver were the main limitations.

The experimental results suggest that transmission through network nodes would not drastically degrade the orthogonally modulated signals. The best choice for transmission dispersion design would be NZDSF in a hybrid- or pre-compensation scheme, while the optimum input power and payload ER have to be adjusted for each transmission link. These results confirm that the IM/FSK and IM/DPSK orthogonal labelling method are suitable for WDM systems and can be feasibly used in practice to upgrade metro-distance WDM transmission systems.

It has been demonstrated that WC in passive HNLF is suitable for optical labelled signals at high bit-rates, as long as the filters involved are sufficiently sharp and stable. In active devices, the design has to match the requirements of the bit-rate of the signal, but offers a higher versatility and a looser requirement on filter stability.

The methods for orthogonal optical label swapping were satisfactory in performance as long as the process involved was able to maintain the same ER for the payload. For most optical labelling swapping nodes, the versatility of combining wavelength conversion with label swapping proved to be the most attractive solution, amongst other things, because a complicated scheme of fast tunable filtering is avoided, and the network is not limited in terms of possible channels to be chosen as output.

The results further demonstrate the potential for the realization of compact label swapping devices based on integrated SOA-MZI wavelength converters, assisted by fast-switching tunable lasers. Such a compact label swapping modules would be a desirable key building block for future core networks.

In conclusion, the successful experimental duplication of the system functionalities of a network node validate labelling and specially orthogonal labelling for all optical packet switched networks, confirming the orthogonal modulation scheme as a promising solution for future ultra-high speed IP-over-WDM networks.

Appendix A

Differential XOR operation with PRBS

Pseudo random bit (PRBS) sequences are a type of Debruijn[1] sequences, which are normally generated by the use of shift registers with feedback [173]. The general case of shift register generation is showed in fig. A.1

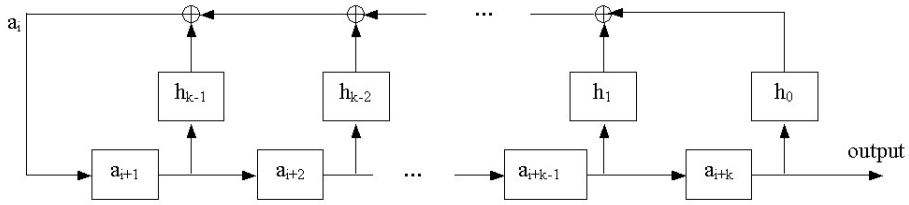

Fig. A.1 : *The general case of a shift register generating a PRBS sequence of period* 2^N*-1.*

The feedback is represented by the factors $h_j = 0,1$. The new left bit, a_i, is calculated as

$$a_i = a_{i+1}\, h_{k-1} + a_{i+2}\, h_{k-2} + \cdots + a_{i+k-1}\, h_1 + a_{i+k}\, h_0 \qquad (1)$$

An *n*-bit shift register can contain 2^n different combinations of ones and zeros. However, only 2^n*-1* of these are possible states when generating sequences since the state consisting of all zeros will result in an output sequence of only zeros. Thus, from an n-bit shift register, the length of the sequence will be

[1] A bit string of length 2^n is called a *(2,n)-deBruijn* sequence if each of the 2^n possible bit strings of length n occurs exactly once as a substring, where wrap-around is allowed

$$N = 2^n - 1 \tag{2}$$

If we define $h_k = 1$, equation (1) can be written as

$$\sum_{j=0}^{k} h_{k-j}\ a_{i+j} = 0 \tag{3}$$

this relationship between $(h_0, h_1, \ldots, h_k)$ and $(a_i, a_{i+1}, \ldots, a_{i+k})$ holds for any i. What it really is saying is that taking any k bits from the PRBS sequence, and multiplying them by $(h_0, h_1, \ldots, h_k)$ this will give us the next bit in the sequence, regardless of where we start from.

Lets now consider the polynomial

$$h_0 + h_1 x + \cdots + h_k x_k \tag{4}$$

and the polynomial corresponding to N successive a_i from the sequence

$$a_{N-1}\, x^{N-1} + a_{N-2}\, x^{N-2} + \cdots + a_1\, x + a_0 \tag{5}$$

The product of these two polynomials is

$$\begin{aligned}
&(h_0 + h_1 x + \cdots + h_k x^k)\,(a_{N-1} x^{N-1} + a_{N-2} x^{N-2} + \cdots + a_0) = \\
&= x^{N-1}\,(h_0 a_{N-1} + h_1 a_{N-2} + \cdots + h_k a_{N-1-k}) + \\
&+ x^{N-2}\,(h_0 a_{N-2} + h_1 a_{N-3} + \cdots + h_k a_{N-2-k}) + \\
&\qquad \vdots \\
&+ x\,(h_0 a_1 + h_1 a_0 + h_2 a_{N-1} + \cdots + h_k a_{N+1-k}) + \\
&+ (h_0 a_0 + h_1 a_{N-1} + h_2 a_{N-2} + \cdots + h_k a_{N-k})
\end{aligned} \tag{6}$$

Counting powers of x modulo N and remembering that the sequence of a_i's is periodic with period N, also the indices of the a_i's may be counted modulo N in other words: $a_{i+N} = a_i$. Using this, the coefficient of x^p in (6) may be written

$$(h_0 a_p + h_1 a_{p-1} + \cdots + h_k a_{p-k}) = \sum_{j=0}^{k} h_{k-j}\ a_{p-k+j} \tag{7}$$

This is the same expression as (3) with $i = p\text{-}k$ which means that the coefficient is *0*. this is true for all coefficients in (6) so the product of the two polynomials is 0. Hence $h(x)$ multiplied with any code word from the shift

register sequence, results in *0*. In other words, *h(x)* may be interpreted as a *multiplum* of the parity check polynomial of the shift register code. This means that if a sequence gives zero when multiplied by *h(x)*, it must be a code word of the PRBS sequence.

If *h(x)* is primitive, i.e. it contains no factors of lower degree it simply is the parity check polynomial of the code. In this case the dimension of the code is *k* since $h_k=1$ was defined. Thus, the code generated by the shift register has 2^k code words that all will be the same word shifted a number of bits (given that the sequence is cyclical with period *N*).

Table A.2 *: Truth table of the XOR operation.*

in_n	out_{n-1}	out_n
0	*0*	*0*
0	*1*	*1*
1	*0*	*1*
1	*1*	*0*

This is a proof of the linearity of the codes generated in this manner. Linearity in this context means that the sum of any two words in the code words must also be a code word. Addition of code words is performed bit by bit modulo 2 (i.e. no carry).

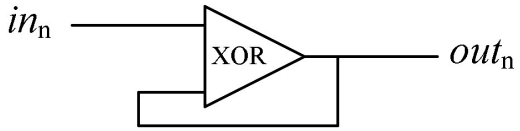

Fig. A.3 *: Generation of a differential encoded signal.*

For studying the differential encoder shown in fig. A.3, we notice that the output is generated by the XOR operation (sum without carry) of the input and the output delayed one position. That is

$$out_n = in_n \oplus out_{n-1} \tag{8}$$

where b_n is the input and a_n is the output. But the characteristics of the XOR operation (see Table A.2) imply that this can be rewritten as

$$in_n = out_n \oplus out_{n-1} \tag{9}$$

Let us therefore consider the case of summing a code word of length N with itself delayed one bit. Being the sum modulo 2, this would render the XOR of the sequence with itself delayed one bit.

Delaying a cyclical sequence represented by a polynomial is simply multiplying it by x^d being d the number of bits we want to the delay the sequence by, as shown:

$$\begin{gathered}(a_0 + a_1 x + a_2 x^2 + \cdots + a_{N-2} x^{N-2} + a_{N-1} x^{N-1}) \cdot x^d = \\ = a_{N-d} + a_{N-d+1} x + \cdots + a_0 x^d + \cdots + a_{N-1-d} x^{N-1}\end{gathered} \tag{10}$$

In particular a 1 bit delay would simply mean multiplying the polynomial by x. Hence adding a sequence with itself delayed one bit will be multiplying the polynomial representing that sequence by $(1 + x)$. Our new sequence will then be

$$\begin{gathered}(a_0 + a_1 x + a_2 x^2 + \cdots + a_{N-2} x^{N-2} + a_{N-1} x^{N-1}) \cdot (1 + x) = \\ (a_0 + a_{N-1}) + (a_0 + a_1) x + (a_1 + a_2) x^2 + \cdots + (a_{N-2} + a_{N-1}) x^{N-1}\end{gathered} \tag{11}$$

In order to make sure that this new sequence also is part of the code (i.e. the same sequence shifted a number of bits) we will have to multiply this polynomial by $h(x)$. If the result is zero, we can conclude that it will be the same PRBS sequence delayed a certain number of bits.

$$\begin{gathered}[(a_0 + a_{N-1}) + (a_1 + a_0) x + (a_2 + a_1) x^2 + \cdots + (a_{N-1} + a_{N-2}) x^{N-1}] \cdot \\ \cdot (h_0 + h_1 x + \cdots + h_k x^k) = \\ \\ = x^{N-1} [h_0 (a_{N-1} + a_{N-2}) + h_1 (a_{N-2} + a_{N-3}) + \cdots + h_k (a_{N-1-k} + a_{N-2-k})] + \\ + x^{N-2} [h_0 (a_{N-2} + a_{N-3}) + h_1 (a_{N-3} + a_{N-4}) + \cdots + h_k (a_{N-2-k} + a_{N-3-k})] + \\ \vdots \\ + x [h_0 (a_1 + a_0) + h_1 (a_0 + a_{N-1}) + \cdots + h_k (a_{N-1-k} + a_{N-2-k})] + \\ + [(a_0 + a_{N-1}) + h_1 (a_{N-1} + a_{N-2}) + \cdots + h_k (a_{N-k} + a_{N-k-1})]\end{gathered} \tag{12}$$

still counting powers of modulo N and a_i's also modulo N (i.e. $a_{i+N} = a_i$). The coefficient of a given x^p can be now written as

$$\begin{gathered}[h_0 (a_p + a_{p-1}) + h_1 (a_{p-1} + a_{p-2}) + \cdots + h_k (a_{p-k} + a_{p-k-1})] = \\ = \sum_{j=0}^{k} h_{k-j} \left(a_{p-k+j} + a_{p-k+j-1}\right) = \sum_{j=0}^{k} h_{k-j}\, a_{p-k+j} + \sum_{j=0}^{k} h_{k-j}\, a_{p-k+j-1}\end{gathered} \tag{13}$$

From (3) we know that each one of these are 0 (they are in fact the same as (3) taking $i = p\text{-}k$ and $i = p\text{-}k\text{-}1$ respectively). Therefore, each of the components in (12) is zero and so is the product of $h(x)$ with (11). This translates into each of the components on the right hand side of (9) being a PRBS signal. Therefore, the new sequence we are analyzing is a code word from the same code as the original one.

From this we can finally conclude that the XOR function of a PRBS sequence with the sequence at the output of the operation delayed one bit, will result in the same sequence shifted a number of bits. In other words, the differential encoding of a PRBS signal gives as a result the same PRBS signal shifted a number of bits. The magnitude of this shift will depend on the values of h_i in the shift register that generates the PRBS sequence.

In order to view this, several PRBS sequences were generated by shift registers of respectively 7, 9 and 11 bits, and their correlation to the same sequence XOR with a 1 bit delay was calculated. The results are shown in the graphs below, showing clearly that after a certain delay the result is the same sequence. The discrete correlation used is defined as follows

$$\rho(i) = \frac{1}{N}\sum_{j=0}^{N-1}(-1)^{a_j + a_{j+i}} \tag{14}$$

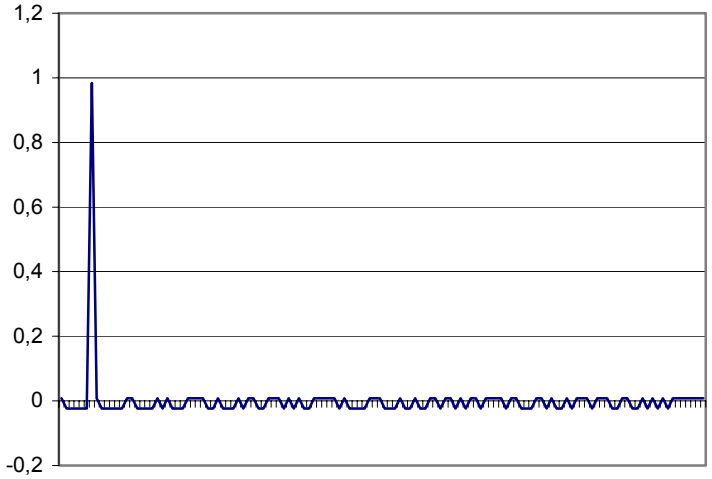

Fig. A.4 *: Correlation of a PRBS sequence generated by a 7-bit shift register and its XOR function with a 1 bit delay of the same sequence. The sequence is 127 bits long and the resulting shift is 6 bits.*

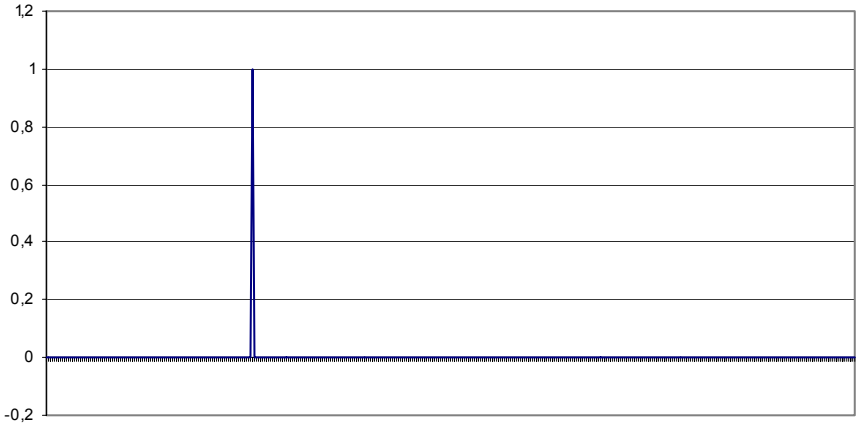

Fig. A.5. *Correlation of a PRBS sequence generated by a 9-bit shift register and its XOR function with a 1 bit delay of the same sequence. The sequence is 511 bits long and the resulting shift is 383 bits.*

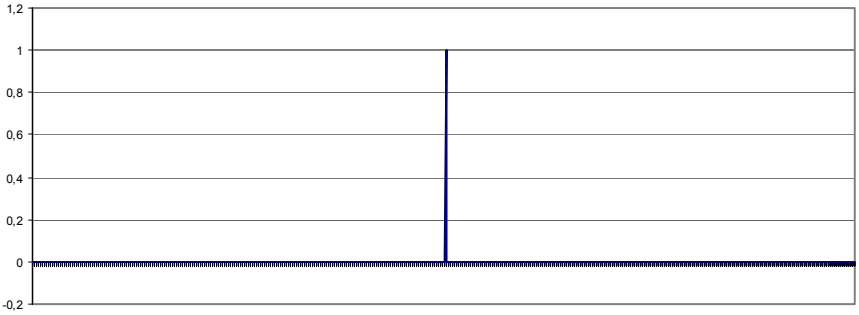

Fig. A.6. *Correlation of a PRBS sequence generated by a 11-bit shift register and its XOR function with a 1 bit delay of the same sequence. The sequence is 2047 bits long and the resulting shift is 1019 bits.*

References

[1] Mike Cansfield, "2004: A year in review", Total-Telecom, www.totaltele.com, January 2005.

[2] Grant Gross, "Study: 2004 was 'turnaround' year for telecom industry", Network World Fusion (www.nwfusion.com), January 2005.

[3] R. E. Wagner, "Interconnection of Metropolitan and Backbone Networks", Optical Fiber Communication Conference (OFC 2003), Atlanta, Georgia, USA, March 23-28, (invited paper) 2003.

[4] Lucas Mearian, ComputerWorld (www.computerworld.com), March 2005.

[5] D. J. Blumenthal, "All-optical label swapping for the future internet", Optics and Photonics News, 13 (3), pp 22-25, March 2002.

[6] S. Yao, B. Mukherjee, S. Dixit, "Advances in Photonic Packet-Switching: An Overview", IEEE Communications Magazine , pp. 84-93, February 2000.

[7] C. Qiao, M. Yoo, "Optical Burst Switching (OBS) – a new paradigm for an optical internet", Special Issue on WDM Networks, J. High Speed Networks, Vol. 8, No.1, pp.69-84, January 1999.

[8] N. Ghani, "Lambda-labeling: a framework for IP-over-WDM using MPLS", Optical Networks Magazine, vol. 1, no.2, pp.45-58, April 2000.

[9] Chunming Qiao, "Labeled Optical Burst Switching for IP-over-WDM Integration", IEEE Communications Magazine, vol. 38, no. 9, pp. 104-114, September 2000.

[10] Bruce Davie and Yakov Rekhter, "MPLS. Technology and applications", Morgan Kaufmann Publishers, San Francisco, 2000.

[11] M. J. Koonen; Sulur, I. Tafur Monroy, J. G. L. Jennen, H. de Waardt, "Orthogonal optical labeling of packets in IP-over-WDM networks", Proceedings of NOC 2002, 7th European Conference on Networks & Optical Communications, 18-21 June 2002, Darmstadt, Germany, 2002, pp. 82-89.

[12] D.J. Blumenthal, B. E. Olsson, G. Rossi, T. E. Dimmick, L. Rau, M. Masanovic, O. Lavrova, R. Doshi, O. Jerphagnon, J. E. Bowers, V. Kaman, L. A. Coldren and J. Barton, "All-optical label swapping networks and technologies", Journal of Lightwave Technology, Vol. 18, No. 12, pp. 2058-2075, Dec 2000.

[13] Tafur Monroy, J. Zhang, Chi Nan, P. V. Holm-Nielsen, C. Peucheret, A. M. Koonen, J. J. Vegas Olmos and G. D. Khoe, "Techniques for labeling of optical signals in burst switched networks", Proceedings of WOBS'03, 16-16, Dallas, Texas, pp. 1-11, October 2003.

[14] F. Ramos, E. Kehayas, J. M. Martinez, R. Clavero, J. Marti, L. Stampoulidis, D. Tsiokos,H. Avramopoulos, J. Zhang, P. V. Holm-Nielsen, N. Chi, P. Jeppesen, N. Yan, I. Tafur Monroy, A. M. J. Koonen, M. T. Hill, Y. Liu, H. J. S. Dorren, R. Van Caenegem, D. Colle, M. Pickavet, and B. Riposati, "IST-LASAGNE: Towards All-Optical Label Swapping Employing Optical Logic Gates and Optical Flip-flops", to be published in Journal of Lightwave Technology, 2005.

[15] D. J. Blumenthal, A. Carena, L. Rau, V. Curri, and S. Humphries, "All-optical label swapping with wavelength conversion for WDM-IP networks with subcarrier multiplexed addressing", IEEE Photon. Technol. Lett., Vol.11, No.1, pp.1497-1499, 1999.

[16] T. Koonen, G. Morthier, J. Jennen, H. de Waardt and P. Demeester, "Optical packet routing in IP-over-WDM networks deploying two-level optical labeling", in Proceedings of the European Conference on Optical Communication, ECOC'01, Amsterdam, The Netherlands, vol. 4, pp. 608-609, paper Th.L.2.1, 2001.

[17] Huang and S. Knauer, "Starlight: A wideband digital switch", in Proc. IEEE Global Telecommun. Conf. (GLOBECOM'84) Atlanta, GA, vol. 1, pp. 121–5, Nov. 1984.

[18] Z. Haas and D. R. Cheriton, "Blazenet: A packet-switched wide-area network with photonic data path", EEE Trans. Commun., Vol. 38, pp.818–829, June 1990.

[19] D. Colle, S. De Maesschalck, C. Develder, P. Van Heuven, A. Groebbens, J. Cheyns, I. Lievens, M. Pickavet, P. Lagasse, P. Demeester, "Data-centric optical networks and their survivability", EEE Journal on Selected Areas in Communications, vol. 20, no.1, pp. 6 -20, 2002.

[20] J.S. Turner, "WDM burst switching for petabit data networks", Optical Fiber Communication Conference, 2000, vol. 2, pp. 47 –49, 2000.

[21] Banerjee, et al., "Generalized Multiprotocol Label Switching: An Overview of Routing and Management Enhancements", IEEE Communication Magazine, pp.144-150, Jan. 2001.

[22] S. J. B. Yoo, Hyuek Jae Lee, Zhong Pan, Jing Cao, Yanda Zhang, Katsunari Okamoto, and Shin Kamei, "Rapidly Switching All-Optical Packet Routing System With Optical- Label Swapping Incorporating Tunable Wavelength Conversion and a Uniform-Loss Cyclic Frequency AWGR", EEE photonics technology letters, vol. 14, no. 8, pp. 1211-3, August 2002.

[23] Takada, J. H. Park, "Architecture of ultrafast optical packt switching ring network", Journal of Lightwave Technology, 20, (12), pp. 2306-2315, 2002.

[24] Y. Gen, Y. Zhang, L. K. Chen, "On Architecture and Limitations of Optical Multiprotocol Label Switching (MPLS) Networks Using Optical-Orthogonal-Code (OCC)/Wavelength Label", OTF, Vol. 8, pp. 43-70, 2002.

[25] B. Meagher, G. K. Chang, G. Ellinas, et al, "Design and implementation of ultra-Low latency optical label switching for packet-switched WDM networks", Journal of Lightwave Technology, Vol.21, No.3, pp 648-663, March 2003.

[26] M. Hickey and L. Kazovsky, "The STARNET Coherent WDM Computer communication network: experimental transceiver employing a novel modulation format", Journal Lightwave Technol., v12, n5, pp876-884, 1994.

[27] M. Hickey, C. Barry, C. Noronha, L. Kazovsky, "Experimental PSK/ASK transceiver for the STARNET WDM computer communication network", IEEE Photon. Technol. Lett., vol. 5, no.5, pp.568-571, 1993.

[28] C. Guillemot, M. Renaud, P. Gambini, C. Janz, I. Andonovic, R. Bauknecht, B. Bostica, M. Burzio, F. Callegati, M. Casoni, D. Chiaroni, F. Clerot, S.L. Danielsen, F. Dorgeuille, A. Dupas, A. Franzen, P.B. Hansen, D.K. Hunter and A. Kloch, "Transparent optical packet switching: The European acts KEOPS project approach", IEEE J. Lightwave Tech., vol. 16, pp. 2117-2134, 1998.

[29] L. Rau, S. Rangarajan, D. J. Blumenthal, H. F. Chou, Y. J. Chiu, J. E. Bowers, "Two-hop all-optical label swapping with variable length 80Gb/s packets and 10Gb/s labels using nonlinear fiber wavelength converters, unicast/multicast output and a single eam for 80- to 10Gb/s packet demultiplexing", Proc. of Optical Fiber Communication Conference 2002, 17-22 Mar 2002.

[30] T. Fjelde, A. Kloch, D. Wolfson, B. Dagens, A. Coquelin, I. Guillemot, F. Gaborit, F. Poingt, and M. Renaud, "Demonstration of 20 Gbit/s all-optical logic XOR in integrated SOA-based interferometric wavelength converter", Electronics Letters, Vol. 36, No. 22, 26 Oct 2000.

[31] Gambini P et al., "Transparent optical packet switching: network architecture and demonstrators in the KEOPS project", IEEE J Selected Areas in Communications, Vol 16, no 7, pp. 1245-57, Sept 1998.

[32] B. E. Olsson, P. Öhlén, L. Rau, G. Rossi, O. Jerphagnon, R. Doshi, D. S. Humphries, D. J. Blumenthal, V. Kaman, and J. E. Bowers, "Wavelength

routing of 40 Gbit/s packets with 2.5 Gbit/s header erasure/rewriting sing all-fiber wavelength converter", Electron. Lett., vol. 31, no. 4, pp. 345–347, Feb. 2000.

[33] S.J. Ben Yoo , "Optical-Packet Switching and Optical-Label Switching Technologies for the Next Generation Optical Internet", Optical Fiber Communication Conference (OFC 2003), Atlanta, Georgia, USA, March 23-28, paper FS5, 2003.

[34] D. Hunter, M. Nizam, M. Chia, I. Andanovic, K. Guild, A. Tzanakaki, M. O'Mahony, J. Bainbridge, M. Stephens, R. Penty, I. White, "WASPNET: A Wavelength Switched Packet Network ", IEEE Communications Magazine, vol.37, no.3, p.120-9, March 1999.

[35] Ian M. White, "A New Architecture and Technologies for High-Capacity Next-Generation Metropolitan Networks", Ph.D. Thesis, Stanford University, August 2002.

[36] Kapil V. Shrikhande, I. M. White, M. S. Rogge, F-T. An, A. Srivatsa, E.S. Hu, S. S-H. Yam and Leonid G. Kazovsky, "Performance Demonstration of a Fast-Tunable Transmitter and Burst-Mode Packet Receiver for HORNET", Optical Fiber Communication Conference (OFC), paper ThG2, Anaheim, California, February 2001.

[37] Ian White, Matt Rogge, Yu-Li Hsueh, Kapil Shrikhande, and Leonid Kazovsky, "Experimental Demonstration of the HORNET Survivable Bi-directional Ring Architecture", Optical Fiber Communication Conference (OFC), paper WW1, Anaheim, California, March 17-22, 2002.

[38] Hideyuki Sotobayashi, Wataru Chujo and Ken-ichi Kitayama, "Photonic Gateway: Multiplexing Format Conversions of OCDM-to-WDM and WDM-to-OCDM at 40 Gbit/s (4 x10 Gbit/s)", Journal of Lightwave Technology, 2002.

[39] Denis J. G. Mestdagh, "Fundamentals of Multiaccess Optical Fiber Networks", Artech House, Inc., 1995.

[40] Carena, M.D. Vaughn, R. Gaudino, M. Shell, D.J. Blumenthal, "OPERA: an optical packet experimental routing architecture with label swapping capability", Journal of Lightwave Technology, vol. 16, no. 12, pp. 2135 – 2145, 1998.

[41] Chlamtac, et. al., "CORD: Contention Resolution by Delay Lines", IEEE J. Selected Areas in Commun., Vol. 14, No. 6, pp. 1014-1029, June 1996.

[42] K.V. Shrikhande, I.M White, D. Wonglumsom, S.M. Gemelos, M.S. Rogge, Y. Fukashiro, M. Avenarius, L.G. Kazovsky, "HORNET: a packet-over-WDM multiple access metropolitan area ring network", IEEE Journal on Selected Areas in Communications, vol. 18, no. 10 , pp. 2004 –2016, 2000.

[43] H.J. Lee, V. Hernandez, V. K. Tsui, S. J. B. Yoo, "Simple, polarization-independent, and dispersion-insensitive SCM signal extraction technique for

optical switching systems applications", Elec. Letters, Vol. 37, No. 20, pp. 1240, 2001.

[44] J. Cheyns, C. Develder, E. Van Breusegem, E. Baert, A. Ackaert, M. Pickavet, P. Demeester, "Routing in an AWG based optical packet switch", Phot. Netw. Comm., Vol. 5, 1, pp. 69-80, January 2003.

[45] H. Rongqing, Z. Benyuan H. Renxiang C.T. Allen, K.R. Demarest, D. Richards, "Subcarrier multiplexing for high-speed optical transmission", Journal of Lightwave Technology, vol. 20, no. 3 , pp.: 417 –427, 2002.

[46] Y. M. Lin, W. I. Way, and G. K. Chang, "A Novel Optical Label Swapping Technique Using Erasable Optical Single-Sideband Subcarrier Label", IEEE Photonics Technology Letters, vol. 12, No. 8, pp. 1088-1090, August 2000.

[47] E. N. Lallas, N. Skarmoutsos, and D. Syvridis, "An Optical FSK-Based Label Coding Technique for the Realization of the All-Optical Label Swapping", IEEE Photonics Letters, vol. 14, no. 10, pp. 1472-1474, October 2002.

[48] K. G. Vlachos, I. T. Monroy, A. M. J. Koonen, C. Peucheret and P. Jeppesen, "STOLAS: Switching Technologies for Optically Labeled Signals", IEEE Communications Magazine, vol. 41, no. 11, pp. S9-15. November 2003.

[49] N. Chi, B. Carlsson, J. Zhang, P. V. Holm-Nielsen, C. Peucheret, P. Jeppesen, "Transmission Performance of All-optically labelled Packets using ASK/DPSK Orthogonal Modulation ", in Proceedings IEEE Laser and Electro-Optics Society Annual Meeting, LEOS'2002, Glasgow, Scotland, U.K., paper MF3, 2002.

[50] Tafur Monroy, E. J. M.Verdurmen, S. Sulur, A. M. J. Koonen, H. de Waardt, G. D. Khoe, N. Chi, P. V. Holm-Nielsen, J. Zhang and C. Peucheret, "Performance of a SOA-MZI wavelength converter for label swapping using combined FSK/IM modulation format", Optical Fiber Technology, vol. 10, no. 1, pp 31-49, 2004.

[51] N. Chi, B. Carlsson, J. Zhang, P. V. Holm-Nielsen, C. Peucheret and P. Jeppesen, "All-optical transparent wavelength conversion of an optically labeled signal in ASK/DPSK orthogonal modulation", in Proceedings IEEE Laser and Electro-Optics Society Annual Meeting, LEOS'2002, Glasgow, Scotland, U.K., paper MF3, 2002.

[52] M. Hickey and L. Kazovsky, "Combined frequency and amplitude modulation for the STARNET WDM computer communication network", IEEE Photon. Technol. Lett., v 6, 1473–1475, Dec. 1994.

[53] R.S. Vodhanel, A.F. Elrefaie, M.Z. Iqbal, R.E. Wagner, J.L. Gimlett and S. Tsuji, "Performance of directly modulated DFB lasers in 10Gb/s ASK/FSK/DPSK lightwave systems", J. Lightwave Technol., v8, 1379-1385, Jan. 1990.

[54] T. Koonen, Sulur, I. Monroy, J. Jennen, H. Waardt, "Optical labeling of packets in IP-over-WDM networks", in Proc. Eur. Conf. Optical Communications (ECOC'02), paper 5.5.2, 2002.

[55] Alvaro Buxéns Azcoaga, "40 Gb/s Optical Transmission Systems", Ph.D. thesis, Research Center COM, Technical University of Denmark, 2003.

[56] M. Renaud, F. Masetti, C. Guillemot, and B. Bostica, "Network and system concepts for optical packet switching", IEEE Commun. Mag., vol. 35, pp. 96–102, Apr. 1997.

[57] Y. Yu, G. Mulvihill, S. O'Duill, R. O'Dowd, B. Moeyersoon and G. Morthier, "STOLAS deliverable D214: Wavelength switching and FSK modulation properties of widely tunable laser diodes and compatibility with network/system requirements", www.ist-stolas.org, 2004.

[58] S. L. Danielsen, B. Mikkelsen, C. Joergensen, T. Durhuus, and K. E. Stubkjaer, "WDM packet switch architectures and analysis of the influence of tunable wavelength converters on the performance", J. Light-wave Technol., vol. 15, pp. 219–27, 1997.

[59] E. Zouganeli, A. F. Mlonyeni, A. Sudbo, O.-P. Rostad, and T. Olsen, "Wavelength routed network using widely tunable transmitters", in Proc. ECOC'2000, Munich, Germany, Sept. 3–7, 10.3.4, 2000.

[60] Sulur, T. Koonen, I.T. Monroy, H. de Waardt, J. Jennen and G. Morthier , "Combined ASK/FSK and ASK/DPSK Modulation Formats for Optically Labeled Signals", in Proc.ONDM'2002, Torino, Italy, Febr. 4–6, 2002.

[61] Sudbø, S. Bjørnstad and E. Zouganeli, "Scalable optical switch based on tunable wavelength converters and arrayed waveguide grating routers", Optical Fiber Communication Conference (OFC 2003), Atlanta, Georgia, USA, March 23-28, 2003.

[62] T. Koonen, E. Zouganeli, C. Peucheret, I. Tafur, Y. Yu, G. Mulvihill, S. O'Duill, R. O'Dowd, B. Moeyersoon and G. Morthier, "STOLAS Deliverable D.121", www.ist-stolas.org, 2004.

[63] C. Bintjas et al., "Clock recovery circuit for optical packets", IEEE Photon. Technol. Lett., vol. 14, pp. 1363-1365, Sep. 2002.

[64] H. J. Lee, H. G. Kim, J. Y. Choi, K. Kim, and J. Lee, "A simple packet level clock extraction scheme using a terahertz optical asymmetric demultiplexer", EEE Photon. Technol. Lett., 11, 1310–1312, 1999.

[65] Y. Shimazu and M. Tsukada, "Ultrafast photonic ATM switch with optical output buffers", J. Lightwave Technol., vol. 10, pp. 265–272 1992.

[66] Christophe Peucheret, "Fibre and Components Induced Limitations in High Capacity Optical Networks", Ph.D. thesis, Research Center COM, Technical University of Denmark, 2003.

[67] C. Develder, M. Pickavet, P. Demeester, "Strategies for an FDL-based feedback buffer for an optical packet switch with QoS differentiation", Proc. Int. Conf. on Optical Internet (COIN2002), paper COIN.TuD1, Cheju Island, Korea, pp. 114-116, Jul. 2002.

[68] Govind P. Agrawal, "Fiber-Optic Communication Systems", John Wiley & Sons, Inc., New York, NY, 2nd edition, 1997.

[69] Kamran Kiasaleh, "A Postdetection Strategy for the Reduction of Error Floors of Optical DPSK Receivers Impaired by Laser Phase Noise", Journal of Lightwave Technology, vol.17, no.2, Feb 1999.

[70] Bruce Carlson, "Communication Systems", Mc Graw-Hill, New York, 1986.

[71] G. Einarsson, J. Strandberg and I. Tafur Monroy, "Error Probability Evaluation of Optical Systems Disturbed by Phase Noise and Additive Noise", Journal of Lightwave Technology, Vol. 13, no. 9, pp 1847-1852, Sept. 1995.

[72] Govind P. Agrawal and Niloy K. Dutta, "Semiconductor Lasers", Kluwer Academic Publishers, Boston, Third Edition, 2001.

[73] N. Chi, L. Xu, J. Zhang, P. V. Holm-Nielsen, C. Peucheret and P. Jeppesen, "Optical Label Switching of 40 Gb/s Payloads Using Orthogonal ASK/DPSK Modulation Format", to be published in Journal of Lightwave Technology, 2005.

[74] J. Zhang, P. V. Holm-Nielsen, N. Chi, C. Peucheret and P. Jeppesen, "DC-balanced line encoding for optical labeling scheme using orthogonal modulation", in Technical Digest Optical Fiber Communication Conference, OFC'04, Los Angeles, California, U.S.A., paper WF2, Feb. 2004.

[75] M. Rohde, C. Caspar, N. Heimes, M. Konitzer, E.J. Bachus and N. Hanik, "Robustness of DPSK direct detection transmission format in standard fibre WDM systems", Electronics Letters, vol.36, no.17, Aug 2000.

[76] L. Becouarn, G. Vareille, P. Pecci and J. F. Marcerou, "3 Tbit/s transmission (301 DPSK channels at 10.709 Gb/s) over 10270 km with a record efficiency of 0.65 (bit/s)/Hz", in Proceedings Euronpean Conference on Optical Communications, ECOC'03, Rimini, Italy, paper PD45, September 2003.

[77] G. Morthier, G Sarlet, R Baets, R. O'Dowd, H. Ishii, Y. Yoshikuni, "The direct modulation bandwidth of widely tunable DBR laser diodes", IEEE Semiconductor Laser Conference, 2000, pp. 87-88.

[78] L. Xu, N. Chi, J. Mork, L. K. Oxenlowe and P. Jeppesen, "Precise measurement of EAM chirp alpha -parameter and theoretical analysis of effective chirp under large signal modulation", in Proceedings of the International Conference on Telecommunications, ICT'2002, pp. 61-63, Beijing, China, June 2002.

[79] J. Zhang, N. Chi, P. V. Holm-Nielsen, C. Peucheret and P. Jeppesen, "A novel optical labeling scheme using a FSK modulated DFB laser integrated with an EA modulator", in Technical Digest Optical Fiber Communication Conference, OFC'03, paper TuQ5, vol. 1, 279-280 2003.

[80] H. Nakajima, J. Charil, "Time-resolved spectrum characteristics of FSK-modulated dual-mode DFB/DBR lasers", IEEE Photonics Technology Letters , vol. 9, no. 6, pp. 821 –823. 1997.

[81] O. A. Lavrova and D. J. Blumenthal, "Detailed transfer matrix method-based dynamic model for multisection widely tunable GCSR lasers", Journal of Lightwave Technology, vol. 18, no. 9, pp. 1274-1283, Sept. 2000.

[82] P.-J. Rigole, S. Nilsson, L. Bäckbom, B. Stålnacke, E. Berglind, J.-P. Weber and B. Stoltz, "Quasi-continuous tuning range from 1560 to 1520 nm in a GCSR laser, with high power and low tuning currents", Electronics Letters, vol. 32, no. 25, pp. 2352-2354, 1996.

[83] A. Saavedra, P.-J. Rigole, E. Goobar, R. Schatz and S. Nilsson, "Amplitude and frequency modulation characteristics of widely tunable GCSR lasers", IEEE Photonics Technology Letters, vol. 10, no. 10, pp. 1383-1385, 1998.

[84] K. Shrikhande, "HORNET project", Stanford University, http://wdm.stanford.edu/iphornet/iphornet.html, 2004.

[85] J. Zhang, et al., "A Novel Method For Optical Subcarrier Label Generation", Optical Fiber Communication Conference (OFC 2003), Atlanta, Georgia, USA, March 23-28, paper TuQ, 2003.

[86] Y. Miyamoto, A. Hirano, K. Yonenega, A. Sano, H. Toba, K. Murata, and O. Mitomi, "320 Gbit/s (8x40 Gbit/s) WDM transmission over 367 km with 120 km repeater spacing using carrier-suppressed return-to-zero format", Electron. Lett., vol. 35, pp. 2041–2042, 1999.

[87] R. Montgomery et al, "A novel technique for double sideband suppressed carrier modulation of optical fields", IEEE Photon. Technol. Lett., 7, (4), pp. 434 -436, 1995.

[88] J. Capmany et al., "Optical label swapping based on subcarrier multiplexing: a network paradigm for the implementation of optical internet", in Proc. 5th Intl. Conf. on Transparent Optical Networks 2003, (Invited Paper) Jun. 2003.

[89] X. Widmer and P. A. Franasek, "A DC-balanced, partitioned-block,8B/10B transmission code", IBM J. Res. Develop., vol. 27, 440–451, 1983.

[90] T. K. Woodward, A. L. Lentine, J. D. Fields, G. Giaretta, and R. Limacher, "First Demonstration of Native Ethernet Optical Transport System Prototype at 10 Gb/s Based on Multiplexing of Gigabit Ethernet Signals", IEEE Photon. Techno. Letter., vol. 12, n8, 1100-1102, 2000.

[91] K.Murata, T. Otsuji, T. Enoki and Y. Umeda, "Exclusive OR/NOR IC for >40Gbit/s optical transmission systems", Electron. Lett., vol. 16, no. 8, pp. 764-765, 1998.

[92] Y. Yamada, Y. Shibata, T. Okugawa and K. Habara, "High level fluctuation tolerant optical receiver for optical packet switch and WDM cross connect", Journal of Lightwave Technology, 16, (12), pp. 2220-2227, 1998.

[93] H. Nishizawa, Y. Yamada, K. Habara and T. Ohyama, "Design of a 10Gb/s burst mode optical packet receiver module and its demonstration in a WDM optical switching network", Journal of Lightwave Technology, 20, (7), pp. 1078-1083, 2002.

[94] Y. Shibata, Y. Yamada, K. Habara and N. Yoshimoto, "Semiconductor laser diode optical amplifiers/gates in photonic packet switching", Journal of Lightwave Technology, 16, (12), pp. 2228-2235, 1998.

[95] M.C. Ho, C.L. Lu, R.T. Hofmeister and L:G: Kazovsky, "Nonlinear crosstalk reduction by spectrum shaping in subcarrier signaling WDM networks", in Proceedings, Conference on Lasers and Electro-Optics (CLEO'98), paper CMG6, 1998.

[96] J. Zhang, N. Chi, P. V. Holm-Nielsen, C. Peucheret and P. Jeppesen, "Method for high-speed Manchester encoded optical signal generation", in Technical Digest Optical Fiber Communication Conference, OFC'04, Los Angeles, California, U.S.A., paper MF76, 2004.

[97] S.P. Gangopadhyay et al., "Performance of linecoded optical heterodyne FSK systems with nonuniform laser FM response", Journal of Lightwave Technology, vol.13, no.4 , pp. 628-638, 1995.

[98] Govind P. Agrawal, "Nonlinear Fiber Optics", Academic Press, San Diego, CA, USA, 3rd edition, 2001.

[99] D.M. Rothnie, J. E. Midwinter, "Improved Standard Fiber performance by Positioning the dispersion compensating fiber", Electronic Letters, Vol.32, No.20, pp.1907-1908, 1996.

[100] C. Peucheret, N. Hanik, R. Freund, L. Molle and P. Jeppesen, "Optimisation of pre- and post-dispersion compensation schemes for 10-Gbit/s NRZ links using standard and dispersion compensating fibers", IEEE Photonics Technology Letters, vol. 12, no. 8, pp. 992-994, 2000.

[101] Torger Tokle, "Optimised Dispersion Management and Modulation Formats for High Speed Optical Communications Systems", Ph.D. thesis, Research Center COM, Technical University of Denmark, 2004.

[102] Birger Carlsson, "A Study on Bit Error Rate Calculation for Optical Labelling Transmission", Mc.S. project, Research Center COM, Technical University of Denmark, 2003.

[103] Quang Nghi Trong Le, "Fibers for 160 Gbit/s Transmission and above", Ph.D. thesis, Research Center COM, Technical University of Denmark, 2003.

[104] Bartłomiej Kozicki, "Wavelegth divisoin multiplexing of optically labelled channels using orthogonal modulation formats", Mc.S. project, Research Center COM, Technical University of Denmark, 2003.

[105] T.-K. Chiang, N. Kagi, T. K. Fong, M. E. Marhic, and L. G. Kazovsky, "Cross-Phase Modulation in Dispersive Fibers: Theoretical and Experimental Investigation of the Impact of Modulation Frequency", IEEE Photon. Technol. Lett., 6(6):733-736, June 1994.

[106] M. Shtaif, "Analytical description of cross-phase modulation in dispersive optical fibers", Optics Letters, vol.23, no.15, Aug 1998.

[107] M. Shtaif and M. Eiselt, "Analysis of Intensity Interference Caused by Cross-Phase Modulation in Dispersive Optical Fibers", IEEE Photonics Technology Letters, vol.10, no.7, July 1998.

[108] S.L. Danielsen, C. Joergensen, B. Mikkelsen and K.E. Stubkjaer, "Analysis of a WDM packet switch with improved performance under bursty traffic conditions due to tuneable wavelength converters", Journal of Lightwave Technology, vol. 16, no. 5, pp. 729 –735, 1998.

[109] K. E. Stubkjaer, S. L. Danielsen, A. Kloch, P. B. Hansen, K. S. Jepsen, H. N. Poulsen, D. Wolfson, A. T. Clausen, E. Limal, A. Buxens, "All-optical wavelength converters", in Proc. of OECC'98, vol. 1, pp. 464-465, Chiba, Japan, (invited paper), June 1998.

[110] B. E. Olsson, P. Ohlen, L. Rau, D.J. Blumenthal, "A simple and robust 40-Gb/s wavelength converter using fiber cross-phase modulation and optical filtering", IEEE Photonics Technology letters, vol.12, no.7, pp. 846-848, 2000.

[111] B. C. Sarker, T. Yoshino, and S. P. Majumder, "All-Optical Wavelength Conversion Based on Cross-Phase Modulation (XPM) in a Single-Mode Fiber and a Mach-Zehnder Interferometer", IEEE Photon. Technol. Lett., 14(3):340-342, Mar. 2002.

[112] S. Bischoff, A. Buxens, H. N. Poulsen, A. T. Clausen and J. Mørk, "Bidirectional four-wave mixing in semiconductor optical amplifiers: theory and experiment", Journal of Lightwave Technology, vol. 17, no. 9, pp. 1617-1625, 1999.

[113] O.A.Lavrova, L.Rau, D.J.Blumenthal, "10 Gbit/s Agile Wavelength Conversion With Nanosecond Tuning Times Using a Multisection Widely Tunable Laser Semiconductor Optical Amplifiers", IEEE Journal of Lightwave Techn., Vol. 20, 4, pp. 712-717, April 2002.

[114] J. Yu, Y. Qian, A. T. Clausen, H. N. Poulsen, P. Jeppesen and S. N. Knudsen, "40 Gbit/s pulsewidth-maintained wavelength conversion based

on a high-nonlinearity DSF-NOLM", Electronics Letters, vol. 36, no. 19, pp. 1633-1635, 2000.

[115] L. K. Oxenloewe, A. T. Clausen and H. N. Poulsen, "Wavelength conversion in an electroabsorption modulator", in Proc. ECOC'2000, paper 9.4.4, pp. 303-304, Munich, Germany, September 2000.

[116] H. Lee, H. Yoon, Y. Kom, and J. Jeong, "Theoretical study of frequency chirping and extinction ratio of wavelength-converted optical signals by XGM and XPM using SOA", IEEE Journal of Quantum Electronics, vol. 35, pp. 1213-1219, August 1999.

[117] S. J. B. Yoo, "Wavelength Conversion Technologies for WDM Network Applications", J. Lightwave Technol., 14(6):955-966, Jun. 1996.

[118] J. Leuthold, P.A. Besse E. Gamper, M. Dülk, S. Fischer, G. Guekos and H. Melchior, "All-Optical Mach-Zehnder Interferometer Wavelength Converters and Switches with Integrated Data- and Control-Signal Separation Scheme", Journal of Lightwave Technology, Vol. 17, No.6, pp1056-1066, June 1999.

[119] S. Tammela, H. Ludvigsen, T. Kajava and M. Kaivola, "Characterization of the chirp and intensity modulation properties of an SOA-MZI wavelength converter", IEEE Photonics Technology Letters, vol. 9, pp. 475-477, 1997.

[120] J. Leuthold, B. Mikkelsen, G. Raybon, C.H. Joyner, J.L. Pleumeekers, B.I. Miller, K. Dreyer and R. Behringer, "all optical wavelength conversion between 10 and 100 Gb/s with SOA delayed interference configuration", Opt. Quantum Electron., vol. 33, pp. 939-952, 2001.

[121] R. Schreieck, M. Kwakernaak, H. Jäckel and H. Melchior, "All-Optical Switching at Multi-100-Gb/s Data Rates with Mach-Zehnder Interferometer Switches", Journal of Quantum Electronics, Vol. 38, No. 8, pp 1053-1061, Aug. 2002.

[122] D. Wolfson, A. Kloch, T. Fjelde, C. Janz, B. Dagens, M. Renaud, "40 Gb/s all-optical wavelength conversion, regeneration and demultiplexing in an SOA-based all-active Mach-Zehnder interferometer", IEEE Phot. Techn. Lett., Vol. 12, pp. 332-334, March 2000.

[123] J. Ramamirtham, J. Turner, "Design of Wavelength Converting Switches for Optical Burst Switching", INFOCOMM 2002, Proceedings Vol. 2,pp.362-370, New York, NY, USA June 2002.

[124] P. Öhlen, B.-E. Olsson, and D. J. Blumenthal, "Wavelength Dependence and Power Requirements of a Wavelength Converter Based on XPM in a Dispersion-shifted Optical Fiber", IEEE Phot. Technol. Lett., 12(5): 522-524, May 2000.

[125] J. Yu and P. Jeppesen, "80Gb/s wavelength conversion based on cross-phase modulation in a high-nonlinearity dispersion-shifted fiber and optical

filtering", IEEE Photonics Technology Letters., vol. 13, no. 8, pp. 833-835, 2001.

[126] T. Clausen, L. Oxenloewe, C. Peucheret, S. N. Knudsen, L. Grüner-Nielsen, A. Bjarklev, S. Barkou, H. N. Poulsen and P. Jeppesen, "Novel single/multiple wavelength RZ pulsesource based on four-wave mixing in newly developed highly non-linear fibre", in Proc. ECOC'2000, paper P3.14, pp. 221-222, Munich, Germany, September 2000.

[127] E. Ciaramella, F. Curti, S. Trillo, "All-optical signal reshaping by means of four-wave mixing in optical fibers", IEEE Photon. Technol. Lett., vol. 13, no.2, pp.142-144, 2001.

[128] T. V. Andersen, K. M. Hilligsoe, C. K. Nielsen, J. Thogersen, K. P. Hansen, S. R. Keiding, and J. J. Larsen, "Continuous-wave wavelength conversion in a photonic crystal fiber with two zero-dispersion wavelengths", Optics Express, 12(17):4113-4122, August 2004.

[129] M. Westlund, J. Hansryd, P. A. Andrekson, S. N. Knudsen, "Transparent wavelength conversion in fibre with 24nm pump tuning range", Electron. Lett., vol.38, no.2, pp.85-86, 2002.

[130] Tina Fjelde, "Traffic analysis and signal processing in optical packet switched networks", Ph.D. thesis, Research Center COM, Technical University of Denmark, 2001.

[131] M.L. Nielsen, M. Nord, M.N. Petersen, B. Dagens, A. Labrousse, R. Brenot, B. Martin, S. Squedin and M. Renaud, "40 Gbit/s standard-mode wavelength conversion in all-active MZI with very fast response", Electron. Letter., vol. 39, no. 4, pp. 385-386, 2003.

[132] Mads Lønstrup Nielsen, "Experimental and Theoretical investigation of Semiconductor Optical Amplifier (SOA) based All-Optical Switches", Ph.D. thesis, Research Center COM, Technical University of Denmark, 2004.

[133] C. Peucheret, B. Zsigri, K. P. Hansen, M. D. Nielsen, and P. Jeppesen, "Photonic crystal fibers for transmission and optical signal processing", IEEE LEOS Newsletter, 18(4):7-8, August 2004.

[134] J.M. Martinez, D. Colle, F. Ramos, R. Van Caenegem, M. Pickavet, J. Marti, "LASAGNE: All-optical label swapping employing optical logic gates in network nodes", Proc. of NOC 2004, Eindhoven, The Netherlands, vol. 9, no. , pp.269-267, June 2004.

[135] www.ciphotonics.com.

[136] Benny Mikkelsen, "Optical Amplifiers and their System Application", Ph.D. thesis, Department of Electromagnetic Systems, Technical University of Denmark, 1994.

[137] J. H. Lee, W. Belardi, K. Furusawa, P. Petropoulos, Z. Yusoff, T. M. Monro, and D. J. Richardson, "Four-wave mixing based 10-Gb/s tunable

wavelength conversion using a holey fiber with a high SBS threshold", IEEE Photonics Technology Letters, 15(3):440-442, March 2003.

[138] Søren Lykke Danielsen, "Traffic Analysis and Signal Processing in High-Capacity Optical Networks", Ph.D. thesis, Department of Electromagnetic Systems, Technical University of Denmark, 1997.

[139] J. Zhang, N. Chi, P.V. Holm-Nielsen, Efstratios Kehayas, Francisco Ramos, M.T. Hill, Y. Liu and H.J.S. Dorren, K. Vyrsokinos, José Martinez, "D.4.1. - First report on simulation results of node functionalities employing all-optical logic gates", IST-LASAGNE Deliverable, www.ist-lasagne.org, 2004.

[140] B. Dagens, C. Janz, D. Leclerc, V. Verdrager, F. Poingt, I. Guillemot, F. Gaborit, and D. Ottenwalder, "Design optimization of all active Mach-Zehnder wavelength converters", IEEE Phonton. Technolo. Letter. vol. 11, no. 4, pp.424-426, vol. 11, no. 4, 1999.

[141] Efstratios Kehayas, Francisco Ramos, J. Zhang, N. Chi, P.V. Holm-Nielsen, M.T. Hill, Y. Liu and H.J.S. Dorren, K. Vyrsokinos, José Martinez, "D.5.1-First report on synchronization, buffering and intra-node interconnection issues for the AOLS node", IST-LASAGNE Deliverable, www.ist-lasagne.org, 2004.

[142] M. L. Nielsen, B. Lavige and B. Dagens, "Polarity preserving SOA-based wavelength conversion at 40 Gbit/s using bandpass filtering", Electron. Letter. pp. 1334-1335, vol. 39, no. 8, Sept. 2003.

[143] T. Durhuus, B. Mikkelsen, C. Joergensen, S. L. Danielsen and K. E. Stubkjaer, "All-Optical Wavelength Conversion by Semiconductor Optical Amplifiers", Journal of Lightwave Technol., vol. 14, pp. 942-954, 1996.

[144] M. L. Nielsen, J. D. Buron, M. Nord and M.N. Petersen, "SOA-based Functional Devices for Future Optical Networks", in Techn. Digest SSDM 2003, paper F-9-1 (invited) Tokio, Japan, 2003.

[145] Viswanathan, N. Feldman, Z. Wang, and R. Callon, "Evolution of multiprotocol label switching", EEE Communi. Mag., vol.36, no.5, pp.165-173, 1998.

[146] Dagens, A. Labroussse, R. Brenot, B. Lavigne, and M. Renaud, "SOA-based devices for all optical signal processing", ThX1, Optical Fiber Communication Conference 2003, Atlanta, USA, 2003.

[147] L. Dittmann et al., "The European IST Project DAVID: a viable approach towards optical packet switching", IEEE J. Select. Areas Commun., vol. 21, pp. 1026-1040, Sept. 2003.

[148] P. Mahgereftech, et al, "Technique for suppression of pattern dependence in a semiconductor-optical-amplifier wavelength converter", IEEE Photon. Technol. Lett., v9, 1583-1585 ,1997.

[149] L. Xu, L.K. Oxenløwe, N. Chi, F. P. Romstad, K. Yvind, J. Mørk, P. Jeppesen, K. Hoppe and J. Hanberg, "Bandwidth and chirp characterisation of wavelength conversion based on electroabsorption modulators", in Proceedings European Congress on Optical Communication, ECOC2002, paper 1.26, 2002.

[150] H. Haug and S. Schimtt-Rink, "Basic mechanisms of the optical nonlinearities of semiconductors near the band edge", J. Opt. Soc. Amer. B, vol. 2, no.7, pp. 1135-1142, 1988.

[151] Cao, J.C. Cartledge, "Characterization of the chirp and intensity modulation properties of an SOA-MZI wavelength converter", J. Lightwave Technol., vol. 20, no. 4, pp 689-695, April 2002.

[152] L. K. Oxenløwe, et. al., "Wavelength conversion in an electroabsorption modulator", in Proceedings of ECOC'00, paper 9.4.4, 2000.

[153] K. Nishimura, et al., "Wavelength conversion with no pattern effect at 40 Gbps using an electroabsorption waveguide as a phase modulator", in Proceedings of ECOC'02, paper 2.3.7, 2002.

[154] Y. Ueno, "All-Optical Signal Processing for over 100 Gb/s Optical-TDM Networks", LEOS Annual Meeting, Tucson, TuY1, Oct. 2003.

[155] J. Cheyns, E. Van Breusegem, C. Develder, A. Ackaert, M. Pickavet, P. Demeester, "Performance improvement of an internally-blocking optical packet/burst switch", ICC 2003 International Conference on Communications, 11-15, Anchorage, Alaska, USA, May 2003.

[156] P. V. Holm-Nielsen, N. Chi, J. Zhang and P. Jeppesen, "Combined Label Swapping and Wavelength Conversion in All-Optical Processing Nodes for 40 Gb/s Labeled Signals", in Proceedings, International Conference on Telecommunications, ICT'05, Capetown, South Africa, May 2005.

[157] Glesk, J. P. Solokoff, and P. R. Prucnal, "All-optical address recognition and self-routing in a 250 Gbit/s packet-switched network", Electronic Letters, 30, 1322-1333, 1994.

[158] Lin Xu, "Electroabsorption modulators used for all-optical signal processing and labelling", Ph.D. thesis, Research Center COM, Technical University of Denmark, 2004.

[159] Gunnar Jacobsen, "Noise in Digital Optical Transmission Systems", Artech House, Inc., 1994.

[160] H. Chen, G. Zhu, Q. Wang, J. Jaques, J. Leuthold, A. B. Piccirilli, and N. K. Dutta, "All-optical logic XOR using differential scheme and Mach-Zehnder interferometer", Electron. Lett., vol. 38, pp. 1271-1273, 2002.

[161] R Ø Andreassen, B E Helvik, "A note on traffic performance gain for optical burst/packet switching", Proc. Optical Network Design & Modelling Conference, ONDM 2004, Feb. 2-4, 2004, Ghent, 2004.

[162] M.T Hill, H. de Waardt, G.D. Khoe and H.J.S. Dorren, "All optical flip-flop based on coupled laser diodes", IEEE Journal of Quantum Electronics 37, 2001.

[163] R. Geldenhuys, Y. Liu, N. Calabretta, M. T. Hill, F. M. Huijskens, G. D. Khoe and H.J.S. Dorren, "All-optical signal processing for optical packet switching", OSA/ Journal of Optical Networking, Vol. 3, No.12, pp.854-865, December, 2004.

[164] K.-H. Park, T. Mizumoto, A. Matsuura, and Y. Naito, "All-optical address extraction for optical routing", J. Lighwave Technol., vol. 16, pp.1129–1136, July 1998.

[165] Yonglin Yu, G. Mulvihill, S. O'Duill, and R. O'Dowd, "Performance implications of wide-band lasers for FSK modulation labeling scheme", IEEE Photonics Technology Letters, vol. 16, no. 1, pp. 39-41, January 2004.

[166] K. E. Stubkjaer, "Semiconductor optical amplifier-based all-optical gates for high-speed optical processing", IEEE Journal on Selected Topics in Quantum Electronics, vol. 6, no. 6, pp. 1428-1435, 2000.

[167] E. Park, A. E. Willner, "Network demonstration of self-routing wavelength packets using an all-optical wavelength shifter and QFSK subcarrier routing control", IEEE photon. Technol. Lett., Vol.8, No.7, pp.114-115, 1996.

[168] J. M. Martinez,F. Ramos, J. Marti, J. Herrera, R. Llorente, "All-optical N-bit XOR gate with feedback for optical packet header processing", in Proceedings of the European Conference on Optical Communication, ECOC'02, Copenhagen, Denmark, paper P.4-08, 2002.

[169] H.J.S. Dorren, M.T. Hill, Y. Liu, N. Calabretta, A. Srivatsa, F.M. Huijskens, H. de Waardt, and G.D. Khoe, "Optical packet switching and buffering by using all-optical signal processing methods", J. Lightwave Technol., vol. 21, no. 1, pp. 2-12, Jan. 2003.

[170] J. Cheyns, E. Van Breusegem, C. Develder, D. Colle, M. Pickavet, P. Demeester, "Evaluating COST functions for OPS node architectures", Proc. ONDM 2004, Ghent Belgium, pp.37-54, Feb. 2-4, 2004.

[171] S. H. Chin, A. Franzan, D. K. Hunter, I. Andanovic, "Synchronisation schemes for optical networks", IEE Proceedings on Optoelectronics, Vol. 147, 6, pp. 423 –427, December 2000.

[172] G.S. Kuo, ed., "Optical Switching", IEEE Comm. Mag., vol. 40, No. 3, pp. 72-101, March 2002.

[173] Carsten Hede, "Experimental investigation of Gigabit electronic switching circuits", Ph.D. Thesis, Electromagnetics Institute, Technical University of Denmark, August 1978.